ROLE OF ZINC IN DENDRITIC CELL ACTIVATION AND THE REGULATION OF COMPLEMENT PROTEIN INTERACTIONS

Dagmara Marta Wiatrek

A Thesis Submitted for the Degree of PhD
at the
University of St Andrews

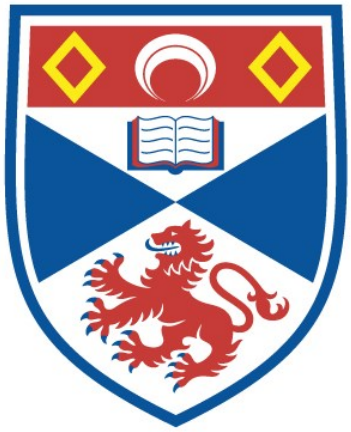

2017

Full metadata for this thesis is available in
St Andrews Research Repository
at:
http://research-repository.st-andrews.ac.uk/

Please use this identifier to cite or link to this thesis:
http://hdl.handle.net/10023/10813

This item is protected by original copyright

This item is licensed under a
Creative Commons License

https://creativecommons.org/licenses/by-nc-nd/4.0

Role of zinc in dendritic cell activation and the regulation of complement protein interactions

Dagmara Marta Wiatrek

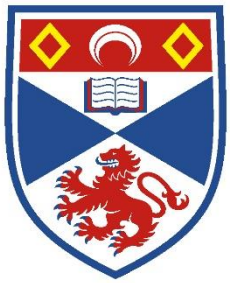

University of
St Andrews

Declaration

Personal declarations

I, Dagmara Marta Wiatrek, hereby certify that this thesis, which is approximately 50,000 words in length, has been written by me, and that it is the record of work carried out by me, or principally by myself in collaboration with others as acknowledged, and that it has not been submitted in any previous application for a higher degree.

I was admitted as a research student in September 2012 and as a candidate for the degree of Ph.D in Medicine; the higher study for which this is a record was carried out in the University of St Andrews between 2012 and 2016.

Date: Signature of candidate:

Supervisor's declarations

I hereby certify that the candidate has fulfilled the conditions of the Resolution and Regulations appropriate for the degree of Ph.D in the University of St Andrews and that the candidate is qualified to submit this thesis in application for that degree.

Date: Signature of supervisor:

Signature of supervisor:

Copyright Declaration

In submitting this thesis to the University of St Andrews I understand that I am giving permission for it to be made available for use in accordance with the regulations of the University Library for the time being in force, subject to any copyright vested in the work not being affected thereby. I also understand that the title and the abstract will be published, and that a copy of the work may be made and supplied to any bona fide library or research worker, that my thesis will be electronically accessible for personal or research use unless exempt by award of an embargo as requested below, and that the library has the right to migrate my thesis into new electronic forms as required to ensure continued access to the thesis. I have obtained any third-party copyright permissions that may be required in order to allow such access and migration, or have requested the appropriate embargo below.

The following is an agreed request by candidate and supervisor regarding the publication of this thesis:

Embargo on both of printed copy and electronic copy for the same fixed time period of two years on the following grounds: publication would be commercially demanding to the researcher and to the supervisors at the University; publication would preclude future publication.

Date: Signature of candidate:

Signature of supervisor:

Abstract

The importance of zinc in immune system is complex and recognised mostly by the effects of zinc deficiency which affects both innate and adaptive immunity. The results presented here provided insight into the complex role of zinc in immunity through examination of the roles of zinc in dendritic cell activation and regulation of complement protein interactions. Little is known about the mechanism by which zinc affects immune cell function. Here we show that Toll-like receptor 4 signalling upon lipopolysaccharide (LPS) binding, alters the expression of zinc transporters, to maintain the stable intracellular free zinc. This indicates the importance of zinc on every level of dendritic cells (DCs) maturation, beginning with antigen recognition, through antigen processing and cell migration to the lymphatic organs, to finally antigen presentation to T-cells. Hydroxyapatite along with LPS can trigger DCs maturation. Following this finding we presented a global picture of proteomic changes that occur in maturing DCs, which was characterised by reduced expression of proteins that drive cellular processes including metabolism and protein translation. Proteomic results may also change the current understanding of antigen presentation by DCs, implicating major histocompatibility complex (MHC) class I in “delayed” antigen presentation. Zinc is also crucial in innate immunity as it inhibits the interaction of complement proteins C1q, Factor H and C3 with histidine rich glycoprotein (HRG). The results suggest for the first time, that binding of complement proteins to HRG is not solely dependent on the N-terminus. Also the role of zinc in the early onset of diseases related to tissue calcification was examined, showing its enhancing effect on HRG binding to hydroxyapatite.

Acknowledgements

Firstly, I would like to express my sincere gratitude to my advisors Dr Alan Stewart and Dr Simon Powis for their continuous support of my Ph.D study and related research, for their patience, motivation, and immense knowledge. Their guidance helped me in all the time of research and writing of this thesis. I could not have imagined having a better advisors for my Ph.D study.

Besides my advisor, I would like to thank the rest of my thesis committee: Prof. David Harrison and Dr. Paul Reynolds, for their insightful comments and encouragement, but also for the hard questions which persuaded me to widen my research from various perspectives.

I thank my fellow labmates in for the stimulating discussions, for the sleepless nights we were working together, and for all the fun we have had in the last four years.

I would like to thank my family: my parents and to my sister and brother for supporting me spiritually throughout writing this thesis and my life in general. Thank you for encouraging me in all of my pursuits and inspiring me to follow my dreams. I always knew that you believed in me and wanted the best for me.

Last but not the least, I owe thanks to a very special person, my fiancé Nikos for his continued and unfailing love, patience and support during my pursuit of Ph.D degree that made the completion of thesis possible. You were always around at times I thought that it is impossible to continue, you helped me to keep things in perspective.

Podziękowania

Pragnę podziękować wszystkim bez których niniejsza praca nie mogłaby powstać.

Po pierwsze, chciałabym wyrazić wdzięczność moim promotorom, dr. Alanowi Stewart i dr. Simonowi Powis za ich ciągłe wsparcie, cierpliwość, motywację i ogromną wiedzę. Ich cenne uwagi merytoryczne niezmiernie mi pomogły podczas moich badań. Nie mogłabym sobie wyobrazić lepszych mentorów na studiach doktoranckich.

Poza moimi promotorami, chciałabym podziękować członkom komisji: Prof. Davidowi Harrison i dr. Paulowi Reynolds, za ich wnikliwe komentarze, zachęty, ale także za trudne pytania, które przekonały mnie, aby rozszerzyć moje badania o kolejne perspektywy.

Pragnę podziękować również koleżankom i kolegom z pracy za stworzenie wspaniałej atmosfery naukowej (i nie tylko), inspirujące dyskusje oraz za bezsenne noce spędzone wspólnie w laboratorium.

Chciałabym podziękować mojej rodzinie: rodzicom, siostrze, bratu, za duchowe wsparcie i zachętę podczas pisania tej pracy. Zawsze wiedziałam, że wierzyliście we mnie i chcieliście dla mnie jak najlepiej.

Na koniec dziękuję wyjątkowej osobie: mojemu przyszłemu mężowi Nikosowi, za jego miłość, cierpliwość i wsparcie.

Contents

Chapter 1. Introduction

1.1. Innate immune system

The innate immune system is the first line of defence against pathogens, providing immediate immune response. After pathogens are recognised through their molecular pattern, granulocytes are attracted to the infected tissue where they migrate via chemotaxis (Amulic et al., 2012). Granulocytes internalise pathogens through phagocytosis and kill them by an oxidative burst with reactive oxygen species (ROS) (Mayer et al., 2014), which was reported to be a zinc dependent process (Maares and Haase, 2016). Additionally, granulocytes secrete chemokines and cytokines, including IL-8 and IL-1 receptor antagonist (IL-1ra), after the contact with bacterial lipopolysaccharides (LPS) (Hasan et al., 2016). Zinc is crucial for granulocyte functioning as zinc deficiency was shown to decrease cytokine production, phagocytosis and chemotaxis. Furthermore, zinc is involved in the formation and release of neutrophil extracellular traps (NETs), used to capture extracellular pathogens (Hasan et al., 2012).

Shortly after granulocyte activation, monocytes migrate to the site of infection. They differentiate into macrophages, and together with granulocytes kill pathogens via phagocytosis and oxidative burst. Additionally, macrophages and dendritic cells (DC) present antigen to T-cells and secrete pro-inflammatory cytokines (Mayer, 2014; Prasad, 2009). Zinc regulates monocyte and macrophage functioning in multiple ways. Zinc deficiency increases phagocytosis and the oxidative burst of monocytes, and increases monocyte maturation into macrophages (Dubben et al., 2010). It also inhibits secretion of IL-12 and the activation of macrophages by the adaptive immune system (TH1 and TH2) and therefore inhibits ROS generation (Bao et al., 2011).

Zinc influences the secretion of pro-inflammatory cytokines in monocytes in a dose dependent, and cell-dependent manner. In monocytes, cytokines are released at low extracellular zinc concentrations, and inhibited at high zinc doses. On the other hand, in peripheral blood mononuclear cells (PBMCs), IL-6-, IL-1b- and TNF-release is induced by high (*ca.* 100 mM) zinc concentrations (Wellinghausen et al., 1996; Wellinghausen et al., 1997). Correspondingly, cytokine production has been shown to be decreased in PBMCs by zinc deficiency (Mayer et al., 2014). However, zinc deficiency does not affect phagocytosis and oxidative burst of PBMCs. Natural killer (NK) cells are crucial for immune response against viral infections and tumours. Haematopoiesis of NK cells from CD34+ common hematopoietic progenitor is enhanced by 10-

20 µM of zinc (Muziolli et al., 2007). Also the number of NK cells is influenced by alterations in extracellular zinc, but are unaffected by intracellular zinc changes, as shown by increased NK cell numbers after zinc supplementation (Metz et al., 2006), but no change in the amount of NK cells after zinc chelation with TPEN (membrane permeable zinc chelator) (Mariani et al., 2008). On the functional level, zinc regulates proper interaction of NK cells with MHC I receptors on target cells (Vales-Gomez et al., 2000) and the addition of zinc increases cytokine production, including IFN-γ (Metz et al., 2006).

Recently the new group of immune cells has been identified. Innate lymphoid cells (ILCs) differentiate from haematopoietic stem cells, via an $ID2^+$ precursor. They belong to lymphocytes but due to the lack of B or T receptors, are unable to respond to an antigen presented via MHC molecules (Walker et al., 2013). Based on the transcription factors that regulate their development and on cytokines secreted, ILCs are divided in to three subgroups: type 1 comprising ILC1s and NK cells (produce IFNγ, perforin and granzymes), type 2 ILCs (ILC2s; produce IL-5, IL-9, IL-13 and amphiregulin) and type 3 comprising ILC3s and lymphoid tissue-inducer (LTi) cells (produce IL-17, IL-22, lymphotoxin and IFNγ) (Spits et al., 2013). ILCs are a multifunctional group. ILC1s play a role in the inflammation, NK-cells are responsible for the immunity against viruses and intracellular pathogens but also tumour surveillance. ILC2s protect against helminthic infection by activating T-cells recruiting and activating mast cells and eosinophils, and stimulate B cell proliferation (Palm et al., 2012). ILC3s are crucial in the intestinal immune system maintaining intestinal homeostasis and protecting against extracellular bacteria (Walker et al., 2013). So far, except well characterised NK cells, it is not known how zinc influences the function of ILCs.

1.1.1. Complement system

The human complement system is a key part of the innate immune system and acts as a first line of defence, performing its function in blood plasma, tissues and within cells (Kolev et al., 2014). It comprises more than 35 plasma and cell membrane bound proteins, produced mainly by the liver (Nan et al., 2013). In plasma, complement proteins are typically present at 0.3-7 µM concentrations (Law and Reid, 1995). There are three complement pathways, which lead to the elimination of pathogens and cytotoxic complexes: classical pathway (CP; antigen-antibody complex interactions), alternative pathway (AP; binding to pathogen surface receptors) and the lectin pathway (LP; initiated by recognition of exposed carbohydrates/ligands by mannose-

binding lectin (MBL) and/or ficolins; (Fig. 1.1; Collard et al., 2001). All three routes lead to a central complement protein C3. C3 is relatively abundant in plasma (*ca.* 5-8.5 µM) compared to other complement proteins (Law and Reid, 1995; Nilsson and Ekdahl, 1998) and additionally, as a modest acute phase protein, shows 50% increase in concentration following complement pathway activation.

To enable detection of pathogens, the AP is constantly active at low grade, and is not influenced by viable host cells. However, the complement system is activated by apoptotic cells, which aids immunological complex clearance and helps cells to maintain normal homeostasis (Lu et al., 2008). Full activation of the complement system occurs only after pathogen recognition, and results in inflammation, as well as opsonisation and phagocytosis of bacteria, viruses and other pathogens. The C5 complement protein is cleaved by C5 convertase to C5b, which then interacts with C6. Subsequent binding of C7, C8 and C9, results in the formation of membrane attack complex (MAC), a large (10 nm-wide) pore in the pathogen or apoptotic cell membrane, leading to the activation of adaptive immune response (Bubeck, 2014).

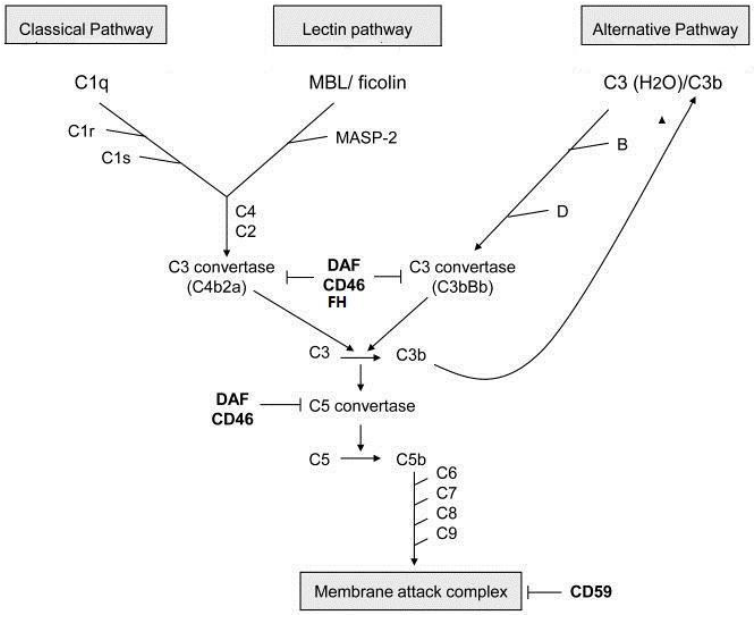

Figure 1.1. A simplified schematic representation of three pathways of complement activation. Abbreviations: mannose binding lectin (MBL); mannose-binding protein-associated serine protease 2 (MASP-2); decay-accelerating factor (DAF); complement regulatory protein, cluster of differentiation 46 (CD46); MAC-inhibitory protein, cluster of differentiation 59 (CD59); complement factor B (B); complement factor D (D) (Asgari et al., 2010).

Classical complement pathway

The first protein component of the classical complement pathway, C1 begins the cascade in which each component activates the next, like domino blocks (Fig. 1.1). The C1 complex, consist of C1q, two molecules of C1r, and two molecules of C1s (C1qr2s2; Ricklin et al. 2010). Because of its extra-hepatic origin, C1q is quite an exceptional complement protein. It is mostly produced by immature dendritic cells, monocytes, and macrophages (Ghai et al., 2007). It has a complex structure, formed by 18 chains of three types, forming six globular target domains attached to a collagen-like region (Fig. 1.2). C1q binds to target molecules based on the charge of their surface. It has over 100 ligands, including IgG and IgM, non-immune complex proteins like C-reactive protein (Kishore et al., 2004) and histidine rich glycoprotein (Manderson et al., 2009). It also binds pathogen-associated molecules such as lipopolysaccharide as well as others (Roumenina et al., 2008). Binding of C1q to its ligands occurs via electrostatic interactions between a Ca^{2+} ion located on the globular head of C1q and negatively charged binding sites on the target.

After binding to the target surface, C1q is initially activated by the proteases (Roumenina et al., 2005). Then, through conformational changes in the complex, binding at the globular head of C1q is detected at C1r (Gaboriaud et al., 2014). Consecutively, conformational changes in C1 complex lead to C1s being cleaved by C1r, which leads to its activation (Gaboriaud et al., 2004) and the formation of a C1r2C1s2 active tetramer. The C1r2C1s2 complex then cleaves C4 into C4a and C4b, and leads to covalent binding of C4b at the cell/pathogen surface. C2 splits into C2aa and C2ba and then C4b binds C2ba, forming C3 convertase (C4b2ba. The convertase cleaves C3 into biologically active C3a and C3b (Gaboriaud et al., 2004; Wallis et al., 2010).

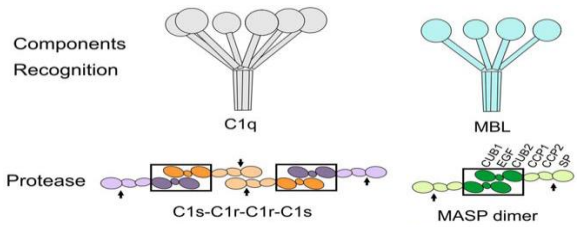

Figure 1.2. Schematic representation of components of the initiating complexes of lectin and classical complement pathways. Abbreviations: mannose binding lectin (MBL); mannose-binding protein-associated serine protease (MASP); CUB1, EGF, CUB2, CCP2 and SP are MASP subdomains (Wallis et al., 2010).

Alternative complement pathway

Under normal physiological conditions, the AP is the only complement pathway active in human plasma. The low-grade activation is crucial to monitor for foreign antigens. This process is known as AP tick-over, which is the hydrolysis of a labile thioester bond, which converts C3 to its hydrolysed, bioactive form, C3(H_2O) (Harboe and Mollnes, 2008). The hydrolysis is spontaneous and can be increased when C3 interacts with some biological or artificial surfaces, including biomaterial and lipid surfaces. During C3 hydrolysis, another complement protein, Factor B (FB) binds to the newly exposed binding site, and forms a complex C3(H_2O)-FB, which is later cleaved by factor D (FD), which acts as a serine protease. Newly formed convertase complex C3(H_2O) Bb cleaves native C3 to C3a and C3b (Nilsson and Nilsson Ekdahl, 2012). During physiological conditions this process creates a loop, where small amount of C3b binds to hydroxyl groups on C3(H_2O). When binding to the surface of host cells, C3b is immediately inactivated, by a sequence of complement regulators. The only exceptions are apoptotic cells, where the number of surface complement regulators is decreased (Verbovetski et al., 2002). To eliminate pathogens, C3(H_2O)Bb convertase is formed on their surface and cleaves C5 into the anaphylatoxin C5a and fragment C5b. The complex enters into cell membranes and interacts with C8 when C5b associates with C6 and C7. That also triggers the binding of several units of C9 that form a membrane attack complex (Ricklin et al., 2010).

Complement pathways are highly regulated. One of the most important regulators is complement factor H (FH), which with its 2–5 μM concentration is a rather abundant plasma protein (Saunders et al. 2006). FH and its shorter splice variant, CFHL1, regulate C3 convertase by competing with factor B to C3b, and by dissociation of C3bBb complex (Zipfel and Skerka, 1999). FH consists of 20 CCP domains, and has at least two binding sites for C3b, at the N-terminus (CCP 1-4) and the C-terminus (CCP19-20) of the protein. Additionally, the N-terminus (CCP1-2) competes with FB for binding to C3b (Fig. 1.3). The interaction between FH and C3b on the surface is quite weak with Kd values in the μM range (Perkins et al., 2012). Additionally, FH binds glycosaminoglycans (GAG) through CCP7 and CCP20. Binding of GAG helps FH recognize heparan sulphate on the cell surface and therefore aids its functional activity (Merle et al., 2015). Another known ligand of FH is C-reactive protein (CRP), which binds to CCP7 and CCP19-20 and through this interaction, boosts complement inhibition (Perkins et al., 2012).

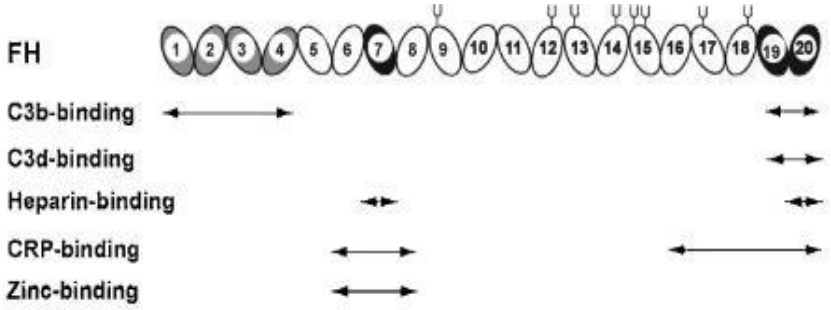

Figure 1.3. Schematic view of Factor H with the position of binding to its ligands. Factor H consists of 20 SCR domains. The positions of two C3b binding sites SCR-1/4, two heparin-binding sites on SCR-7 and SCR-20, two C3d binding sites on SCR-19 and SCR-20, two C-reactive protein (CRP) binding sites at SCR-6/8 and SCR-16/20, and zinc binding sites at SCR-6/8 are shown. The location of eight N-linked glycosylation sites is shown by symbols; a ninth site at SCR-4 is not occupied (Perkins et al., 2012).

FH has an additional control mechanism, involving five FH-related proteins (CFHR1-5) that belong to FH family. They are splice variants of the gene, coding for FH and therefore show high sequence homology with FH. However, their sequences are shorter than FH, with only 5 to 9 CCP domains (Skerka et al., 2013). CFHRs increase complement activation by binding of CFHR3 and CFHR4 to C3b, C3d and GAG on the cell surface, which as a result prevents FH from binding. A high degree of sequence similarity exists between the C-termini of CFHR3 and CFHR4, and FH (Heinen et al., 2009).

Lectin complement pathway

The lectin pathway is initiated by the binding of mannose-binding lectin (MBL), protein that possesses a collagen-like domain and a CRD to carbohydrates of microorganisms (Turner, 1996). The overall structure of MBL is a bit similar to C1q, however MBL forms multiple oligomers (trimers, tetramers and higher ordered oligomeric forms) (Fig. 1.2) (Matsushita and Fujita, 2001). MBL is linked to MBL-associated serum protease-1 (MASP-1), MASP-2, and MASP-3 (Jack et al., 2001). The interaction is calcium dependent and in the absence of Ca^{2+} ions, lectin complement pathway cannot be activated (Teillet, 2005). When MBL is bound to its target, MASPs become active and cleave C4 and C2, which results in the formation of C3 convertase (C4b2ba), which is then followed by the rest of the complement cascade (Takahashi et al., 2007).

Complement related diseases

Complement proteins and associated pathways are involved in many diseases. For example, C5 plays pathophysiological role in myocardial ischemia and reperfusion injury (Busche and Stahl, 2010). Some polymorphisms in FH, particularly in GAG-binding sites, can create imbalance in complement regulation and cause or contribute to various diseases (Brandstatter et al., 2012). One of them is the life-threatening kidney disease, haemolytic uraemic syndrome (HUS), where the majority of patients demonstrate dysfunctional FH due to mutations or FH autoantibodies (Brandstatter et al., 2012). This was found to be associated with a homozygous deletion in CFHR1 (Hofer et al., 2013). Additionally, mutations in C-terminus of FH (CCP19–20) were identified in numerous HUS patients. Those mutations prevent the interaction between FH and C3b, or FH and GAG, or both, which leads to lack of surface protection against a complement attack (Ferreira et al., 2009; Merle et al., 2015). In addition, autoimmunity is strongly associated with complement proteins, mainly with deficiency of the early components of the classical pathway: C1q and C4 (Sturfelt and Truedsson, 2005). Addition of zinc to FH causes it to form oligomers containing 4-10 monomers, which inhibit its activity. FH-zinc oligomer formation is thought to be relevant in age-related macular degeneration (AMD) and occurs when zinc levels increase to above 60 µM (Perkins et al., 2010).

1.2. Dendritic cells – a link between innate and adaptive immune system

Dendritic cells (DCs) serve as a link between innate and adaptive immunity and are considered as professional antigen presenting cells (APCs). T-lymphocytes cannot recognize antigen by themselves. To initiate an immune response DCs are needed. Immature DCs are present in non-lymphoid tissue where they meet the antigen and recognise it through specialized pattern recognition receptors (PRRs). DCs retain the memory of captured antigen and when they maturate and migrate to lymph nodes the uptake of further antigen is being reduced. In the lymph node the antigen is then being processed and presented through MHCII molecules to both lymphocytes T and B.

Primary DCs are very rare with the frequency of only 0.02–0.06 x 10^6 cells/ml of blood (Stemcell Technologies; 2nd Sep 2016). Recent research showed that based on molecular markers and cell function, DCs can be divided into a few subsets. The two main groups are plasmacytoid DCs that express CD123 and BDCA-2, myeloid DCs that express BDCA-1 and BDCA-3 and Langerin DCs that express CD1a and CD14 markers. Due to DCs being present in the blood, lymphoid tissues, skin

and lungs, additional variability in surface markers expression is introduced by environmental differences. Therefore, to standardize the identification of DCs, multiple research is now being carried to compare DC subsets at the transcriptional level (Patel and Metcalf, 2016).

1.2.1. Dendritic cell maturation

Maturation increases the abilities of DCs to present antigen, this includes phenotypic and functional maturation. During a process called phenotypic maturation, the morphology of DCs changes, more specifically their size increases and characteristic cytoplasmic projections develop. Mature DCs lack several surface antigens including CD19, CD20 molecules to interact with B-cells, CD3 for T-cells, CD56 for NK cells, CD14 for monocytes and CD34 for haemopoietic stem cells (Tan et al., 2010). Instead, other surface molecules appear, which are crucial for their antigen presenting function. Those maturation markers are peptide–MHC class I and II molecules, and T cell costimulatory molecules like CD80 and CD86 (Turley et al., 2000; Trombetta et al., 2003), and are being highly expressed on the surface of mature DCs. Functional maturation progresses nearly in parallel to phenotypic maturation. However, in contrast to phenotypic maturation, which can be induced by many environmental stimuli, for functional maturation DCs need to sense microbial compounds through its PPRs. Functional changes include altered endocytosis, and later, migration to the nearest lymph node to meet T-cells. In addition, cytokine expression significantly increases upon DC maturation (Hammer and Ma 2013).

1.2.2. Toll-like receptors signalling

Innate immune response relies on the pattern-recognition receptors (PRRs), which recognize microbial structures, known as pathogen-associated molecular patterns (PAMPs). Dendritic cells express various PRRs, including nucleotide-binding oligomerization domain (NOD)-like receptors (NLRs), retinoic acid-inducible gene I (RIG-I) -like receptors (RLRs), Toll-like receptors (TLRs) and C-type lectins including β-glucan receptor - Dectin-1 which is involved in response against fungal pathogens. (Brown, 2006). It was thought that in healthy hosts, protection against fungal infection relies on Th1-cell immune response (Romani, 2004). Nonetheless, recently discovered subset of T helper cells – Th17, are now considered substantial for immune response against microbial pathogens including fungi (Vautier et al., 2010).

TLRs are a type of membrane bound PRR. In humans, there are ten TLRs classified so far (TLR1-TLR10). Mice have additionally TLR11-13, but lack TLR10 (Gay and Gangloff, 2007). Based on the similarities among cytoplasmic domains, TLRs, together with the interleukin-1 receptors (IL-1Rs)

form the toll/interleukin-1 (TIR) superfamily. Extracellular domains of TLR are formed by tandem repeats of leucine-rich regions. This so-called leucine-rich repeats differ between TLRs, which allows the binding of specific ligands. Additionally to ligand specificity, TLRs are discriminated based on cellular localization and signal transduction (Dowling and Dellacasagrande, 2016). Localization depends on ligands being recognised. Receptors detecting mainly bacterial membrane components (TLR1, TLR2, TLR4, TLR5, TLR6) are located on the plasma membrane, whilst other TLRs are present on organelles and other intracellular compartments (TLR3, TLR7, TLR8 and TLR9) when detecting foreign nucleic acids. However, small amounts of the so-called "intracellular TLRs" can be also found on the cell surface, probably to detect low amounts of circulating nucleic acids (Guerrier et al., 2014).

The main function of TLRs is to initiate an innate immune response. They induce the phenotypic and functional maturation of antigen presenting cells and the production of cytokines (Kawai and Akira, 2010). TLR3, TLR4, TLR7, TLR8, and TLR9 signalling activates Th1-type immune responses characterized by secretion of proinflammatory cytokines, while TLR2 and TLR5 initiate Th2-type immune responses which are associated with secretion of anti-inflammatory cytokines (Duthie et al., 2011). Furthermore, TLR3, TLR7, and TLR9 stimulate proliferation, maturation, and survival of B cells (Crampton et al., 2010; Green et al., 2012). It is also suggested that intracellular TLRs play a role in autoimmunity, because their prolonged activation leads to overstimulation of B cells (Green and Marshak-Rothstein, 2011).

After interaction with specific ligands, two TLR receptor chains dimerize and undergo conformational changes that results in recruitment of the intracellular adaptor protein, MyD88 (myeloid differentiation primary response gene 88), which initiates signalling. Additionally, after ligand binding TLR4 can be rapidly internalised by a clathrin- and dynamin-mediated process (Chaturvedi and Pierce, 2009). The only exception is TLR3, which signals via TRIF. TLR2, TLR4, TLR5 and TLR9 can also, in addition to MyD88 pathway, activate the TRIF cascade (Nilsen et al., 2015; Robinet et al., 2016). Regardless of adaptor protein, activation leads to the activation of NF-kB, p38, JNK, and/or IFN-regulatory factor (IRF) signalling. As a result, inflammatory cytokines are produced (Fig. 1.4; Perkins and Vogel, 2015). TLR signalling bears the information about the type of immunogen; therefore, the expression of TLRs differs between DC subsets to customize the response.

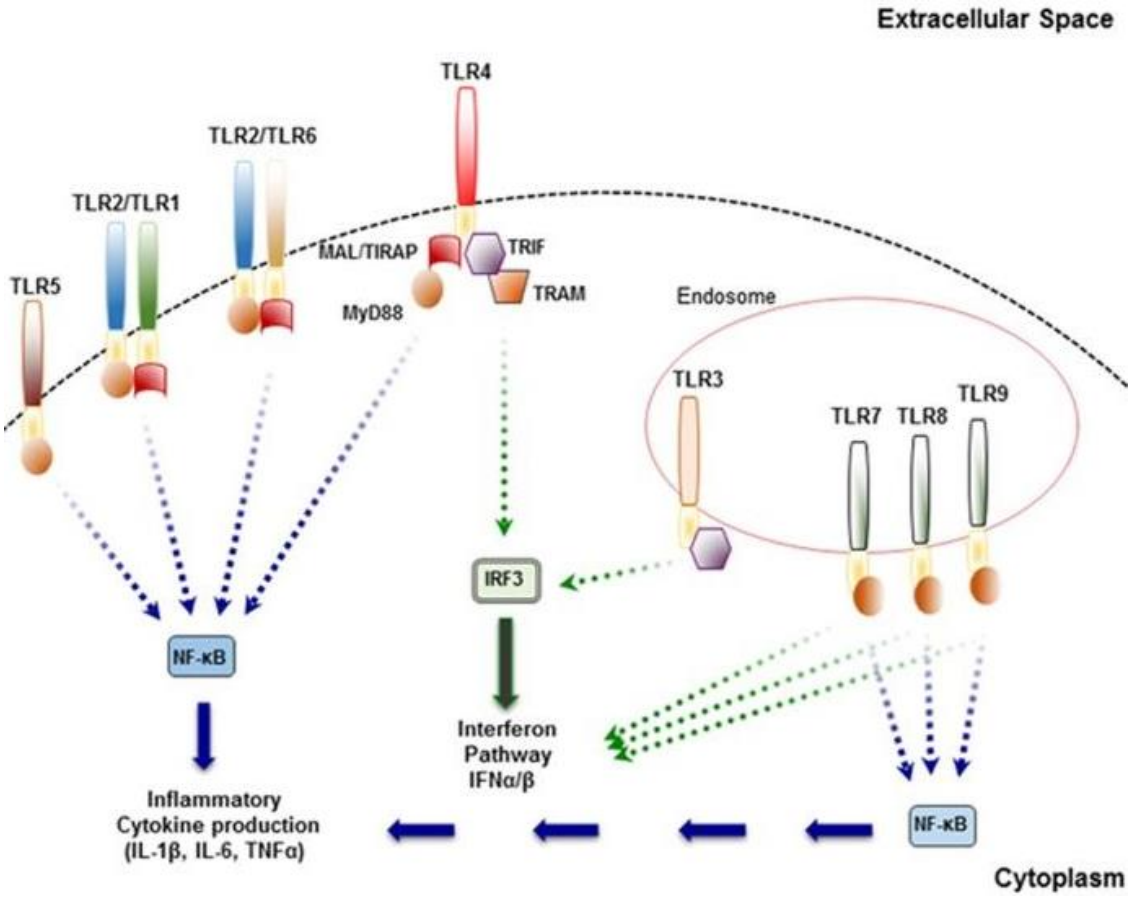

Figure 1.4. Signalling pathways of toll-like receptors (TLRs). After interaction with specific ligands, TLRs activate MyD88 or TRIF signalling pathway. Regardless of adaptor protein, activation leads to the activation of the NF-kB, p38, JNK, and/or IFN-regulatory factor (IRF) signalling. As a result, inflammatory cytokines are being produced (Dowling and Mansel, 2016).

Some events in TLR1, TLR2 and TLR4 signalling may be zinc-dependent. It was shown in numerous studies, that signalling cascade induced by recognition of bacterial components is influenced by zinc on many levels, including MAPKs activation, which is enhanced by the addition of zinc, or blocked when zinc is chelated. Additionally, the expression of pro-inflammatory cytokines like TNF-α, IL-1β and IL-6 by macrophages and primary monocytes, is limited by the chelation of intracellular zinc (Haase et al., 2008) and enhanced by the addition of physiological zinc concentrations (Yamasaki et al., 2007; Haase et al., 2008). A lack of zinc was also reported to selectively affect post-LPS phosphorylation of several kinases (inhibitor of nuclear factor kappa-IKK, mitogen-activated protein kinases-MAPKs and mitogen-activated protein kinase kinase-MKK) but not influence interleukin-1 receptor-associated kinase 1 (IRAK1; Dowling and

Mansel, 2016). To summarise, zinc is required to prevent dephosphorylation of several kinases, and for NF-kB activation, and thereby for transcription and release of a number of cytokines.

1.2.2.1. TLR4 signalling after activation with LPS and hydroxyapatite (HAP)

TLR4 was the first TLR identified in mammals and recognizes the active, lipid A component of lipopolysaccharide (LPS) from Gram-negative bacteria (Dowling and Mansel, 2016). The interaction starts with LPS-binding protein (LBP) in the serum binding LPS on the bacterial membranes and LPS aggregates in aqueous solutions. LBP facilitates extraction of LPS monomers by CD14 protein by changing the arrangement of LPS aggregates. LPS is transferred by albumin and then bound by N-terminal highly hydrophobic pocket of CD14. Subsequently, with the assistance of albumin, CD14 transfers LPS to MD-2 in the TLR4/MD-2 complex and later "M" shaped dimers of TLR4/MD-2 complexes are being formed. Then through the phosphate groups of lipid A, LPS interacts with positively charged amino acids of TLR4 (Plociennikowska et al., 2014).

LPS is not the only known ligand for TLR4. There are numerous endogenous activators including: CD138, endoplasmin, fibrinogen, fibronectin, heparan sulphate, HSP22, HSP60, HSP70, HSP72 (Yu et al., 2010), but also divalent metal cations nickel and cobalt have been shown to trigger activation of human TLR4. The interaction of those metals occurs with non-conserved histidine residues, and may mediate TLR4 dimerization even in the absence of MD2 (Daringer et al., 2015). It is not known whether other metal cations, including zinc can trigger TLR4 activation. In addition, hydroxyapatite (HAP), a calcium phosphate mineral, can induce inflammatory reaction via TLR4 signalling as shown in macrophages exposed to HAP particles (Grandjean-Laquerrière et al., 2007). Both LPS and HAP ligands induce the same sequence of TLR4 signals, starting with TLR binding TIRAP and MyD88, which results in phosphorylation of MAPKs and early activation of NF-kB (Fig. 1.5) (Haase et al., 2008). Additionally, after activation of MyD88, binding of TRAM and TRIF adaptors to TLR4 receptor causes delayed activation of NF-kB (Kagan et al., 2008). Late activation of NF-kB also triggers the activation IFN regulatory factor 3 (IRF3) (Fitzgerald et al., 2003), which then, together with TRIF induce IFN-β production (Monroe et al., 2010). IFN-β is crucial for induction of expression of surface molecules required for antigen presentation such as CD40, CD80, and CD86 (Hoebe et al., 2003).

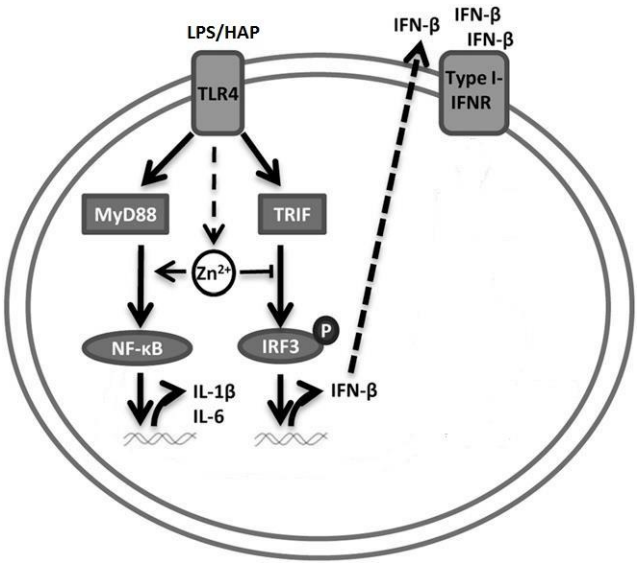

Figure 1.5. The role of zinc in TLR4 signalling. After binding LPS or HAP, TLR4 initiates a signalling cascade involving the adaptor proteins MyD88 or TRIF, which result in the production of proinflammatory cytokines (Brieger et al., 2013).

1.2.3. Antigen presentation

Antigen presentation is the capacity of some immune cells, called antigen presenting cells (APC), to capture antigens and then allow their recognition by T-cells. It is important because during their development in the thymus, only T-cells that show dual specificity (recognize self-carrier molecules, but only non-self-antigens) are picked during positive selection for further development. Therefore, antigens are processed and presented via major histocompatibility complex (MHC; also called called human leukocyte antigen, HLA) or cluster of differentiation 1 protein (CD1) molecules. There are two subgroups of MHCs: class I and class II which present peptides at the cell surface to $CD8^+$ and $CD4^+$ T-cells, respectively (Vyas et al., 2008). CD1 on the other hand are involved in the presentation of lipid antigens to T cells (Porcelli, et al., 1989). MHC I molecules are present on all nucleated cells (Kulski et al., 2003) and their function is to present endogenous proteins including pathogen peptides, degraded by cytosolic and nuclear proteasomes. Degraded peptides are transported via transporter associated with antigen presentation (TAP) into the endoplasmic reticulum (ER), where MHC class I molecules are waiting, stabilized by chaperones, including calreticulin, ERp57 and tapasin. After peptide binding, peptide–MHC class I complexes leave the ER and via Golgi migrate to the cell surface for antigen presentation to CD8+ T-cells via T-cell receptor (TCR; Fig. 1.6 A) (Huges et al., 1997).

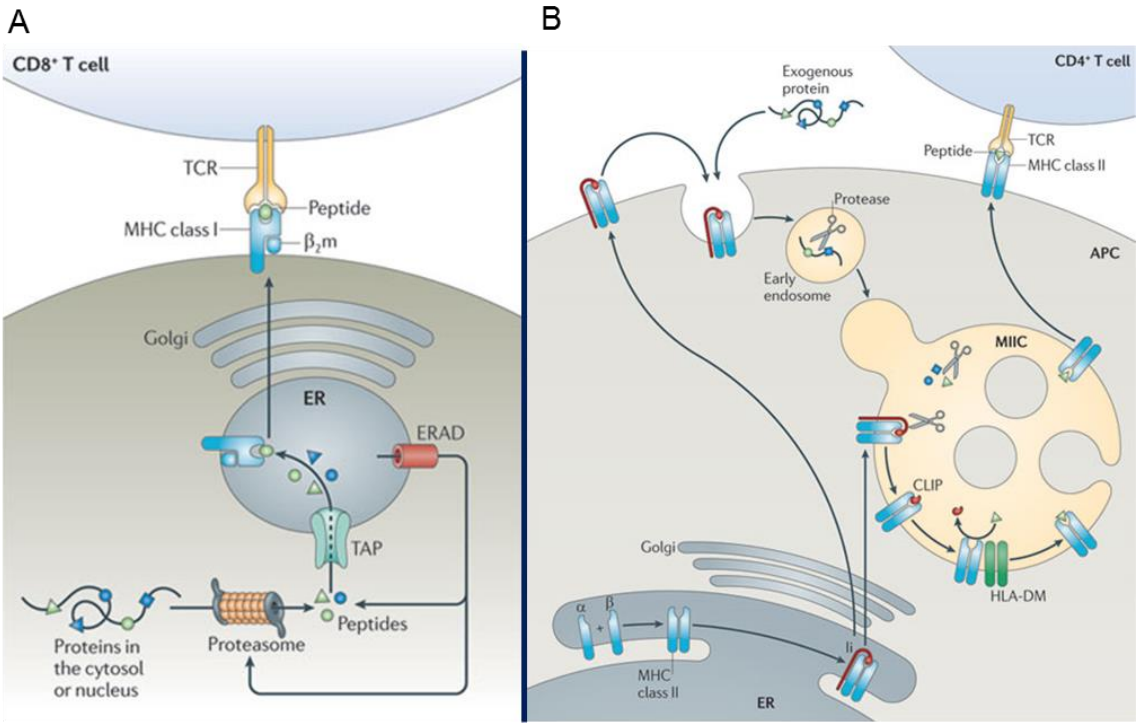

Figure 1.6. Antigen presentation by MHC class I (A) and MHC class II (B) presentation pathways. (A) For the presentation of intracellular antigenic peptides by MHC class I molecules peptides are first degraded by the proteasome. Then, translocated via transporter associated with antigen presentation (TAP) into the endoplasmic reticulum (ER) lumen where MHC class I molecules are being loaded. Released peptide–MHC class I complexes migrate to the cell surface where the antigen is being presented to $CD8^+$ T cells. (B) MHC class II molecule complexed with invariant chain (Ii) are transported to late endosomes, where Ii is being digested and only class II-associated Ii peptide (CLIP) fragment remains complexed with MHC class II. CLIP is then exchanged for antigenic peptide and MHC class II molecules are transported to the plasma membrane to present antigenic peptides to $CD4^+$ T cells. APC, antigen-presenting cell; β_2m, β_2-microglobulin; ERAD, ER-associated protein degradation; MHC class II compartment (MIIC); TCR, T cell receptor (Neffies et al., 2011).

Additionally, in the process known as cross-presentation, exogenous antigens are being presented by MHC class I to CD8+ T cells via one of the two main intracellular pathways: 'cytosolic' and 'vacuolar' pathways (Fig. 1.7). In the cytosolic pathways, antigens are degraded by the proteasome and then trimmed by amino-terminal peptidases prior to being loaded on MHC class I. Cut peptides are transported by transporter associated with antigen processing 1 (TAP1) and TAP2 into the ER. There MHC class I molecules are loaded with peptides the same

way as in the classical MHC class I-mediated antigen presentation pathway. Alternatively, after degradation by proteasomes, antigens can be transported back into phagosomes and loaded there. In vacuolar pathway of antigen cross-presentation, antigen is being degraded and loaded on MHC class I molecules in endocytic compartments. Vacuolar pathway is therefore independent of TAP and proteasome (Fig. 1.7; Joffre et al., 2012).

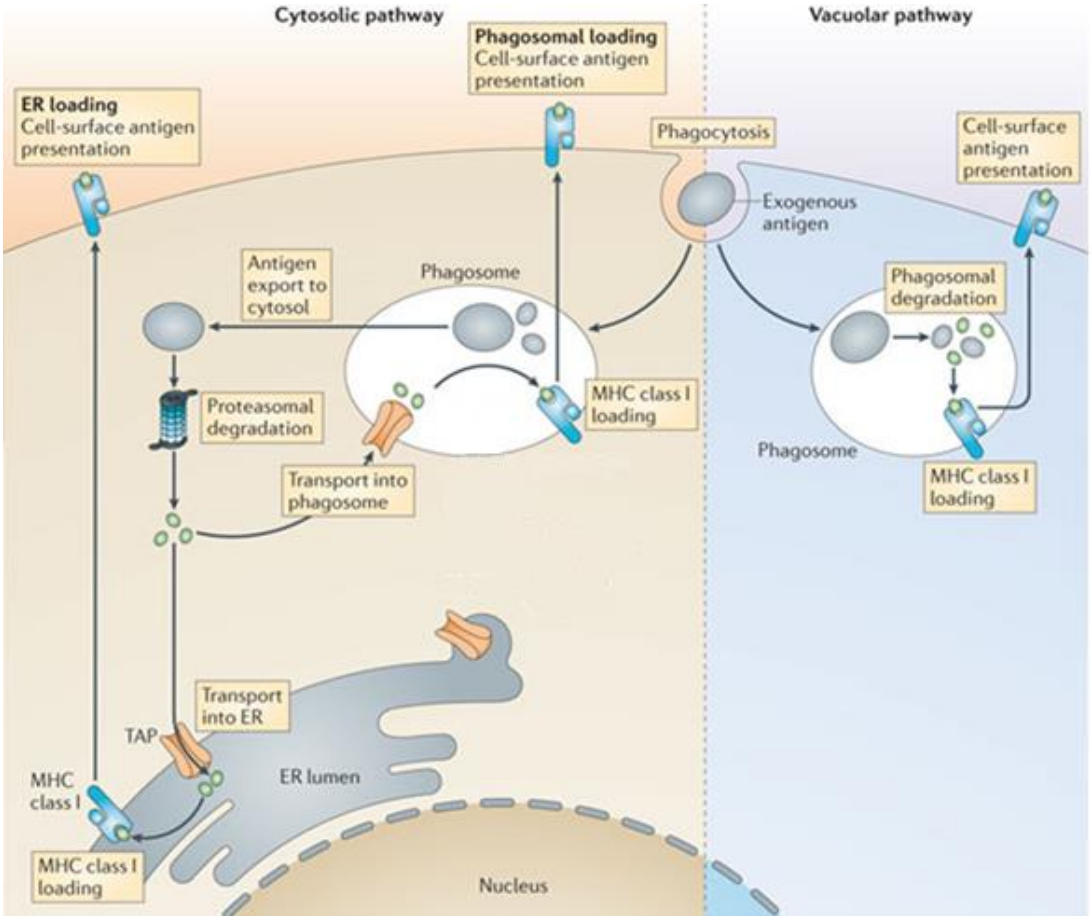

Figure 1.7. Intracellular pathways for cross-presentation in dendritic cells. After phagocytosis, exogenous antigens can be processed in two ways, either by cytosolic pathway, which involves degradation in the proteasome and on MHC class I in endoplasmic reticulum (ER) or vacuolar pathway where antigens are degraded into peptides in the phagosome, where they are then loaded on MHC class I molecules (Joffre et al., 2012).

MHC II molecules are present only on the surface of APCs (macrophages, certain B-cells and dendritic cells). Each MHC II protein complex is composed of two proteins, α and β. Those two membrane spanning proteins, together with Ii chain, form trimeric αβIi complexes (Roche et al.,

1991). MHC II αβIi complexes are transported to early endosomes, which then together develop into the late endosomes (Fig. 1.6 B). In late endosomes, Ii is degraded, leaving a residual class II-associated Ii peptide (CLIP) in the peptide-binding groove of the MHC class II heterodimer. CLIP fragment is then exchanged for an antigenic peptide degraded in the endosomal pathway. This exchange is facilitated by HLA-DM molecule. Loaded MHC class II then migrate to the cell surface to present antigens to CD4+ T-cells (Neefjes et al., 2011).

Antigens are loaded mostly in late endosomes, but some MHC II-protein complexes can be formed in early endosomes or lysosomes, or even at the plasma membrane (Griffin et al., 1997; Pinet and Long, 1998). Expression of MHC II changes during DC maturation. In immature cells, complexes are formed and stored for a very short time on their surface, and then endocytosed and degraded. As maturation progresses, both the generation of new complexes and their turnover on the cell surface gradually increases. In fully mature DCs cell surface expression of MHC II is more than 10 times higher than in immature DCs (van Niel et al., 2008).

Bacterial lippopolisacharide (LPS) and other TLR ligand are crucial in the presentation of previously internalised antigens. It was shown by Turley et al., (2000) that complex formation between previously internalized antigens and MHC class II molecules and also trafficking of those complexes to the cell surface was effective only following treatment of DCs with LPS. LPS also stimulated antigen cross-presentation via MHC class I (Delamarre et al., 2003). Proinflammatory TLR signaling in macrophages or DCs also stimulates phagosome maturation, antigen processing and favours presentation phagosomal cargo being TLR ligand via MHC class II (Mantegazza et al., 2013).

1.3. Zinc in immune system

Zinc is one of the most abundant metallic chemical elements on earth, and it is known for its exceptional biological importance (Hambidge and Krebs, 2007). Zinc is referred to as a trace element because of its low concentration in plasma; nonetheless, it is one of the essential trace elements in the human body. Most of the total 3 g of zinc in the body is bound to proteins (Scott and Bradwell, 1983; Rink and Gabriel, 2000). The importance of zinc in humans was only recognised in the 1960s. Now deficiency of zinc is considered one of the main reasons of malnutrition and is estimated to affect over 25% of the world's population, and considered the eleventh most important health risk factor in the world (Maret and Sandstead, 2006). Copenhagen Consensus 2008 stated that zinc deficiency (along with vitamin A deficiency) is the

number one global health issue that can be addressed in a cost effective manner, to reduce child morbidity and mortality (Copenhagen Consensus 2008 Challenge Paper, Hunger and Malnutrition; *www.copenhagenconsensus.com*).

In mammals, zinc is absorbed from the diet by enterocytes that line the gut through the action of the Zip4 transporter protein; it is then released into the portal circulation by the ZnT1 transporter protein for systemic distribution (Cousins, 2010). The physiological plasma zinc concentration is in the range of 15-20 µM (Gorgani et al., 1999b), with zinc mostly (75%) bound to serum albumin. This accounts for as much as 98% of exchangeable/deliverable zinc. The rest is bound to other plasma proteins such as alpha-2 macroglobulin (Lu et al., 2012) and histidine rich glycoprotein (HRG). Of great importance is the fact that the affinity of zinc for those proteins drops in low pH. Conditions of local acidosis (e.g. ischemia or hypoxia) generally can be caused by problems with blood vessels, with resultant damage to or dysfunction of tissue (Borza and Morgan, 1998, Jones et al., 2005b). The concentration of unbound Zn^{2+} ions in plasma is in the range of 0.5-1 µM (Vallee and Falchuk, 1993, Tubek et al., 2008) and in the cells in extremely low nanomolar and even picomolar concentrations (Maret, 2015). In some pathological states, the zinc level can be highly elevated (intracellular zinc level of up to 60 µM in age-related macular degeneration (AMD)) (Perkins et al., 2010). Localised zinc concentrations can be also increased, such as at the cell surface following its release from activated platelets (Leung et al., 1983). Zinc concentration in platelets is 30-60 times higher than in plasma. It is accumulated in cell cytoplasm and in α-granules (Marx et al., 1993). Other cells able to release zinc are erythrocytes, lymphocytes and neutrophils (Whitehouse et al., 1982). In addition, as a result of lipopolysaccharide (LPS) administration, nitric oxide can cause release of zinc from thiol groups of zinc fingers, which increases free zinc levels (Andonova et al., 2001, Kolb and Kolb-Bachofen, 1998).

Zinc is required for the activities of over 300 enzymes, including deoxythymidine kinase, which is essential for DNA synthesis and cell division, and is important for the structural integrity of nearly 2000 transcription factors (Prasad, 2012). It also plays a huge role in cell integrity and cellular metabolism, protein synthesis (Maret, 2009) and wound healing (Heyneman, 1996). There is a group of calcium-dependent zinc-containing endopeptidases called matrix metalloproteinases (MMPs). MMPs are members of the metzincin group of proteases which share the conserved zinc-binding motif in their catalytic active site. They mainly act as regulators of extracellular tissue signalling networks and also degrade the various components of the

extracellular matrix (ECM) (LÖffek et al., 2011). MMPs contribute to the homeostasis of many tissues and participate in several physiological processes, including bone remodelling, angiogenesis, cell migration and proliferation. Dysregulated MMPs activity leads to pathological conditions such as arthritis, inflammation and cancer (LÖffek et al., 2011). It was also shown that several MMPs are directly involved in the immune response and innate immunity. Those include MMP-7 in the lung which by cytokine release recruit neutrophils (Chen et al., 2009) and recruitment of immune cells by macrophage derived MMP-2 and MMP-9 in a monocyte-driven model of autoimmune kidney inflammation (Triantafyllopoulou et al., 2010).

Because of this, zinc deficiency has many dangerous effects, particularly immunological disorders (Ibs and Rink, 2003). The effect of zinc deficiency on the immune system is complex and influences both innate and adaptive immunity, contributing to several chronic inflammatory diseases including acrodermatitis enteropathica, rheumatoid arthritis (RA), chronic asthma, systemic lupus erythematosus and Alzheimer disease (Bonaventura et al., 2015).

1.3.1. Zinc in innate immunity

The exact mechanisms by which zinc influences the innate immune system are not yet fully understood. It is known that zinc supplementation increases chemotaxis of granulocytes (Hujanen, 1995) and that a lack of zinc increases phagocytosis and cytotoxicity of monocytes (Mayer et al., 2014). Additionally, both zinc deficiency and surplus have a role in the neutralization of pathogens, through the regulation of superoxide anion production whose role is the destruction of pathogens after phagocytosis (Hasegawa et al., 2000). Another role of zinc is to promote adhesion of monocytes to endothelial cells (Chavakis et al., 1999). Also the importance of zinc for the production of cytokines such as interleukins IL-1β, IL-6 and TNF-α (Fig. 1.8) was observed for many cell types, including monocytes where zinc deficiency inhibited the production of IL-6 and TNF-α (Mayer et al., 2014). Zinc deficiency also causes reduction of NK cell activity (Allen et al., 1983), decreased cell production, reduction in cell mediated immunity and phagocytosis, lymphocyte proliferation, and affects the maturation of dendritic cells (Kitamura et al., 2006). According to Kitamura et al (2006), LPS induced maturation of DCs triggers decrease in intracellular free zinc, which is crucial for the increased expression of MHC-II and co-stimulatory molecules on the DCs surface. These results imply zinc is a crucial element in antigen presentation and therefore activation of the adaptive immune response.

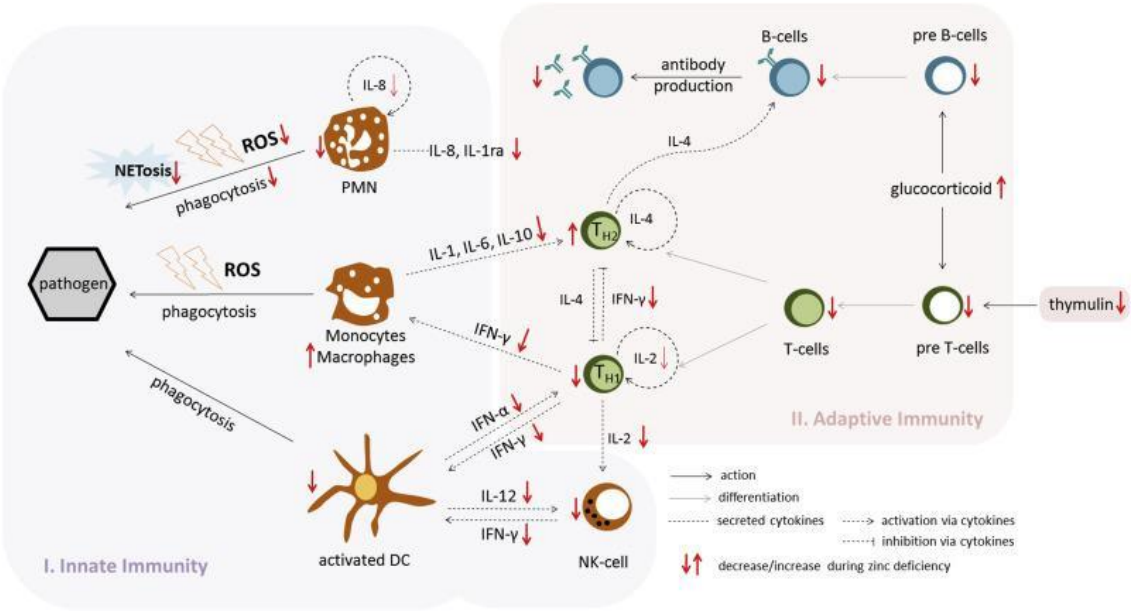

Figure 1.8. The effect of zinc deficiency on the innate and adaptive immune cells and their interactions. The number of most of immune cells decreases as a result of zinc deficiency, however immune defence against pathogens is maintained. Mainly cytokines production is affected (Maares and Haase, 2016).

1.3.2. Zinc in adaptive immunity

Changes in zinc homeostasis have been shown to affect adaptive immunity in multiple ways. For example, zinc influences lymphocyte formation and the production of cytokines, which in fact leads to changes in activity and function (Maares and Haase, 2016). Also T-cells are very sensitive to zinc; zinc deficiency is known to cause thymus atrophy, reduction in Th1 cell numbers (T-cell lymphopenia) and decreased activity of thymulin, a zinc dependent hormone produced by thymic epithelial cells (Dardenne et al., 1982, Mitchell et al., 2006). The role of thymulin is to induce the differentiation of T-cells and enhances several functions of the various T-cell subsets (Bach and Dardenne, 1989). In addition, studies on mice showed that a lack of zinc during T-cell maturation leads to significant apoptosis of T-cell precursors (King et al., 2005). Another role of zinc is to maintain the balance between the Th1 and Th2 subsets as its deficiency significantly affects the production of Th1 cytokines and (although less significantly) the Th2 response (Prasad, 2000). Other effects of zinc deficiency on T-cells includes inhibition of the development of pro-inflammatory Th17 cells (Kitabayashi et al., 2010) and increases the number of cytotoxic and memory T-cells (Prasad, 2000), which could lead to autoimmune reactions.

B-cells are in general less affected by zinc than T-cells. Yet, zinc has an influence on their development as its deficiency causes a reduction of immature and pre-mature B-cells. Additionally, antibody production by those cells is affected by zinc deficiency (Stefanidou et al., 2006).

1.3.3. Zinc and inflammation

Zinc is indirectly associated with inflammation. Zinc deficiency triggers increased cytokine production, including IL-1-β release (Summersgill, 2014), which is involved in the pathogenesis of rheumatoid arthritis. That suggests that a lack of zinc contributes to the disease and zinc supplementation could be used as a treatment (Dore-Duffy, 1990). Other cytokines whose levels are elevated when zinc is reduced are IL-6, IL-8 and TNF-α (Mariani et al., 2006). Furthermore, zinc deficiency potentiates proliferative response of T and B lymphocytes as a result of IL-6 and IL-2 signalling but in contrary lessens IL-4 signalling, leading to an impairment of the immune system (Gruber et al., 2013).

1.4. Zinc homeostasis

Surprisingly, despite its many functions, our body has only a limited ability to store zinc and such stores are inadequate for long periods of zinc deficiency (Liuzzi et al., 2005). For this reason, zinc homeostasis is strictly controlled. Transport through the plasma/cellular membrane occurs via ZIP and ZnT transporters: ZIP (encoded by the Slc39 genes) transports Zn to the cell cytosol and ZnT (encoded by the Slc30 genes) transports Zn from the cell cytosol (Cousins et al., 2006), (Palmiter and Huang, 2004; Eide, 2004). Another mechanism involves the storage and release from “zincosomes” controlled by the same zinc transporters (Wellenreuther et al., 2009). The last mechanism is binding zinc by metalothioneins (MTs) (Maret, 2009).

Metallothioneins, small cysteine rich proteins, have a great zinc binding capacity and chelate zinc in the cytoplasm. Each of this protein can bind up to seven Zn^{2+} ions, depending on the oxidation of metallothioneins thiol residues (Krezel and Maret, 2007; Maret 2006). They can also act as an exchangeable zinc pool, releasing zinc when needed (Blewett and Taylor, 2012). MTs react with zinc in two ways; they are either buffering or muffling of zinc. Under normal physiological conditions their function is to buffer zinc with different affinities at the nano- to picomolar range (Krezel and Maret, 2007). However, in case of elevated cytosolic zinc, the role of zinc-binding proteins is to move it out of the cell or store it within subcellular compartments.

The difference between those two processes is that muffing is much slower than buffering (Gunzel et al., 2007). MTs can also bind heavy metals, with the capacity very often higher than for zinc. For example, Cd^{2+}MT complexes are 100 to 1000-fold more stable than Zn^{2+}–MT complexes (Carpene et al., 2007; Bell and Vallee, 2009).

Another mechanism of zinc homeostasis is the reversible storage of zinc in "zincosomes". These intracellular vesicles can store milimolar amounts of zinc, and then release it back to the cytoplasm when needed (Haase and Maret, 2005). For a long time, zinc stored in those vesicles was considered as free or just loosely bound. In fact, it is not free but present as complexes, mainly bound to light, redox-inactive ligands (sulphur, histidine and oxygen; Wellenreuther et al., 2009).

1.5. Zinc transporters as the main mechanism of zinc homeostasis

Zinc enters the body as a divalent, hydrophilic cation with a single oxidative state, which means it cannot be oxidized or reduced. Zn^{2+} ions cannot cross the membrane by passive diffusion and thus specialized transporters are required to facilitate transport of zinc in and out of the cytosol. Zip (Zrt-Irt-Protein) and ZnT (Zn-transporter) transporters are important components of a network that builds zinc homeostasis. Mammalian zinc transporters are grouped based on their predicted membrane topology, into two major families, encoded by solute-linked-carrier (SLC) genes, the SLC30 (ZnT) and SLC39 (Zip) families. There are 10 isoforms of ZnTs and 14 of Zips encoded in the human genome (Kambe, 2013). Zip proteins are grouped into four subfamilies, I, II, Gufa and LIV-1. Most of them (9 in total) belong to the LIV-1 subfamily (Zip 4, 5, 6, 7, 8, 10, 12, 13, 14; Jeong and Eide, 2013).

X-ray crystal structures of zinc transporters are not yet available, thus both structure and mechanisms of transport are yet to be discovered. It is however postulated that ZIP proteins transport zinc independently of ATP, by symporters, or secondary active transport (Hojyo and Fukada, 2016). Additionally, Zip2-mediated zinc transport was shown to be very likely a co-transport with HCO^{3-} (Gaither and Eide, 2000). In contrast, ZnT transport seems to require ATP as it was shown by Ohana et al (2009) that the proton gradient generated by V-type ATPases powers zinc transport into the Golgi apparatus. Nonetheless, the exact molecular mechanisms remain unclear.

Most ZIP members have eight predicted transmembrane (TM) domains with their N- and C-termini facing the extracytoplasmic space and a histidine-rich region between TM3 and TM4.

This histidine rich loop was postulated to be a zinc binding site but its specific function is still not known. The greatest homology amongst Zip transporters exists within a signature 12 amino acids sequence (HSVFEGLAVGLQ), localised to TM4 (Eng et al., 1998). Transporters from LIV-1 subfamily are different from other Zips by having a highly conserved putative metalloprotease motif (HEXPHEXGD) in TM5. Additional histidine residues on the N-terminal ectodomain and extracellular loop between TM2 and 3 are also found in LIV-1 subfamily members (Taylor et al., 2004). These histidine residues located on N-terminal domain are thought to bind zinc, making more zinc accessible for transport. Additionally, there are three glycosylation sites located near to the N-terminus (Taylor et al., 2005; Wang et al., 2004).

ZnT family members have six conserved TMs with both N- and C-termini facing the cytoplasm. In contrast to ZIP proteins, the C-terminal tails of ZnTs are long and consist of 82 to 203 amino acids (longest in ZnT6). Between TM2 and TM3 is a conserved serine flanked by two histidines. Zinc transporter activity depends on the histidine-rich zinc binding region located between TMs IV and V. ZnTs can form hetero- (SLC30A5/SLC30A6) or homodimers (SLC30A7), which is especially important for ZnT6 as it cannot transport zinc itself but only modulate the activity of other transporters (Ohana et al., 2009; Suzuki et al., 2005).

1.5.1. Subcellular localisation

Both families of zinc transporters (except ZnT10) have been well characterised in many cell types. In humans, Zip1 and ZnT1 are ubiquitously expressed, whereas other Zips and ZnTs show more tissue/cell-specific expression.

The majority of the Zip transporters can be found at the plasma membrane. Zip1 is mostly present on the plasma membrane, when cells are cultured in a media with low zinc concentration, it serves as the main zinc importer. However, when sufficient amounts of zinc is present, Zip1 can translocate to intracellular organelles (Milon et al., 2001). Zips 2-6 and Zip8, Zip10 and Zip14 are also located on at the plasma membrane (Table 1.1; Jeong and Eide, 2013). Zip4 is responsible for zinc uptake in the small intestines, where it is located on enterocytes at the plasma membrane (Cousins, 2010). Zip3 and Zip8 are additionally located on lysosomes. Zip7, Zip9 and Zip13 are present on intracellular organelles and therefore can only transport zinc from the cytoplasm into intracellular stores (Table 1.1).

Zip	cell membrane	intracellular organelles (ER, Golgi)	membrane of secretory vesicles	exosomes	cytoplasmic vesicles	cytoplasm	enterocytes	mitochondria
1	x			rat	x			
2	X							
3	X		X					
4	X		X				X	
5	X			human			X	
6	X							
7		x			x			
8	X		X					X
9		X						
10	X							
11								
12								
13		x			x			
14	x			human				

Table 1.1. Known subcellular localizations of ZIP zinc transporters (Jeong and Eide, 2013).

ZnT1 is localized on the plasma membrane as it is the main exporter of zinc from the cell cytosol to the extracellular space. Other exporters found on plasma membrane but also on organelles are ZnT2, ZnT4 and ZnT5. ZnT3, ZnT6, ZnT7, ZnT8 and Znt9 are located on intracellular membranes and transport zinc to stores or organelles (Table 1.2). The subcellular localization of ZnT10 is not known (Schweigel-Röntgen, 2014).

ZnT	cell membrane	intracellular organelles	membrane of secretory vesicles	exosomes	cytoplasmic vesicles	cytoplasm
1	X			rat		
2	X	X	X			
3		X	X			
4	X	X	X	mouse		
5	X	X			X	
6		X			X	
7		X			X	
8		X	X			
9						X
10				rat		

Table 1.2. Known subcellular localizations of ZnT zinc transporters (Huang and Teppamorndech, 2013).

1.5.2. The role of zinc transporters in the immune system

As described above, zinc deficiency is known to cause defects in the immune system. These effects are manifested through deficits in macrophage and neutrophil chemotaxis and phagocytosis, reduced secretion of pro-inflammatory cytokines by macrophages and reduced NK activity. The acute phase response to stress, trauma, and infection includes a transient and rapid decline in the plasma zinc concentration. Such observations also suggest that zinc affects the immune system in a dose dependent manner, with low concentrations of zinc being pro-inflammatory and high, anti-inflammatory (Foster and Samman, 2012).

Many Zip and ZnT transporters are expressed in immune cells and there are a few links found between their functioning and effective immune responses (Overbeck et al., 2008). The expression of most zinc transporters are influenced by LPS treatment. For example, it was shown that stimulation of macrophages with LPS and TNF-α caused uptake of zinc from extracellular space by upregulation of Zip8. This in fact weakened the pro-inflammatory response as zinc bound NF-κB and inhibited IκB kinase β (Liu et al., 2013). In addition, expression of ZIP14 in macrophages is upregulated as a result of LPS (or LPS plus IFN-γ) stimulation. Similar to ZIP8, this inhibited the pro-inflammatory response by impairing IL-6 and TNF-α release (Sayadi et al., 2013). A study on human T-cells, showed that immune activation causes upregulation of several zinc transporters, with the highest effect seen for Zip8. Additionally, ZIP8 regulates efflux of zinc from the lysosomes and consequently controls IFN-γ expression (Aydemir et al., 2009). Also, ZnT5 is required for the mast cell activation in mast cell-mediated allergic reactions (Nishida et al., 2009).

Despite zinc transporters being deeply involved in the immune functioning, their presence in dendritic cells (DCs) is still not fully characterised. Current studies have shown that LPS stimulation caused downregulation of ZIP6 and ZIP10 transporters in DCs, but increased expression of ZnT1, ZnT4 and ZnT6. The effect was associated with a decrease in intracellular zinc concentration, which was suggested to be necessary for LPS-induced DC maturation (Kitamura et al., 2006). Defective or dysregulated zinc transporters are involved in the development and/or progression of many diseases; therefore, it is crucial to understand their expression pattern in cells essential for the proper immune response.

1.6. Histidine-rich glycoprotein (HRG)

Histidine-rich glycoprotein (HRG) is a 75 kDa glycoprotein, present at relatively high concentrations in human plasma (*ca.* 100-150 μg/ml). Human HRG plasma levels increase with age (Drasin and Sahud, 1996). The protein is synthesised by the parenchymal cells of the liver (Koide et al., 1986; Hulett and Parish, 2000).

HRG has a multidomain structure, composed of 507 amino acids, with six predicted N-linked glycosylation sites (Poon et al., 2010a). It consists of two cystatin like N-terminal domains (N1 and N2), a central histidine rich region (HRR) flanked by two proline rich regions (bigger PRRI and smaller PRR2) and a C-terminal domain (C; Fig. 1.9; Jones et al., 2005a). The HRR region bears an extraordinary repeating amino acid sequence (GHHPH) between residues 330 and 389 and is implicated in metal binding (Morgan, 1981; Koide et al., 1986). The domains are held together by six disulfide bonds (Sorensen et al., 1993), however only five disulfide bonds might be essential for the native conformation of the protein (Ronca and Raggi, 2015), as the Cys185-Cys399 bond is amenable to redox activity (Kassaar et al., 2014).

HRG has a high binding capacity for Zn^{2+} and other divalent cations. The binding occurs via histidine residues, with a stoichiometry for Zn^{2+} of approximately 1:1-1:10 (Morgan, 1978). Nonetheless, when other plasma proteins that compete for zinc are present, HRG chelates only 1% of the metal (Fu and Horn, 2002). The binding of other divalent metal cations was examined for rabbit HRG and showed that Hg^{2+}, Cu^{2+}, Zn^{2+}, Ni^{2+}, Cd^{2+}, and Co^{2+} bind in descending order of binding affinity (Mangani et al., 2003). The affinity of HRG for zinc is pH dependent. HRG with isoelectric point of 7.09 (calculated by ExPasy based on protein sequence), at pH 7.4 is negatively charged and can bind Zn^{2+} to neutral histidine residues. Whereas at low pH, positively charged protein binds Zn^{2+} by protonation of histidines and possibly causes a conformational change of HRG (Borza et al., 1996). Also binding of HRG to its ligands, heparin and heparan sulfate was shown to be pH dependent (Fu and Horn, 2002; Borza and Morgan, 1998).

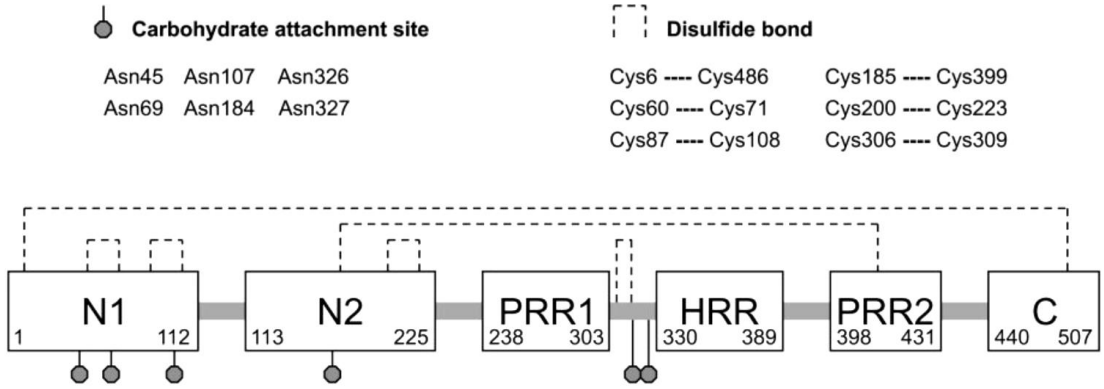

Figure 1.9. Schematic representation of protein domains, post-translational modifications of human HRG (Poon et al., 2010a).

HRG is not found only in humans but also in many other vertebrates (Jones et al., 2005b). Rabbit plasma HRG is very similar to human protein, with two homologous N-terminal domains, histidine rich region flanked by two proline-rich regions and a C-terminal domain. The sequence alignment of human HRG (GenBank under the accession number AAI50592.1) and rabbit HRG (XP_008264798.1), show that the two proteins share 292 identical amino acids (60% identity), 385 semi-conserved and conserved amino acids (68% positives) and 53 gapped amino acids (9% gap) over 545 residues, as calculated by the NCBI BLAST software. The highest similarity homology occurs at the N1 and N2 terminal domains, with the proteins sharing 84% overall identity (Fig. 1.10; Ronca and Raggi, 2015).

A

```
rbHPRG          LTPTDCKTTKPLAEKALDLINKWRRDGYLFQLLRVADAHLDGAESATVYYLVLDVKETDC  60
huHPRG          VSPTDCSAVEPEAEKALDLINKRRRDGYLFQLLRIADAHLDRVENTTVYYLVLDVQESDC  60
                ::****.:.:* **********.***********:****** .*.:*********:*:**

rbHPRG          SVLSRKHWEDCDPDLTKRPSLDVIGQCKVIATRYSDEYQTLRLNDFNCTTSSVSSALANT  120
huHPRG          SVLSRKYWNDCEPPDSRRPSEIVIGQCKVIATRHSHESQDLRVIDFNCTTSSVSSALANT  120
                ******:*:**:*  :.***  **********:* * * **: ****************

rbHPRG          KDSPVLFDFIEDTEPFRKSADKALEVYKSESEAYASFRVDRVERVTRVKGGERTNYYVDF  180
huHPRG          KDSPVLIDFFEDTERYRKQANKALEKYKEENDDFASFRVDRIERVARVRGGEGTGYFVDF  180
                ******:**:**** :**.*:**** **.*.: :*******:***:**.*** *.*:***

rbHPRG          SVRNCSRSHFHRHP-AFGFCRADLSFDVEASNLENPEDVIISCEVFNFEEHGNISGFRPH  239
huHPRG          SVRNCPRHHFPRHPNVFGFCRADLFYDVEALDLESPKNLVINCEVFDPQEHENINGVPPH  240
                *****.* ** *** .******** :**** :**.*::::*.****: :** **.*. **

rbHPRG          LG--------------KTPLGTDGSRDHHHPHKPHKFGCPPPQEGEDFSEGPPSQGGTPP  285
huHPRG          LGHPFHWGGHERSSTTKPPFKPHGSRDHHHPHKPHEHGPPPPPDERDHSHGPPLPQGPPP  300
                **              *.*: . ************:.* *** :  *.* ***   *.**

rbHPRG          LSPPSGPRCRHRPFGTNETHRFPHHRNFSEHHPHGPPPHGHHPHGPPPHGHHPHGPPPHG  345
huHPRG          LLPMSCSSCQHATFGTNGAQRHSHNNNSSDLHPHKHHSHEQHPHGHHPHAHH--------  355
                * * * . *.* .**** ::*..*:.* *: ***   .* :****  **.**

rbHPRG          HPPHGPPPHGHPPHGPPPHGHPPHGPPPHGHPPHGPPPHGHPPHGPPPHGHPPHGPPPHG  405
huHPRG          --------------------------PHEHDTHRQHPHGHHPHGHHPHGHHPHGHHPHG  385
                                         ** * .*   **** ***  **** ***  ***

rbHPRG          HPPHGHGFHDHGPCDPPSHKEGPQDLHQHGHGPPPKHPGKRGPGKGHFPFHWRRIGSVYQ  465
huHPRG          HHPHCHDFQDYGPCDPPPHNQGH---CCHGHGPPPGHLRRRGPGKGPRPFHCRQIGSVYR  442
                * ** *.*:*:******.*::*      ******* *  .******  *** *.*****.

rbHPRG          LPPLQKGEVLPLPEANFPSFSLRNHTHPLKPEIQPFPQVASERCPEEFNGEFAQLSKFFP  525
huHPRG          LPPLRKGEVLPLPEANFPSFPLPHHKHPLKPDNQPFPQSVSESCPGKFKSGFPQVSMFFT  502
                ****.***************.* :*.*****: ***** .** ** :*:. *.*:* **.

rbHPRG          STFPK  530
huHPRG          HTFPK  507
                 ****
```

B

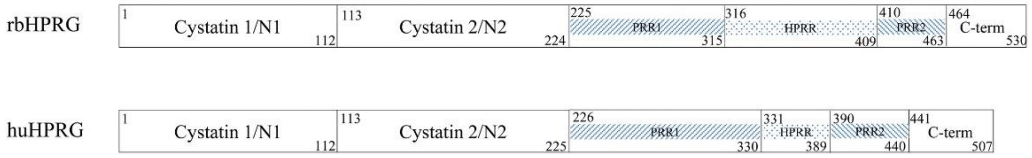

Figure 1.10. (A) Alignment of human HRG (GenBank under the accession number AAI50592.1) and rabbit HRG (XP_008264798.1). (B) Domain structure of human and rabbit HRG proteins (Ronca and Raggi, 2015).

Through its ability to interact with numerous ligands, HRG serves as a regulator of numerous physiological processes including angiogenesis by both stimulatory (Simantov et al., 2001; Klenotic et al., 2010) and inhibitory (Dixelius et al., 2006) mechanisms. It has been also shown

that HRG acts in the coagulation system (Tsuchida-Straeten et al., 2005) by interaction with many molecules including: heme, plasminogen (Lijnen et al., 1980), heparanase (Poon et al., 2010b), fibrinogen (Leung et al., 1983) and heparin (Kassaar et al, 2015). HRG also plays an important role in the immune system. It is involved in immune complex clearance by binding to various components of the immune system including the complement proteins within both the classical and alternative pathways, antibodies, F_{ab} region on immunoglobulin G and membrane attack complex components. HRG also modulates formation and function of immune complexes. Despite of its huge importance, immune complexes can become toxic by building deposits in small blood vessels and lead to pathologies such as rheumatoid arthritis, vasculitis or glomerulonephritis. To streamline transport of the immune complex to the liver and spleen, where the phagocytosis occurs, complement proteins need to be involved. HRG modulates complement (by augmentation or inhibition) through interactions with C8, C9, factor D and S-protein. It also binds strongly to C1q, FH, C4b-binding protein, C3, C4 and IgG (Manderson et al., 2009, Chang et al., 1992). As the whole process of pathogen recognition, complex formation and clearance is very complicated, a vast array of proteins is needed to control, including HRG. The most abundant serum immunoglobulin that forms complexes is IgG. It is already known that HRG bind to all IgG subclasses and also to IgM, but the affinity is dependent on L-chain isotype. The average Kd value for this interaction is 85 nM but higher for those with Lλ chain than Lκ and is decreased in the presence of zinc (Gorgani et al., 1997a, Gorgani et al., 1999b). Interestingly, HRG in physiological concentrations can inhibit insoluble IgG immune complexes formation but also promote the phagocytosis of soluble complexes by macrophages (Gorgani et al., 1999a).

It is of great importance to eliminate necrotic cells (Jones et al., 2005b, Jones et al., 2005c) and apoptotic cells (Gorgani et al., 2002) from the immune system. HRG regulates activation of complement on necrotic cells, via interactions with C1q. This interaction occurs in the late stage of cell death when the cell membrane becomes permeable (Manderson et al., 2009). Zinc is thought to inhibit the interaction of HRG with C1q (Gorgani et al., 1997b). However, the effect of zinc on other complements remains to be determined. HRG also regulates other immune processes including antitumor (Huang et al., 2011), antibacterial (Rydengard et al., 2006, Rydengard et al., 2007, Kacprzyk et al., 2007) and antifungal (Rydengard et al., 2008) activities. As mentioned above it also modulates complement proteins by augmentation or inhibition (Easterbrooksmith et al., 1988, Gorgani et al., 1997a, Chang et al., 1992) and controls phagocytosis (Poon et al., 2010a).

Activated platelets can release zinc into plasma. Incidentally, activated platelets simultaneously can also release HRG in localised areas (Leung et al., 1983). Zinc concentrations in the cytoplasm and alpha-granules of human platelets is 30–60-fold higher than in plasma (Morgan, 1981). It has been proposed by Kluszynski et al. that platelets release Zn^{2+} ions from α-granules (Kluszynski et al., 1997; Gorodetsky et al., 1993), which serves as a cofactor for the binding HRG molecules to heparin (for heparin neutralization; Kassaar et al, 2015) and also to tropomyosin on endothelial cells (to exert an antangiogenic effect; Jones et al., 2005b). It is important that zinc is released locally because it provides better control for fibrinogenesis and angiogenesis.

It has been postulated by Lu et al. (2012), that HRG activation by zinc may occur pathophysiologically through fatty acid-mediated inhibition of zinc binding by albumin. Albumin is the most abundant plasma protein (600 μM) and contains 588 amino acids in three domains. It has many functions, but its main functions are the transport and delivery of molecules such as fatty acids, metal ions and drugs. Fatty acid transport is achieved through five major and up to five additional low-affinity binding sites (Leung et al., 1983). There is also evidence that zinc dependent activation of HRG may be important for development of thrombotic disorders. As thrombotic disorders often co-exist with disorders connected with high levels of plasma fatty acids (diabetes, obesity), there is a potential relation between fatty acids binding to albumin, the subsequent release of zinc and the increased complexation of zinc with HRG (Fig. 1.11; Stewart et al., 2009).

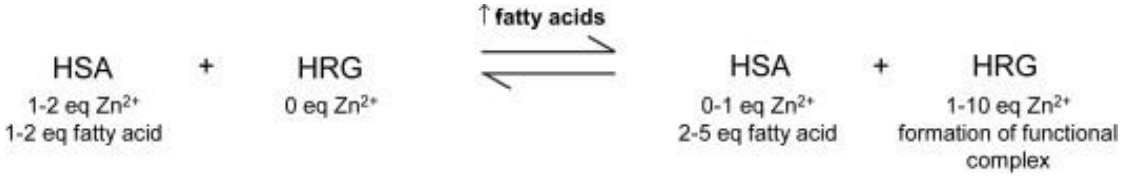

Figure 1.11. With high levels of HRG associated with thrombotic disorders, there must be a relation between fatty acids binding to albumin, subsequent release of zinc and the increase of zinc-HRG complex formation. Increasing fatty acid level shifts the equilibrium towards the right (Stewart et al., 2009).

1.7. Age-related macular degeneration (AMD)

Age-related macular degeneration (AMD) is the leading cause of irreversible central vision loss in elderly people. It affects nearly 8.7 % of the population over the age of 55, which is estimated to 196 million people by the year 2020 (Wong et al., 2014). It is associated with the development of drusen between retinal pigment epithelium (RPE) and Bruch's membrane. Drusen are pathological extracellular deposits primarily containing glycolipids, proteins, and cellular debris (Liu et al., 2012). Besides age, certain risk factors contribute to the development of the disease, including smoking and family history (Klein et al., 2004; Thornton, 2005). It is now known that genetic factors can be responsible for as much as 50 to 70% of the total variability in disease risk. Further familial studies also showed that genetic factors play a significant role in the variability in the severity of AMD (Seddon et al., 2005).

AMD is connected with the development of drusen between retinal pigment epithelium (RPE) and Bruch's membrane, which block exchange of nutrients from the vasculature leading to cell death and sensory loss within the central visual field. The late stage of the disease can be characterised as either wet-AMD (neovascular) or dry-AMD (non-neovascular), also called geographic atrophy caused by degeneration of photoreceptors. In neovascular disease, newly formed, abnormal vessels, grow in the sub-retinal space causing RPE detachment. Both forms result in vision damage through cell death (Tan, 2016).

1.7.1. Retinal immune defence

The retina is crucial for vision. It is constituted by four major layers of cells. Phototransduction occurs in the rods and cones of the neurosensory retina. The next layer, the retinal pigment epithelium (RPE) serves as a blood/eye barrier, regulates nutritional transport and phagocytes outer segments of photoreceptors (Strauss, 2005). The third retinal layer, Bruch’s membrane (BM) is actually a multilayer extracellular matrix and serves as a carriage of wastes and nutrients between choroid and RPE. The outermost layer of retina, the choriocapillaris is highly vascularized and connects the retina with the choroid, which provides nutrients and oxygen (Fig. 1.12) (Lutty et al., 2010).

The macula is the central part of the retina. It has not only many more rods and cones, but also RPE cells. The central macula (fovea) is especially rich in photoreceptors, with 30 cones per each RPE cell, and the central part of fovea, is built only by red and green cones. That assures high visual acuity. The number of rods may vary and during aging decrease by 30%, however the

number of cones is not affected by age. Additionally, during AMD development, rod degeneration is much higher than cones; nonetheless, rod loss triggers also cone damage. The macula has exceptionally high choroidal circulation, to maintain oxygen needs of photoreceptor cells (Algvere et al., 2016).

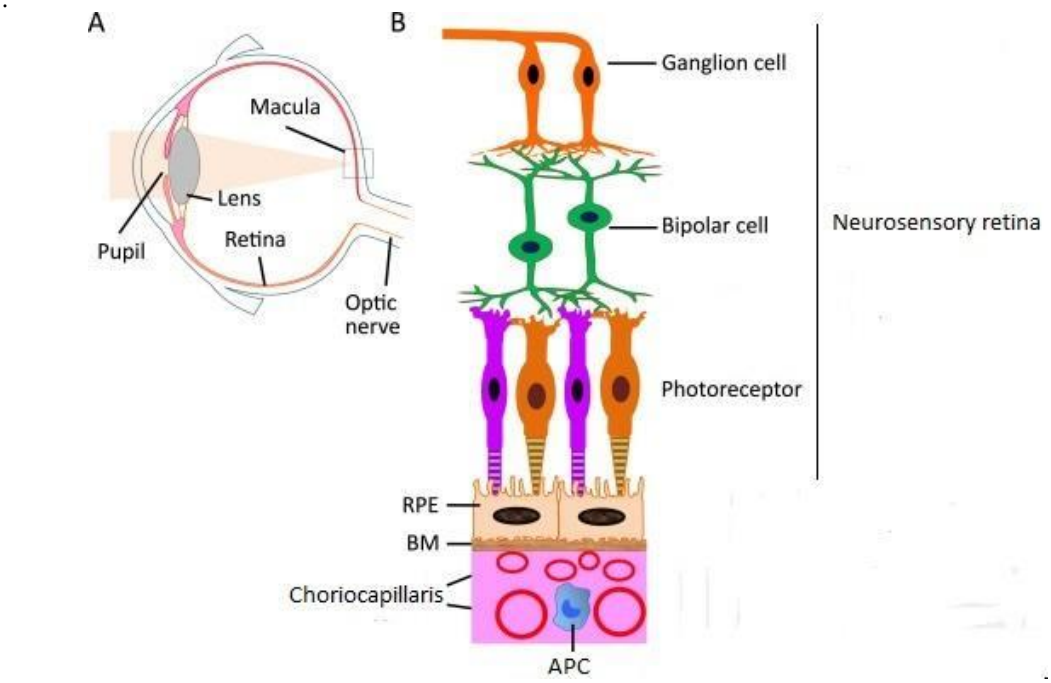

Figure 1.12. The neuronal structure of the retina. The diagram of a human eye, showing the path of a light beam (A) passing through the pupil, lens and reaching the macula. The retina is built by four main layers (B): choriocapillaris that connects the retina with choroid, Bruch's membrane (BM), retinal pigment epithelium (RPE), and neurosensory retina with photoreceptors (Xu and Chen, 2016).

The retina is sometimes called an immune privileged tissue as it has unique mechanisms that reduce the risk of infection and reduce inappropriate immune response (Forrester et al., 2008). Those mechanisms include a blood/retina barrier, to prevent circulating pathogens from entering the retina and also preventing the activation of T-cells in blood (Forrester and Xu, 2012). Additionally, due to the lack of a lymphatic system, APC present in choroid cannot respond to the pathogens in retina when the blood/retina barrier is intact. Finally, the retina has its own, internal immunoregulatory mechanism maintained by retinal cells (Streilein, 1999; Wenkel and Streilein, 2000).

The innate immune system of the retina is formed by three types of immune cells and a complement system. Innate immune cells in the retina are: $CD11b^+$ microglia, $CD11b^+CD14^+CD45^+$ macrophages and DCs (Forrester et al., 2010; Xu et al., 2009). In mice, $CD11c^+$ $DEC205^+$ DCs (Gregerson and Yang, 2003) and MHC II^+33D1^+ DCs (Xu et al., 2007) have been identified. These were shown to be activated in the early inflammation of the retina and phagocytose dead ganglion cells (Lehmann et al., 2010). During the late inflammation and in diseases such as AMD, microglia are activated (Karlstetter et al., 2015).

1.7.2. Complement activation and regulation in the retina in relevance to AMD

The complement system is a second line of innate immune defence in the retina as demonstrated in the RPE and choroid of both human (Anderson et al., 2010) and mouse eyes (Luo et al., 2011). It has been proposed for a long time (first reports date back to late 1800s), that dysregulated immune response can be a cause of AMD (Tan et al., 2016). Several proteins pertained to alternative complement pathway (AP) were linked to the disease. As the retina is separated from the blood circulation, complement proteins together with complement regulatory proteins are produced by retinal microglia and RPE cells (Luo et al., 2011). These include FH, which is being expressed by RPE cells (Chen et al., 2007) and the choriocapillaris (Fett et al., 2012). In fact, retina expresses only selected complement proteins, which suggests that for full activation of the complement system, the blood/retinal barrier needs to be broken. The complement system of the retina can be upregulated because of obsolescence (Chen et al., 2010), but is also regulated by inflammatory cytokines, such as TNF-α and IFN-γ (Chen et al., 2008; Lau et al., 2011).

Multiple evidence suggest that the complement system is involved in the pathogenesis of AMD. Individuals suffering from AMD were reported to have increased plasma levels of C3a, C3d, Bb, and C5a (Lechner et al., 2016). Various complement components, including C3, C5b-9, FB, and FH were also identified in drusen and in AMD lesions (Anderson et al., 2010). Additionally, polymorphisms in a number of complement genes, FH, FB, C2, SERPING1, and C3 increase the risk of AMD (Cipriani et al., 2012; Edwards, 2008). In relation to AMD, a polymorphism in FH has the biggest significance with about 40% of affected individuals carrying an “at-risk” SNP (T1277C) in one or both copies of their complement factor H (CFH) gene (Haines, 2005). This polymorphism in the FH gene leads to a change in the protein at amino acid 402 from a tyrosine

to histidine (Y402H). Because of this mutation, FH is thought to more readily forms oligomers, which inhibit its activity.

AMD is also associated with complement factor H related proteins (CFHR). CFHR comprise a group of five plasma proteins: CFHR1, CFHR2, CFHR3, CFHR4 and CFHR5, which can each bind to the central complement component C3b. Mutations, genetic deletions and duplications in the individual *CFHR* genes are associated with a numerous diseases including AMD where the homozygous deletion of CFHR1 and CFHR3 is associated with a lower risk for AMD (Hughes et al., 2006). It is probably caused by the competition between CFHR1 and CFHR3 with factor H for binding to C3b. On the other hand, it was shown that a particular CFHR1 variant, CFHR1A, is strongly associated with AMD and genetically linked to risk variant Y402H (Martinez-Barricarte et al., 2012).

1.7.3. Sub-retinal pigment epithelial deposit formation

During obsolescence, the retina experiences multiple changes, including shifts in the number and distribution of photoreceptors (Curcio et al., 2000), thickening of BM (Feeney-Burns and Ellersieck, 1985), accumulation of sub-RPE deposits (Strauss, 2005) and upregulation of the retinal complement system (Chen et al., 2010). The formation of small, “hard” drusen deposits in sub-RPE is also a normal age related change and do not indicate disease. However, the second type of drusen, “soft” with no distinct borders accumulating between BM and RPE or in RPE itself, concur with the development of the AMD (Jager et al., 2008). Drusen are pathological extracellular deposits primarily containing over 40% of lipids, proteins (including complement proteins), and cellular debris (Liu et al., 2012). It is also believed that the place of drusen formation is also the main site of immune complex formation in AMD (Tan et al., 2016).

Recently Thompson et al., (2015) proposed a novel mechanism of drusen formation (Fig. 1.13). According to the authors, drusen originate as cholesterol rich lipids, secreted by RPE and then enrolled in the BM. These micrometre sized lipid droplets are then coated by insoluble HAP, the mineral that is known for high protein binding capacity. Once sub-RPE HAP coated spherules are formed, they bind various, RPE secreted proteins, including FH, amyloid beta and vitronectin. It is also very likely that during AMD pathogenesis, the blood/retina barrier has been broken, as plasma protein HRG was also identified on HAP coated spherules. It suggests that serum proteins might be retained by binding to the HAP surface and therefore build up the deposits to clinically relevant size.

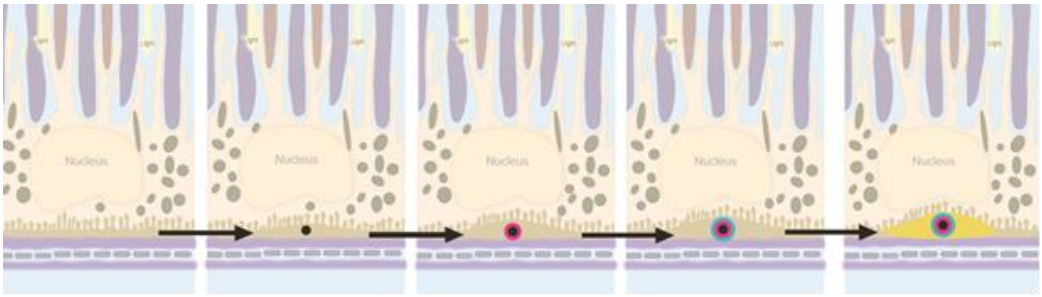

Figure 1.13. Proposed mechanism for growth and/or initiation of sub-RPE deposit formation. Formation is initiated by the HAP deposition (magenta) onto cholesterol-containing droplets (black). Consequently, proteins (blue) bind to the HAP surface facilitating further deposition in a self-driven oligomerisation process ultimately to form the visible deposit (yellow; Thompson et al., 2015).

Zinc also appears to play a role in AMD development. In the healthy eye, the BM contains 47 ppm of zinc. However, in AMD the amount increases to 137 ppm in the membrane and approximately 232 ppm in deposits (Dr Imre Lengyel, personal communication). It is feasible that together FH-zinc oligomer formation (Perkins et al. 2010), FH-HRG binding and the interaction between HRG, complement proteins and HAP are essential for drusen formation and occurs when zinc levels are elevated (Perkins et al., 2010).

1.8. Hypothesis and aims

The major hypothesis underlying this thesis is that zinc is an important regulator of multiple aspects of immunity including antigen presentation and immune complex clearance. The primary aims of this work are directed towards gaining better insight into the complex role of zinc in dendritic cell activation and regulation of complement protein interactions.

The specific aims of this thesis are therefore to:

1. Get an insight into the mechanism of zinc homeostasis during DC maturation, by characterising alterations in the expression of chosen zinc transporters.
2. Quantitatively describe global proteomic changes in DCs upon LPS and hydroxyapatite (HAP) induced maturation.
3. Define the role of zinc in immune complex clearance, by characterizing its influence on HRG–complement interactions and determine whether these interactions occur via N terminus of HRG and to investigate whether zinc and pH alterations may contribute to AMD development by promoting HRG-hydroxyapatite interactions.

Chapter 2. Zinc homeostasis and the role of zinc in dendritic cell function

2.1. Introduction

2.1.1. Zinc in immune cell signalling

Zinc is one of the crucial trace elements in human body. The physiological zinc plasma concentration is in the range of 15-20 µM (Gorgani et al., 1999b), with zinc mostly (75%) bound to albumin and other plasma proteins. This accounts for as much as 98% of deliverable zinc. The concentration of non-protein bound Zn^{2+} ions in plasma is in the range of 0.5 to 1 µM (Tubek et al., 2008).

Zinc functions as a cofactor for nearly 3,000 proteins, which represent 10 % of human genome (Passerini et al., 2009). Its importance highlighted by the effects of zinc deficiency (Prasad, 2009), which leads to many pathological states including inflammation (Haase and Rink, 2009), neurodegeneration (Sensi et al., 2009) and cancer (Taylor at al., 2008).

In immune cells, zinc has several functions, one of them being signal transduction. It serves as a second messenger, with the signalling pathways including T-cell activation, signalling after antibody recognition by Fcε, and after activating of pattern recognition receptors (PRRs; Kabu et al., 2006; Nishida et al., 2008). PPRs are a "primitive" part of the immune system as they evolved before adaptive immunity and other components of immune system. PPRs enable immune cells to recognise damaged host cells through damage-associated molecular patterns (DAMPs) or pathogen through pathogen associated molecular patterns (PAMPs). PRRs can be either membrane bound or cytoplasmic. Toll like receptor 4 (TLR4) is an example of a membrane-bound PAMPs. It is activated mainly by bacterial lipopolysaccharide (LPS; West et al., 2006), but also by hydroxyapatite (HAP) (Velard et al., 2013). There is a growing evidence that zinc acts as a second messenger to trigger the activation of dendritic cells through Myeloid Differentiation Primary Response 88 (MyD88) or TIR-domain-containing adapter-inducing interferon-β (TRIF) signalling pathways (Kitamura et al., 2006; Brieger et al., 2013; Haase et al., 2008) in response to TLR4 activation. MyD88 is the early signalling pathway, where zinc acts as phosphatase inhibitor resulting in the production of inflammatory cytokines. Later, TRIF-dependent signalling leads secretion of interferon β (IFN-β) and expression of surface molecules required for T-cell

activation during antigen presentation (Brieger et al., 2013). The level of free zinc in the cytoplasm transiently increases via zinc release from zinc binding proteins or by transport from intracellular stores through zinc channels (Maret, 2008).

2.1.2. Zinc homeostasis in dendritic cells

Dendritic cells (DCs) primarily function as antigen presenting cells (APCs). They are crucial to initiate immune response. Immature DCs are present in non-lymphoid tissue where they become activated by antigens through PRRs, including TLRs. After activation, they maturate and migrate to lymph nodes where the antigen is processed and presented. Zinc deficiency causes defects in immune response and includes: hypoplasia of lymphoid tissues, reduction of T-helper cell numbers (Prasad, 2000), reduction of NK cell activity (Allen et al., 1983), decreased cell production, reduction in cell mediated immunity and phagocytosis, as lymphocyte proliferation, IL-2 production, DTH response, Ab response . Zinc deficiency is also known to cause thymus atrophy, reduction in Th1 cells number and decrease thymulin activity (Dardenne et al., 1982, Mitchell et al., 2006). This, together with the knowledge that zinc acts as a second messenger in immune cell signalling, suggests that zinc homeostasis influences dendritic cells function. Mainly zinc transporters control cellular zinc homeostasis. There are 24 such transporters in humans; 14 Zrt-, Irt-like proteins (Zips encoded by the Slc39A genes), which transport Zn^{2+} to the cell cytosol and 10 Zn transporters (ZnTs encoded by the Slc30A genes), which transport Zn^{2+} from the cell cytosol (Cousins et al., 2006; Palmiter and Huang, 2004; Eide, 2004). Both families of zinc transporters (except ZnT10) have been characterised in many groups of cells. Zip1 is ubiquitous in human cells, whereas other Zips and ZnTs exhibit more tissue-specific expression. Several zinc transporter isoforms have been implicated in the function of immune cells; examples include ZnT5 in allergic response, and Zip8 and Zip14 in cytokine release (Nishida et al., 2009; Aydemir et al., 2009; Sayadi et al., 2013). Although zinc transport is strongly linked to immune functioning, the expression of zinc transporters and their specific roles in dendritic cells are still not well characterised. A study by Kitamura et al. in 2006, demonstrated that stimulation of the TLR system in DCs by LPS induces significant alterations in the expression of several zinc transporters (Kitamura et al., 2006). However, in this study the relative expression levels were only measured until 6 hours post-LPS stimulation. The life span of dendritic cells differs between cell populations and ranges between 7 to 14 days (Merad and Manz, 2009).

The aims of this chapter are to examine the importance of zinc for DC maturation and to get an insight into the mechanism of zinc homeostasis during this process, by characterising alterations

in the expression of chosen zinc transporters. Changes in levels of mRNA transcript encoding for those transporters will be assessed using qPCR. Alterations in the expression of zinc transporter proteins during LPS-induced maturation will also be determined using immunofluorescence microscopy as well as flow cytometry. Intracellular free zinc levels is examined using the zinc-specific membrane permeable fluorophore, ZnAF-2F DA and flow cytometry. In addition, intracellular zinc will be visualised by fluorescent microscopy using the same fluorophore. Finally, by measuring cytokine release, it will be determined whether LPS and hydroxyapatite can trigger DCs maturation and therefore initiate immune response.

2.2. Materials and methods

2.2.1. Cell culture methods

2.2.1.1. Cell culture of human monocyte derived dendritic cells (moDCs)

Monocyte-derived DCs used for all the studies were prepared according to a well-established protocol (Zhou and Tedder, 1996). Blood was obtained from a healthy donors and purified over density gradient (Histopaque, Sigma Aldrich, Haverhill, UK), at room temperature to isolate peripheral blood mononuclear cells (PBMC). Monocytes were then enriched by a two-hour adhesion step (adherence to culture dishes), with non-adherent cells being washed away. As a result, on average, 0.7 x 10^6 monocytes were isolated per 1 ml of blood used. MoDCs were then obtained from these human monocytes by culturing in RPMI 1640 medium (Gibco, Thermo Fisher Scientific) supplemented with 10% foetal calf serum (FCS), 50 ng/ml interleukin-4 (IL-4; eBioscience, Haltfield, UK) and 50 ng/ml granulocyte-macrophage colony-stimulating factor (GM-CSF; Abcam, Cambridge, UK) for 5 days. The resultant, immature, moDCs were then treated with 100 ng/ml of bacterial LPS (Sigma Aldrich) for up to 72 h. All tissue culture procedures were performed in a class 2 containment cabinet. Cells were grown in 6, 12, or 24-well culture dishes, in an incubator at 37^{o}C in a humidified atmosphere of 5% CO_2.

Ethical approval for the use of moDCs was granted by the University of St Andrews School of Medicine Ethics Committee.

2.2.1.2. Cell counting

For cell counting, 10 µl of cell suspension was mixed 1:1 with trypan blue dye and incubated at room temperature for 2 min. The number of viable and dead cells (viable cells do not take up the dye) was then measured either by haemocytometer or by an automated cell counter (TC20, BioRad).

2.2.1.3. Cell isolation

During cell culture, moDCs attach to the culture dish. Therefore, to harvest mature moDC, cells were firstly washed with sterile phosphate-buffered saline (PBS; 137 mM NaCl, 2.7 mM KCl, 10 mM Na_2HPO_4, 1.8 mM KH_2PO_4 pH 7.4). Followed by a quick rinse with a few drops of trypsin solution (Trypsin-EDTA, 0.05%; Gibco), cells were incubated with 100 µl of fresh trypsin for 5 min at 37^{o}C.

2.2.2. Western blotting

2.2.2.1. The comparison of chemiluminescent and near infrared (NIR) western blot techniques

Western blot is a technique commonly used for protein detection and analysis. Chemiluminescent protein detection is made possible due to the use of enzyme-conjugated antibodies, which allow detection with X-ray films or CCD camera. With all its advantages, this traditional Western blot technique has also some limitations. It does not allow the use of a mixture of primary antibodies, which means that only one protein can be analysed at a time. Therefore, the target protein and control have to be detected separately, with the membrane stripped in between or samples re-run. Stripping is useful and a very common practice as it allows investigating more than one protein at the same blot, however it is not advisable to make quantitative comparison of targets probed after stripping. Even very careful stripping removes some sample protein from the membrane. To overcome these issues fluorescently-labelled antibodies (with emission in near-infrared (NIR) spectrum) are now commonly used in western blotting. The reason behind using the NIR part of the spectrum is to limit auto-fluorescence of membranes and biological molecules as seen at longer wavelengths. There is a big choice of secondary antibodies directly labelled with NIR fluorophores, which can be distinguished based on emitted colour. For increased accuracy, a mixture of antibodies can be used with one of them directed against housekeeping protein that serves as an internal, normalization control. Fluorescent detection also shows much higher sensitivity than chemiluminescent detection and exceeds visible fluorescence detection. Overall, it is fast, accurate and quantitative method of protein analysis.

2.2.2.2. Protein extraction

MoDCs were grown on 6 or 12-well plates and stimulated with LPS as described above (2.2.1.1.). When cells were mature, culture plates was placed on ice and cells were washed twice with cold phosphate buffered saline (PBS), followed by the addition of 200 µl of 10x RIPA buffer (Cell Signalling Technology, Danvers, MA, U.S.A.) diluted to a 1x solution using ddH_2O. Cells were incubated for 10 min, then scrapped with cell scrapper, transferred to Eppendorf tubes and lysed for an additional 10 min, at 4^{o}C. Cell lysates were centrifuged at 14,000 rpm at 4^{o}C for 10 min, to pellet cell debris. The resultant supernatants were then transferred to fresh tubes.

2.2.2.3. Protein quantification

To determine the protein concentrations in the cell lysates, the BCA protein assay kit (optimised for 96-well plates) was used (Pierce, Thermo Fisher Scientific). The BCA Protein Assay is a formulation based on bicinchoninic acid (BCA) for the colorimetric detection and quantitation of total protein (Smith et al., 1985). The absorbance at 570 nm was measured using a Dynex MRX microplate reader (Dynex Technologies, Worthing, UK). Protein concentrations were calculated using a standard curve created using solutions of bovine serum albumin at known concentrations.

2.2.2.4. Sodium dodecyl sulfate-polyacrylamide gel electrophoresis (SDS-PAGE)

The quantified protein samples were resuspended in NuPAGE LDS Sample Buffer (Invitrogen, Thermo Fisher Scientific) with an addition of 10% β-mercaptoethanol for reducing conditions. Then denatured by heating at 95°C for 5 min. Samples were loaded into precast NuPAGE 4-12% Bis-Tris 1.0 mm protein gels (Invitrogen, Thermo Fisher Scientific), and run for approximately 1 h at 160 V in running buffer (NuPAGE MES SDS Running Buffer, Thermo Fisher Scientific). After electrophoresis, gels were electroblotted to allow immuno-detection of proteins (Western blot).

2.2.2.5. Western blotting

To detect zinc transporters and TLR 4 in moDC cell lysates, NIR immunoblotting technique was used.

To minimize the background, which is especially important when using the fluorescent secondary antibodies, Immobilon-FL PVDF membrane was used (Millipore, Billerica, U.S.A.). The membrane was pre-conditioned with 100% methanol for 5 min, and then soaked with transfer buffer (25 mM Tris, 190 mM glycine, 20% methanol) for 10 min. The SDS-PAGE protein gel, prepared as described above (2.2.3.4.), was equilibrated with transfer buffer for 10-15 min, and so were other elements of the "blotting sandwich". The sandwich was arranged in a semi-dry electrophoretic transfer cell system (Trans-Blot SD; Bio-Rad, Hemel Hempstead, UK), from the platinum anode with: extra thick filter paper/membrane/gel/extra thick filter paper. Air bubbles were removed between each layer. The transfer was carried out at 16 V for 30 min, and then the membrane was carefully removed, rinsed with water, and placed in blocking solution (1:1 PBS and Odyssey Blocking solution, PBS based; Li-Cor, Cambridge, UK) for an hour, with agitation, at room temperature.

Membranes were incubated with primary antibodies at the following dilutions: β-actin at 1:1500 (C4, Santa Cruz Biotechnology, Dallas, U.S.A.), Zip7 at 1: 1500 (Thermo Fisher Scientific), pZip7 at 1:150 (a gift from Dr Kathryn Taylor, Cardiff University, UK), Zip6 at 1:100 (also a gift from Dr Kathryn Taylor), ZnT1 at 1:1500 (Abcam, Cambridge, U.S.A.), ZnT7 at 1:1500 (Sigma-Aldrich), TLR4 at 1:1000 (ProSci Inc., Poway, U.S.A.). All antibodies were diluted in PBS (or in the case of pZip7 TBS) supplemented with 0.01% Tween 20 and 0.01% SDS. The primary antibody was incubated with the blot overnight at 4^{o}C with agitation. This was followed by four 5 min washes and a 20 min wash with TBS, PBS or TBS containing 0.05% Tween 20 (TBST) respectively.

Membranes were then incubated with a mixture of either donkey anti-goat IRDye 680 (1:20,000 dilution, Li-Cor) and donkey anti-mouse IRDye 800 (1:15,000 dilution, Li-Cor), or donkey anti-goat IRDye 700 (1:20,000 dilution, Li-Cor) and donkey anti-rabbit IRDye 800 (1:15,000 dilution, Li-Cor) for 45 min at room temperature, agitating. Antibodies were diluted in PBS supplemented with 0.01% Tween 20 and 0.01% SDS, except of pZip7, which was prepared in TBS supplemented with 0.01% Tween 20 and 0.01% SDS. Excessive secondary antibody was washed away with four times 5 min washes with either TBS or PBS both containing 0.01% Tween 20, followed by 20 min wash with TBS or PBS. Membrane was then left to dry on a filter paper at 37^{o}C for 1 h. Fluorescent protein bands were detected using an Odyssey imager (Li-Cor).

The NIR blots allow quantification of proteins using an internal software Image Studio 4.0. The software measures density of each band end then compares it to the density of corresponding control band. Further calculations were performed using Microsoft Excel, with the assumption that the expression of β-actin control was not influenced by experimental conditions and remained stable between samples.

2.2.3. Immunofluorescence

To visualise alterations in zinc transporter expression upon TLR 4 signalling, immunofluorescence (IF) microscopy was used. This technique is a type of immunohistochemistry that uses fluorophores to visualise the target protein. There are two main types of IF; direct, when primary antibody is directly linked to fluorophore, or indirect, with two-step detection method where primary antibody binds to a target protein and a secondary antibody has a fluorophore conjugate. Indirect IF is more sensitive and was therefore used to immunostain zinc transporters and TLR4 receptor.

PBMC isolated from fresh blood as described above (2.2.1.1.), were cultured on sterilised, 13 mm in diameter, round cover slips on 24-well cell culture dish. After two hours, non-adherent cells were washed away and only monocytes remained attached to the culture surface. Immature moDC were then obtained and treated with bacterial LPS as described above (2.2.1.1.). Cells were then washed once with PBS and fixed for 10-20 min, on ice with 4% *p*-formaldehyde (prepared from in PBS from 16 % formaldehyde solution, Sigma-Aldrich), followed by permeabilization with ice-cold methanol, for 5 min at –20°C. Cells were then rinsed twice with PBS prior to blocking with 1% bovine serum albumin (BSA) dissolved in PBS, supplemented with 0.05% Tween 20, for 30 min at room temperature, followed by another wash with PBS. All subsequent incubations were performed in a humidified chamber to prevent cells from drying out. For IF the same antibodies as above (2.2.3.) were used. All antibodies were used at a concentration of 5 µg/ml, except for anti-pSLC39A7, which was used at 20 µg/ml. Antibodies were diluted in blocking solution. For each cover slip, 100 µl of diluted antibody was applied and incubated overnight at 4°C. Cells were then washed four times in 5 min intervals, in PBS supplemented with 0.05% Tween 20.

Secondary antibodies, Donkey Anti-Rabbit AlexaFluor 568 (Thermo Fisher Scientific), or Donkey Anti-Mouse AlexaFluor 647 (Thermo Fisher Scientific), were diluted 1:200 in wash buffer, 100 µl was applied per cover slip and incubated for 1 h at room temperature. Cells were then washed again four times in 5 min intervals, in PBS supplemented with 0.05% Tween 20. For mounting 10 µl of SlowFade Diamond Antifade Mountant with DAPI (Thermo Fisher Scientific) was used. Mounted microscopy slides were were allowed to cure for 24 h at room temperature in the dark. After that time, excess mounting solution was drawn using a filter paper, and edges were sealed with nail varnish. Slides were stored in the dark and viewed the following day, under 20x magnification and 100x magnification oil immersion, using fluorescent microscope Leica CTR 5500 (Leica Microsystems, Milton Keynes, UK).

2.2.4. Zinc imaging

To investigate the relationship between TLR 4 signalling and the abundance of intracellular zinc in moDCs, zinc was measured using the membrane permeable zinc-specific fluorescent probe, ZnAF-2F DA (AdipoGen, Liestal, Switzerland). MoDCs were grown on the coverslips as described above (2.2.4.) and treated with 100 ng/ml of bacterial LPS for up to 72 h. Cells were then washed twice with PBS, to remove serum that was added to media, and incubated with 10 µM ZnAF-2F DA in PBS at 37°C for 30 min in a humidified incubator. Cells were then washed once with PBS

and then once with PBS supplemented with 100 µM of ethylenediaminetetraacetic acid (EDTA; to remove excess extracellular zinc). EDTA chelates extracellular zinc, which would otherwise result in increased background on IF images. For mounting, SlowFade® Diamond Antifade Mountant with DAPI (Thermo Fisher Scientific) was used. Slides were allowed to cure for 24 h in the dark, as advised by the manufacturer and edges were sealed with nail varnish. To avoid photo bleaching, all the procedures were performed in the dark, and microscopy slides were stored in the dark at all times. As a control, unstained cells of 0 and 24 h post LPS stimulation time points were prepared. Due to the nature of the assay, which was a one-step, direct staining, no other controls were prepared. Slides were viewed under 20x magnification and 100x magnification with oil immersion on Leica CTR 5500 microscope (Leica Microsystems).

2.2.5. Flow cytometry

Based on the emitted fluorescence, flow cytometry allows three types of data are generated. Using forward scatter (FSC) approximate cell size is calculated. Side/orthogonal scatter (SSC) allows investigating cell complexity or granularity and finally labelling cell with fluorescent antibodies directed against specific molecules is used to investigate cell function. Cells analysed by flow cytometry can be either directly stained, using fluorophores or fluorophore conjugated primary antibodies; or indirectly stained, with fluorophore conjugated secondary antibodies. Flow cytometry allows analysing multiple biophysical properties of each cell, at rates of over 1000 particles per second. This makes the approach semi-quantitative, as equal number of particles will be analysed in each sample, and therefore samples can be compared.

Flow cytometry was used to measure the alterations in zinc transporter expression, TLR4 receptor expression and the levels of intracellular zinc following LPS-triggered maturation of moDCs. MoDCs were treated with bacterial LPS for 24 h to 72 h as described above. Mature moDCs were dissociated using trypsin for 5 min at 37^{o}C and washed twice with PBS. Cells were plated on 96-well, transparent, round bottom plate and either stained with 10 µM of cell permeable zinc fluorophore, ZnAF-2F DA at 37^{o}C for 30 min to label intracellular zinc; or with primary and secondary antibodies for an indirect protein staining. Cells stained with zinc fluorophore were washed with PBS and then with 100 µM EDTA prior to fixation with 2% *p*-formaldehyde for 15 min on ice (prepared from in PBS from 16 % formaldehyde solution, Sigma-Aldrich). Prior to primary antibody staining, cells were fixed with 1% *p*-formaldehyde for 15 min on ice. Cells were washed twice with PBS and blocked with 3% BSA in PBS for 30 min at room temperature. Primary antibodies used for flow cytometry were the same as above (2.2.3.). All

antibodies were used at 1:1000 dilution, except of anti-pSLC39A7, which was used at 1:500 dilution; dissolved in PBS supplemented with 3% BSA. Cells were incubated with primary antibodies for 1 h at room temperature and washed three times for 5 min with cold PBS. Secondary antibodies, donkey anti-rabbit AlexaFluor 568 (Thermo Fisher Scientific), or donkey anti-mouse AlexaFluor 488 (Thermo Fisher Scientific), were diluted 1:100 in 1% BSA in PBS, and incubated for 30 min, at room temperature, in the dark. Cells were then washed again three times in 5 min intervals, with cold PBS. Stained cells were kept at 4^{o}C in the dark for 2 days. The instrument used was Guava easyCyte 8HT (Merck Millipore) and samples were analysed using Guava 2.7 software.

2.2.6. The Human Tumor Necrosis Factor-alpha (TNF-α) assay

Macrophages and mature dendritic cells are known to secrete TNF-α after TLR4 signalling upon LPS stimulation, which indicates that cells are active and functional. The response of dendritic cells for hydroxyapatite (HAP) stimulation is not known. To see whether generated moDC are functional and to verify that HAP can indeed activate moDCs, aliquots of cell culture media were analysed using an enzyme-linked immunosorbent assay (ELISA) for the quantitative determination of TNF- α. Cells were obtained as described before (2.2.1.1.). Differentiated moDCs were stimulated with 100 ng/ml of LPS over 72 h or cultured with up to 20 mg/ml of ethanol-sterilised HAP nanopowder (Sigma-Aldrich) for 24 h. Next, the culture media was collected and TNF-α concentration measured using the TNF alpha Human ELISA Kit (Invitrogen, Thermo Fisher Scientific). This kit is a sandwich ELISA assay, which comes with plates pre-coated with specific anti-TNF-α antibody. After addition of the sample to the wells, detection involved addition of biotinylated anti-TNF-α antibody followed by a streptavidin-HRP conjugate. The plate was then washed to remove unbound substances and substrate for HRP was applied. After the reaction was stopped using ELISA stop solution, the absorbance at 450 nm was measured using a Dynex MRX microplate reader (Dynex Technologies, Worthing, UK). The concentration of TNF-α in the samples was determined based on standards supplied with the kit.

2.2.7. Polymerase chain reaction to semi-quantify gene expression

Polymerase chain reaction (PCR) is a common molecular biology technique used to amplify DNA. It is a versatile technique and during 30 years since its discovery, many variations have been developed. Those include reverse transcription PCR (RT-PCR) where RNA is converted to cDNA, which is then amplified and can be used inter alia to determine the relative expression of a gene,

and quantitative PCR (qPCR) which allows quantitative measurement of target gene in a sample. Quantitative PCR is very precise as it measures the amount of amplified product in real time using fluorescent DNA-binding dyes, such as SYBR Green.

2.2.7.1. RNA extraction

Prior to RT-PCR and qPCR procedures, RNA was purified using phenol-chloroform RNA extraction protocol. MoDCs were trypsinised for 10 min at 37^{o}C. Following centrifugation (10,000 rpm for 5 min), the media was removed and cells were washed with PBS. TRIzol Reagent (1 ml; Invitrogen, Thermo Fisher Scientific) was added to cells, mixed and incubated for 5 min at room temperature. Then 200 µl of chloroform was added, shaken vigorously for 15 s and incubated for 5 min at room temperature. Following incubation, samples were centrifuged for 15 min at 13,000 rpm at 4^{o}C. The colourless upper aqueous phase, containing RNA was transferred to a fresh tube. To precipitate the RNA, 0.5 ml of isopropanol for every 1 ml of TRIzol was added and then incubated at room temperature for 10 min, followed by centrifugation at 11,000 rpm at 4^{o}C. The pellet containing the RNA was visible on the side of the tube. After precipitation, the supernatant was removed and the pellet was washed with 1 ml of 75% ethanol for every 1 ml of TRIzol used. Samples were mixed by vortexing and centrifuged at 16,000 rpm for 5 min at 4^{o}C. RNA was resuspended in 30 µl of RNAse-free water and incubated at 55^{o}C, until the pellet completely dissolved. To check the concentration and quality of obtained RNA (based upon absorbance measurements) a NanoVue spectrophotometer (GE Healthcare, Little Chalfont, UK) was used. RNA was considered to be of sufficient purity when 260/280 nm absorbance ratio was between 1.95 and 2.1. To remove any DNA contaminations, 4 µg of RNA was mixed with 1 µl of DNAse (Ambion, Thermo Fisher Scientific) and compatible 10x reaction buffer, followed by incubation at 37^{o}C for 25 min. Next 1 µl of inactivation reagent was added and samples were incubated at room temperature for 5 min and centrifuged at 10,000 × g for 15 min to remove pelleted DNA. RNA was quantified again and stored at -80^{o}C until required.

2.2.7.2. Synthesis of cDNA from RNA

To synthesise cDNA for subsequent amplification, 2 µg of total RNA was used. The volume of the RNA in solution was increased to 12.5 µl with addition of UltraPure™ DNase/RNase-Free Water. The total reaction volume was 20 µl and included 12.5 µl of diluted RNA, 1 µl of dNTP (Sigma-Aldrich), 1 µl of Oligo (dT) 15 Primer (Promega, UK), 200 units (1 µl) of reverse transcriptase (Revert Aid, Thermo Fisher Scientific) and 0.5 µl of RiboLock RNase Inhibitor (Thermo Fisher Scientific) in the appropriate reaction buffer. All steps were performed on ice in a PCR-grade

cabinet to avoid DNA contamination. Samples were incubated for 1 h at 42°C. The quality of obtained DNA was assessed using a NanoVue spectrophotometer (GE Healthcare, Little Chalfont, UK) as above. DNA was stored at -20°C until required.

2.2.7.3. Reverse transcription-PCR

RT-PCR was performed to determine the expression (semi-quantitatively) of zinc transporters (ZnT 1, 4, 5, 6, 7, 9 and Zip 1, 3, 6, 7, 8, 9, 10, 11 and 12) in moDC treated with LPS. The reaction volume of the RT-PCR reactions was 20 µl and included, 10 µl of BIO-X-ACT™ Short Mix (Bioline, London, UK), 7 µl of ultrapure water, 1 µl (250 nM) of each forward and reverse primers and 1 µl (made from 100 ng RNA) of cDNA. As a negative control, samples without the addition of cDNA ware included. As a positive control and reference gene, primers for ribosomal protein RPLP0 were used. All primers were made by Eurofins MWG (Luxembourg). The thermal cycling steps were as follows: 1 cycle as initial denaturation at 95°C for 2 min, followed by 40 cycles of denaturation at 95°C for 30 s, annealing at 58°C for 30 s and extension at 68°C for 30 s. Final extension was done in 1 cycle at 68°C for 5 min.

RPLP0 forward primer	5'- GAGTGATGTGCAGCTGATCAAGACTGG-3'
RPLP0 reverse primer	5'- CAGAGTTTCCTCTGTGATATCAAGCACTTCAG-3'
SLC30A1 (ZnT1) forward primer:	5'- CATGCTGTCGGACGTGCTGG-3'
SLC30A1 (ZnT1) reverse primer	5'- GCTGAAGCCGCTGTGATGGTG-3'
SLC30A4 (ZnT4) forward primer:	5'- CGTTCTGTACTTGCTTTTCATGATTGGAG-3'
SLC30A4 (ZnT4) reverse primer	5'- CCAACAGCTGCGGTGATGAGC-3'
SLC30A5 (ZnT5) forward primer:	5'- GCTCTCTGTCGACGTTGGTGG-3'
SLC30A5 (ZnT5) reverse primer	5'- CCTGGTGTGCTGCTTTGTTCATAGC-3'
SLC30A6 (ZnT6) forward primer:	5'- CGAAGGTCCTGGAAGATACTGCTC-3'
SLC30A6 (ZnT6) reverse primer	5'- CAGCCAGGACTTCTAATCTTTCAAACC-3'
SLC30A7 (ZnT7) forward primer	5'- CCTGTCCATCAAAGACGATGAATACAAAC-3'
SLC30A7 (ZnT7) reverse primer	5'- GCCAGAACTTCCGCTCTAACATACC-3'
SLC30A9 (ZnT9) forward primer	5'- CCTGAGTCAAGTAAAGTTGTACTCCAC-3'
SLC30A9 (ZnT9) reverse primer	5'- GCTTCCACATCTGATCTCAAGTATACAG-3'
SLC39A1 (Zip1) forward primer	5'- CGAGGCGGTAGCTTCAGAGC-3'
SLC39A1 (Zip1) reverse primer	5'- GCCAGGATGAACTCTTGCAGTGG-3'
SLC39A3 (Zip3) forward primer	5'-CCTCTCTCTCTGCAACACCTTTGG -3'
SLC39A3 (Zip3) reverse primer	5'-CCATGAAGGGGCTCTCATACTCC -3'

SLC39A6 (Zip6) forward primer	5’-CATGACTCAGATAGTTCAGGTAAAGATCC -3’
SLC39A6 (Zip6) reverse primer	5’-CTTTGATGCATTGAAACACTCCTGAGG -3’
SLC39A7 (Zip7) forward primer	5’-CTCACGAGAGCATCTGGCATGG -3’
SLC39A7 (Zip7) reverse primer	5’-CTGAGCAAGATCTGAAGTAGAGAGC -3’
SLC39A8 (Zip8) forward primer	5’-CCACTTTGGAAATGATAACTTTGGTCCTC -3’
SLC39A8 (Zip8) reverse primer	5’-CTGAAGGAGAGACAAGGTGCAGG -3’
SLC39A9 (Zip9) forward primer	5’-GGAACGACTGAAGCTGGTGACTG -3’
SLC39A9 (Zip9) reverse primer	5’-CTTGCTGCTTCTGGATCGTCAGTAG -3’
SLC39A10 (Zip10) forward primer	5’-GCTTCACAGACAGCATCGTGGAATG -3’
SLC39A10 (Zip10) reverse primer	5’-GATTATGGGAATGCTGGTGGTTATGTG -3’
SLC39A11 (Zip11) forward primer	5’-CGTGTTCGTATTCTCTAGTGGACAG -3’
SLC39A11 (Zip11) reverse primer	5’-GGATCAGACTTCTTCTTCATCAACGTAG -3’
SLC39A12 (Zip12) forward primer	5’-CAGATGCACTATTACTAATAGCTGGAGG -3’
SLC39A12 (Zip12) reverse primer	5’-GCACCTTCACTGCTCACTATTCCAG -3’

Table 2.1. Sequences of gene-specific primers used in RT-PCR reactions.

2.2.7.4. Agarose gel electrophoresis

After the PCR amplification 3 µl of 6x DNA loading dye (Thermo Fisher Scientific) was added to tube and 15 µl of this mixture loaded onto a 1% agarose gel. Gels were prepared by melting 1% (w/v) agarose (Sigma-Aldrich) in Tris-acetate-EDTA buffer (TAE; 40 mM Tris pH 7.6, 20 mM acetic acid, 1 mM EDTA) with the addition of SYBR Safe DNA Gel Stain (Life Technologies) to enable detection of DNA bands. Sample wells were formed by inserting a comb into the gel before it set. Hyperladder IV (Bioline, 100-1,000 bp) was loaded into one well to allow identification of DNA sizes. DNA bands were separated at 150 V for approximately 40 min. DNA was visualised in a Gel Doc XR+ Imager and band intensities analysed using the Image Lab 2.0 software (Bio-Rad Laboratories, Inc.).

2.2.7.5. Quantitative PCR

For quantitative measurement of alterations in genes coding for zinc transporters in moDCs, qPCR was performed using the ViiA™ 7 Real-Time PCR System (Thermo Scientific) with PerfeCTa® SYBR® Green FastMix, ROX™ (Quanta Bioscience). Assays were performed on MicroAmp® Optical 384-Well Reaction Plate (Life technologies). The reaction volume was 10 µl and reaction

set up as follows: 5 µl of SYBR Green Mix, 0.3 µl (250 nM final concentration) of each forward and reverse primer, 1 µl (made from 100 ng of RNA) of cDNA and ultrapure water. To avoid pipetting errors and maximise assay precision, the plate was set up using a high-precision automated PCR setup, pipetting robot (QIAgility; QIAGEN).

The following thermal cycling protocol was used: 1 cycle as initial denaturation at 95°C for 1 min, then 40 cycles of 95°C for 15 s and 60°C for 45 s. For Melt Curve (dissociation stage) the PCR cycling was 95°C for 15 s followed by 60°C for 1 min and again 95°C for 15 s.

β-actin forward primer	5'-AGAGCTACGAGCTGCCTGAC-3'
β-actin reverse primer	5'-AGCACTGTGTTGGCGTACAG-3'
RPLP0 forward primer	5'-CATGTGAAGTCACTGTGCCAG-3'
RPLP0 reverse primer	5'-GATCAGCTGCACATCACTCAG-3'
SLC30A1 (ZnT1) forward primer:	5'-AACACCCTGGTGGCCAATAC-3'
SLC30A1 (ZnT1) reverse primer	5'-TCTGGGGTTTTCTGGGTCTGC-3'
SLC30A7 (ZnT7) forward primer	5'-CATGATCATGCTCATGGACATGG-3'
SLC30A7 (ZnT7) reverse primer	5'-CACCAATACTTCCAAGTGTATCTG-3'
SLC39A6 (Zip6) forward primer	5'-CAGCGATGGCCTAGCAATTG-3'
SLC39A6 (Zip6) reverse primer	5'-CATGCCAGCCTTTAGTAGAACAG-3'
SLC39A7 (Zip7) forward primer	5'-GGTTCTCAGTGGAATTGTTGCC-3'
SLC39A7 (Zip7) reverse primer	5'- CTCTTGTCTTCCATGTCCATGAC-3'

Table 2.2. Sequences of gene-specific primers used in qPCR reactions.

To validate qPCR efficiency, an initial validation standard curve for each primer set was generated. Amplification efficiency is a rate at which the PCR amplicon is produced and shows the overall performance expressed as a percentage value. Each assay is defined as having 100% efficiency when the quantity of PCR product doubles during the geometric phase of amplification. Standard amplification curves were plotted for each primer pair using serial dilution of DNA. Reaction efficiencies and correlation coefficient (R2) (Table 2.3) were calculated automatically by ViiA™ 7 Real-Time PCR System Software based on standard curves plotted (see Appendix 1).

Target	R2	Primer efficiency (%)	Error
SLC30A1 (ZnT1)	0.993	97.91	0.101
SLC30A7 (ZnT7)	0.995	75.3	0.119
SLC39A6 (Zip6)	0.994	96.65	0.109
SLC39A7 (Zip7)	0.995	96.77	0.092
β-actin	0.998	88.9	0.051
RPLP0	0.996	91.96	0.075

Table 2.3. To calculate amplification efficiency, reaction was set up for each primer pair, with a serial dilution of cDNA. That allowed to plot amplification standard curves expressed as a quantity of gene amplified per threshold cycle (CT). ViiA™ 7 Real-Time PCR System Software based on standard curves plotted calculated reaction efficiencies for all primer pairs automatically. R2 value indicates correlation coefficient.

Normalisation was performed using two reference genes (β-actin and RPLP0). These were chosen as they were expected to maintain a constant level of the expression in all of the samples irrespectively of the treatment. To analyse relative quantification of genes, Comparative C_T Method ($\Delta\Delta CT$) was used. $\Delta\Delta CT$ values when using the two reference genes were calculated using the following equation:

$$\Delta\Delta CT = (Ct\ target\ treated - \sqrt{Ct\ \beta actin\ treated\ x\ Ct\ RPLP0\ treated}) -$$

$$(Ct\ target\ untreated - \sqrt{Ct\ \beta actin\ untreated\ x\ Ct\ RPLP0\ untreated})$$

2.3. Results

2.3.1. Morphological characteristic of DCs

MoDCs were differentiated from purified monocytes using interleukin-4/granulocyte–macrophage colony-stimulating factor treatment, a well-established method (Soo et al., 2012). The cells obtained exhibited morphological characteristics typical of mature dendritic cells (Tan et al., 2010; Verdijk et al., 2004) with characteristic long cytoplasmic projections (Fig. 2.1).

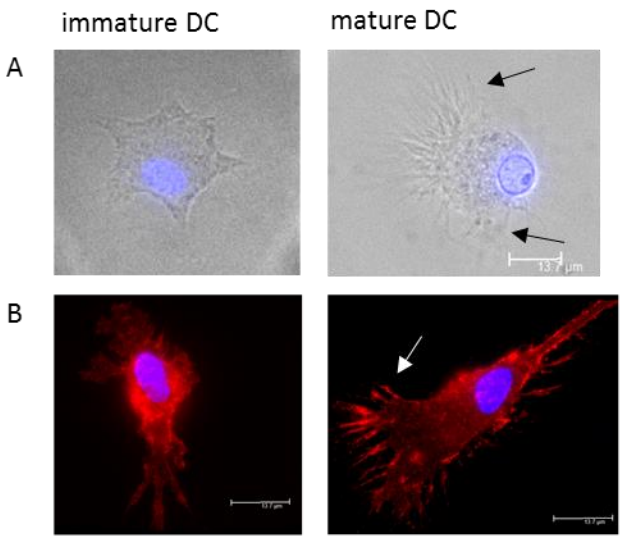

Figure 2.1. Microscopy images (at 100× magnification) of immature and mature moDCs in (A) bright-field and (B) stained with AlexaFluor 568 recognising anti-Zip6 and DAPI. DCs displayed a typical morphology with long cytoplasmic projections (as indicated by the arrows).

2.3.2. Characteristic of zinc transporters in moDC

2.3.3.1. Alterations in mRNA expression

Zinc transporters are the main regulators of zinc homeostasis. Therefore, to establish the link between TLR4 signalling and zinc homeostasis in moDCs, it is necessary to characterise the changes in expression of those transporters upon DC maturation. In order to do this moDCs were treated with LPS over a 10 h period with samples being taken after 2, 6, and 10 h (Fig. 2.2). LPS triggers dendritic cell maturation through TLR4 signalling. As a control, moDCs untreated with

LPS were used. RNA was isolated using trizol-chloroform extraction method and RT-PCR was performed. For this preliminary study, the RNA expression of six ZnT (1, 4, 5, 6, 7, 9), and nine Zip (1, 3, 6, 7, 8, 9, 10, 11, 12) transporters was verified. As a loading control, RPLP0 was used, a housekeeping gene encoding for ribosomal protein P0. Unfortunately, the control revealed that there was less template used for 10 h time point.

Changes in expression differed between the transporters. For ZnT4, Zip3, Zip10 and Zip11 mRNA expression decreased gradually up to 10 h post-LPS treatment. Whilst ZnT1, ZnT7, ZnT9, Zip1, and Zip8 mRNA transcript expression increased up to 6 h post maturation, and then dropped significantly between 6 to 10 h (Fig. 2.2). Zip6 and Zip7 exhibited abrupt increases in expression with the peak at 2-6 h. Interestingly LPS treatment did not appear to affect the expression of ZnT5, ZnT6 and Zip12, with ZnT5 being the only plasma membrane associated zinc "exporter" expressed of those assessed. After 10 h post-LPS treatment Zip3 and Zip8 were the only zinc importers expressed of those assessed (Fig. 2.2).

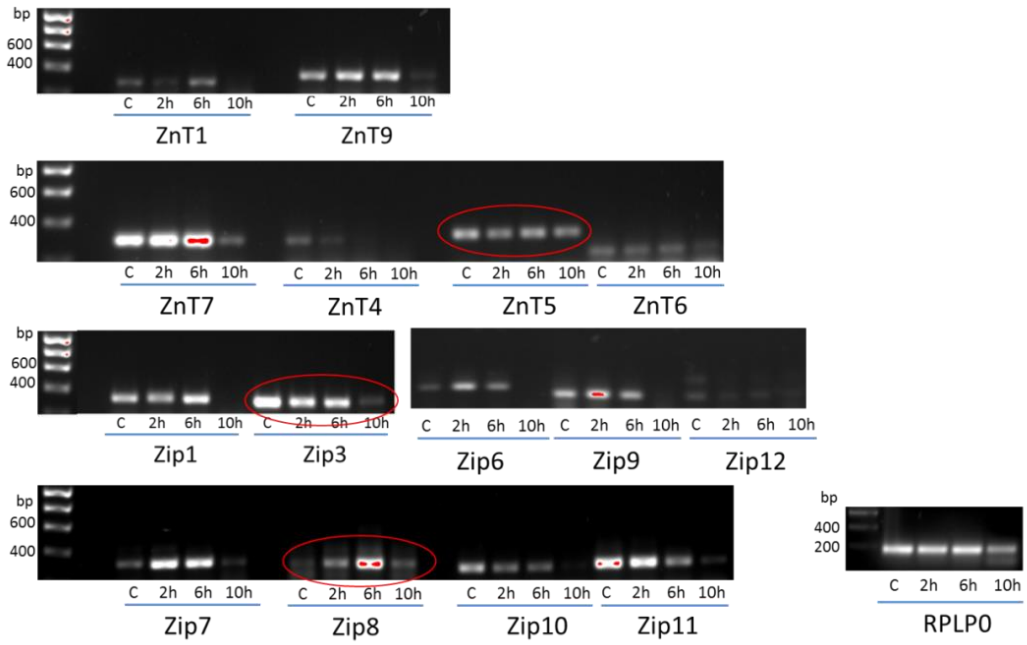

Figure 2.2. Bacterial LPS alteration of zinc transporters in moDCs is time dependent. Cells were cultured with LPS in the concentration of 100 ng/ml over 10 h with sampling done after 2, 6 and 10 h and without the addition of LPS as a control (C). The expression of almost all of the zinc transporters (both Zips and ZnTs) is decreasing gradually over time with only two zinc importers and one exporter (circled in red) being expressed after 10 h of LPS treatment.

The significant changes in zinc transporter expression observed between 6-10 h suggest this period to be crucial for DC functioning and may represent the point at which DCs migrate in the lymphatic system (Alloatti et al., 2016). It is also very interesting to know if there are other significant alterations in mRNA transcript encoding for zinc transporters after 10 h post- LPS stimulation. Most of the zinc transporters assessed are present on both, cell membrane and membrane of cytoplasmic vesicles. It is therefore impossible to bring any conclusions about the compartmental movement of zinc during dendritic cell maturation, migration, and antigen presentation based solely on obtained results. To confirm previous findings and gain more insight into particular transporters, quantitative PCR (qPCR) was used. For this study, two zinc importers (Zip6 and Zip7) and two zinc exporters (ZnT1 and ZnT7) were chosen. Zip6 is present on the cell membrane and thus transports zinc from the extracellular space into the cytosol. ZnT1 is also present on the cell membrane but maintains the transport of zinc in the opposite direction. Zip7 and ZnT7 are both located on intracellular organelles and cytoplasmic vesicles, where ZnT7 transports zinc into the storage, and Zip7 releases zinc from endoplasmic reticulum (ER) into the cytoplasm. It was important that for more detailed studies, transporters located on either cell membrane or intracellular membranes were assessed.

Mature monocyte-derived DCs were prepared and treated with 100 μg/ml of bacterial LPS, for up to 72 h. LPS-induced alterations in zinc transporter expression and the significant changes observed may indicate crucial period for DC function. Because of very high sensitivity of qPCR, careful design is crucial in this approach. All primers pairs used were designed to be located on separate exons, to prevent amplification of genomic DNA. Primers efficiency was calculated using standard amplification curve for 10-fold serial dilution of DNA. Efficiencies for all primer pairs were above 90%, except for ZnT7 with 75% and β-actin with 89% efficiency, with R2> 0.99 (Table 2.3).

The expression of mRNA transcripts encoding ZnT1 and ZnT7 were significantly upregulated after 12 h. For ZnT1, expression reached a 4-fold increase after 24 h and then a gradual decrease in expression was observed up to 72 h post-LPS stimulation (Fig. 2.3 A). For ZnT7, a 2 to 3-fold increase (relative to control) was prolonged with no significant changes between 24 h and 72 h (Fig. 2.3 B). In general, changes in mRNA expression of Zip transporters achieved 1.5-fold increases. Zip6 transporter after 6 h post LPS treatment, mRNA expression decrease and then steadily increase up to 48 h (Fig. 2.3 C). There was a slight increase in the expression of Zip7 24 h post-LPS treatment and the effect is prolonged up to 72 h (Fig. 2.3 D).

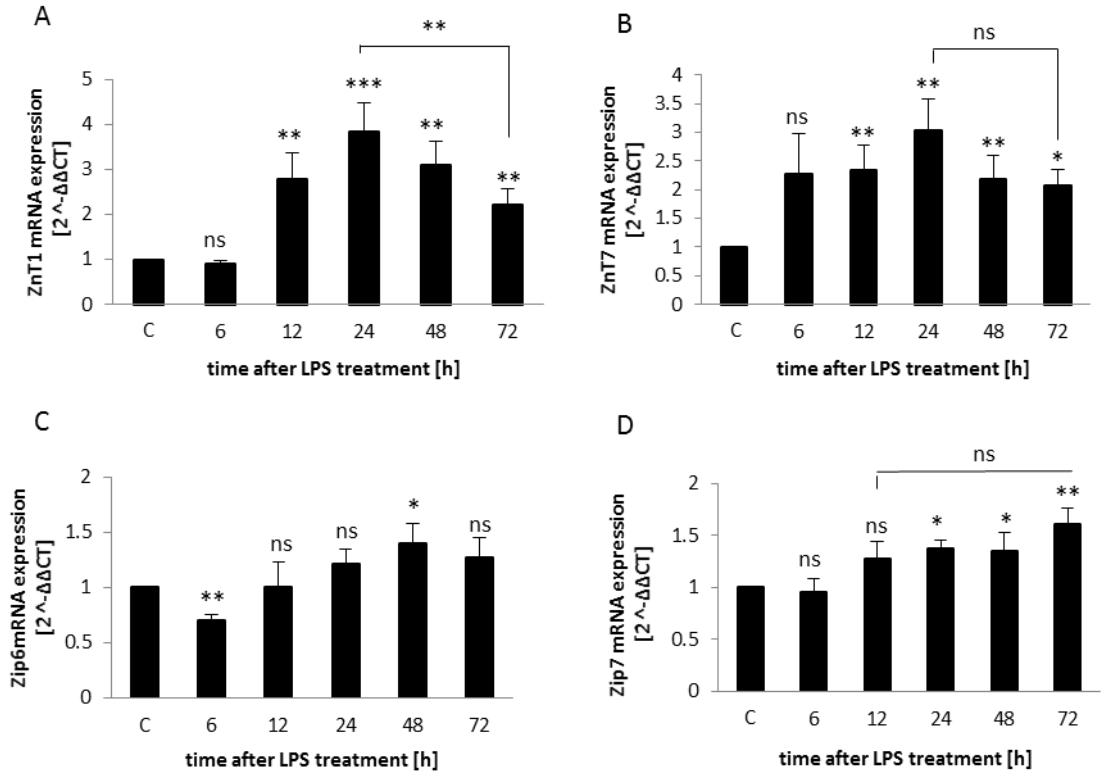

Figure 2.3. LPS-induced alterations in zinc transporter expression. Real-time PCR of the relative amounts of mRNA transcripts encoding various zinc transporters (vertical axes) left untreated or treated for up to 72h with LPS. All results were normalised to the amount of two housekeeping genes, β-actin and RPLP0. Results are the average ± SD of six independent experiments. $p>0.05$ (ns), $p\leq0.05$ (*), $p\leq0.01$ (**), $p\leq0.001$ (***).

Zip proteins transport zinc into the cytoplasm (Zip6 from the extracellular space and Zip7 from the intracellular vesicles) and ZnT proteins act as zinc exporters (ZnT1) or move zinc to storage vesicles (ZnT7). Given the observed differences in the expression of Zips and ZnTs, these results suggest that stimulation of TLR4 causes dramatic movement of zinc out of the cytoplasm (Fig. 2.3). It also showed that in response to LPS stimulation, the message for ZnT7 production increases prior to ZnT1. This indicates that zinc is firstly transported into the storage vesicles and then the excess is removed to the extracellular space.

2.3.2.2. Alterations in protein expression

To determine whether alterations in mRNA levels are translated to protein production, Near Infrared (NIR) western blot with fluorophore-linked, secondary antibodies was performed on

cells lysates from moDC. This method allows detection of two different targets on the same blot, which allows normalisation against an internal control without stripping and re-probing of the blots. Cells were prepared exactly as described previously and treated for 72 h with bacterial LPS followed by cell lysis and protein quantification. To examine alterations in protein expression caused by LPS-mediated TLR4 activation, NIR western blot of four zinc transporters (ZnT1, ZnT7, Zip6 and Zip7) and the TLR4 receptor were performed. Additionally, a NIR western blot probing for Zip7 in its phosphorylated state was also carried out. This was particularly important as zinc transporters are activated through phosphorylation.

Cell lysates from three independent biological repeats were prepared in the same way as previously described. Each membrane was incubated simultaneously with antibody against one of the zinc transporters (or antibody against TLR4) and anti-β-actin as a control (Fig. 2.4). Bi-colour detection with near infrared fluorescence, IRDye® secondary antibodies were used. Generally, this approach gave very reliable results although some non-specific binding (as indicated by the presence of extra bands) was observed when probing with anti-Zip6 and anti-phospho-Zip7 antibodies. The anti-phospho-Zip7 antibody revealed protein bands of distinct sizes (Fig. 2.4 F). The upper band is the phosphorylated Zip7 (Taylor et al. 2008). The lower band however is of very similar size to the band shown for total Zip7 protein as can be compared with Fig. 2.4 E. Two of the blots (for ZnT7 (Fig. 2.4 C, D) and Zip6 (Fig. 2.4 G, H)) are presented as two figures, control and target separately, as the band sizes for both target and control proteins are very similar and would overlap on one image.

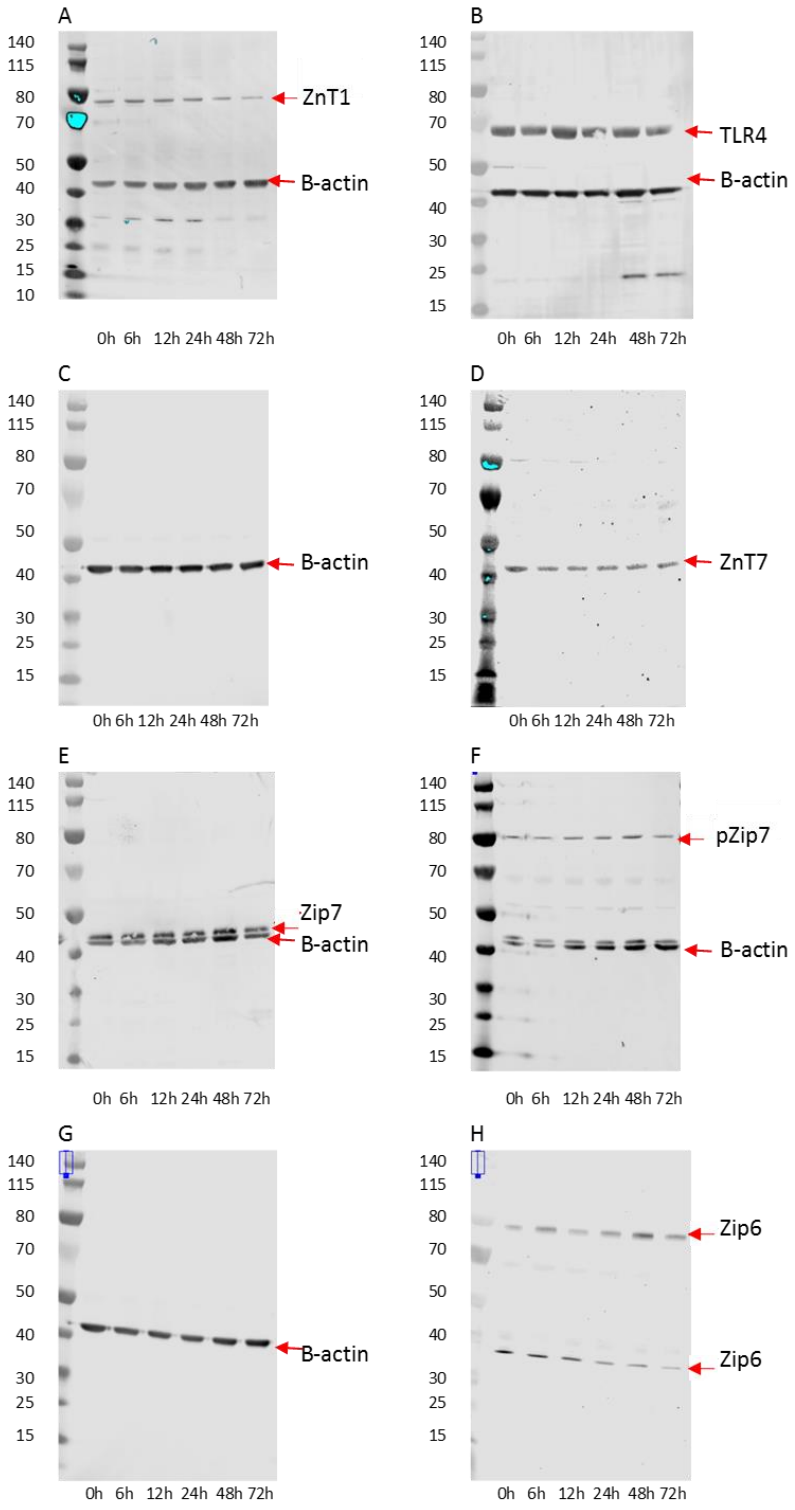

Figure 2.4. NIR Western blot analysis of LPS-induced alterations in zinc transporter expression and TLR4 receptor. Dendritic cells were treated with LPS for up to 72 h. Each membrane was incubated subsequently with target antibody and antibody against β-actin control. Images C and D, and G and H represent the same membrane. Two secondary antibodies labelled with

spectrally distinct NIR fluorescent dyes were used. Here shown in greyscale. Results are the representative images for three independent experiments.

The Odyssey imaging system has internal software, which allows quantitative analysis of NIR western blots. The expression of target protein was normalised to the expression of the β-actin control, for each probed western blot membrane. The results were then plotted using Microsoft Excel. Results are presented in arbitrary units and represent protein alterations of analysed zinc transporters (Fig. 2.5). The expression patterns differed between the transporters. Expression of ZnT1 increased slightly after 6 h and then gradually decreased up to 72 h, with the largest changes observed after 24 h post LPS stimulation (Fig. 2.5 A). The expression of ZnT7 transporter decreased after the first 6 h of the experiment then remained stable until 12 h, followed by slight decrease up to 24 h. Due to considerable variation between replicates, it is hard to say whether the expression of ZnT7 changed at 48 h of experiment. Nonetheless, when compared to the 24 h time point, increased expression of ZnT7 at 72 h was observed (Fig. 2.5 B). The protein level of the Zip6 transporter appeared stable over the first 12 h post-LPS treatment. Then a decrease in the expression was observed at 24 h, followed by gradual increase at the 72 h time point (Fig. 2.5 E).

For Zip7, a gradual decrease in expression at the protein level was observed had almost halved (relative to the initial protein amount) at 24 h post-LPS treatment (Fig. 2.5 C). In addition, this transporter exhibited maximum phosphorylation at 6 h. A degree of dephosphorylation then occurs (observed at 12 h post-LPS treatment) and the level of phosphorylated protein stabilises until 72 h (Fig. 2.5 D). It is worth highlighting that Zip7 is located on the membrane of storage vesicles and transports zinc into the cytoplasm. Therefore, the Western blot results reveal that at 6 h post-LPS stimulation, the transport of zinc into storage vesicles was likely favoured as phosphorylation activates Zip7. Given that LPS is a ligand for TLR4 and the alterations in zinc transporters expression are a result of TLR4 signalling, it was important to check the expression of TLR4 itself over the course of the experiment (Fig. 2.5 F). Western blotting revealed that the expression of this receptor gradually increases up to 12 h and then fluctuates by increasing and decreasing every 24 h. Those fluctuations might mean that cells try to maintain the amount of receptor on stable level.

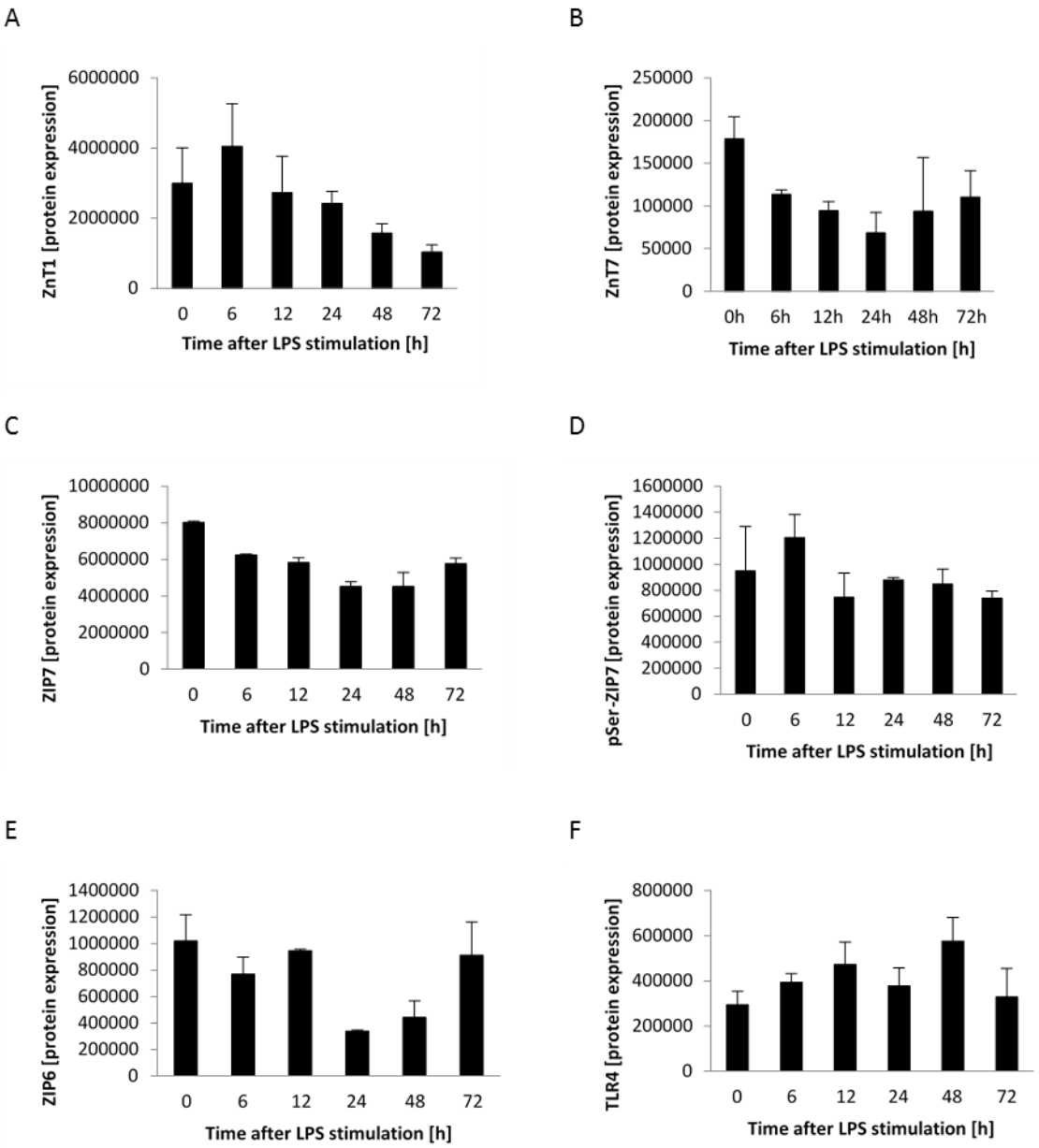

Figure 2.5. LPS-induced alterations in zinc transporter expression. NIR Western blot analysis of various zinc transporters and TLR4 receptor left untreated or treated for up to 72h with LPS. Results were normalised to the amount of β-actin. Results are the mean ± S.D. based upon three independent experiments.

To help confirm the western blot findings and to gain more insight into TLR4-mediated regulation of zinc transporter expression (and additionally to look at the cellular localisation of chosen zinc transporters), immunofluorescence microscopy and flow cytometry were used. As

shown by immunoblotting (Fig. 2.5), the most significant changes in transporters expression occurred after 24 h post-LPS stimulation. Therefore, for further experiments only the 24 h time point versus untreated control were compared.

For IF imaging moDCs were grown on microscopy cover slips for 24 h following addition of bacterial LPS. The transporters were detected using primary antibodies against zinc transporters combined by matching secondary Alexa Fluor antibodies and images taken under x20 magnification. Images of treated and untreated sample for each transporter were taken with the same microscopy and camera settings. The general observation showed that the protein expression of all zinc transporters decreased after 24 h of LPS treatment (Fig. 2.6 A). It has previously been suggested that ZnT1 is localised exclusively on the cell membrane (Schweigel-Röntgen, 2014). However, on the microscopy images it was visible in the cytosol and was particularly evident in this location after LPS treatment. Moreover, its localisation looked granular in appearance and therefore could represent its presence on vesicles. This may suggest that TLR4 signalling causes the main zinc exporter to internalize. Also the expression of ZnT1 decreased after LPS-stimulation compared to the control. Cellular localisation of another zinc exporter, ZnT7 did not change upon treatment but the expression level decreased. Also expression of Zip6, which is thought to remove zinc from intracellular organelles to the cytoplasm, decreases but its subcellular localisation does not change. There were no changes in expression of TLR4 observed (Fig. 2.6 A). Collectively, these data are in agreement with western blot results.

To support IF imaging data, and to assess the alterations in zinc transporters expression in a quantitative manner, flow cytometry was used. Cells were grown and prepared as described above, and treated with LPS for 24 h. After the incubation with primary and matching secondary antibodies, the fluorescence (representative of 5,000 cells per sample) was measured. The results are expressed as a percentage relative to the untreated control and revealed alterations in the protein expression of analysed zinc transporters. The findings were consistent with IF data and WB data (Fig. 2.6 B). The results from both fluorescent microscopy and flow cytometry showed decreases in protein expression of ZnT1, ZnT7 and Zip6 transporters after 24 h post-LPS treatment (Fig. 2.6). Those findings were consistent with previous western blotting results. Expression of TLR4 receptor did not change after 24 h relative to the untreated control (Fig. 2.6). However, when there were more time points (Fig. 2.5 F), fluctuations in expression were observed every 24 h after the initial 12 h of expression increase.

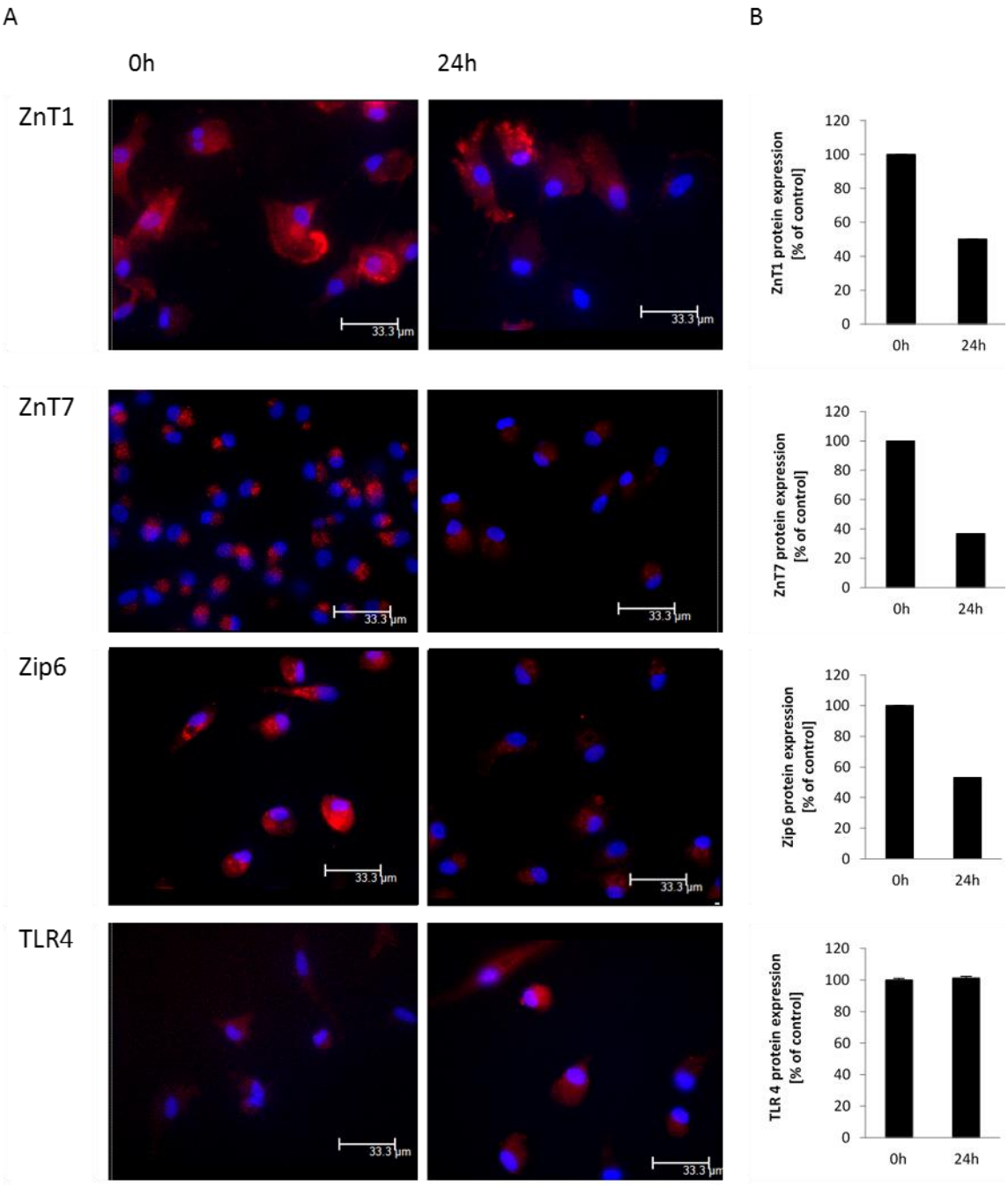

Figure 2.6. LPS-induced changes in the expression of zinc transporters in DCs. Fluorescent microscopy imaging of zinc transporters distribution inside moDC (A) and flow cytometry of zinc transporters, detected with Alexa Fluor® 594 dye (B), in DCs left untreated (as a control) or treated for 24 h with LPS.

2.3.2.3. Phosphorylation of Zip 7 transporter

No commercial phospho-protein antibodies are available for zinc transporters. However, a phospho-Zip7 directed antibody was obtained as a gift from Dr Kathryn Taylor (Cardiff University). It allowed to perform not only western blot analysis of Zip7 transporter levels in the phosphorylated state compared to the total Zip7 (Fig. 2.4; 2.5), but also to examine the cellular localization of the phosphorylated form of the Zip7 transporter (Fig. 2.7) and to perform quantitative analysis of the phosphorylation level (Fig. 2.8).

Reversible phosphorylation plays a significant regulatory role in many cellular processes, by altering the conformational state of a protein to activate or inhibit its function. The activation of Zip7 occurs via its phosphorylation by protein kinase CK2 (Taylor et al., 2012). As a result, activated Zip7 releases zinc from endoplasmic reticulum (ER) into the cytoplasm. Phosphorylation and therefore activation of the zinc transporter Zip7, can give an important insight into zinc homeostasis of dendritic cells. MoDCs were cultured on microscopy cover slips with the addition of bacterial LPS for 12 or 24 h. Transporters were detected using bi-color staining with Alexa Fluor antibodies of distinct absorbance. Images were obtained under 100x magnification with oil immersion.

The IF images reveal co-localization of phosphorylated and total Zip7 transporters (Fig. 2.7), therefore for this particular transporter phosphorylation does not change the localization of the protein. The level of phosphorylation of Zip7 was low in the untreated control (Fig. 2.7; 0 h). After 12 h of LPS stimulation, phosphorylation increased and then at 24 h the level of phosphorylation decreased but did not reach the initial level (Fig. 2.7). For more quantitative measurement of the Zip7 transporter phosphorylation, flow cytometry was employed. Cells were grown and prepared as previously but treated with LPS for up to 72 h. After LPS treatment, cells were stained with either Zip7 or phospho-Zip7 antibody at a time. Results are presented as the expression of phosphorylated Zip7 and total Zip7 (Fig. 2.8) presented in arbitrary units (Fig. 2.8).

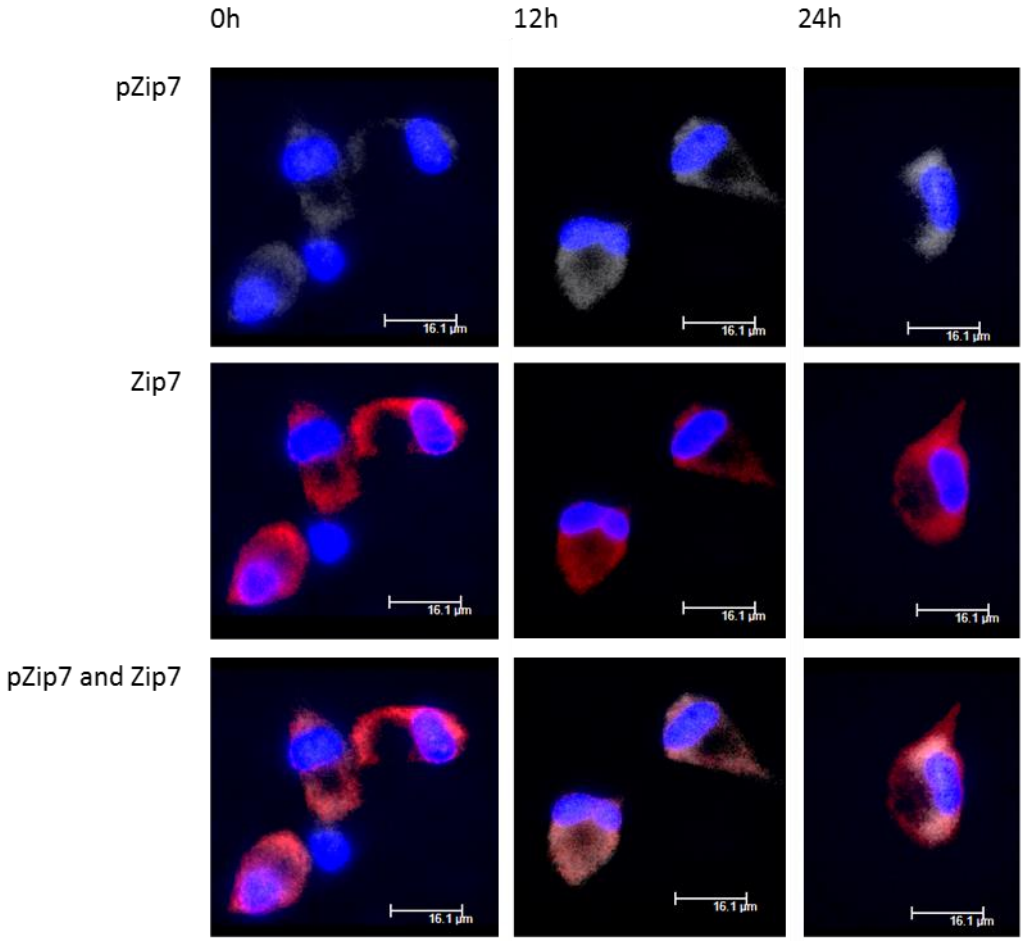

Figure 2.7. Fluorescent microscopy imaging of total Zip7 (red) and Zip7 in the phosphorylated state (white) in MoDCs. Cells were treated with LPS for 24 h. Signal was detected with Alexa Fluor® 594 (red) and Alexa Fluor® 647 (white) conjugate.

Flow cytometry data suggests that TLR4 signalling activates the Zip7 transporter. The highest phosphorylation is present after 12 h of LPS treatment with more than 50% of total protein phosphorylated. Zip7 remained phosphorylated until 48 h of the LPS treatment. After 72 h de-phosphorylation occurred.

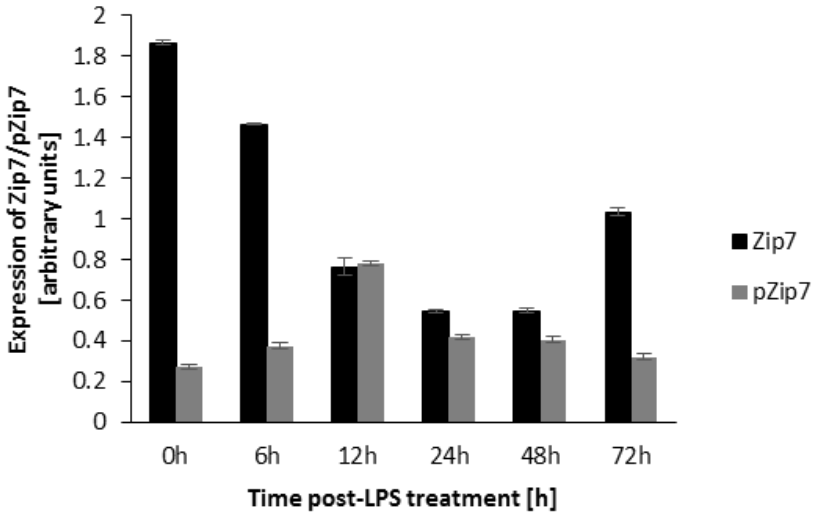

Figure 2.8. Phosphorylation of Zip7 transporter induced by LPS stimulation over 72 h. Expression of phosphorylated Zip7 and total Zip7 transporter, presented in arbitrary units.

2.3.3. Toll-like receptor 4-mediated alteration in intracellular zinc level in DCs

It has been postulated by Kitamura and colleagues (Kitamura et al., 2006), that alterations in zinc transporters expression caused by LPS-mediated stimulation of the TLR4 receptor result in a decrease in the free zinc concentrations in DCs. However, in that study expression was only examined for 6 h after LPS stimulation. In addition, the zinc probe used in this study was Newport green (also known as dichlorofluorescein, DCF). This fluorescent probe is zinc-specific but has only moderate zinc-binding affinity (Kd for Zn^{2+} is around 1 µM; DCF-N7991; Thermo Fisher Scientific). It is therefore not in a suitable range to detect intracellular free zinc concentrations, which are in the low nanomolar range (Maret, 2015). To gain a better insight into the alteration in zinc transporters expression pertaining to zinc homeostasis during moDCs maturation, current examination extends the Kitamura et al. study to 72 h post LPS-stimulation. To investigate the relationship between TLR4 signalling and the abundance of intracellular zinc fluorescent microscopy and flow cytometry with zinc probe ZnAF-2F DA were used.

Cells were prepared and treated with LPS as described before and stained with ZnAF-2F DA. This fluorophore permeates the cell membranes of living cells and is then hydrolysed in the cytosol, such that it is then retained in the cell. ZnAF-2F DA was chosen because of its high affinity for

zinc. The levels of intracellular labile zinc (free or loosely bound zinc) in most of the cells are in the nanomolar range. Most of the available fluorescent zinc probes have dissociation constant (K_d) values for zinc in micromolar range, including Newport Green (K_d = 1 µM) and Fluozin (K_d = 2 µM). In contrast, the K_d of ZnAF-2F DA for zinc is 5.5 nM, which affords sufficient sensitivity for biological applications. Additionally, ZnAF-2F DA is highly selective for zinc as it does not fluoresce in the presence of high concentrations of other biologically important cations including 5 mM Ca^{2+}, Mg^{2+}, Na^{+} or K^{+} or 1 µM Cu^{2+} or Fe^{2+} (Hirano et al., 2002).

Monocytes are adherent cells and attach to culture dish after approximately 1 h of culture. Nevertheless, when kept in culture for more than 24 h mature moDCs can detach from the surface. The process can be observed in the presented microscopy images (Fig. 2.9).

The results showed that upon LPS treatment, the amount of zinc decreased (Fig. 2.9) at 2 h post LPS treatment and then remained stable until 72 h of LPS stimulation. Controls, cells not stained, showed no fluorescence at 488 nm wavelength (data not shown).

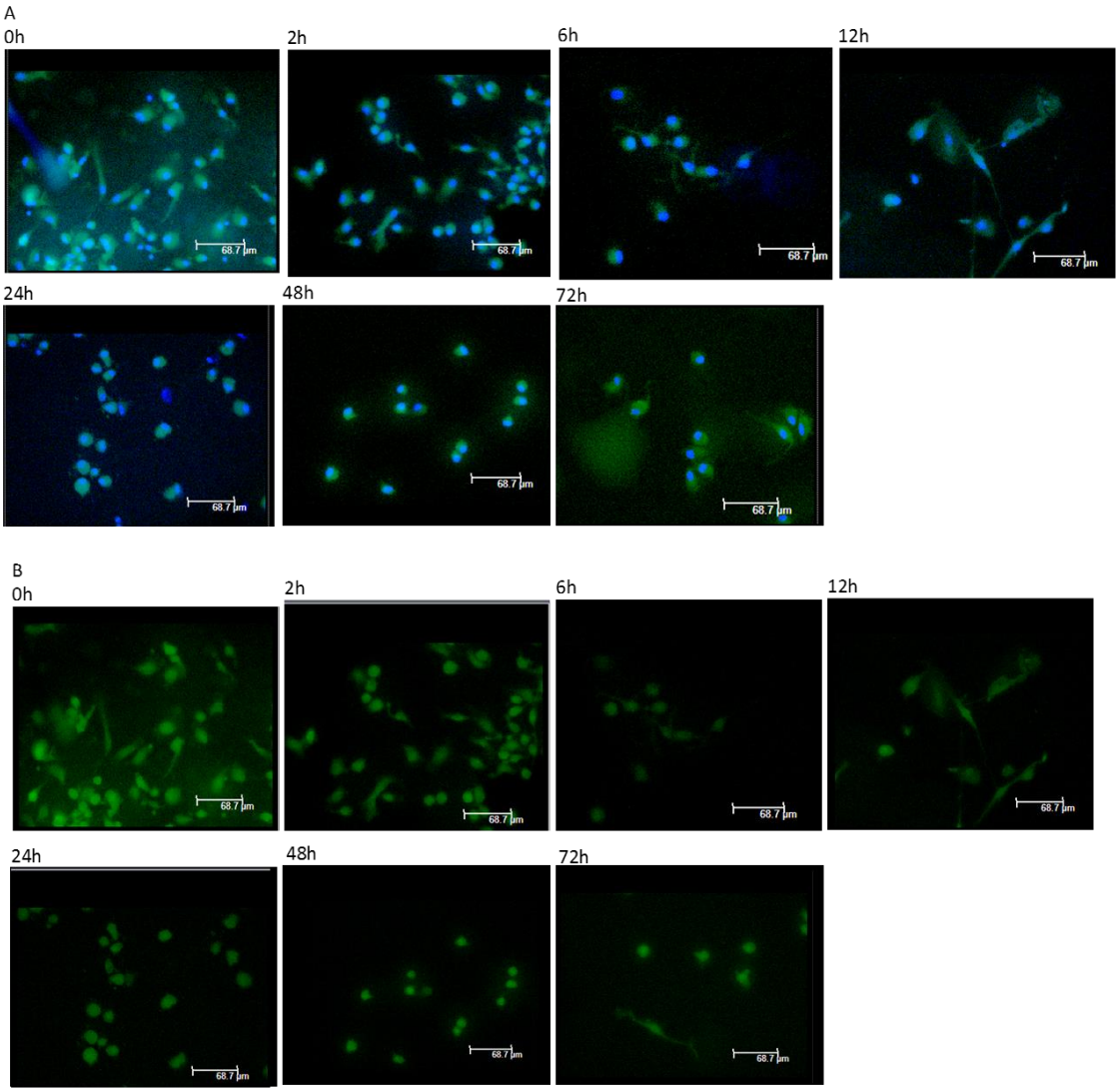

Figure 2.9. Fluorescent microscopy imaging of zinc distribution inside dendritic cell. MoDC were treated with LPS over 72h and incubated with ZnAF-2F DA (AdipoGen) - membrane permeable zinc fluorophore prior fixation. (A) Cells stained with ZnAF-2F DA (green) and DAPI (blue), (B) cells stained with ZnAF-2F DA only. Images were taken under x 20 magnification. Scale bar represent 68.7 µm.

To support IF results, showing LPS induced zinc alterations in moDC, flow cytometry was used. To make the results comparable to IF studies, the same zinc fluorophore, ZnAF-2F DA was used, as its λem = 515 nm made it suitable for both methods. Prior to staining, cells were trypsynised and transferred to round bottom 96-well plates, suitable for flow cytometry. To set up threshold, unstained, untreated cells were used. For each sample, fluorescent signal of 5000 cells was

measured. Results are present in a logarithmic scale of arbitrary units, showing changes in green fluorescence (Fig. 2.10). Minor fluctuations in the levels of zinc can be observed throughout the LPS treatment. These findings are consistent with IF data, which also showed no major alterations in intracellular, zinc in moDCs, caused by TLR4 signalling (Fig. 2.9).

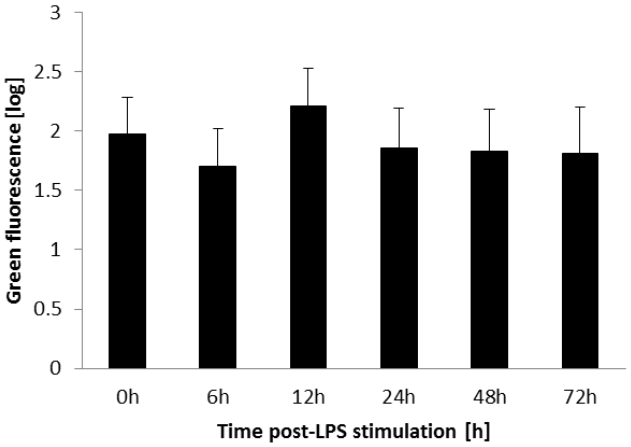

Figure 2.10. Flow cytometry of intracellular free zinc, detected with ZnAF- 2F DA, in DCs left untreated or treated for up to 72 h with LPS.

2.3.4. The effect of LPS and hydroxyapatite on TNF-α secretion by moDC

TLRs are localised on either the cell membrane or intracellular compartments. The isoforms known to be localised on the cell surface are TLR1, TLR2, TLR4, TLR5 and TLR6, which mainly recognise bacterial products such as LPS. Some non-bacterial particles can also be recognised by TLRs. These include the mineral, hydroxyapatite (HAP) which is a ligand for TLR4 and at least one more TLR (Velard et al., 2013). Following activation, TLRs activate signalling pathways that induce the production of chemokines, co-stimulatory molecules, and cytokines including TNF-α. Specifically, TLR4, after binding its ligand undergoes conformational changes that initiate MyD88 signalling pathway. This triggers the activation of a downstream pathway that results in translocation of nuclear factor κB (NF-κB) from the cytoplasm to the nucleus and finally production of pro-inflammatory cytokines including TNF-α.

Mature dendritic cells are known to secrete TNF-α through TLR4 signalling. However, the reaction of dendritic cells to HAP stimulation is not known. To gain insight into the role of HAP in TLR4 signalling in moDCs, and to confirm moDC functionality, aliquots of supernatants were analysed by ELISA for the expression of TNF- α. ELISA kit used had a very high sensitivity of 1.7

pg/mL. MoDCs were grown with the addition of LPS for up to 72h. Media was then collected and secreted TNF-α concentrations measured. The maximum TNF-α secretion detected in the supernatant of mature DCs was 7 ng/ml (Fig. 2.11 A), which was observed at 12 h after LPS stimulation. This was followed by a gradual decrease at 48 h, lowering to almost 50% of the maximum value, and then increasing again after this time point. In the experiment, two controls were used. The first one was the culture of moDCs without the addition of LPS to control for any compounds found in the culture media that may trigger a response from DCs. The second control was RPMI media supplemented with 10% FCS.

The secretion of TNF-α by moDCs upon HAP stimulation was also examined (Fig. 2.11 B). Differentiated moDCs were grown in the presence of sterile HAP powder for 24 h at the variety of concentrations. After stimulation, the cell culture media was collected and TNF-α concentrations were measured. It was found that HAP does initiate an immune response from moDCs (as indicated by an increase in TNF-α secretion). However, secreted TNF-α levels were generally lower from cells treated with HAP compared to LPS-activated cells, with the peak of 350 pg/ml (at 5 mg of HAP per ml of media). With higher concentrations of HAP, TNF- α secretion becomes lower again and at 20 mg/ml of HAP almost reached the level of TNF-α secretion of an untreated control. Cells untreated with HAP were used as a control and showed 200 pg/ml TNF-α secretion. This would suggest that even though HAP can activate DCs, the response is not as strong as with LPS (Fig. 2.11 B).

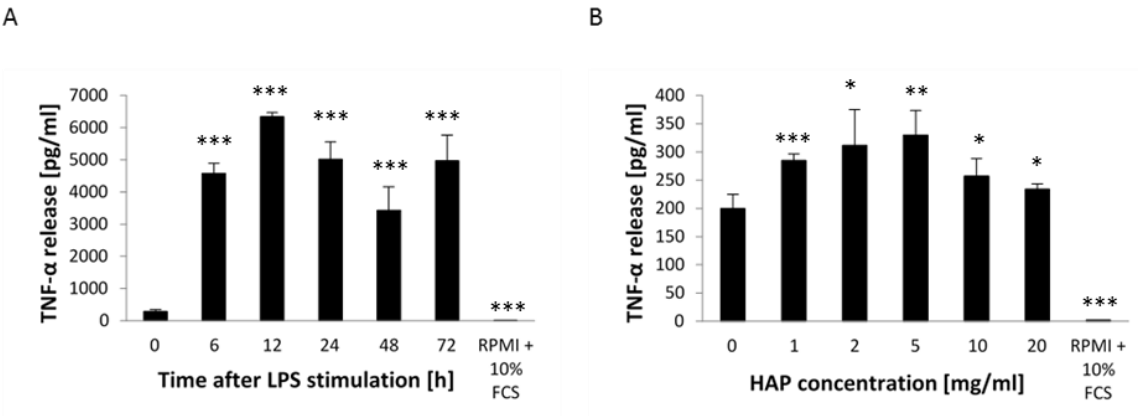

Figure 2.11. TNF-α release from moDCs following stimulation with LPS and HAP. MoDCs were cultured in RPMI media supplemented 10% FCS. Next cells were stimulated with 100 µg/ml of bacterial LPS for up to 72 h (A) or with hydroxyapatite nanopowder for 24 h (B) and TNF-α secretion was measured using Human TNF-α ELISA Kit (Life Technologies). p≤0.05 (*), p≤0.01 (**), p≤0.001 (***).

2.4 Discussion

2.4.1. Morphological characteristic of moDC

DCs can be directly purified from blood; however, their number is very low at just 0.02-0.06 x 10^6 cells/ml of blood. DCs can be also generated *in vitro* by culturing CD14+ monocytes (Soo et al., 2012) or CD34+ bone marrow cells (Tan et al., 2010), with the addition of GM-CSF and IL-4. Obtained immature DCs can be then stimulated with antigen to induce maturation. Upon maturation, DCs undergo morphological and functional changes, including development of extensive cytoplasmic projections in many directions from the cell body. Additional characteristics of mature moDCs are the presence of MHC class II and co-stimulatory molecules, including CD40, CD80 and CD86 (Reis e Sousa, 2006), as demonstrated through immunophenotyping using flow cytometry.

The DCs used in this chapter were generated from peripheral blood monocytes. Great care was taken during cell preparation to maintain cell structure. Therefore, cells were grown directly on microscopy coverslips, as attaching cells to the microscopy slide by centrifugation (cytospin) could cause severe damage. Microscopy imaging in both bright field and using fluorescence antibodies revealed the abundance of characteristic cytoplasmic projections upon LPS-induced maturation. Cells were prepared using a well-established protocol (Soo et al., 2012), therefore, no further characterisation (immunophenotyping) was done.

2.4.2. Zinc homeostasis in moDC upon LPS stimulation

Zinc deficiency causes defects in cellular immunity. Therefore, it is crucial to establish the link between zinc homeostasis and dendritic cells function. One of the components of a network that build zinc homeostasis are Zip and ZnT transporters. A study by Kitamura et. al. (2006) demonstrated that in dendritic cells (DC), stimulation by bacterial LPS induced significant alterations in the expression of zinc transporters. In this study, expression was assessed up to 6 hours after LPS stimulation. The main aim of the current study was to confirm these results and extend the timescale of experiment beyond 6 hours post-LPS stimulation. Therefore, mature monocyte-derived DCs were treated with 100 ng/µl of bacterial LPS for up to 72 h. The presented data show that LPS-induced alterations in zinc transporters expression maintain stable level of intracellular free zinc.

Stimulation of moDCs with bacterial LPS caused significant changes in zinc transporters expression observed for both mRNA transcripts and protein. Firstly, the expression of mRNA transcripts encoding for six ZnT (1, 4, 5, 6, 7, 9) and nine Zip (1, 3, 6, 7, 8, 9, 10, 11, 12) transporters was verified, until 10 h of LPS induced maturation. Changes in expression differed between the transporters. For ZnT4, Zip3, Zip10, and Zip11 the expression reduced gradually until 10 h post-LPS treatment. ZnT1, ZnT7, ZnT9, Zip1, and Zip8 mRNA expression increased after 6 h of maturation, and then decreased between 6-10 h. Zip6 and Zip7 exhibited an abrupt increase in expression after treatment with the peak at 2-6 h. Interestingly, LPS treatment did not alter the expression of ZnT5, ZnT6 and Zip12.

These findings are extremely interesting in the context of a study done by Kitamura et al. (2006). According to Kitamura (2006), expression of Zip6 slightly decreases, and expression of Zip10 is not altered after 6 h of LPS treatment. Though those findings are consistent with current results, the most interesting observations start beyond the 6 h time point where the expression of not only Zip6 and Zip10, but also Zip1 and Zip9 decreased almost to the basal level. Published results also suggest reduction in ZnT1, ZnT4 and ZnT6 mRNA expression after 6 h of treatment (Kitamura et al., 2006). The results obtained demonstrate that while expression of ZnT4 decreases over time, expression of ZnT6 does not change. Also ZnT1 expression was found to increase over 6 h and then decrease.

To gain more insight into the role of transporters in zinc homeostasis during DC maturation, quantitative PCR (qPCR) was used. For this study, two zinc importers (Zip6 and Zip7) and two zinc exporters (ZnT1 and ZnT7) were chosen. Zip6 is present on the cell membrane and thus transports zinc from the extracellular space into the cytosol. ZnT1 is also present on the cell membrane but maintains the transport of zinc in the opposite direction. Zip7 and ZnT7 are both located on intracellular organelles and cytoplasmic vesicles, where ZnT7 transports zinc into the storage, and Zip7 releases zinc from endoplasmic reticulum (ER) into the cytoplasm. It was important that for detailed study of zinc in moDC maturation, transporters either located on the cell membrane or on intracellular membranes were characterised.

The expression of mRNA transcripts encoding for Zip7 increased by ~0.25-fold at 24 h post-LPS stimulation. The expression of mRNA transcripts encoding for Zip6 decreased by 0.2-fold at 6 h, and then increased by 0.5-fold at 24 h and stabilised. The mRNA expression of ZnT transporters (ZnT1 and ZnT7) also increased, but the changes were more rapid and significant than for zinc

importers, and appeared after 12 h of LPS treatment (3-fold for ZnT1 and 2.5-fold for ZnT7). Additionally, the mRNA expression of zinc exporters decreased gradually until 72h.

The results of protein expression studies surprisingly did not mirror those observed in the gene expression studies. The expression of zinc exporters at the protein level gradually decreased until to 72h of LPS stimulation, when compared to the untreated control. The expression of Zip6 decreased dramatically after 24 h, but then slowly recovered. In contrast, the expression of Zip7 did not change, but the phosphorylation occurred after 12 h of LPS stimulation.

The biological explanation of this observation is not immediately obvious, however, chosen time points are highly likely to replicate the period of *in vivo* post-LPS stimulation (i.e. exposure to a pathogen) when the DC processes the antigen, leaves the site of pathogen exposure and reaches the lymph nodes to initiate an immune response. Immature DCs are located in non-lymphoid tissues, where they permanently explore the presence of microorganisms or bacteria products. As soon as DCs recognise the pathogen, they undergo a complex process termed “maturation”, which changes their morphology and function to enhance the ability of antigen uptake and processing (Granucci et al., 1999; Reis e Sousa, 2006). During these developmental changes, the expression of MHC class II and co-stimulatory molecules, including CD40, CD80, and CD86 increases. In addition, the secretion of inflammatory cytokines and chemokines is also increased (Reis e Sousa, 2006). The whole process of DC maturation can be divided into three main phases: early maturation (0-6 h of stimulation), maturing DCs (7-18 h of stimulation), and fully mature DCs (over 18 h of stimulation; Alloatti et al., 2016). The early maturation of DCs starts after an antigen is recognised through PRRs, such as TLRs. Antigens can be either pathogen- or damage-associated molecular pattern molecules, and include bacterial LPS, which is a ligand for TLR4. During the early phase of maturation, an antigen is taken up by DCs. In the next phase, antigen uptake and the ability to degrade and process antigens is decreased in order to preserve the antigen for processing in the lymph node. Throughout the process of maturation, DCs travel to the lymph nodes. Fully mature DCs present the antigen to CD4+, but the process of cross-presentation of newly acquired antigens to CD8+ T-cells is downregulated. It is estimated that after 40 h of antigen stimulation, the ability of the cell to present antigen ends or is at least very circumscribed (Alloatti et al., 2016; Reis e Sousa, 2006).

There is a growing evidence that following activation, zinc acts as a second messenger to trigger the activation of dendritic cells through MyD88 or TRIF signalling pathways (Kitamura et al., 2006; Brieger et al., 2013; Haase et al., 2008). MyD88 is the early signalling pathway, where zinc

acts as phosphatase inhibitor, resulting in the production of inflammatory cytokines. Later, TRIF dependent signalling causes the secretion of IFN-β and expression of surface molecules that together are required for T-cell activation during antigen presentation (Brieger et al., 2013). Current findings support this observation, as the data now shows that intracellular zinc levels are not changing during the whole process of antigen recognition, uptake, and processing. One of the mechanisms to ensure sufficient zinc level in the cytoplasm is its release from ER storage, through Zip7 transporter.

Zip7 is an exception amongst zinc transporters. It is ubiquitously expressed among organisms, including orthologues in *Drosophila* (CATSUP) and *Arabidopsis* (IAR1; Taylor and Nicholson, 2003; Stathakis et al., 1999); and among cell types (Taylor et al., 2004). Studies on the variety of cell types, including erythroleukemia cells, lung fibroblasts and mammary epithelial cells, showed that Zip7 subcellular localisation is limited to the membrane of the Golgi or endoplasmic reticulum (ER), or both (Kambe, 2011; Huang et al., 2005). Its gene expression and cellular localization are not affected by the alterations in zinc levels. Nonetheless, elevated zinc levels can extinguish Zip7 protein translation (Huang et al., 2005).

Zip7 has multiple functions. Activation of Zip7 is essential for the release of zinc from the ER, and initiates the signalling cascade, which promotes cell proliferation (Taylor, 2008; Taylor 2008b). Additional functions include zinc-mediated inactivation of protein phosphatases, which results in the activation of tyrosine kinases (Hogstrand et al., 2009).

As demonstrated with the prokaryotic Zip homologue ZipB, Zip transporters act as ion channels (Hogstrand et al., 2009). The mechanisms that regulates zinc transport are not entirely clear; however, Zip7 (and other Zips) are known to be activated (at least in part) by phosphorylation. There is multiple evidence to support this concept, including presence of phosphorylation sites and MAPK-binding motifs located on the cytoplasmic site of the Zip7 transporter (Hogstrand et al., 2009). Gated release of zinc from the ER has been observed after phosphorylation of Zip7 by protein kinase CK2. As a result, released zinc activates tyrosine kinase, which leads to the phosphorylation of AKT and kinases 1 and 2 (ERK1/2) (Taylor et al., 2012).

The presented data suggest that zinc homeostatic control is an important part of the antigen presentation process. The later time points (>6 h) are likely to correspond to the period in vivo post-LPS stimulation (i.e. exposure to a pathogen) when the DC has left the site of pathogen exposure and is migrating to a local lymph node to initiate an immune response. Collectively, the findings help to build a more complete picture of the behaviour of Zip and ZnT transporters

that occurs during this crucial period for DCs. Additionally, presented data now implicate zinc homeostasis as important in this process and provides a strong background for future functional studies of zinc and DCs in the immune system in health and disease.

2.4.3. HAP and LPS induced TNF-α secretion

The presented data show that HAP can induce the secretion of pro-inflammatory cytokines by DCs, however to a lesser extent than LPS. Calcium phosphate biomaterial particles, typically HAP or beta-tricalcium phosphate (b-TCP), are known to trigger an immune response (Velard et al., 2013) in a number of immune cells studied, including monocytes, macrophages and fibroblasts (Nandra et al., 2005). Such responses are usually measured by monitoring the secretion of pro-inflammatory cytokines, including TNF-α and do not depend on the size, type or shape of particles used in the study (Lange et al., 2009; Lange et al., 2011). The cellular pathways involved in the response remain unclear (Velard et al., 2013). Production of TNF-a by macrophages exposed to HAP particles is partially TLR4 dependent (Grandjean-Laquerrière et al., 2007), which would indicate a joint signalling pathway between HAP and LPS stimulation.

Chapter 3. Proteomic alterations in maturing dendritic cells

3.1. Introduction

3.1.1. Proteomic studies on maturing human dendritic cells

Tissue-resident immature dendritic cells (iDCs) exhibit very high capacity to capture exogenous and cellular antigens through endocytosis and phagocytosis upon activation of surface receptors. The antigens are recognised through pattern recognition receptors (PRRs) including toll like receptors (TLRs; West et al., 2006). IDCs are highly phagocytic, however their antigen presenting ability is very limited. After antigen recognition, iDCs begin a maturation process which can be divided into five steps. Firstly, the morphology of DC changes whereby the cell grows and develops cytoplasmic projections, a process involving cytoskeleton rearrangement. In this first phase cell motility increases by the loss of adhesive molecules (West et al., 2004). In the second phase, maturing DCs express T-cell co-stimulatory molecules (CD40, CD54, CD80 and CD86) on the cell surface (Ferreira et al., 2010). The third phase is a migration to the lymph nodes and spleen and the expression of a lymph-node homing chemokine receptor (CCR7), which enables cell to enter lymphatic vessels (Yanagihara, 1998). DCs express MHC class II antigen presenting molecules on their cell surface, and in the final phase chemokines and cytokines are secreted (Ferreira et al., 2010). At this point, DCs become fully mature and cannot take up new antigens but are ready to present the processed antigens to chemo-attracted, antigen-specific T-cells to therefore initiate the immune response (Banchereau et al., 2000). Overall DCs are considered as mature when they can activate T-cell through distinct mechanisms. The first mechanism of signalling is the interaction of MHC II molecule with T-cell receptor (TCR). Second mechanism is the interaction between costimulatory molecules CD80/CD86 on the DC cell surface with CD28 on the T cells. DC signalling determines the balance between different subsets of T-cells (Ferreira et al., 2010).

Proteomics can be defined as the simultaneous study of multiple (usually many) proteins in a particular cell or tissue at a given time. This can incorporate aspects of cellular localisation, interactions between proteins, post-translational modifications and protein functions. Such data provides an insight into the biological processes and the functional state of the cell and very often is complementary to genomic studies. Most of the proteomics studies performed so far in DCs are fairly primitive and based primarily on traditional electrophoresis-based techniques,

such as 2-D gel electrophoresis and 2-D DIGE (2-D gel electrophoresis with an internal standards). Other non-gel based techniques that have been used to study DCs are liquid chromatography combined with mass spectrometry (LC-MS/MS) and multidimensional protein identification technology (MudPIT; Ferreira et al., 2010). Several of those studies focused on alterations in protein expression during DCs maturation. Those were performed either on the whole cell lysate or on the fractionated samples of DCs, including exosome (Andre et al., 2004; Thery et al., 2002) and secretome (Gundacker et al., 2009).

One of the earliest proteomic studies of DCs was carried out by Angenieux et al. (2001). They identified 10 proteins (Table 3.1) which expression differed between monocytes and immature monocyte derived DCs (moDCs). They identified proteins involved in antigen processing, including chaperones, and proteins involved in cytoskeletal remodelling upregulated on protein level and mRNA transcript in immature moDCs. Soon another two papers were published examining protein and gene expression changes upon differentiation and TNF-α induced maturation of moDCs. Richards and colleagues using 2-D gel electrophoresis were able to detect a total of 900 distinct proteins, from which expression levels of only 37 were identified to have changed (Le Naour et al., 2001; Richards et al., 2002). Their most interesting observation was that during moDC maturation, only a small number of genes were altered at the RNA level, which points to importance of post-transcriptional and post-translational modifications. Among the identified proteins were chaperones, proteins involved in cell structure and fatty acid-binding proteins (Table 3.1), which suggested that protein-folding pathways and alterations in lipid metabolism play a role in antigen processing and presentation.

Another proteomic study confirmed the importance of post-translational modifications in moDCs maturation (Pereira et al., 2005). In this study lipopolysaccharide (LPS) was used to induce maturation and then combined CBB G-250 stained 2-D gels with LC-MS/MS to identify proteins in cell lysates. They observed 50 spots on 2-D gels, which corresponded to 36 separate altered proteins upon maturation (note that many spots appear in multiple electrophoretic forms). The identified altered proteins were mostly involved in cell structure including multiple forms of actin, but also chaperones and MHC class I molecule (Table 3.1).

A study by Ferreira et al. (2008) used a more sensitive gel electrophoresis technique, 2-D DIGE combined with MALDI-TOF/TOF-MS. This allowed identification of 74 proteins exhibiting altered expression upon moDC maturation. The authors analysed the protein expression profile of immature and mature moDCs. Again, similar to previous studies, they were mostly involved in

cytoskeleton remodelling, including gamma actin, fascin and lamin; in signal transduction, interferon-induced GTP-binding protein Mx1 and tyrosine-protein phosphatase; and in cellular metabolism, pyruvate carboxilase and alpha enolase. In addition proteins involved in MHC II antigen processing pathway (cathepsin B, D and S) were also altered.

STUDY	MATERIAL STUDIED	ACTIVATION METHOD	IDENTIFIED PROTEIN	UNIPROT
Angenieux et al. 2001	Immature moDCs		Vimentin	P08670
			Mn SOD	P04179
			ARP2/3 34kDa	O15144
			Glutamate dehydrogenase	P00367
			grp94-gp96	P14625
			GBI-2	P04899
			grp78	P11021
			Prx III	P30048
			EF-Tu	P49411
			Annexin H	P07355
Le Naour et al. 2001 Richards et al., 2002	moDC	TNF-α	Up-regulated:	
			hsp73	5729877
			Vimentin 3-a	2119204
			Macrophage capping protein	4502561
			Guanylate kinase	4504221
			hsp27 3-a	123571
			Ferritin light chain	120523
			Fatty acid binding protein (FABP) 5 3-a	4557581
			FABP4	4557579
			ACBP	118276
			S100C	5032057
			Down-regulated:	
			Calreticulin 3-a	4757900
			RNCC protein	4337097
			myeloid-related proteins (MRP) 14 3-a	4506773
			MRP8 3-a	115442
Pereira et al., 2005	moDC	LPS	Up-regulated:	
			Heat shock cognate 71 kDa protein	P11142
			Lymphocyte-specific protein 1	P33241
			Grp58	P30101
			Thioredoxin	P10599
			Vimentin	P08670
			Down-regulated:	
			Actin, cytoplasmic 1	P02570
			Chloride intracellular channel (RNCC)	O00299
			Fibrinogen gamma chain	P02679
			Grp78	P11021
			Glutathione S-transferase P	P09211
			Lymphocyte-capping protein	P40121

Gundacker et al. 2009	moDC	LPS	Up-regulated: Interferon-induced GTP-binding protein Mx1 (MxA) Interferon-induced 17 kDa protein Interferon-induced protein with tetratricopeptide repeats 3 Calpain-1 catalytic subunit CD54 antigen Interferon-induced guanylate-binding protein 1 Rho/Rac guanine nucleotide exchangefactor 2 (GEF-H1) ISG20	 P20591 P05161 O14879 P07384 P05362 P32455 Q92974 Q96AZ6

Table 3.1. An overview of various proteomic studies performed on DCs.

Individual proteins differ between described studies, with only few proteins in common. This may be due to the sensitivity and accuracy of the methods used as well as the method of sample preparation and the protocol used for moDC maturation, which were varied. Ferreira et al. (2008) used a combination of LPS and IFN-γ, Pereira et al. (2005) used GM-CSF with IL-4 and LPS and Le Naour et al. (2001) used IL-4, GM-CSF and TNFa. It was later shown that the inducer used for moDC maturation has great influence on the proteomic profile of matured cells and therefore also their functional state (Gundacker et al., 2009). In this study shotgun analysis identified 1690 cytoplasmic proteins. The greatest alterations in protein expression were observed upon LPS induced maturation. Activation of moDCs with 1-palmitoyl-2-arachidoyl-sn-glycerol-3-phosphorylcholin (OxPAPC) or with human rhinovirus (HRV) also induced alterations in protein expression, however these were lesser than those observed following LPS-treatemnt (Gundacker et al., 2009). Another known inducer of DCs maturation is hydroxyapatite (HAP). HAP a calcium phosphate mineral, can induce inflammatory reaction via TLR4 signalling as shown in macrophages exposed to HAP particles (Grandjean-Laquerrière et al., 2007). So far no studies describing proteomic changes during DCs maturation induced with HAP have been reported.

The proteomic studies of DCs maturation described above highlighted involvement of similar groups of proteins, including proteins involved in cytoskeletal remodelling, chaperones and antigen processing and presentation proteins. Nevertheless, specific identified proteins differ between the studies, which might be due to the technical limitations of proteomic methods used, which varied from traditional 2-D electrophoresis to basic mass spectrometry-based

approaches. Also the preparation and maturation of cells has a big influence on the proteome of mature DCs. The majority of methods used in the studies described above are semi-quantitative at best. The proteomic technique that will be described next, SWATH is fully quantitative and has vast coverage.

3.1.2. SWATH

Mass spectrometry (MS)-based proteomic approaches are a quickly developing field of research. In comparison to traditional techniques used for protein analysis such as western-blotting or enzyme-linked immunosorbent (ELISA) assays, which serve mostly for protein identification, (MS)-based proteomics allows higher throughput, specificity and quantitative analysis (Ong and Mann, 2005).

The most commonly used MS-based proteomic technique is quantitative LC-MS/MS, which is a combination of liquid chromatography and two or more mass spectrometry based techniques. This technique requires the use of isotopically-labelled standards, which show similar chromatographic behaviour to the target, but can be discriminated based on the mass. Prior to analysis, the analyte is proteolytically cleaved and then the resultant peptides are separated by liquid chromatography. Next the sample can be processed in one of the two main strategies used for LC-MS/MS. The first is known as shotgun proteomics, where separated peptides are analysed by a tandem mass spectrometry (MS/MS). MS/MS involves two steps. The first step (MS1) is the formation of ions by the ion source and their separation by mass-to-charge ratio and then fragmentation. In the second stage (MS2), fragmented ions are separated and detected. It is then possible to assign fragmented ion spectra to their corresponding peptide sequences using a database. The second strategy used is a targeted proteomics. In this method a set of searched peptides have to be specified prior to experiment. It then allows quantitative search of only this limited number of peptides in the sample, by calculating the likelihood that a group of transition signals generated by ions are delivered from the searched peptide (Gillet et al., 2012). The two described LC-MS/MS techniques have many advantages but also some limitations. Shotgun proteomics allows identification of a large number of proteins in a sample, but does not suit an accurate quantification (Liu et al., 2004). In contrast, targeted proteomics allows an accurate quantification and reproducible detection, but just for a set of specific proteins (Picotti et al., 2009). Therefore even a combination of both methods, cannot provide simultaneous quantitative identification of a large number of proteins (Gillet et al., 2012).

Sequential Window Acquisition of all Theoretical fragment-ion spectra (SWATH) is a label-free quantitative, proteomic technique. Samples are quantified by comparison of peak areas received for the sample under one or more biological conditions or a biological timeline and normalised to one or more internal standards, that are unaffected upon the course of experiment. This allows calculation of the fold-change of the identified protein between the conditions tested. SWATH can analyse a large number of digested peptides from 1000s of proteins simultaneously, collecting the fragmentation spectra by using wide range precursor-isolation windows (Gillet et al., 2012). In the first quadrupole of a standard SWATH acquisition, precursor windows (30 to 50), with variable mass widths are sequentially selected. This allows to full coverage of the mass-to-charge range (m/z) 400-1250. In the second quadrupole, transmitted ions are fragmented. These fragmented ions are then detected by the ToF (time of flight) mass analyser (Fig. 3.1). For each precursor-isolation window, ToF analyser generates a 3D fragment-ion m/z intensity-retention time map. To identify proteins corresponding to fragmented ions, a reference map is generated by information-dependent acquisition (IDA) experiment. Peptides are then quantified based on fragmented-ion peaks, using spectral libraries, which are generated using SWATH compatible mass spectrometer operated in data dependent acquisition mode (Chang et al., 2015).

Overall, SWATH quantitatively identifies proteins by combining precursor mass, chromatography retention and ion transitions. SWATH is the proteomic method that comprise both high throughput, and full quantification of proteins in the sample. In addition, it requires the minimal sample preparation and much lower costs, compared to other MS techniques such as SILAC (stable isotope labelling with amino acids in cell culture), which requires isotopic labelling of cells. It provides quantification that is incomparably more accurate than not only traditional immunoblotting, but also LC-MS/MS.

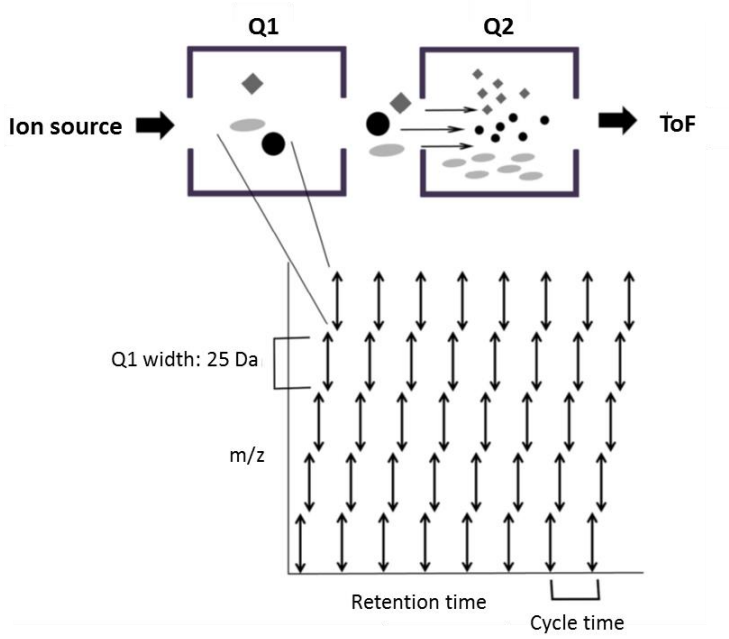

Figure 3.1. Overview of SWATH acquisition. The first quadrupole (Q1) contains 25 Da windows across the entire m/z range of interest. In second quadruple (Q2) ions that pass from Q1 are fragmented by collision-induced dissociation. Those fragmented ions are then monitored by ToF mass analyser.

SWATH has previously been used to quantitatively characterise proteins in human plasma (Haverland, 2016), and to study protein interaction dynamics including synaptosomes, from human Alzheimer's disease autopsy tissue (Chang et al., 2015), human leukocyte antigen (HLA)-associated proteome (Caron et al., 2015) and of nucleic acid binding and regulatory proteins in HIV-1-infected macrophages (Haverland et al., 2014). SWATH proteomics has never been used to identify infection-related proteomic changes in the most potent antigen presenting cells – DCs.

The aims of this chapter are to quantitatively describe global proteomic changes in DCs upon LPS and HAP induced maturation. In addition, those proteomic changes will be related to specific cellular pathways involved in metabolism, protein production and antigen presentation. That will allow to characterise for the first time quantitative proteomic changes that occur during antigen processing and presentation, which is a crucial time period for DCs.

3.2. Methods

3.2.1. Sample preparation

3.2.1.1. Cell culture

Blood was obtained from a healthy donor and purified over a ficoll gradient at room temperature to isolate peripheral blood mononuclear cells (PBMC; Histopaque, Sigma Aldrich). PBMC were plated on 3 wells of 6 well plate, then monocytes were isolated and differentiated into dendritic cells as described before (2.2.1.1.). MoDCs were treated with 4 mg of sterile hydroxyapatite nanopowder (Sigma) or with 100 ng/ml of bacterial LPS, or left untreated as control. HAP nanopowder was washed twice in 70% ethanol, then washed twice with sterile RPMI serum free media and then resuspended 10 µl of RPMI 10% FCS and applied to cell culture dish. Cell culture was carried for 24h.

3.2.1.2. Assessment of Cytokine Production.

Macrophages and mature dendritic cells are known to secrete TNF-α after TLR4 signalling upon LPS stimulation, which indicates that cells are active and functional. The response of dendritic cells for hydroxyapatite (HAP) stimulation is not known. To see whether generated moDC are functional and to find the amount of HAP that triggers the highest response of DCs, aliquots of supernatants were analysed using an enzyme-linked immunosorbent assay (ELISA) for the quantitative determination of TNF- α. Differentiated moDCs matured by 4 mg of HAP and 100 ng/ml of LPS stimulation as described above (3.2.1.1.) for 24 h. Next, the culture media was collected and TNF-α concentration measured using the TNF alpha Human ELISA Kit (Invitrogen, Thermo Fisher Scientific). This kit is a sandwich ELISA assay, which comes with plates pre-coated with specific anti-TNF-α antibody. After addition of the sample to the wells detection involved addition of biotinylated anti-TNF-α antibody, followed by streptavidin-HRP conjugate. The plate was then washed to remove unbound substances and substrate for HRP was applied. After the reaction was stopped, the absorbance at 450 nm was measured using a Dynex MRX microplate reader (Dynex Technologies, Worthing, UK). The concentration of TNF-α in the samples was determined based on standards supplied with the kit.

3.2.1.3. Cell lysis and quantification

Cells were washed on ice with 1x PBS and lysed for 30 min at 55^{o}C with 300 µl of lysis buffer (10 mM HEPES, 1.5 mM $MgCl_2$, 10 mM KCl, 0.5 mM DTT, 0.5 % Rapi Gest, pH 7.9). Cells were further

lysed using syringe. Next cell debris was spun down at 14000 rpm, 4°C, for 5 min, supernatant transferred to a fresh Eppendorf tube and protein quantified using the BCA protein assay kit (Thermo Fisher Scientific) as described before (2.2.3.3). For the analysis 30 µg of protein per 50 µl solution was submitted.

3.2.2. LC-ESI-MSMS analysis

LC-ESI-MSMS analysis, including library generation and SWATH were carried out by The Mass Spectrometry and Proteomics Facility (University of St Andrews) and Dr Swati Arya. Prior to analysis 20 µg of proteins were first denatured with 6-8 M Urea and subsequently reduced and alkylated with 1 mM tris(2-carboxyethyl)phosphine (TCEP) and 5 mM iodoacetamide. The reaction was stopped with 10 mM dithiothreitol (DTT). The resulting samples were then digested with trypsin (1:50 ratio (w/w), 0.2 µg/µl trypsin; Promega), overnight at 30°C. To stop the digestion, 0.5% (v/v) trifluoroacetic acid was added. Tryptic peptides were desalted using Pierce C18 spin column (Thermo Fisher Scientific) and concentrated down, using a SpeedVac (Thermo Savant).

3.2.2.1. Library generation

For spectral library generation, an AB SCIEX TripleTOF 5600+ System mass spectrometer was used. All samples were analysed on an Eksigent nanoLC AS-2/2Dplus system coupled with a SWATH-MS-enabled AB SCIEX TripleTOF 5600+ System utilising trap elute methods. The samples were loaded in loading buffer (2% acetonitrile and 0.05% trifluoroacetic acid) and bound to an Aclaim pepmap 100 µm x 2 cm trap (Thermo Fisher Scientific), and washed for 10 min to waste. The trap was turned in line with the analytical column, Aclaim pepmap RSLC 75 µm x 15 cm and the peptides eluted. The analytical solvent system consisted of buffer A (2% acetonitrile and 0.1% formic acid in water) and buffer B (2% water with 0.1% formic acid in acetonitrile) at a flow rate of 300 nl/min with the following gradient: linear 1-20% of buffer B over 90 min, linear 20-40% of buffer B for 30 min, linear 40-99% of buffer B for 10 min, isocratic 99% of buffer B for 5 min, linear 99-1% of buffer B for 2.5 min and isocratic 1% solvent buffer B for 12.5 min. The mass spectrometer was operated in DDA top20 positive ion mode, with 250 and 150 ms acquisition time for the MS1 (m/z 400-1200) and MS2 (m/z 230-1800) scans respectively, and 15 s dynamic exclusion. Rolling collision energy with a collision energy spread of 15 eV was used for fragmentation.

The library of identified 845 proteins was generated using Protein Pilot v5.0.1. The following search parameters were used, with urea denaturation as special factors, Homo sapiens as species, trypsin as the cleavage enzyme and carbamidomethyl as a fixed modification of cysteines. The search was carried out against the Swissprot database downloaded June 2015, restricted to Human only species. The iRT peptides had been added to this fasta database.

3.2.2.2. Sequential Window Acquisition of all Theoretical fragment-ion spectra (SWATH) mass spectrometry

DIA mass spectrometry (SWATH-MS)

For SWATH-MS data acquisition, the same mass spectrometer and LC-MS/MS setup was operated essentially as described before above, but using 50 windows of variable Da effective isolation width (with an additional 1 Da overlap on the left side of the window) and with a dwell time of 50 ms to cover the mass range of 400–1,250 m/z in 2.6 s in TOF-MS mode. MS/MS data is acquired over a range of 230-1800 m/z with high sensitivity setting. The collision energy for each window was set using the collision energy of a 2^+ ion centred in the middle of the window with a spread of 15 eV

3.3. Results

3.3.1. Cytokine Production.

Immature DCs were obtained from fresh blood taken from a single donor following culture of purified human peripheral blood monocytes with GM-CSF and IL-4. Maturation was induced by the addition of either LPS or HAP nanopowder. TLR4 recognise bacterial products present in the extracellular space such as LPS. Some non-bacterial particles can also be recognised by TLRs. One of them is the mineral HAP, which is a ligand for TLR4 and at least one more TLR (Velard et al., 2013). Following activation, TLRs activate signalling pathways that induce the production of chemokines, co-stimulatory molecules, and cytokines including TNF-α (Kolanowski et al., 2016). DCs matured upon LPS treatment exhibit a strong T cell stimulatory capacity, however the functional phenotype of DC matured upon HAP stimulation is not known.

To confirm cell functionality, aliquots of the culture media were analysed for TNF-α production, using a commercial ELISA kit. DCs maturated in response to addition of LPS secreted 5.00±0.86 ng/ml TNF-α and cells maturated following addition of HAP nanopowder secreted 0.42±0.04 ng/ml TNF-α. Immature dendritic cells (control) secreted 0.26±0.04 ng/ml TNF-α. (Fig 4.1). These results indicate that hydroxyapatite can induce DCs maturation.

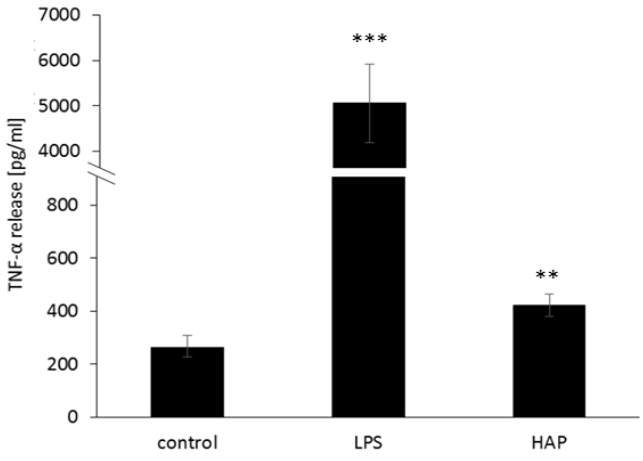

Figure 3.2. TNF-α release from moDCs following stimulation with LPS and HAP. MoDCs were cultured in RPMI media supplemented 10% FCS. Next cells were stimulated with 100 µg/ml of bacterial LPS or 4 mg/ml of HAP for 24 h. TNF-α secretion was measured using Human TNF-α ELISA Kit (Life Technologies). p≤0.01 (**), p≤0.001 (***). The experiment was replicated with similar results obtained.

3.3.2. Identification of proteins upregulated upon moDC maturation

3.3.2.1. Proteins upregulated upon LPS induced maturation

SWATH analysis allowed identification of 845 proteins, from which 260 proteins exhibited a significant change in expression (p value <0.05) in cell lysates taken from moDCs differentiated upon LPS stimulation. From those 260 proteins, 19 (7.3%) were upregulated upon maturation. The highest up regulation, of more than 30-fold change, was observed for three proteins: Interferon-induced GTP-binding protein, interferon-induced protein with tetratricopeptide repeats 3 (IFIT3) and ubiquitin-like protein ISG15 (Table 3.2). The two "interferon-induced" proteins are involved in immune defence against a wide range of viruses (Pichlmair et al., 2011). Additionally, those proteins act as regulators of apoptosis, IFN-induced GTP binding protein as enhancer (Li and Youssoufian, 1997), and IFIT3 as a negative regulator (Stowowczyk et al., 2011). Ubiquitin-like protein ISG15 is also involved in immune response to viral (Hsiang et al., 2009) and bacterial (Bogunovic et al., 2012) infection. In fact it is a key protein in the innate immune response and acts either via binding to a target protein as a tag (ISGylation) or as an unconjugated protein. Besides the response against bacterial and viral infection, ISG15 negatively regulates protein ubiquitination (Okumura et al., 2008) and type I interferon production, but induce natural killer cell proliferation, act as a chemotactic factor for neutrophils, induce interferon-gamma production and is involved in type I interferon signalling pathway playing an essential role in antibacterial immunity (Bogunovic et al., 2012).

Other proteins with more than 10-fold up regulation upon LPS-induced maturation, were TNF receptor-associated factor 1 (TRAF1) and fascin. TRAF1 regulates cells survival and apoptosis as part of E3 ubiquitin-protein ligase complex, which promotes ubiquitination of target proteins. TRAF1 is also an inducer of nuclear factor-κB (NF-κB), transcription factor that regulates genes involved in innate and adaptive immune response including cytokine release (Irmler et al., 2000). Additionally, as a TNF binding protein, was involved in the regulation of TNF-mediated signalling pathway (Wicovsky et al., 2009). Fascin is a protein involved in maintaining anatomical cell structure by organising actin filaments into bundles. Plays a role in the formation of membrane ruffles, positive regulation of filopodium, and podosome assembly, anatomical structure morphogenesis and the formation of cell-cell junction involved in cell communication (Chen et al., 2010; Yamashiro et al., 1998). Also several keratins were upregulated after LPS induced maturation. Similarly, to fascin, they are involved in maintaining cell structure as structural constituents of cytoskeleton (Kobayashi et al., 1996; Kobayashi et al., 1999). Furthermore, one

of them, keratin, type II cytoskeletal 1, is a part of skin barrier against pathogens and as that regulate immune response via activation of lectin complement pathway (Collard et al., 2001). It is also possible that those keratins may be contaminating proteins, as those can be found in dead skin and dust and although great care is taken during sample preparation it is difficult to be absolutely sure these were not introduced during the experiment. Another protein involved in cytoskeletal organisation is coronin-1B. It is involved in actin filament branching and in filament bundle assembly (Makhov et al., 2008) and also in cell migration (Holoweckyj et al., 2005).

Three alleles of α-chain of major histocompatibility complex class I (MHC class I) were identified as upregulated proteins. MHC class I is present on antigen presenting cells (including dendritic cells) and is involved in the presentation of foreign peptide antigen to CD8+ T-cells, and to natural killer (NK) cells. MHC class I is also involved in IFN-γ and type I IFN signalling pathways. Additionally, MHC calls I regulates DC differentiation during viral infection (Huang et al., 2009).

Several enzymes were upregulated upon DC maturation. Creatine kinase catalyses the transfer of phosphate from ATP to phosphogens. The activity of this enzyme is crucial to energy transduction when energy demands are high. Another catalyst, thioredoxin, catalyses dithiol-exchange reactions. Amongst its many functions are cell to cell signalling, cell proliferation, cell movement (Miller et al., 2000). Thioredoxin also assists in protein folding and repair. Calpain-1 is a calcium-regulated protease which is involved in cytoskeletal remodelling and signal transduction. Tryptophan-tRNA ligase, regulates activation of ERK, Akt, and *endothelial nitric oxide synthase* (eNOS) signalling pathways, that are associated with angiogenesis, cell proliferation and cytoskeletal reorganization (Tzima et al., 2003; Bange et al., 1992). The last identified enzyme, with 1.67 fold increase upon DC maturation, was kynureninase. Through its enzymatic activity, kynureninase is involved in 'de novo' biosynthetic of nicotinamide adenine dinucleotide (NAD) and involved in response to IFN-γ (Walsh and Botting, 2002).

Finally, there were two proteins with small but significant, 1.3-fold upregulation upon LPS induced maturation. Those are CD44 antigen, and WD repeat- and FYVE domain-containing protein 4 (WDFY4). CD44 antigen is a receptor for hyaluronic acid (HA) and other ligands including collagens and metalloproteinases. Through those interactions, CD44 antigen mediates cell-cell interactions and cell migration. It is involved in lymphocyte activation, monocyte aggregation (Selbi et al., 2004), IFN-γ signalling pathway and negative regulation of apoptosis

(Bourguignon et al., 2009). CD44 antigen also regulates peptidyl-serine and peptidyl-tyrosine phosphorylation (Shi et al., 2006).

UNIPROT	PROTEIN NAME	FOLD INCREASE	P VALUE
P20591	Interferon-induced GTP-binding protein	37.52	0.001
O14879	Interferon-induced protein with tetratricopeptide repeats 3	34.16	0.001
P05161	Ubiquitin-like protein ISG15	30.98	0.001
Q13077	TNF receptor-associated factor 1	17.87	0.008
Q16658	Fascin	11.09	0.004
P30466	Major histocompatibility complex class I, B-18 alpha chain	7.42	0.019
P35527	Keratin, type I cytoskeletal 9	7.06	0.013
P12277	Creatine kinase B-type	3.45	0.009
P01889	Major histocompatibility complex class I, B-7 alpha chain	3.42	0.002
Q07000	Major histocompatibility complex class I, Cw-15 alpha chain	3.19	0.011
P10599	Thioredoxin	2.88	0.001
P04264	Keratin, type II cytoskeletal 1	2.58	0.019
P07384	Calpain-1 catalytic subunit	2.43	0.036
P23381	Tryptophan--tRNA ligase, cytoplasmic	2.41	0.009
Q16719	Kynureninase	1.67	0.008
Q8NHM4	Putative trypsin-6	1.66	0.036
Q9BR76	Coronin-1B	1.51	0.048
P35908	Keratin, type II cytoskeletal 2 epidermal	1.45	0.001
P16070	CD44 antigen	1.35	0.050
Q6ZS81	WD repeat- and FYVE domain-containing protein 4	1.30	0.009

Table 3.2. List of the proteins upregulated, after stimulation of dendritic cells with LPS. Calculated p value is the confidence that the fold change described is legitimate across the technical and biological replicates, based on the instrumentation and software used.

3.3.2.2. Proteins upregulated upon HAP induced maturation

SWATH identified 190 proteins (from 845) that significantly changed in expression level (p value <0.05) in cell lysates from moDCs upon HAP stimulation. From those 190 proteins, only 5 (2.6 %) were upregulated upon maturation (Table 3.3). Two of the proteins, Interferon-induced protein with tetratricopeptide repeats 3 and WD repeat- and FYVE domain-containing protein 4 were also upregulated upon LPS-induced maturation.

Second highest fold-change was observed integrin beta-3 (ITGB3), a receptor for vast array of ligands, including cytotactin, fibronectin, fibrinogen, laminin, plasminogen, prothrombin, thrombospondin and vitronectin. ITGB3 is involved in numerous process, including cell adhesion (Longhurst et al., 1999), migration and growth (Lee et al., 2012), and also negatively regulates chemotaxis (Riches et al., 2013).

Thymidine phosphorylase provides energy for nucleotide synthesis by catalysing the reversible phosphorolysis of thymidine. The produced molecules are then utilized as carbon and energy sources (Usuki et al., 1992). Thymidine phosphorylase is also involved in cell differentiation.

Finally, the last protein upregulated upon HAP induced maturation was ubiquitin thioesterase, an enzyme involved in adaptive immune response by regulating CD4+ T-cell energy via interaction with RNF128. Ubiquitin thioesterase is also involved in cellular response to DNA damage (Nakada et al., 2010) and response to IL- 1.

UNIPROT	PROTEIN NAME	FOLD CHANGE	P VALUE
O14879	Interferon-induced protein with tetratricopeptide repeats 3	2.46	0.040
Q6ZS81	WD repeat- and FYVE domain-containing protein 4	1.34	0.021
P05106	Integrin beta-3	1.27	0.038
P19971	Thymidine phosphorylase	1.19	0.018
Q96FW1	Ubiquitin thioesterase	1.17	0.049

Table 3.3. List of the proteins upregulated, after stimulation of dendritic cells with HAP nanopowder.

3.3.3. Identification of proteins down-regulated upon moDC maturation

3.3.3.1. Proteins that exhibit reduced expression following LPS induced maturation of moDC

Upon LPS induced maturation of DCs, the majority of proteins detected in cell lysate were down-regulated. This accounts for as much as 92.7% of the total proteins detected (Table 3.4). Those proteins are involved in many cellular processes including cell metabolism, antigen presentation and protein production. Proteins were therefore grouped into specific pathways, using KEGG database: Kyoto Encyclopedia of Genes and Genomes – GenomeNet (*www.genome.jp/**kegg**).*

UNIPROT	PROTEIN NAME	FOLD DECREASE	P VALUE
Q9BVJ7	Dual specificity protein phosphatase 23	13.40	0.001
Q15717	ELAV-like protein 1	10.98	0.001
Q6NUK1	Calcium-binding mitochondrial carrier protein SCaMC-1	9.53	0.009
P38571	Lysosomal acid lipase/cholesteryl ester hydrolase	7.63	0.001
P36543	V-type proton ATPase subunit E 1	6.12	0.012
P00390	Glutathione reductase, mitochondrial	5.09	0.001
P07339	Cathepsin D	4.91	0.003
P55263	Adenosine kinase	4.43	0.000
P17900	Ganglioside GM2 activator	4.29	0.042
Q96CN7	Isochorismatase domain-containing protein 1	4.11	0.019
P10644	cAMP-dependent protein kinase type I-alpha regulatory subunit	3.88	0.026
Q8IV08	Phospholipase D3	3.82	0.025
P35270	Sepiapterin reductase	3.62	0.025
P22626	Heterogeneous nuclear ribonucleoproteins A2/B1	3.47	0.011
P62805	Histone H4	3.38	0.012
Q9Y5X3	Sorting nexin-5	3.32	0.008
P24666	Low molecular weight phosphotyrosine protein phosphatase	3.25	0.049
P60891	Ribose-phosphate pyrophosphokinase 1	3.23	0.022
P34897	Serine hydroxymethyltransferase, mitochondrial	3.22	0.024
P61916	Epididymal secretory protein E1	3.22	0.012
Q99880	Histone H2B type 1-L	3.15	0.002
P07858	Cathepsin B	3.14	0.001
P11310	Medium-chain specific acyl-CoA dehydrogenase, mitochondrial	3.10	0.034
P09622	Dihydrolipoyl dehydrogenase, mitochondrial	3.10	0.032
P22102	Trifunctional purine biosynthetic protein adenosine-3	3.08	0.029
Q96HC4	PDZ and LIM domain protein 5	2.99	0.052
Q9Y3F4	Serine-threonine kinase receptor-associated protein	2.85	0.040
O75369	Filamin-B	2.83	0.003
P15090	Fatty acid-binding protein, adipocyte	2.82	0.001
P07910	Heterogeneous nuclear ribonucleoproteins C1/C2	2.81	0.015
P01034	Cystatin-C	2.81	0.021
P06748	Nucleophosmin	2.78	0.012
Q9BTM1	Histone H2A.J	2.72	0.004
P08697	Alpha-2-antiplasmin	2.70	0.016
P17844	Probable ATP-dependent RNA helicase DDX5	2.65	0.032
Q9UBR2	Cathepsin Z	2.64	0.001
P61960	Ubiquitin-fold modifier 1	2.64	0.004
P19878	Neutrophil cytosol factor 2	2.58	0.021

P10253	Lysosomal alpha-glucosidase	2.53	0.013
P15531	Nucleoside diphosphate kinase A	2.52	0.006
P00505	Aspartate aminotransferase, mitochondrial	2.50	0.048
Q92945	Far upstream element-binding protein 2	2.44	0.030
O00764	Pyridoxal kinase	2.42	0.010
P52790	Hexokinase-3	2.41	0.019
P46776	60S ribosomal protein L27a	2.38	0.033
P63173	60S ribosomal protein L38	2.30	0.022
P28676	Grancalcin	2.30	0.001
P02774	Vitamin D-binding protein	2.27	0.036
P30043	Flavin reductase (NADPH)	2.27	0.042
Q13838	Spliceosome RNA helicase DDX39B	2.27	0.025
P62136	Serine/threonine-protein phosphatase PP1-alpha	2.24	0.049
Q99536	Synaptic vesicle membrane protein VAT-1 homolog	2.23	0.002
Q09666	Neuroblast differentiation-associated protein AHNAK	2.23	0.004
O00757	Fructose-1,6-bisphosphatase isozyme 2	2.22	0.003
P08670	Vimentin	2.20	0.001
P20036	HLA class II histocompatibility antigen, DP alpha 1 chain	2.20	0.035
P06703	Protein S100-A6	2.14	0.040
Q13510	Acid ceramidase	2.12	0.034
O00154	Cytosolic acyl coenzyme A thioester hydrolase	2.09	0.040
P11215	Integrin alpha-M	2.07	0.013
P24844	Myosin regulatory light polypeptide 9	2.07	0.001
Q92598	Heat shock protein 105 kDa	2.07	0.007
P07686	Beta-hexosaminidase subunit beta	2.06	0.000
P07954	Fumarate hydratase, mitochondrial	2.06	0.032
P26599	Polypyrimidine tract-binding protein 1	2.00	0.016
P04080	Cystatin-B	1.96	0.013
P22897	Macrophage mannose receptor 1	1.96	0.050
P35268	60S ribosomal protein L22	1.91	0.001
P42765	3-ketoacyl-CoA thiolase, mitochondrial	1.88	0.047
Q9H4A4	Aminopeptidase B	1.87	0.041
Q13075	Baculoviral IAP repeat-containing protein 1	1.87	0.027
Q99798	Aconitate hydratase, mitochondrial	1.85	0.006
O75874	Isocitrate dehydrogenase [NADP] cytoplasmic	1.85	0.005
P55084	Trifunctional enzyme subunit beta, mitochondrial	1.85	0.038
P05107	Integrin beta-2	1.84	0.000
P25788	Proteasome subunit alpha type-3	1.83	0.050
P31946	14-3-3 protein beta/alpha	1.82	0.014
P15586	N-acetylglucosamine-6-sulfatase	1.82	0.016
Q01469	Fatty acid-binding protein, epidermal	1.81	0.000
P06576	ATP synthase subunit beta, mitochondrial	1.81	0.050
O75368	SH3 domain-binding glutamic acid-rich-like protein	1.81	0.015

P21980	Protein-glutamine gamma-glutamyltransferase 2	1.80	0.006
Q86TI2	Dipeptidyl peptidase 9	1.79	0.024
P23469	Receptor-type tyrosine-protein phosphatase epsilon	1.78	0.012
P51659	Peroxisomal multifunctional enzyme type 2	1.77	0.019
P23526	Adenosylhomocysteinase	1.77	0.018
P18510	Interleukin-1 receptor antagonist protein	1.76	0.005
P34932	Heat shock 70 kDa protein 4	1.76	0.000
Q14103	Heterogeneous nuclear ribonucleoprotein D0	1.76	0.019
Q9NNX6	CD209 antigen	1.75	0.004
Q9ULV4	Coronin-1C	1.75	0.019
P45974	Ubiquitin carboxyl-terminal hydrolase 5	1.74	0.029
P48735	Isocitrate dehydrogenase [NADP], mitochondrial	1.74	0.030
P83731	60S ribosomal protein L24	1.74	0.020
P62913	60S ribosomal protein L11	1.72	0.029
P40939	Trifunctional enzyme subunit alpha, mitochondrial	1.71	0.018
P09467	Fructose-1,6-bisphosphatase	1.70	0.013
Q15257	Serine/threonine-protein phosphatase 2A activator	1.68	0.050
O95571	Persulfide dioxygenase ETHE1, mitochondrial	1.68	0.009
Q8N392	Rho GTPase-activating protein 18	1.67	0.050
P50995	Annexin A11	1.66	0.006
Q9Y6N5	Sulfide:quinone oxidoreductase, mitochondrial	1.65	0.019
P01903	HLA class II histocompatibility antigen, DR alpha chain	1.65	0.016
Q9NTK5	Obg-like ATPase 1	1.65	0.046
P68032	Actin, alpha cardiac muscle 1	1.65	0.040
Q96G03	Phosphoglucomutase-2	1.64	0.016
P30044	Peroxiredoxin-5, mitochondrial	1.64	0.030
P62917	60S ribosomal protein L8	1.63	0.013
P21281	V-type proton ATPase subunit B, brain isoform	1.63	0.000
P29350	Tyrosine-protein phosphatase non-receptor type 6	1.63	0.019
P62158	Calmodulin	1.63	0.001
P19823	Inter-alpha-trypsin inhibitor heavy chain H2	1.63	0.000
Q15582	Transforming growth factor-beta-induced protein ig-h3	1.62	0.011
P31948	Stress-induced-phosphoprotein 1	1.62	0.003
Q9UBQ7	Glyoxylate reductase/hydroxypyruvate reductase	1.60	0.017
P38117	Electron transfer flavoprotein subunit beta	1.60	0.015
P14550	Alcohol dehydrogenase [NADP(+)]	1.60	0.014
P38646	Stress-70 protein, mitochondrial	1.59	0.006
O15143	Actin-related protein 2/3 complex subunit 1B	1.59	0.008
P61160	Actin-related protein 2	1.59	0.001
O14773	Tripeptidyl-peptidase 1	1.59	0.003
P60842	Eukaryotic initiation factor 4A-I	1.58	0.021
P18124	60S ribosomal protein L7	1.57	0.028
P62269	40S ribosomal protein S18	1.57	0.005

P40925	Malate dehydrogenase, cytoplasmic	1.57	0.002
P38606	V-type proton ATPase catalytic subunit A	1.54	0.004
P30046	D-dopachrome decarboxylase	1.54	0.020
P63244	Guanine nucleotide-binding protein subunit beta-2-like 1	1.53	0.000
Q96TA1	Niban-like protein 1	1.53	0.036
P26447	Protein S100-A4	1.53	0.044
P50502	Hsc70-interacting protein	1.52	0.023
Q9BRA2	Thioredoxin domain-containing protein 17	1.52	0.016
P62424	60S ribosomal protein L7a	1.51	0.022
P14314	Glucosidase 2 subunit beta	1.51	0.041
P06744	Glucose-6-phosphate isomerase	1.50	0.010
P84077	ADP-ribosylation factor 1	1.50	0.000
P09960	Leukotriene A-4 hydrolase	1.49	0.014
P06753	Tropomyosin alpha-3 chain	1.49	0.039
P62826	GTP-binding nuclear protein Ran	1.49	0.029
P31146	Coronin-1A	1.49	0.030
Q16698	2,4-dienoyl-CoA reductase, mitochondrial	1.49	0.018
P40121	Macrophage-capping protein	1.49	0.007
Q9BUF5	Tubulin beta-6 chain	1.48	0.001
P50990	T-complex protein 1 subunit theta	1.48	0.022
O75608	Acyl-protein thioesterase 1	1.47	0.034
P25787	Proteasome subunit alpha type-2	1.47	0.029
P02768	Serum albumin	1.47	0.017
Q04917	14-3-3 protein eta	1.47	0.044
Q9Y2Q3	Glutathione S-transferase kappa 1	1.46	0.001
Q06830	Peroxiredoxin-1	1.45	0.011
P04406	Glyceraldehyde-3-phosphate dehydrogenase	1.45	0.025
P47756	F-actin-capping protein subunit beta	1.44	0.001
Q9BSJ8	Extended synaptotagmin-1	1.44	0.006
P61088	Ubiquitin-conjugating enzyme E2 N	1.44	0.001
P51149	Ras-related protein Rab-7a	1.43	0.010
P27797	Calreticulin	1.43	0.005
Q7Z4W1	L-xylulose reductase	1.43	0.014
P52566	Rho GDP-dissociation inhibitor 2	1.42	0.062
Q9NY33	Dipeptidyl peptidase 3	1.42	0.024
P52209	6-phosphogluconate dehydrogenase, decarboxylating	1.41	0.001
P10809	60 kDa heat shock protein, mitochondrial	1.41	0.008
P12081	Histidine--tRNA ligase, cytoplasmic	1.41	0.002
P28072	Proteasome subunit beta type-6	1.41	0.008
P37837	Transaldolase	1.40	0.002
P13489	Ribonuclease inhibitor	1.40	0.044
P09382	Galectin-1	1.39	0.002
Q969H8	Myeloid-derived growth factor	1.39	0.021

P04040	Catalase	1.39	0.001
P11413	Glucose-6-phosphate 1-dehydrogenase	1.39	0.013
P00918	Carbonic anhydrase 2	1.38	0.009
P49411	Elongation factor Tu, mitochondrial	1.38	0.005
Q02878	60S ribosomal protein L6	1.38	0.005
O60664	Perilipin-3	1.38	0.021
P62277	40S ribosomal protein S13	1.38	0.016
O14818	Proteasome subunit alpha type-7	1.38	0.045
P07741	Adenine phosphoribosyltransferase	1.38	0.007
P62851	40S ribosomal protein S25	1.37	0.017
P50226	Sulfotransferase 1A2	1.37	0.031
P40926	Malate dehydrogenase, mitochondrial	1.37	0.001
Q15121	Astrocytic phosphoprotein PEA-15	1.37	0.004
P61981	14-3-3 protein gamma	1.37	0.011
P61313	60S ribosomal protein L15	1.37	0.013
O43399	Tumor protein D54	1.36	0.029
P28482	Mitogen-activated protein kinase 1	1.36	0.007
O00754	Lysosomal alpha-mannosidase	1.36	0.045
P05387	60S acidic ribosomal protein P2	1.36	0.007
P07355	Annexin A2	1.36	0.035
O75083	WD repeat-containing protein 1	1.35	0.004
P30041	Peroxiredoxin-6	1.35	0.002
P62888	60S ribosomal protein L30	1.35	0.026
P30040	Endoplasmic reticulum resident protein 29	1.35	0.013
P62829	60S ribosomal protein L23	1.34	0.022
P06737	Glycogen phosphorylase, liver form	1.34	0.033
P14618	Pyruvate kinase PKM	1.34	0.013
P47755	F-actin-capping protein subunit alpha-2	1.33	0.004
Q15084	Protein disulfide-isomerase A6	1.33	0.016
Q9NUQ9	Protein FAM49B	1.33	0.001
P01911	HLA class II histocompatibility antigen, DRB1-15 beta chain	1.32	0.030
Q9Y3Z3	Deoxynucleoside triphosphate triphosphohydrolase SAMHD1	1.32	0.028
O43707	Alpha-actinin-4	1.32	0.020
P19105	Myosin regulatory light chain 12A	1.32	0.005
P14174	Macrophage migration inhibitory factor	1.32	0.001
P00558	Phosphoglycerate kinase 1	1.32	0.010
P07237	Protein disulfide-isomerase	1.31	0.017
P11142	Heat shock cognate 71 kDa protein	1.31	0.001
O15144	Actin-related protein 2/3 complex subunit 2	1.31	0.018
P62937	Peptidyl-prolyl cis-trans isomerase A	1.30	0.040
P14625	Endoplasmin	1.29	0.023
P13716	Delta-aminolevulinic acid dehydratase	1.29	0.019
P62258	14-3-3 protein epsilon	1.29	0.029

P11021	78 kDa glucose-regulated protein	1.28	0.020
O95336	6-phosphogluconolactonase	1.28	0.041
P78417	Glutathione S-transferase omega-1	1.28	0.006
P00488	Coagulation factor XIII A chain	1.28	0.007
P13796	Plastin-2	1.27	0.026
Q01105	Protein SET	1.27	0.018
P35237	Serpin B6	1.27	0.037
P55786	Puromycin-sensitive aminopeptidase	1.26	0.019
P46940	Ras GTPase-activating-like protein IQGAP1	1.26	0.000
Q00610	Clathrin heavy chain 1	1.25	0.043
P30101	Protein disulfide-isomerase A3	1.25	0.061
O60749	Sorting nexin-2	1.25	0.033
Q01813	ATP-dependent 6-phosphofructokinase, platelet type	1.25	0.039
P28066	Proteasome subunit alpha type-5	1.24	0.010
P36578	60S ribosomal protein L4	1.23	0.037
P04075	Fructose-bisphosphate aldolase A	1.23	0.009
P06396	Gelsolin	1.21	0.032
P06733	Alpha-enolase	1.21	0.016
P05388	60S acidic ribosomal protein P0	1.19	0.024
P55072	Transitional endoplasmic reticulum ATPase	1.19	0.047
O75390	Citrate synthase, mitochondrial	1.14	0.032
P26641	Elongation factor 1-gamma	1.14	0.005
P50914	60S ribosomal protein L14	1.08	0.028

Table 3.4. List of the proteins exhibiting reduced expression in dendritic cells stimulated with LPS.

Cell metabolism

From the identified, down regulated proteins, 15 were assigned as being involved in the glycolysis/gluconeogenesis pathway. Glycolysis is a sequence of enzymatic reactions that result in the conversion of glucose into pyruvate. The energy produced in this process is used to form adenosine triphosphate (ATP) and reduced nicotinamide adenine dinucleotide (NADH). Gluconeogenesis, is a process of generation of glucose from non-carbohydrate carbon substrates like glucogenic amino acids, glycerol, pyruvate and lactate (Berg et al., 2012).

LPS-induced maturation inhibits a number of enzymatic reaction in glycolysis and gluconeogenesis pathway (downregulated enzymes are highlighted in red, Fig. 3.3). Starting with the first step of glycolysis, phosphorylation of glucose to form glucose 6-phosphate (G6P), where two enzymes are downregulated, phosphoglucomutase-2 (5.4.2.2) and hexokinase 1 (2.7.1.1).

This is an energy consuming reaction, which stimulates continuous influx of glucose into the cell. G6P is then converted into fructose 6-phosphate (F6P) by glucose-6-phosphate isomerase (5.3.1.9). This reaction is reversible in case of high concentration of F6P, however normally the glycolysis moves to the next step, which is phosphorylation of F6P. This second phosphorylation is catalysed by a phosphofructokinase-1 (2.7.1.11) and results in the production of β-D-Fructose 1,6-bisphosphate (F1,6BP) and energy use by ATP hydrolysis. This pathway is irreversible and therefore during gluconeogenesis, alternative pathway with fructose-bisphosphatase 1 (3.1.3.11) for dephophorylation of F1,6BP to F6P. Next the hexose ring of F1,6BP is split by fructose-bisphosphate (4.1.2.13) into two triose sugars, glyceraldehyde 3-phosphate (GADP) and glycerine phosphatase which is rapidly converted to a second GADP. This is the end of the first phase of glycolysis, the energy consuming process, where is converted into two triose sugars (Berg et al., 2012). Enzymes catalysing all described steps were downregulated upon LPS induced maturation of DCs.

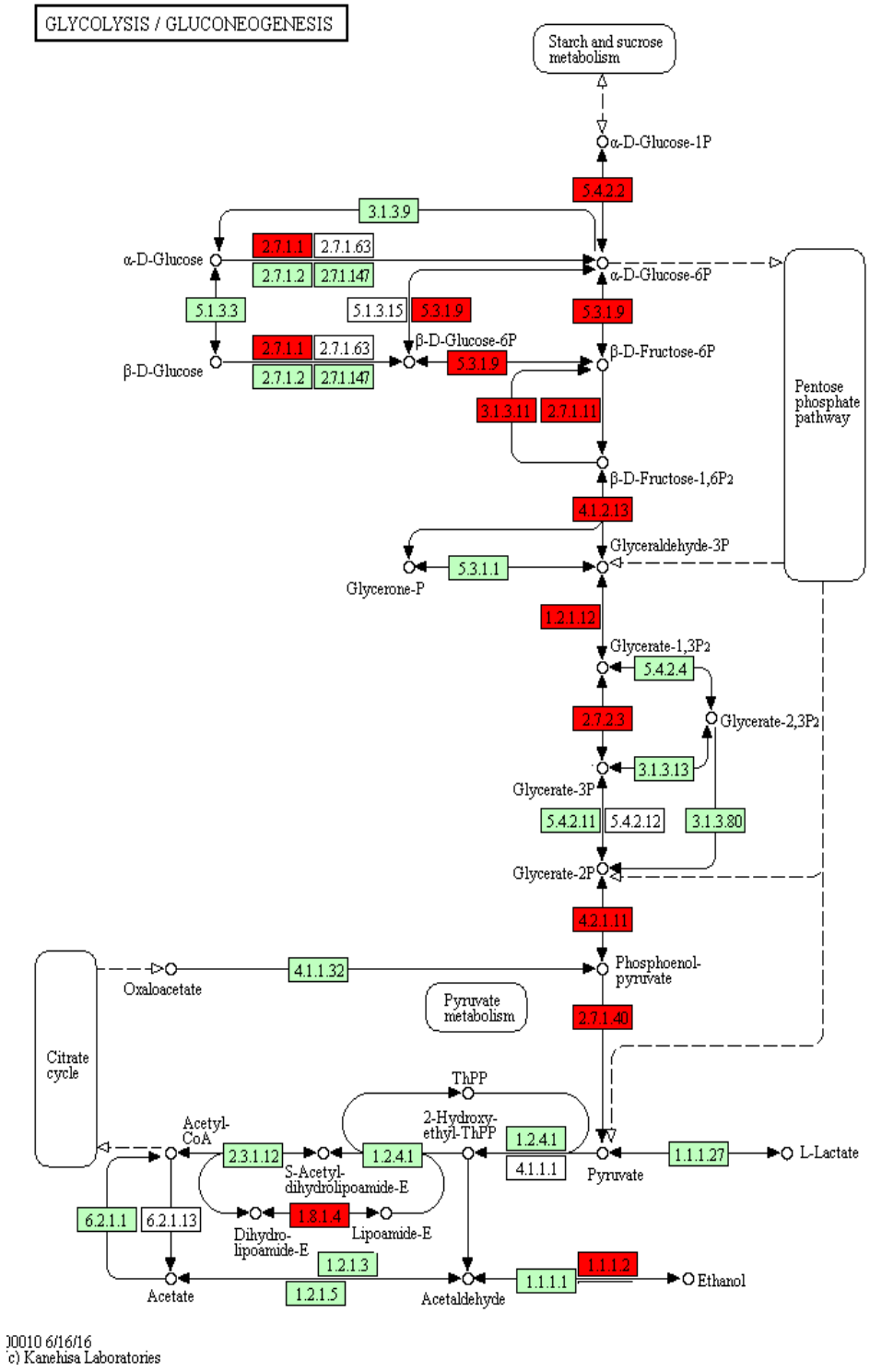

Figure 3.3. Glycolysis/gluconeogenesis pathway. Proteins down regulated during LPS induced maturation of moDC are highlighted in red. Both proteins highlighted in red and in green are members of human pathway. Pathway was plotted using KEGG Orthology Based Annotation System (*www.genome.jp/**kegg**).*

In the second phase of glycolysis is an energy gaining process where for each of the trio sugars, two ATP molecules and one NADH molecule are gained. GADP sugars are oxidised and phosphorylated by glyceraldehyde phosphate dehydrogenase (GAPDH; 1.2.1.12) giving two molecules of glycerate-1,3-phosphatase and also releasing two molecules of NADH. In the next step phosphate group is being transferred from glycerate-1,3-phosphatase to ADP by phosphoglycerate kinase 1 (2.7.2.3), forming ATP and 3-phosphoglycerate. This is followed by de-phosphorylation of 3-phosphoglycerate into 2-phosphoglycerate by phosphoglycerate mutase (5.4.2.11) an enzyme that is not downregulated by DC maturation. Enolase (4.2.1.11) then forms phosphoenolpyruvate from 2-phosphoglycerate. In the final step, pyruvate kinase (2.7.1.40) de-phosphorylates phosphoenolpyruvate to pyruvate and phosphorylates a molecule of ADP to ATP (Berg et al., 2012).

In the post glycolytic processes, NADH is oxidised back to NAD^+. In nonaerobic conditions this is done by pyruvate converting to lactate or by the pyruvate first converting to acetaldehyde and then by aldo-keto reductase (1.1.1.2) to ethanol. In aerobic conditions, NADH generated in glycolysis, is transferred to mitochondria where it is converted to acetyl-CoA, which then enters citric acid cycle.

The citric acid cycle (or Krebs cycle) is another metabolic pathway negatively affected by LPS induced maturation of moDCs. In this cycle, energy is generated through the oxidation of acetyl-CoA in the reactions carried out by 8 enzymes. Five of those enzymes are downregulated upon DC maturation (Fig. 3.4, highlighted in red).

Acetyl-CoA can be provided from glycolysis, or as a product of fatty acid oxidation or amino acid metabolism. The cycle begins with the transfer of carbon groups by citrate synthase (2.3.3.1) from acetyl-CoA to oxaloacetate, to form citrate. Citrate then undergoes isomerisation catalysed by aconitase (4.2.1.3) to form isocitrate. Then isocitrate is converted to 2-oxoglutaratein in two reactions catalysed by isocitrate dehydrogenase (1.1.1.42). Firstly, oxidation of isocitrate to oxalosuccinate occurs with the production of NADPH molecule, followed by decarboxylation of oxalosuccinate to 2-oxoglutarate. It is then oxidised to succinyl-CoA with the release of another NADH molecule. Subsequently succinyl-CoA is dephosphorylates into sonicate which is oxidised to form fumarate. Another downregulated enzyme, fumarate hydratase (4.2.1.2) is then hydrating a C-C double bond of fumarate, which results in the formation of L-malatate. In the last reaction of the citric cycle, L-malatate is oxidised by malate dehydrogenase (1.1.1.37) to give

oxaloacetate and release another NADPH. The next step is again step one, where acetyl-CoA donates carbon group to oxaloacetate (Berg et al., 2012).

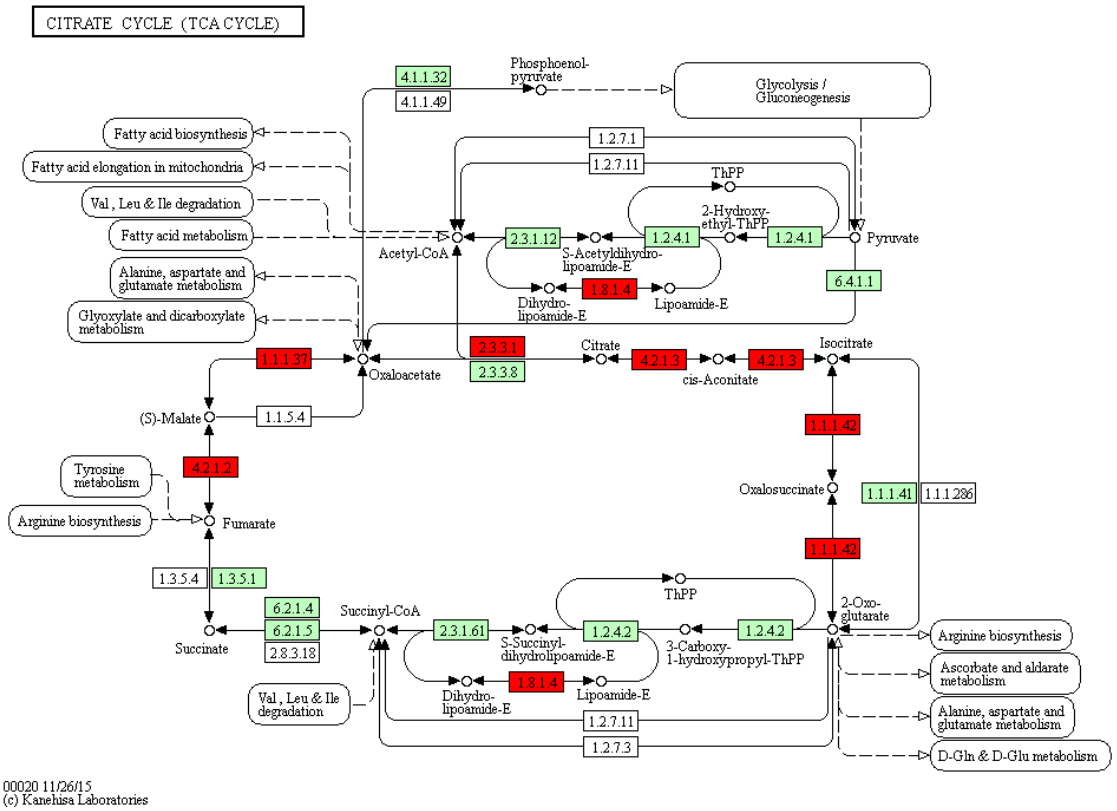

Figure 3.4. The citric acid cycle. Proteins down regulated during LPS induced maturation of moDC are highlighted in red. Both proteins highlighted in red and in green are members of human pathway. Pathway was plotted using KEGG Orthology Based Annotation System (*www.genome.jp/**kegg**).*

Another metabolic pathway affected by LPS induced moDC maturation is the pentose-phosphate pathway, where 11 enzymes are downregulated. In this sequence of biochemical reactions glucose-6-phosphate is oxidised to ribulose-5-phosphate and NADPH is produced. NADPH production is the main objective of this pathway, as it is necessary to carry out the reduction reaction in the cytoplasm and the synthesis of pentose sugars. The pentose phosphate pathway is divided into two phases, the oxidative phase where two molecules of $NADP^+$ are reduced to NADPH and the non-oxidative phase (Fig. 3.5; Berg et al., 2012).

Firstly, glucose 6-phosphate, through dehydrogenation with glucose-6-phosphate dehydrogenase (1.1.1.49), is converting to glucono-1,5-phospholactone releasing one NADPH

molecule. Glucono-1,5-phospholactone is then hydrolysed to 6-phosphogluconate by 6-phosphogluconolactonase (3.1.1.31), which is then converted to ribulose-5-phosphate by donating electron to $NADP^+$ and as a result generating another molecule of NADPH, and CO_2. The enzyme catalysing this reaction is phosphogluconate dehydrogenase (1.1.1.44).

The non-oxidative phase begins with the isomerisation of ribulose-5-phosphate, either to ribulose-5-phosphate by ribose 5-phosphate isomerase (5.3.1.6) or to xylulose 5-phosphate by ribulose-5-phosphate-3-epimerase (5.1.3.1). xylulose 5-phosphate and ribose 5-phosphate together undergo a reaction catalysed by transketolase (2.2.1.1) that gives glyceraldehyde 3-phosphate and sedoheptulose 7-phosphate which then together undergo a reaction performed by transaldolase 1 (2.2.1.2) and gives erythrose 4-phosphate and fructose 6-phosphate. Other enzymes form pentose phosphate pathway down-regulated upon LPS induced maturation were fructose-bisphosphate aldolase (4.1.2.13) converting glyceraldehayde to fructose-1,6-phosphate, which is then dephosphorylated to fructose 6-phosphate by fructose-bisphosphatase (3.1.3.11) which can be reversed by 6-phosphofructokinase (2.7.1.11); fructose 6-phosphate is be reversibly converted to glucose-6-phosphate by glucose-6-phosphate isomerase (Fig. 3.4; 5.3.1.9). Also two enzymes from post pentose phosphate reaction were downregulated; phosphoribosyl pyrophosphate synthetase 1-like (2.7.6.1) and phosphoglucomutase 2 (5.4.2.2 and 5.4.2.7).

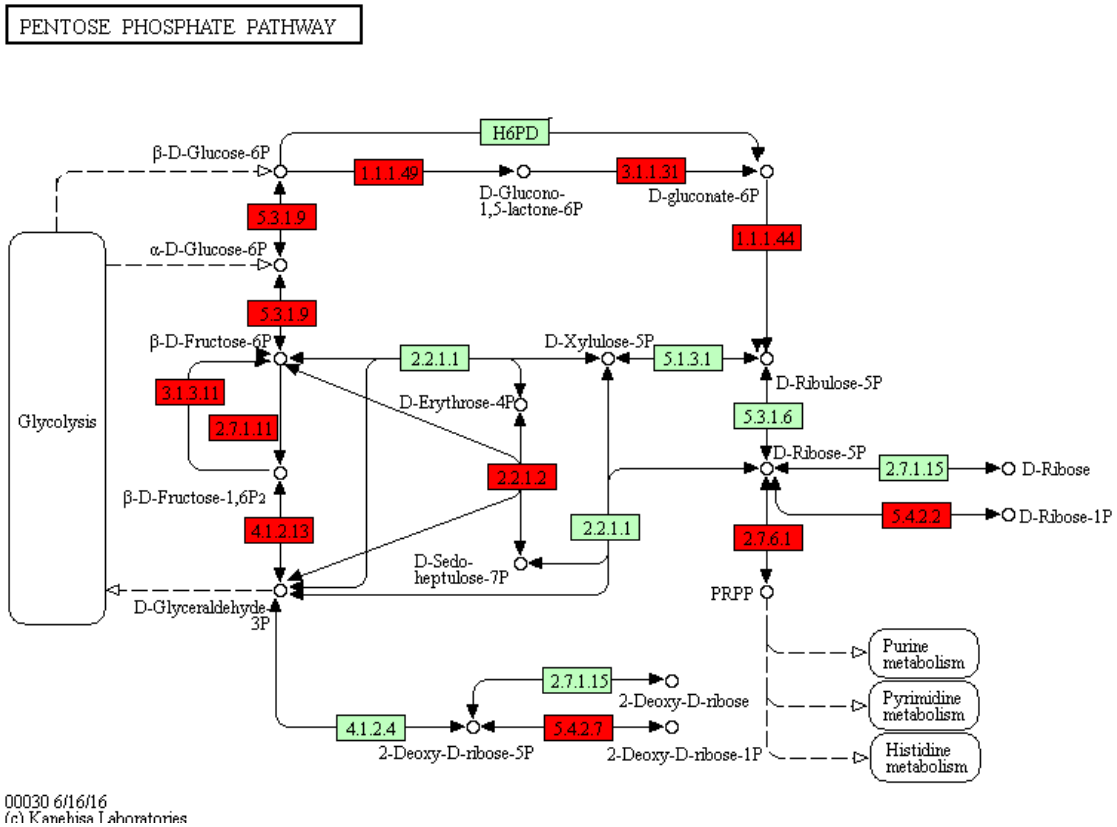

Figure 3.5. The pentose phosphate cycle. Proteins down regulated during LPS induced maturation of moDC are highlighted in red. Both proteins highlighted in red and in green are members of human pathway. Pathway was plotted using KEGG Orthology Based Annotation System (*www.genome.jp/**kegg**).*

Antigen presentation

DCs are the most potent antigen presenting cells and proteomic studies identified expression changes in several proteins involved in antigen processing and presentation. Proteins downregulated upon LPS-induced moDCs maturation were identified in both MHC class I and MHC class II pathways. After antigen presentation by MHC class I and II, T-cells, can establish the tolerance for self-antigen, and adaptive immunity against exogenous antigens. Additionally MHC I presents antigens produced by the cell itself, and MHC II presents foreign antigens.

Antigen processing by MHC I starts with the protein degradation by proteasome. Cytosolic proteins are then cut into 8-10 amino acid (aa) peptides, which are stabilised and directed towards endoplasmic reticulum (ER) by two chaperones, heat shock protein 70 (Hsp70; Fig. 3.6)

and heat shock protein 90 (Hsp90). Peptides are then being transferred into the endoplasmic reticulum (ER) by transporter associated with antigen processing (TAP). The TAP structure is formed of two proteins: TAP-1 and TAP-2 (TAP1/2). The TAP transporter can be also found in the lumen where it is linked to the large multimeric peptide-loading complex (PLC). PLC is formed by TAP, β2 microglobulin (β2M), calreticulin (CALR), ERp57 and tapasin (TAPBP), and MHC I and holds MHC I molecules until they have been fully loaded with peptides (Antoniou et al., 2003). When MHC I is loaded (on the Fig 3.6 shown together with its component β2M), the PLC dissociates, and MHC I leaves ER through the secretory pathway to reach the cell surface. It then interacts via α_3 domain with the extracellular IgV-like domain of CD8-α on CD8+ T-cells (Devine et al., 1999), or with killer-cell immunoglobulin-like receptor (KIR) on the surface of NK-cells. Current results show, that Hsp70, ERp57, CALR and heat shock protein family A member 5 (Hsp70A5; BiP on Fig. 3.6) are downregulated after LPS-induced DCs maturation.

Exogenous antigens are endocytosed and cleaved by cathepsin B (CATB), gamma-interferon-inducible lysosomal thiol reductase (GILT), legumin (AEP) and other endo/lysosomal proteases into small peptides of 14-20 aa (Blum et al., 2013). MHC II molecules are being synthetised in ER from α and β chains complexed with an invariant chain (Ii). Ii chai, blocks antigen binding site on MHC II until it is fused with late endosome, containing antigenic peptides. Ii the helps in the export of MHC II fused with endosomes into the Golgi and then Ii chain is degraded by cathepsins, including CATB, which is downregulated upon LPS-induced DC maturation. MHC II is then stabilised and transported in vesicles to the cell surface, where it presents the antigen to CD4+ T-cells.

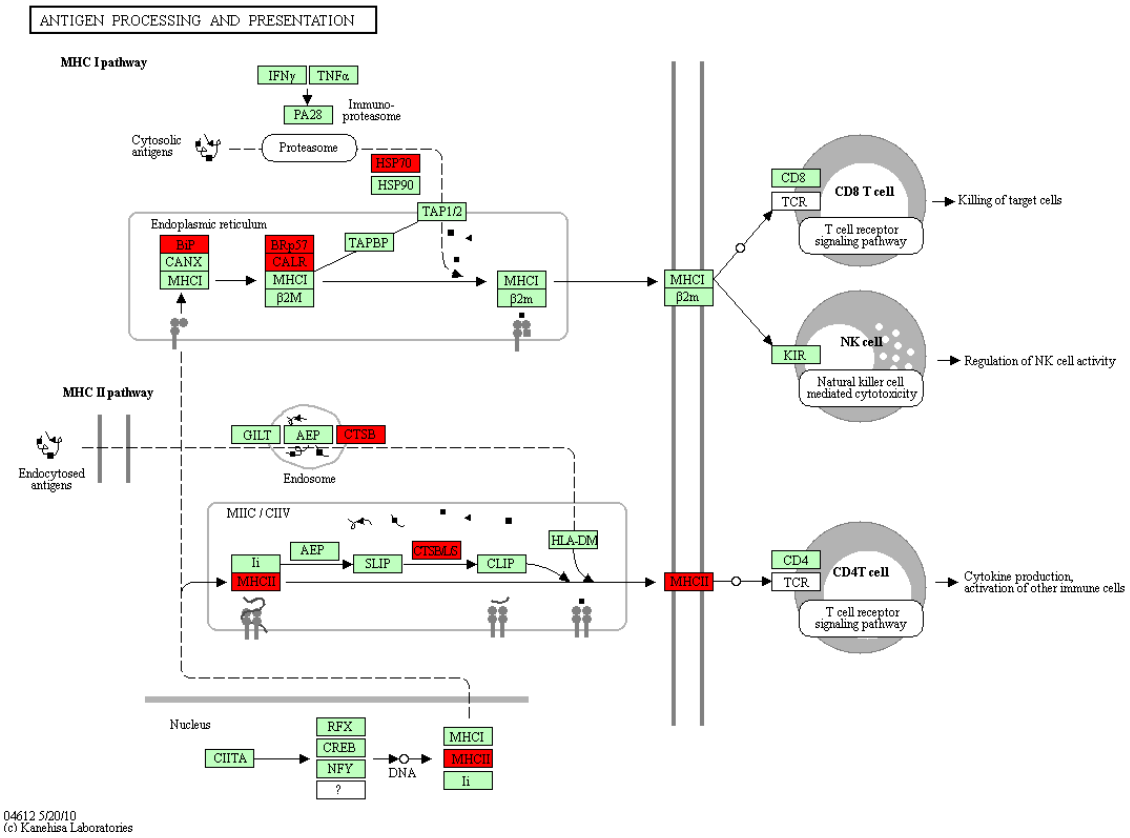

Figure 3.6. Antigen processing and presentation by DCs. Proteins down regulated during LPS induced maturation of moDC are highlighted in red. Both proteins highlighted in red and in green are members of human pathway. Pathway was plotted using KEGG Orthology Based Annotation System (*www.genome.jp/**kegg**).*

It was mentioned previously that exogenous antigens, prior to processing and presentation, are internalised by endocytosis. Endocytosis can be subdivided into two main subcategories, clathrin-mediated and clathrin-independent endocytosis. Several proteins from the clathrin-dependent pathway were down-regulated upon LPS induced maturation. The first identified protein was clathrin itself, which together with associated proteins plays critical role in the shaping of rounded vesicles for intracellular trafficking. Following clathrin, another downregulated protein was Arp2/3 complex, responsible for maintaining intracellular motility of endosomes and other intracellular vesicles (Fig. 3.7). Another downregulated protein was the heat shock cognate 70 (Hsc70), which together with the phosphatase auxilin is involved in removal of clathrin and associated protein from the surface of vesicles, prior to formation of early endosomes. Also two proteins associated with early endosomes, F-actin-capping protein

subunit beta and alpha (CAPZA and CAPZB), which function is to stabilise actin filaments were down-regulated.

Down-regulated proteins associated with late endosomes were Rab7 and sorting nexins 1/2 and 5 (SNX 1/2 and 5). Rab7 plays central role in the endocytosis, by participating in in multiple regulation mechanisms in endosomal sorting, biogenesis of lysosome and phagocytosis (Zhang et al., 2009). The role of SNX 1/2 and 5 proteins is protein sorting from endosomes to lysosomes.

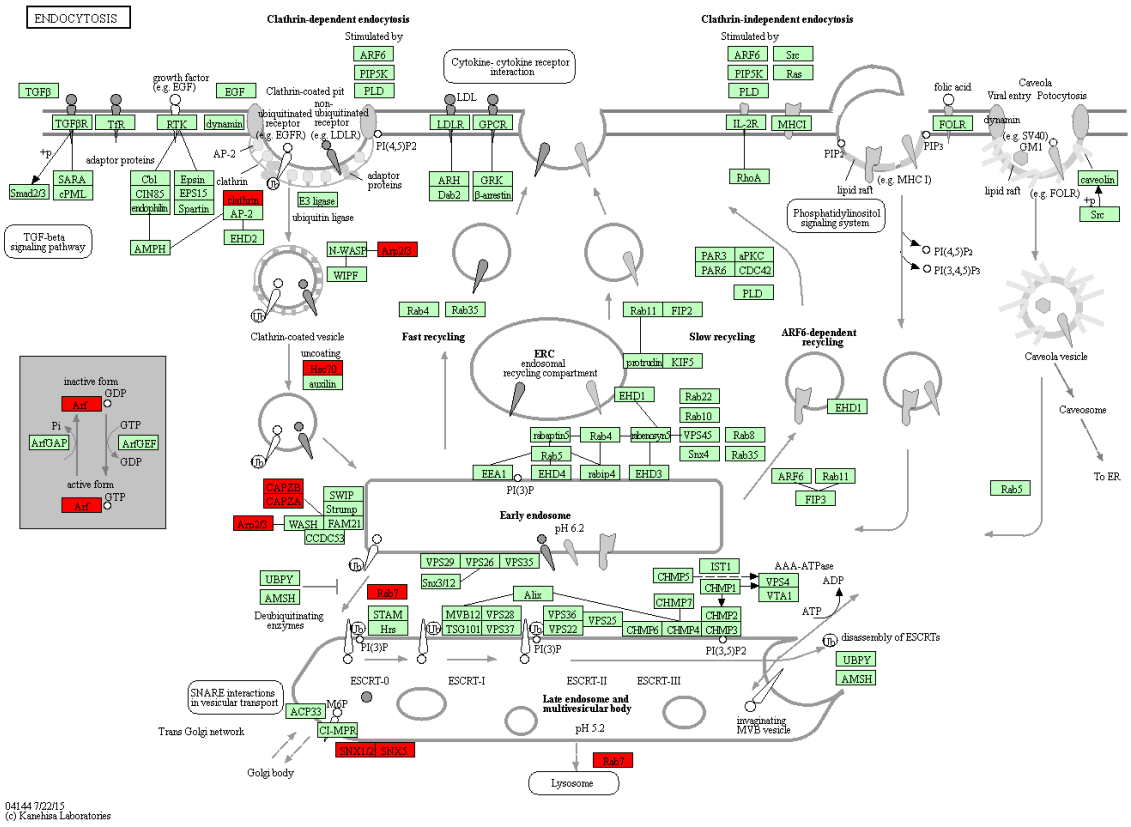

Figure 3.7. Endocytic pathway. Proteins down regulated during LPS induced maturation of moDC (highlighted in red) belong to clathrin dependent endocytic pathway. Both proteins highlighted in red and in green are members of human pathway. Pathway was plotted using KEGG Orthology Based Annotation System (*www.genome.jp/**kegg**).*

Lysosomal and phagosome protein

Several lysosomal enzymes were also down-regulated upon LPS-induced maturation. Those include proteases: cathepsins and tripeptidyl-peptidase 1 (TTP1), glycosidases: acid alpha-

glucosidase (GAA), hexosaminidase subunit alpha and beta (HEX A/B), and lysosomal alpha-mannosidase (LEMAN). Also sulfatase, glucosamine (N-acetyl)-6-sulfatase (GNS), lipase, lysosomal acid lipase/cholesteryl ester hydrolase (LIPA), ceramidase, N-acylsphingosine amidohydrolase 1 (ASAH1) and ganglioside GM2 activator (GM2A) were down-regulated. In addition, adaptor related protein complex 1 mu 2 subunit (AP-1) and clathrin, both involved in the transport of synthetised lysosomal enzymes are downregulated.

Upon LPS-induced maturation several proteins involved in phagosome function were downregulated. Those proteins were: coronin, ATPase H+ transporting V0, ras-related protein (Rab-7), tubulin β and calreticulin (CALR). In addition four phagocytosis promoting receptors were also downregulated: complement C3r receptor (CR3), integrin alpha M (αMβ), phospholipase A2 receptor and C-type lectin domain family 4 member M.

Protein synthesis and processing

The process of protein biosynthesis can be divided into three main parts; transcription of genomic DNA into mRNA occurring in the nucleus, translation of mRNA into amino acids by ribosomes and finally post-translational modifications, which involves covalent and enzymatic reactions, modifying polypeptide chain, to form mature protein.

Upon LPS-induced DCs maturation, 19 ribosomal proteins and 11 proteins involved in protein processing in ER, were found to be down-regulated. This indicates that maturation not only affects metabolic pathways and antigen presentation, as described above but also inhibits the synthesis of new proteins by DCs.

Ribosomal proteins downregulated upon LPS-induced maturation have different functions during translation, like initiation, elongation and termination. They are a components of either large 60S or small 40S ribosomal subunit, which together consist of around 80 proteins. Downregulated proteins from large ribosomal subunit are elongation factors thermo-unstable (ET-Tu): L4e, L8e, L23e, L11e, L7e, L14e and L27Ae; elongation factor thermos-unstable G (ET-Tu,G): L30e and L7Ae. Also proteins that were considered stable irrespectively of the cell treatment and are frequently used as housekeeping genes during PCR, were found to be downregulated upon LPS-treatment. These were the neutral phosphoprotein ribosomal protein P0 (RPLP0; LP0 on Fig. 3.8) and ribosomal phosphoproteins P1 and P2 (RPLP1 and RPLP2; LP1 and LP2 on Fig. 3.8). Other downregulated proteins from large ribosomal subunit were L15e,

L24e, L6e, L22e and L38e. Only three proteins belonging to small ribosomal subunit were downregulated. These were S18e, S13e involved in the initiation of translation and S25e.

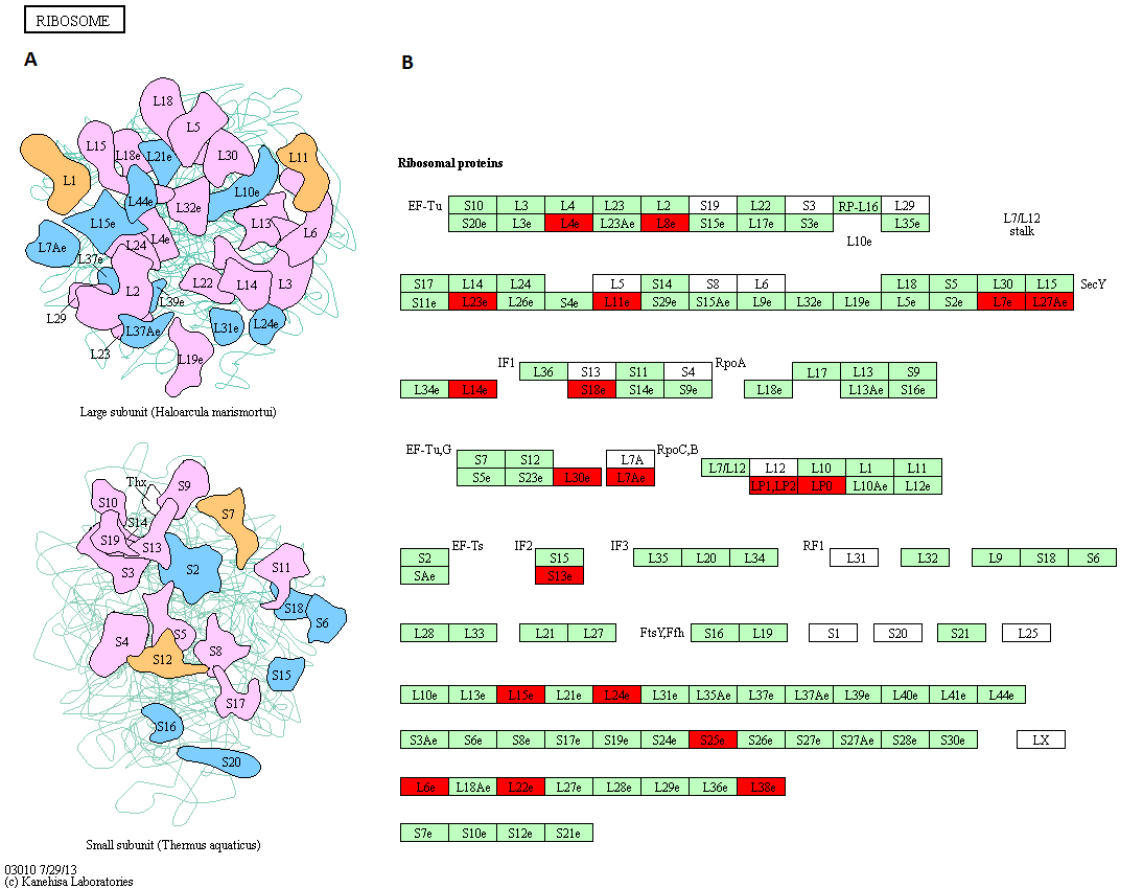

Figure 3.8. The structure of large and small subunit of ribosome. (A) Protein composition of large and small subunits of ribosome. (B) A list of ribosomal proteins with the proteins downregulated during LPS induced maturation of moDC highlighted in red. Both proteins highlighted in red and in green are components of human ribosome. Pathway was plotted using KEGG Orthology Based Annotation System (*www.genome.jp/**kegg**).*

Once a protein is translated from mRNA, the polypeptide chain is directed into the ER by signal recognition particle (SRP; Fig. 3.9). Once the protein enters ER, it is recognised by molecular chaperones including the downregulated proteins, binding immunoglobulin protein (BiP) and heat shock protein 90 kDa beta member 1 (GRP94). In addition to protein recognition, they are crucial for proper protein folding and Bip is also required to transport protein into ER lumen. Another downregulated protein, an enzyme alpha 1,3-glucosidase (GlcII) which catalyses N-glycosylation and also de-glycosylation during protein processing in endoplasmic reticulum.

Other downregulated endosomal proteins are protein disulfide isomerase family A member 3 (ERP57), calreticulin (CRT) and protein disulfide isomerase family A member 6 (PDIs).

In addition to ER proteins, also three proteins involved in ER-associated protein degradation (ERAD) pathway were downregulated; heat shock protein family A (Hsp70), heat shock protein family H (NEF) and valosin containing protein (p97). The function of ERAD is targeting of misfolded proteins for ubiquitination and later degradation by phagosome.

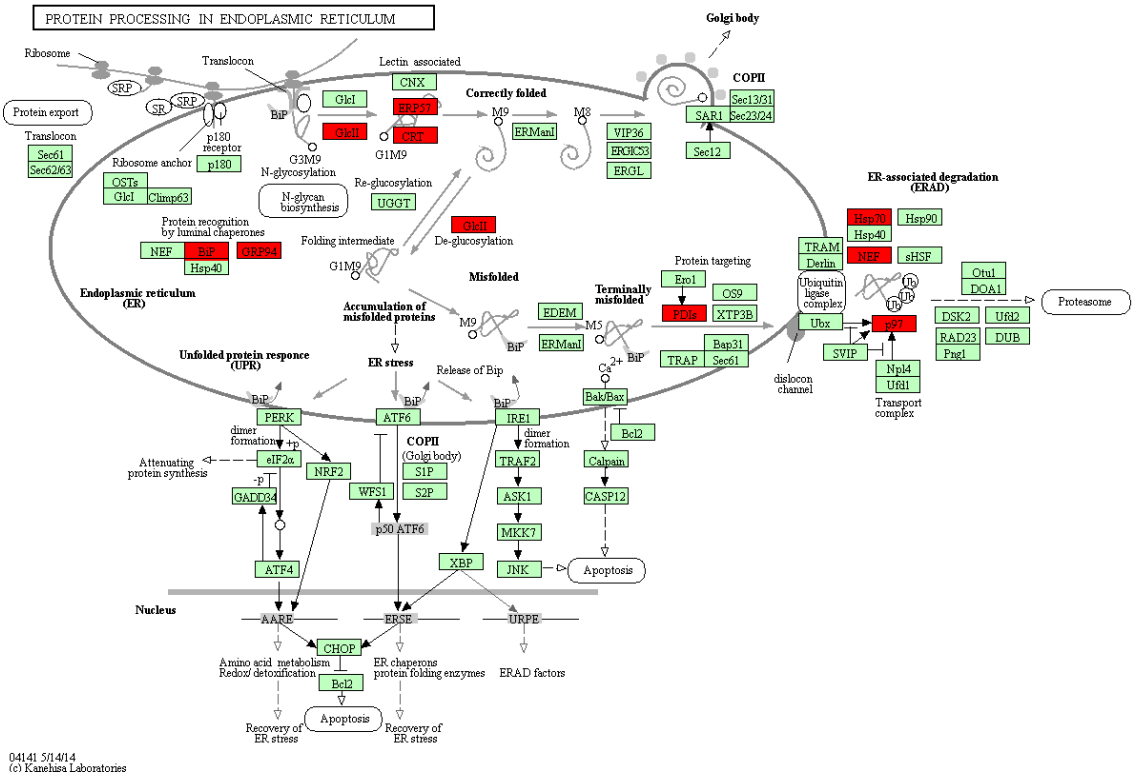

Figure 3.9. Protein processing in ER. Proteins down regulated during LPS induced maturation of moDC are highlighted in red. Both proteins highlighted in red and in green are members of human pathway. Pathway was plotted using KEGG Orthology Based Annotation System (*www.genome.jp/kegg).*

3.3.3.1. Proteins that exhibit reduced expression following HAP-induced maturation of moDC

Upon HAP-induced maturation of DCs, the majority of proteins in cell lysates which exhibited alterations in protein expression were down-regulated. This accounts for more than 97% of these proteins (Table 3.5). Among these, are proteins involved in many cellular processes

including cell metabolism, antigen presentation and protein synthesis. Proteins were therefore grouped into specific pathways using KEGG – GenomeNet (*www.genome.jp/kegg).*

UNIPROT	PROTEIN NAME	FOLD DECREASE	P VALUE
Q01105	Protein SET	57.25	0.000
Q92882	Osteoclast-stimulating factor 1	44.00	0.001
P13667	Protein disulfide-isomerase A4	25.62	0.016
Q92945	Far upstream element-binding protein 2	24.77	0.006
Q13075	Baculoviral IAP repeat-containing protein 1	22.08	0.002
P27797	Calreticulin	20.67	0.003
O95379	Tumor necrosis factor alpha-induced protein 8	19.67	0.037
P05455	Lupus La protein	18.58	0.000
Q9Y5X3	Sorting nexin-5	16.04	0.017
P61923	Coatomer subunit zeta-1	15.49	0.001
Q15435	Protein phosphatase 1 regulatory subunit 7	14.02	0.017
P08238	Heat shock protein HSP 90-beta	13.95	0.053
P08697	Alpha-2-antiplasmin	13.12	0.002
P19338	Nucleolin	11.71	0.000
P06748	Nucleophosmin	11.09	0.005
Q16543	Hsp90 co-chaperone Cdc37	10.89	0.001
P36543	V-type proton ATPase subunit E 1	10.53	0.026
Q6DKI2	Galectin-9C	9.83	0.009
O60234	Glia maturation factor gamma	9.76	0.027
Q13838	Spliceosome RNA helicase DDX39B	9.15	0.034
Q9Y315	Deoxyribose-phosphate aldolase	8.98	0.027
O60763	General vesicular transport factor p115	8.57	0.021
P16403	Histone H1.2	8.02	0.002
P07237	Protein disulfide-isomerase	7.65	0.000
P07437	Tubulin beta chain	7.57	0.000
P07910	Heterogeneous nuclear ribonucleoproteins C1/C2	6.97	0.001
Q9Y3F4	Serine-threonine kinase receptor-associated protein	6.85	0.000
P08758	Annexin A5	6.62	0.004
P52566	Rho GDP-dissociation inhibitor 2	6.26	0.020
Q00839	Heterogeneous nuclear ribonucleoprotein U	5.69	0.050
Q13451	Peptidyl-prolyl cis-trans isomerase FKBP5	5.58	0.025
Q15084	Protein disulfide-isomerase A6	5.23	0.003
P15090	Fatty acid-binding protein, adipocyte	5.02	0.003
P06702	Protein S100-A9	4.94	0.004
P14317	Hematopoietic lineage cell-specific protein	4.88	0.044
P61956	Small ubiquitin-related modifier 2	4.88	0.048

P55209	Nucleosome assembly protein 1-like 1	4.81	0.000
P14314	Glucosidase 2 subunit beta	4.68	0.028
P62136	Serine/threonine-protein phosphatase PP1	4.61	0.048
P30040	Endoplasmic reticulum resident protein 29	4.61	0.009
P19823	Inter-alpha-trypsin inhibitor heavy chain H2	4.52	0.002
P51572	B-cell receptor-associated protein 31	4.52	0.035
Q9BUF5	Tubulin beta-6 chain	4.50	0.002
P55084	Trifunctional enzyme subunit beta, mitochondrial	4.50	0.040
P60866	40S ribosomal protein S20	4.50	0.050
P63173	60S ribosomal protein L38	4.48	0.006
P02774	Vitamin D-binding protein	4.38	0.013
Q9H0E2	Toll-interacting protein	4.08	0.040
P05109	Protein S100-A8	3.87	0.022
Q9H4B7	Tubulin beta-1 chain	3.86	0.015
P23284	Peptidyl-prolyl cis-trans isomerase B	3.80	0.049
Q9UBR2	Cathepsin Z	3.77	0.046
P19105	Myosin regulatory light chain 12A	3.53	0.005
P30101	Protein disulfide-isomerase A3	3.40	0.018
P50502	Hsc70-interacting protein	3.39	0.022
P07858	Cathepsin B	3.33	0.019
Q9Y6N5	Sulfide:quinone oxidoreductase, mitochondrial	3.14	0.019
Q9NQC3	Reticulon-4	3.07	0.009
P09382	Galectin-1	3.03	0.018
P15880	40S ribosomal protein S2	2.97	0.028
O43396	Thioredoxin-like protein 1	2.96	0.020
P68366	Tubulin alpha-4A chain	2.93	0.025
P26599	Polypyrimidine tract-binding protein 1	2.90	0.024
Q8N392	Rho GTPase-activating protein 18	2.88	0.050
P62847	40S ribosomal protein S24	2.84	0.032
Q9H223	EH domain-containing protein 4	2.83	0.048
O00560	Syntenin-1	2.81	0.009
P07355	Annexin A2	2.75	0.001
P21980	Protein-glutamine gamma-glutamyltransferase 2	2.68	0.007
P68371	Tubulin beta-4B chain	2.65	0.055
P07339	Cathepsin D	2.63	0.021
P51659	Peroxisomal multifunctional enzyme type 2	2.59	0.001
P26447	Protein S100-A4	2.58	0.030
P62913	60S ribosomal protein L11	2.55	0.010
Q99536	Synaptic vesicle membrane protein VAT-1 homolog	2.53	0.016
Q71U36	Tubulin alpha-1A chain	2.52	0.032
P60660	Myosin light polypeptide 6	2.50	0.006
P41240	Tyrosine-protein kinase CSK	2.46	0.047
P30050	60S ribosomal protein L12	2.46	0.035

P49411	Elongation factor Tu, mitochondrial	2.42	0.020
P54920	Alpha-soluble NSF attachment protein	2.40	0.019
P19878	Neutrophil cytosol factor 2	2.39	0.014
P14625	Endoplasmin	2.38	0.013
P18124	60S ribosomal protein L7	2.38	0.013
P11021	78 kDa glucose-regulated protein	2.28	0.003
P60842	Eukaryotic initiation factor 4A-I	2.27	0.032
Q9Y3Z3	Deoxynucleoside triphosphate triphosphohydrolase SAMHD1	2.24	0.034
P28676	Grancalcin	2.22	0.028
P31948	Stress-induced-phosphoprotein 1	2.21	0.010
P62241	40S ribosomal protein S8	2.19	0.039
P53621	Coatomer subunit alpha	2.19	0.025
P61978	Heterogeneous nuclear ribonucleoprotein K	2.18	0.014
P05387	60S acidic ribosomal protein P2	2.16	0.002
P35579	Myosin-9	2.14	0.024
P02776	Platelet factor 4	2.12	0.009
P62906	60S ribosomal protein L10a	2.12	0.009
P62081	40S ribosomal protein S7	2.11	0.002
P52790	Hexokinase-3	2.09	0.015
P62269	40S ribosomal protein S18	2.09	0.003
P26641	Elongation factor 1-gamma	2.08	0.004
Q9UBW5	Bridging integrator 2	2.06	0.040
O94925	Glutaminase kidney isoform, mitochondrial	2.05	0.048
O14773	Tripeptidyl-peptidase 1	2.05	0.008
P07686	Beta-hexosaminidase subunit beta	2.04	0.052
Q13177	Serine/threonine-protein kinase PAK 2	2.00	0.031
P05388	60S acidic ribosomal protein P0	2.00	0.002
Q9NTK5	Obg-like ATPase 1	1.99	0.001
P08865	40S ribosomal protein SA	1.98	0.039
P18510	Interleukin-1 receptor antagonist protein	1.96	0.020
Q14103	Heterogeneous nuclear ribonucleoprotein D0	1.95	0.019
Q02878	60S ribosomal protein L6	1.89	0.019
P12956	X-ray repair cross-complementing protein 6	1.89	0.019
P62280	40S ribosomal protein S11	1.89	0.031
P23396	40S ribosomal protein S3	1.88	0.049
P26373	60S ribosomal protein L13	1.88	0.041
Q13510	Acid ceramidase	1.85	0.018
P83731	60S ribosomal protein L24	1.85	0.011
P46783	40S ribosomal protein S10	1.84	0.052
P62888	60S ribosomal protein L30	1.84	0.000
P63244	Guanine nucleotide-binding protein subunit beta-2-like 1	1.80	0.036
P15153	Ras-related C3 botulinum toxin substrate 2	1.80	0.045
P62158	Calmodulin	1.77	0.047

O75915	PRA1 family protein 3	1.77	0.043
P51148	Ras-related protein Rab-5C	1.74	0.059
P38646	Stress-70 protein, mitochondrial	1.73	0.042
P23526	Adenosylhomocysteinase	1.69	0.057
P23526	Adenosylhomocysteinase	1.69	0.057
P36578	60S ribosomal protein L4	1.68	0.033
Q14697	Neutral alpha-glucosidase AB	1.68	0.058
P62829	60S ribosomal protein L23	1.68	0.031
P05386	60S acidic ribosomal protein P1	1.68	0.042
Q01469	Fatty acid-binding protein, epidermal	1.67	0.013
P62277	40S ribosomal protein S13	1.67	0.011
P46777	60S ribosomal protein L5	1.67	0.033
P01911	HLA class II histocompatibility antigen, DRB1-15 beta chain	1.67	0.006
O43488	Aflatoxin B1 aldehyde reductase member 2	1.66	0.030
P04080	Cystatin-B	1.62	0.051
Q9UI12	V-type proton ATPase subunit H	1.61	0.050
P61916	Epididymal secretory protein E1	1.60	0.038
Q9ULV4	Coronin-1C	1.60	0.011
P46782	40S ribosomal protein S5	1.59	0.020
Q9Y2Q3	Glutathione S-transferase kappa 1	1.58	0.010
Q9BTM1	Histone H2A.J	1.58	0.026
O75347	Tubulin-specific chaperone A	1.56	0.007
P12081	Histidine--tRNA ligase, cytoplasmic	1.56	0.027
Q9P0L0	Vesicle-associated membrane protein-associated protein A	1.55	0.010
P00918	Carbonic anhydrase 2	1.55	0.029
P61353	60S ribosomal protein L27	1.53	0.022
Q8WUM4	Programmed cell death 6-interacting protein	1.53	0.008
Q99798	Aconitate hydratase, mitochondrial	1.51	0.055
O15143	Actin-related protein 2/3 complex subunit 1B	1.47	0.018
P61026	Ras-related protein Rab-10	1.46	0.024
P10809	60 kDa heat shock protein, mitochondrial	1.46	0.018
Q86VP6	Cullin-associated NEDD8-dissociated protein 1	1.45	0.023
P47755	F-actin-capping protein subunit alpha-2	1.42	0.042
P61163	Alpha-centractin	1.41	0.028
P28482	Mitogen-activated protein kinase 1	1.39	0.008
P38606	V-type proton ATPase catalytic subunit A	1.39	0.023
P17987	T-complex protein 1 subunit alpha	1.38	0.040
P67936	Tropomyosin alpha-4 chain	1.38	0.014
P14550	Alcohol dehydrogenase [NADP(+)]	1.38	0.028
Q96TA1	Niban-like protein 1	1.37	0.036
P40121	Macrophage-capping protein	1.34	0.050
P50395	Rab GDP dissociation inhibitor beta	1.32	0.001
P21281	V-type proton ATPase subunit B, brain isoform	1.31	0.042

O75874	Isocitrate dehydrogenase [NADP] cytoplasmic	1.30	0.043
P52209	6-phosphogluconate dehydrogenase, decarboxylating	1.29	0.011
P09467	Fructose-1,6-bisphosphatase 1	1.27	0.049
O14818	Proteasome subunit alpha type-7	1.26	0.055
P40925	Malate dehydrogenase, cytoplasmic	1.26	0.007
P51452	Dual specificity protein phosphatase 3	1.25	0.011
P13639	Elongation factor 2	1.24	0.063
P16050	Arachidonate 15-lipoxygenase	1.24	0.045
O60664	Perilipin-3	1.23	0.015
P28066	Proteasome subunit alpha type-5	1.19	0.025
P06744	Glucose-6-phosphate isomerase	1.19	0.031
P50990	T-complex protein 1 subunit theta	1.17	0.004
P37837	Transaldolase	1.15	0.032
P84077	ADP-ribosylation factor 1	1.15	0.015

Table 3.4. List of the proteins downregulated, after stimulation of dendritic cells with HAP.

Cell metabolism

HAP induced maturation affected cellular metabolism but to a much lower extent than LPS-induced maturation. Only four components of glycolysis and six proteins from the pentose phosphate pathway were downregulated.

Downregulated proteins involved in glycolysis, were also found to be downregulated upon LPS stimulation, those proteins are: glucose-6-phosphate isomerase (Fig. 3.3 5.3.1.9), an enzyme converting glucose 6-phosphate into fructose 6-phosphate (F6P); hexokinase 1 (2.7.1.1); fructose-bisphosphatase 1 (3.1.3.11) which dephophorylates β-D-fructose 1,6-bisphosphate to F6P. Also one protein involved in the post glycolytic processes is downregulated. Aldo-keto reductase (1.1.1.2) is involved in the oxidation of NADH to NAD^+ under non-aerobic conditions.

Another metabolic pathway affected by HAP-induced moDC maturation is the pentose-phosphate pathway where four of the downregulated enzymes correspond to enzymes downregulated upon LPS stimulation. Those enzymes are: phosphogluconate dehydrogenase (Fig. 3.5 1.1.1.44), transaldolase 1 (2.2.1.2), fructose-bisphosphatase (3.1.3.11) and glucose-6-phosphate isomerase (5.3.1.9). There are also several downregulated enzymes involved in pentose phosphate pathway that were not downregulated upon LPS induced maturation. Those enzymes are glucose 1-dehydrogenase (H6PD), which belongs to oxidoreductases and catalyses conversion of β-D-glucose- 6 phosphate to D-gluconate-6 phosphate; and deoxyribose-

phosphate aldolase (4.1.2.4), which produces D-glyceraldehyde 3-phosphate and acetaldehyde from 2-deoxy-D-ribose 5-phosphate.

Antigen presentation

Proteins involved in antigen presentation that were downregulated upon HAP induced moDCs maturation were identified in both MHC class I and MHC class II pathways. In general downregulated proteins corresponded to the ones identified upon LPS induced DC maturation. For MHC I pathway those were HSP90, ERp57, CALR and BiP, for MHC II pathway CTSB and CTSB/LiS. However in contrast to LPS induced maturation, MHC II molecule itself was not downregulated upon HAP stimulation.

Protein biosynthesis

The biggest difference in the protein expression between LPS and HAP induced moDC maturation, were observed in protein biosynthesis. Upon HAP-induced DCs maturation, 27 ribosomal proteins and 9 proteins involved in protein processing in ER, were found to be down-regulated. From the downregulated ribosomal proteins 12 correspond to the ones identified upon LPS induced maturation, these proteins are L4e, L6e, L7e, L11e, L23e, L24e, L30e, L38e, RPLP0, LP1/2, S13e and S18e. Other proteins downregulated upon HAP induced maturations were EF-Tu proteins: S20e, S3e, S11e, S2e and L5e, and EF-Tu,G proteins S5e and L30e (Fig. 3.10). In addition down-regulated proteins belonging to the large subunit were: L10Ae, L12e, L13e and L27e; and belonging to small ribosomal subunit: Sae, S8e, S24e, S7e and S10e.

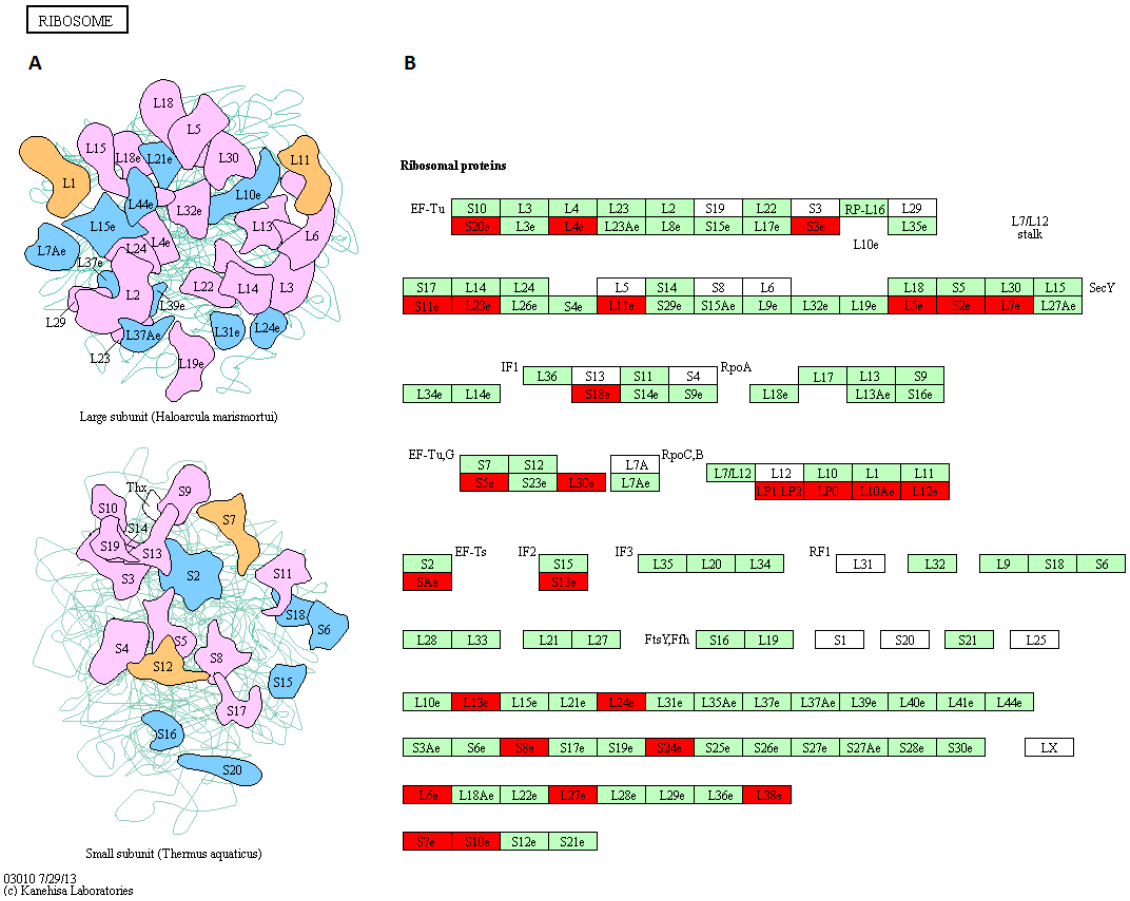

Figure 3.10. The structure of large and small subunit of ribosome. (A) Protein composition of large and small subunits of ribosome. (B) A list of ribosomal proteins with the proteins downregulated during HAP-induced maturation of moDC highlighted in red. Both proteins highlighted in red and in green are components of human ribosome. Pathway was plotted using KEGG Orthology Based Annotation System (*www.genome.jp/**kegg**).*

Upon HAP-induced maturation, downregulated ER proteins involved in posttranslational processing, correspond to the proteins downregulated upon LPS stimulation, namely Bip, GRP94, GlcII, ERP57, CRT and PDIs. The difference was observed for ERAD pathway, where only heat shock protein 90 alpha (Hsp90) and B-cell receptor-associated protein 31 (Bap31), leading to ERAD were downregulated.

3.4. Discussion

DCs are initiators of immune response and inflammation processes. However, to fulfil this role they need to be activated upon contact with an antigen and undergo a process called maturation, which comprises multiple cellular changes. The aims of maturation are, to allow morphological and physiological changes of DCs that aid antigen processing and the subsequent migration to the lymphatic organ for antigen presentation. Here we performed a novel proteome profiling study of human DCs during the maturation induced with LPS and HAP. Although there were numerous proteomic studies performed previously examining DCs in different functional states (Angenieux et al., 2001; Le Naour et al., 2001; Richards et al., 2002; Pereira et al., 2005; Ferreira et al., 2008; Gundacker et al., 2009), the tool used for this study, SWATH proteomics has never used before to characterise DCs proteome. Due to its accuracy and sensitivity, the current study can for the first time provide detail of maturation-induced proteomic changes in a comprehensive and fully quantitative manner and would be impossible using traditional techniques such as 2-D gel electrophoresis or shotgun proteomics. In addition, this study for the first time uses HAP to induce DC maturation and provides quantitative analysis of subsequent proteomic changes. This can bring important insight into the pathology of inflammatory diseases associated with tissue calcification, such as age-related macular degeneration, atherosclerosis and Alzheimer's disease and, or into the mechanisms of bone graft rejection.

SWATH analysis allowed identification of 845 proteins in cell lysates from moDCs from which 260 proteins and 190 proteins were significantly altered when DCs were differentiated upon LPS stimulation and HAP stimulation, respectively. From those, twenty (7.7%) were upregulated upon LPS-induced maturation and only six (3.2%) upon HAP induced maturation (Fig. 3.11). Proteins that exhibited the largest, more than 30-fold increase upon LPS induced maturation were three interferon induced proteins, IFN-induced GTP binding protein, IFN-induced protein with tetratricopeptide repeat 3 and ubiquitin-like protein ISG15. These observation match exactly to the previously published results by Gundacker et al. (2009). Using shotgun proteomics, they also identified those three particular proteins as being the main upregulated proteins upon LPS-induced maturation of DCs. Nevertheless, in contrast to Gundacker's study, current results are fully quantitative. In addition, one of those proteins, IFN-induced protein with tetratricopeptide repeats 3, was also the most upregulated upon HAP-induced maturation,

albeit the increase was just 2.5-fold. Those proteins are involved in antiviral and antibacterial defence and ubiquitin like protein serves additionally as a negative regulator of ubiquitination.

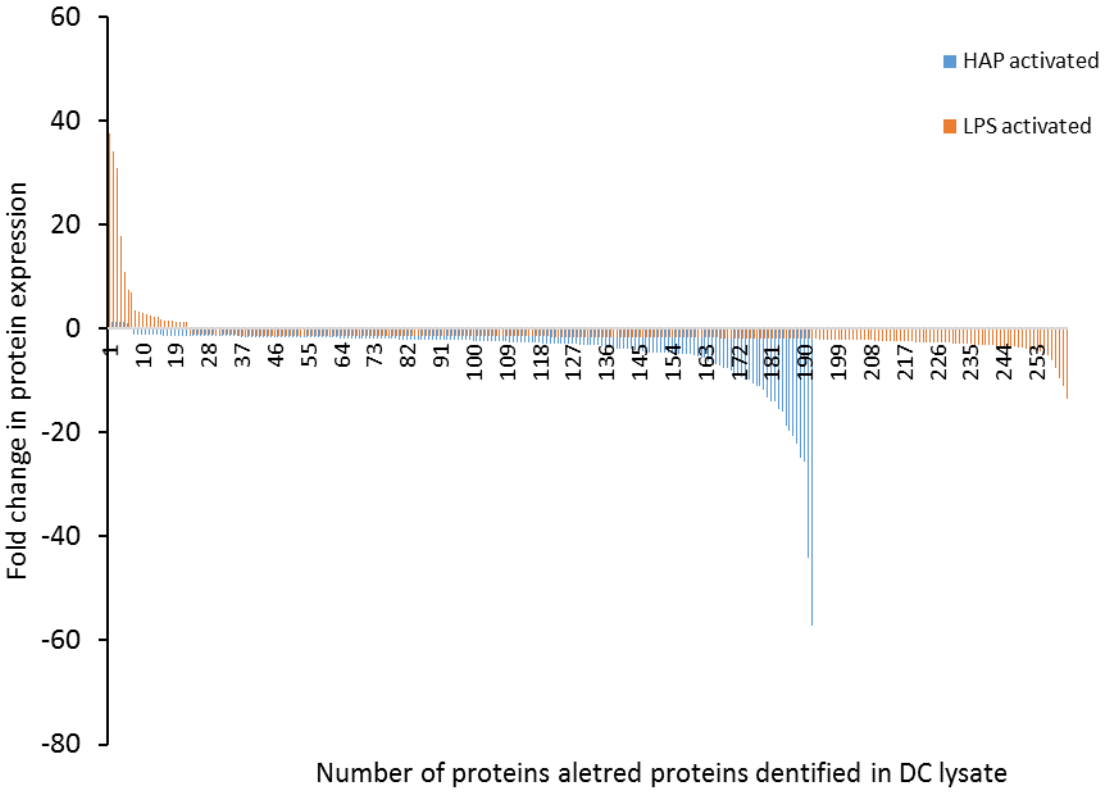

Figure 3.11. Schematic summary of protemic data, demonstrating differences and similarities between dendritic cells (DC) activated with LPS (orange) and HAP (blue). 260 proteins and 190 proteins were significantly altered when DCs were differentiated upon LPS stimulation and HAP stimulation, respectively.

Other proteins identified to be upregulated upon LPS-induced maturation, can be assigned into functional groups. Firstly, a group of proteins identified are known to be involved in the positive regulation of ubiquitination. Ubiquitination targets protein for destruction and is an important post-translational regulator of the immune response on many levels including innate and adaptive immunity and antimicrobial defence (Jiang and Chen, 2011). Ubiquitination also regulates the antigen presenting function of DCs by influencing TLR4 signalling in multiple ways. The TLR4 pathway is activated after binding LPS or HAP and follows either MyD88 or TRIF route,

which was described in detail in the introduction. Ubiquitination is involved in the regulation of both routes by activation NF-κB and MAPK cascade downstream of both routes (Kayagaki et al., 2007) and also ubiquitination of TRAF3, which leads to INF secretion (Kagan et al., 2008). Ubiquitination is also crucial for antigen presentation by both MHC class I and II (Oh and Shin, 2015). In DCs, MHC II is ubiquitinated via lysine of of the β subunit (Shin et al., 2006), which is mediated by the ubiquitin ligase, membrane-associated RING-CH1 (MARCH1; Nice et al., 2010). The role of MHC II ubiquitination is reduction of MHC II surface expression and therefore antigen presentation as a response to IL-10 and regulatory T-cells. In addition, it promotes cytokine production and aids the ability of DCs to activate CD4+ T-cells, even when less antigen is being presented (Oh and Shin, 2015). The ubiquitination of MHC I is also mediated via MARCH1 and leads to rapid endocytosis and degradation (Lang et al., 2013).

Another group of proteins up-regulated upon LPS-induced maturation consisted of proteins involved in stabilising cell structure and cytoskeletal remodelling. These include fascin, keratin type I and II, calpain and actin binding coronin 1B. Upon maturation, DCs undergo morphological and functional changes, including development of extensive cytoplasmic projections in many directions from the cell body (Tan et al., 2010; Verdijk et al., 2004). This process involves cytoskeletal remodelling; therefore, it was expected to find upregulated proteins involved in this process. Fascin (Al-Alwan et al., 2001) and calpain (Gundacker et al., 2008) were previously reported to be highly expressed during DC maturation. In addition coronin 1B is required for efficient cell migration of maturing DCs to the lymphatic organs (Cai, et al., 2005). Also one protein up-regulated during HAP induced DCs maturation ITGB3 is involved in migration and growth (Lee et al., 2012).

The SWATH analysis identified a massive decrease in global protein expression upon DC maturation. This accounts for as much as 92% of altered proteins for LPS activated cells and almost 97% of altered proteins for HAP activated DCs. For LPS activated cells, 55 proteins (23% of the total downregulated proteins) are involved in cellular metabolism. For HAP activated cells, 23 proteins involved in metabolism are downregulated (12.5% of the total downregulated proteins). The pathways that are mostly affected, are the ones involved in carbon metabolism: glycolysis, gluconeogenesis, pentose phosphate pathway and citrate cycle. Interestingly, proteins involved in fatty acid metabolism and biosynthesis of amino acids are not affected at 24 h of maturation.

The groups of proteins most affected by DC maturation were ribosomal proteins and proteins involved in protein processing in ER. Upon LPS-induced maturation 19 ribosomal and 11 ER proteins were downregulated and upon HAP-induced maturation, 27 and 9 proteins were downregulated, respectively. This suggests that protein translation and post-translational modifications are very important for DC-directed immune response. There are multiple studies linking inflammation, innate immunity, and post-transcriptional regulation (Todd et al., 2008).

Ribosomal proteins together with some of the ER components make a complex cellular machinery responsible for protein synthesis through translation and post-translational modifications. For a long time ribosomal proteins were considered only to be important collectively, but now it is clear that many of those proteins are multifunctional and play an important role in the regulation of cell growth and death (Warner and McIntosh, 2009).

Global protein synthesis is increased between 8 to 12h of LPS induced maturation followed by a gradual decrease (Ceppi et al., 2009). This increased protein synthesis is tightly controlled during DC activation as it correlates to activation of translational proteins, eIF4E-binding proteins (4E-BPs) and S6 ribosomal protein (S6) and dephosphorylation of negative regulator of translation, alpha-subunit of eukaryotic translation initiation factor 2 (eIF2α; Ceppi et al., 2009). This sudden activation of the translational process then reverted back to the steady state, which correlated with the global protein synthesis pattern. Nonetheless, the authors observed that relative transcription and translation intensity was maintained even at 16 h of maturation. Current results now extended the observation of translational machinery to 24 h of maturation. Downregulation of translational machinery at 24 h post LPS activation, is also in agreement with the large number of proteins to which a decrease in expression was observed. Current results also revealed for the first time that HAP-induced maturation of DCs can lead to changes in protein translation and post-translational modifications. With many identified proteins being downregulated after 24 h post HAP stimulation.

Upon DC maturation it was found that MHC class I molecules, which are known to be involved in antigen presentation, were up-regulated. Three subunits of MHC class I molecules were identified with 3 to 7-fold increase in expression after LPS stimulation. MHC I presents self-antigens, which are either partially degraded proteins, proteins that were previously functional or newly synthesised but defective proteins (Apcher et al., 2012; Rock et al., 2014). Activated DCs are known to secrete type-I IFN and other cytokines (Liu et al., 2005), which in return potentiate MHC I mediated antigen presentation. Most of the proteins involved in antigen

presentation in either LPS- or HAP-activated DCs were downregulated during cell maturation. This includes MHC class II antigen presenting molecule, but also proteins from MHC I and II pathways, involved in antigen processing and loading. It is therefore possible that there is other, unexpected source of antigen, which are then presented on MHC I, but are not involved in traditional antigen processing and presentation pathway. It was postulated by Apcher et al. (2012) that prematurely terminated full length peptides generated from defective mRNA and rejected by the non-sense mediated decay pathway after first round of translation are rapidly degraded in the cytosol and presented via MHC I. There is also growing evidence suggesting that the translation of immature mRNA can occur in the nucleolus (Apcher et al., 2013; Rugjee et al., 2013). This could be another potential source of antigen for MHC I presentation, which can be loaded obviating traditional pathway.

Another explanation for only MHC class I being upregulated during DC maturation may be increased presentation of exogenous antigen by MHC I even though it is usually maintained by MHC class II molecules (Lelouard et al., 2007). We have shown that upon LPS- and HAP-induced activation of human DCs, expression of a great number of ribosomal proteins is decreased. It is very likely caused by type-I IFN stimulation as it was shown before to induce decrease in mRNA encoding for ribosomal proteins (Taylor et al., 2004c; Taylor et al., 2007), but the same effect was observed on the protein level upon LPS stimulation (Lelouard et al., 2007). Also the increased expression of positive regulators of ubiquitination after DC stimulation (e.g. creatine, TNF receptor-associated factor 1) supports this concept. It was observed that in response to microbe stimulation (LPS), aggregates made of newly synthesised but ubiquitinated proteins are formed in the DC cytoplasm (Lelouard et al., 2002; Lelouard et al., 2004). This aggregation is probably the result of protein overproduction at 8 to 12 h of maturation (Ceppi et al., 2009). Those aggregates are protected from degradation and stabilised for up to 16 h. The highest ability of antigen presentation by MHC class I occurs several hours after DCs activation, thus this aggregates serve as important store of antigens for delayed antigen presentations (Lelouard et al, 2004).

In summary, SWATH proteomics enabled the identification of a large number of proteins during DCs maturation. Results presented in this chapter provided for the first time a fully quantitative analysis of proteins during this process. In addition, proteomic changes in maturing DCs induced by HAP were observed for the first time.

Chapter 4. The role of zinc in complement protein interactions

4.1 Introduction

4.1.1. Complement proteins

The human complement system forms part of the innate immune system and comprises more than 35 plasma and cell membrane bound proteins (Nan et al., 2013). There are three complement pathways, which lead to the elimination of pathogens and cytotoxic complexes: classical, alternative and lectin (Collard et al., 2001). The first components of complement pathways are C1q for the classical pathway and C3 for the alternative pathway.

The complement pathways are very carefully regulated and play key roles in in tissue regeneration (Clark et al., 2008), blood clotting, the clearance of cellular debris (Pickering and Walport, 2000) and are implicated in the pathophysiology of many diseases (Alchi and Jayne, 2010; Sweigard et al., 2014). One of the most important regulators is complement Factor H (FH), the major regulator of C3b. Polymorphisms in FH can cause or contribute to various diseases. One of them is the life-threatening kidney disease, haemolytic uremic syndrome (HUS), where the majority of patients demonstrate dysfunctional FH due to mutations or FH autoantibodies (Brandstatter et al., 2012). Addition of zinc to FH causes it to form oligomers containing 4-10 monomers, which inhibit its activity. FH-zinc oligomer formation is relevant to age-related macular degeneration (AMD) and occurs when zinc levels increase to above 60 μM (Perkins et al., 2010).

4.1.2. The role of zinc, complement proteins and histidine-rich glycoprotein (HRG) in AMD development

AMD is the leading cause of irreversible central vision loss in elderly people. It is associated with the development of drusen between retinal pigment epithelium (RPE) and Bruch's membrane. Drusen are pathological extracellular deposits primarily containing glycolipids, proteins, and cellular debris (Liu et al., 2012), which block exchange of nutrients from the vasculature leading to cell death and sensory loss within the central visual field. Recent work has shown that drusen contains cholesterol-containing droplets, coated with insoluble hydroxyapatite (HAP) known as HAP spherules. It has been shown in AMD-affected individuals that these spherules bind proteins, including amyloid β, vitronectin, FH and HRG (Fig. 4.1) (Thompson et al., 2015). It is

thought that the binding of such proteins to HAP spherules is a primary mechanism leading to deposit formation.

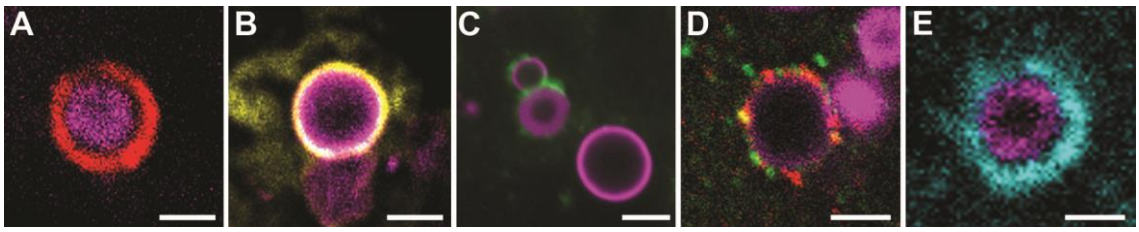

Figure 4.1. Molecular constituents of the outer surface of HAP spherules, identified in eyes of individuals with AMD. Immunohistochemical fluorescent-labelling with protein-specific antibodies, showed HAP spherules (A-E, magenta) to be coated with amyloid beta (A, red), vitronectin (B, yellow), and FH (C, green), colabelled by a combination of amyloid beta (red) and FH (green) (D) or HRG (E, cyan). Scale bars: 2 µm. Figure adapted from Thompson *et al.*, 2015, with new data (part E) from Dr Imre Lengyel, UCL Instiute of Ophthalmology.

Given its role as an important regulator of the classical complement pathway, the introduction of endogenous FH is being considered as an alternative or supplementary strategy to correct complement dysregulation in AMD. Purified human FH has been used in vivo as an experimental treatment in an animal model (Fakhouri et al., 2010). Whether such an approach may be useful clinically is still to be established.

Zinc also appears to play a role in AMD development. In the healthy eye, the Bruch's membrane contains 47 ppm of zinc. However, in AMD the amount increases to 137 ppm in the membrane and approximately 232 ppm in deposits (Dr Imre Lengyel, personal communication). It is feasible that together FH-zinc oligomer formation (Perkins et al., 2010), FH-HRG binding and the interaction between HRG, complement proteins and HAP are essential for drusen formation and occurs when zinc levels are elevated (Perkins et al., 2010).

4.1.3. The role of HRG in the immune system

Human histidine rich glycoprotein (HRG) is an abundant plasma protein with a multi-domain structure, composed of 507 amino acids, with six predicted N-linked glycosylation sites (Poon et al., 2010a). It consists of two cystatin like N-terminal domains (N1 and N2), a central histidine

rich region (HRR) flanked by two proline rich regions (bigger PRRI and smaller PRR2) and a C-terminal domain (C) (Jones et al., 2005a).

Through its ability to interact with numerous ligands (mainly through the N- and C-terminal domains), HRG serves as a positive (Simantov et al., 2001, Klenotic et al., 2010) and negative (Dixelius et al., 2006) regulator of physiological processes including angiogenesis through a variety of mechanisms. It has been also shown that HRG acts in the coagulation system as an anticoagulant and antifibrinolytic agent (Tsuchida-Straeten et al., 2005) by interaction with many molecules including: haem, plasminogen (Lijnen et al., 1980), heparanase (Poon et al., 2010b), fibrinogen (Leung et al., 1983) and heparins (Koide et al., 1989).

In the immune system, HRG plays an important role. It modulates the formation and function of immune complexes (IC) but also prevents the build-up of IC deposits, which are detrimental to small blood vessels. Those deposits can lead to pathologies such as rheumatoid arthritis, vasculitis or glomerulonephritis. HRG, through binding to various components of the immune system including the complement proteins (within both classical and alternative pathways), antibodies and Fc receptors on immunoglobulins, maintains streamline transport of the immune complexes to the liver and spleen (Gorgani et al., 1997; Gorgani et al., 1999).

Another role of HRG in the immune system is modulation of complement function by augmentation or inhibition through interactions with C8, C9, D and S-protein. It also binds strongly to C1q, FH, C4b -binding protein, C3, C4 and IgG (Manderson et al., 2009; Chang et al., 1992). It is thought that the binding between HRG and complement proteins, occurs via N-terminus. Through those interactions HRG is involved in elimination of necrotic (Jones et al., 2005b, Jones et al., 2005c) and apoptotic (Gorgani et al., 2002) cells from the immune system in two ways. HRG can either bind heparan sulfate (HS) on the surface of phagocytes, to promote necrotic cell uptake (Poon et al., 2010), or regulate activation of complement on necrotic cells, via interactions with C1q. This interaction occurs in the late stage of cell death when the cell membrane becomes permeable (Manderson et al., 2009). Zinc is thought to inhibit the interaction of HRG with C1q (Gorgani et al., 1997b) and to affect many other proteins within the complement system. For example in guinea pig, concentrations of zinc between 25 to 500 μM inhibit most of the complement factors and affects overall complement activity (Montgomery et al., 1979). The inhibitory effects of zinc were also observed on C9 (Yamamoto and Takahashi, 1975), C3-convertase, FH, C1q and C4b functions (Blom et al., 2003). On the other hand, zinc has stimulatory effect on C3 (Downing et al., 1989).

The aims of this chapter are to characterise HRG–complement interactions, using an ELISA based method, and to determine whether these interactions occur via N terminus of HRG, a common ligand-binding region. In addition, the role of zinc in regulating the interaction of HRG with complement proteins and heparin will be examined. Second aim of this chapter is to investigate whether zinc and pH alterations may contribute to AMD development by promoting HRG-hydroxyapatite interactions. Those interactions will be studied using, newly established, magnetic beads binding assay.

4.2. Materials and methods

4.2.1. Purification of human and rabbit HRG

HRG was purified from either human or rabbit plasma using immobilised-metal affinity chromatography (IMAC). A HisTrap HP column (GE Healthcare) was equilibrated with binding buffer (10 mM Tris, 150 mM NaCl, 5 mM imidazole, pH 8) and then loaded with filtered serum following addition of 5 mM imidazole. For elution, the imidazole concentration was increased across linear gradient of 0-30% of 500 mM imidazole over 5 min and then 30-100% over another 5 min. Fractions were collected and analysed using sodium dodecyl sulfate polyacrylamide gel electrophoresis (SDS-PAGE). For the final purification step, a size exclusion HiLoad 26/600 Superdex 200 pg column (GE Healthcare) was used with 10 mM Tris, 150 mM NaCl, pH 8 as the running buffer, and with a flow rate of 0.5 ml per minute. Eluted fractions were again analysed using SDS-PAGE. Human and rabbit HRG were concentrated using a Vivaspin 20 concentrator (10 kDa MWCO; GE Healthcare) to 10 mg/ml. Purified sample was aliquoted and flash frozen in liquid nitrogen before final storage at -80°C. Additionally, gel bands of relevant size, were extracted using sterile razor blade and sent for mass spectrometry analysis (MS).

4.2.2. Purification of human factor H (FH)

FH was purified from pooled human serum using a three-step process. Serum was centrifuged (4,200 rpm for 30 min at 4^{o}C) and filtered (0.45 µm filter), and pH adjusted to 6.0 prior to purification. For the first step a cation exchange column (CEX), (HisTrap SPFF; GE Healthcare) was used. This column was equilibrated with binding buffer (20 mM tri-sodium citrate, pH 6.0), and loaded with filtered serum. The column was then washed with binding buffer, until the absorbance reached 0 mAU. For elution, the ionic strength was increased across a linear gradient of 0-100% of 200 mM NaCl (20 mM Tris-HCl, 200 mM NaCl, pH 6.0). Fractions were collected and analysed using SDS-PAGE. Chosen fractions were pooled and dialysed overnight against 5 L of 20 mM Tris-HCl pH 8.6 (4^{o}C, stir) and then loaded onto an anion exchange column (AEX), HisTrap QFF (GE Healthcare) equilibrated by 20 mM Tris-HCl pH 8.6. Factor H was eluted with ionic strength increased across linear gradient 0-100% of 250 mM NaCl (20 mM Tris-HCl, 250 mM NaCl, pH 8.6). Fractions were collected and analysed using SDS-PAGE. For the final purification, the size exclusion column HiLoad 26/600 Superdex 200 pg (GE Healthcare) was used with 10 mM Tris, 150 mM NaCl, pH 7.5 buffer, and with a flow rate of 0.5 ml per minute. Eluted fractions were again analysed using SDS-PAGE. Fractions containing FH were pooled and either

concentrated using a Vivaspin 20 concentrator (10 kDa MWCO; GE Healthcare), and flash frozen in liquid nitrogen, or freeze-dried (using liquid nitrogen and Edwards Modulyo EF4 freeze-drier). Prior to freeze-drying sample was dialyzed for two days at 4°C against 5 L of 50 mM ammonium carbonate buffer (dialysis buffer was replaced after 24h). Both flash frozen and freeze-dried samples were stored at -80°C until required. Additionally, gel band of relevant size, was extracted from the final SDS gel using sterile razor blade and sent for mass spectrometry analysis (MS).

4.2.3. SDS-PAGE and Western blotting

Protein samples were resuspended in NuPAGE® LDS 4x Sample Buffer (Invitrogen, Thermo Fisher Scientific, Dartford, UK) for non-reducing conditions and the same buffer with the addition of 5% β-mercaptoethanol for reducing conditions. Following denaturation by heating at 90°C for 5 min, samples were loaded into precast NuPAGE® 4-12% Bis-Tris 1.0 mm protein gels (Invitrogen, Thermo Fisher Scientific), and run for approximately 1 h at 160 V in running buffer (NuPAGE® MES SDS Running Buffer, Thermo Fisher Scientific). After electrophoresis, gels were stained using Coomassie Brilliant Blue.

4.2.4. TEV protease preparation

A recombinant catalytic domain of the Nuclear Inclusion a (Nia) protein from tobacco etch virus (TEV) was produced to allow proteolytic cleavage of the His-tag from a recombinant form of the HRG N1/N2-domain (see below). The TEV protease uses a catalytic triad of residues, Cys-Asp-His to catalyse peptide hydrolysis. The enzyme was expressed recombinantly using pRK793 vector in *E. coli* strain BL21 (DE3)-RIL This domain is engineered to have an N-terminal His-tag and a C-terminal polyarginine tag and is purified as MBP fusion protein that cleaves itself in vivo.

Pre-culture of BL21 (DE3)-RIL expressing catalytic domain of TEV protease was set up from a glycerol stock in 20 ml of Luria broth (LB) supplemented with 100 µg/ml of ampicillin and grown for 12 h at 37°C with shaking (200 rpm). The following day, the main culture was set up in 1 L of the same medium in 1:100 dilution of initial culture and left at 37°C, 200 rpm until OD_{600} reached 0.7 AU. Protein expression was induced with 1 mM isopropyl β-D-1-thiogalactopyranoside (IPTG) and the temperature lowered to 25°C. Cultures were incubated for 16 h with shaking (180 rpm). The bacterial pellet was harvested by centrifugation for 40 min, 6,000rpm at 4°C, then weighed and resuspended for 30 min at 4°C in binding buffer (50 mM Tris, 150 mM NaCl, 20 mM

imidazole, pH 8.0) at a 1:5 (w/v) ratio. Cells were lysed by sonication with Ultrasonic Cell Disruptor with 40 % amplitude for 2 min of 10 s pulses with 10s intervals. Cell debris was removed following centrifugation for 20 min, 20,000 rpm at 4^{o}C. The supernatant was then filtered (0.44 µm membrane; Millipore, Consett, UK.) and applied to a His Trap HP column (GE Healthcare,) pre-washed with lysis buffer. Protein was eluted with a linear gradient up to 400 mM imidazole (10 column volumes (CV) to reach 10% of elution buffer, 20 CV to reach 100% and then 100% over 5 CV). Eluted fractions were immediately diluted in a 1:1 (v/v) ratio with dialysis buffer (20 mM Tris HCl, 500 mM NaCl, pH 7.5) and then dialysed over night at 4^{o}C with stirring. Protein was concentrated to 2 mg/ml using a Vivaspin 20 column (10 kDa MWCO; GE Healthcare), diluted 1:1 with glycerol, frozen with liquid nitrogen and stored at -80 ^{o}C.

4.2.5. Production of recombinant HRG N1/N2 domain fragment

4.2.5.1. Molecular cloning

Construction of expression vectors

To amplify the cDNA sequence encoding the N1/N2-domains of human HRG for insertion into pETM11 *E. coli* expression plasmid (Fig. 4.2), 10 ng of template DNA was used. The template was a plasmid I.M.A.G.E clone containing the full length human HRG coding sequence purchased from Source Bioscience (Nottingham, UK). To the template DNA, 25 µl of BIO-X-ACT™ Short Mix (Bioline, London, UK) was added. This is a ready 2× mixture of DNA polymerase, $MgCl_2$ and dNTP. Forward (5'-TAAGCAGAATTCATGAAGCACCACCACCAC-3') and reverse primers (5'-TGCTTAGCGGCCGCTCATTT GAGCTCT-3') (Eurofins Scientific, Luxembourg) were added at a final concentration of 0.6 µM. Molecular grade water was added to a final volume of 50 µl. The PCR amplification reaction was performed using a Phoenix 2 thermal cycler (Helena Bioscience, Tyne and Wear, UK). PCR cycling was as follows: 1 cycle as initial denaturation at 95^{o}C for 2 min, followed by 40 cycles of denaturation at 95^{o}C for 30 s, annealing at 64^{o}C for 30 s, and extension at 72^{o}C for 30 s. Final extension was in 1 cycle at 72^{o}C for 5 min.

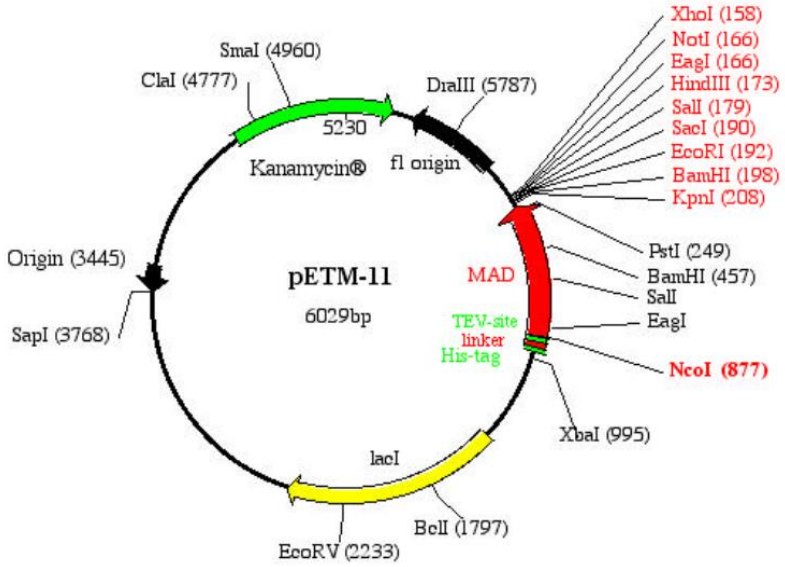

Figure 4.2. PETM-11 expression vector, used for the N1/N2 – domain expression. The multiple cloning site (MSC) was the location of gene insertion. The expression is driven by the T7-lac promoter. A kanamycin resistance gene allows for the selection of colonies.

Restriction enzyme digest

A double restriction enzyme digest was performed to cleave the pETM11 plasmid at the sites where N1/N2-domain will be inserted (inside the multiple cloning site and immediately downstream and in-frame from a hexameric His-tag and TEV protease site). A similar digest was also performed on the amplified dsDNA fragment to prepare this for insertion into pETM11 and to subsequently confirm the presence of proper insert (following insertion/transformation). For this 1 µg of DNA was digested with the high fidelity restriction enzymes SacI-HF® and NcoI-HF® (NEB, Hitchin, UK) in 1x CutSmart® Buffer (NEB). Reactions were incubated for 90 min at 37°C. Additionally, to prevent re-ligation of compatible ends, the DNA was treated with 1 µl of calf intestine alkaline phosphatase (NEB) in the appropriate buffer and incubated for additional 30 min at 37°C. The treated DNA was then purified by agarose gel electrophoresis.

Agarose gel electrophoresis

Gels were prepared by melting 1% (w/v) agarose (Sigma-Aldrich, Haverhill UK) in Tris-acetate-EDTA buffer (TAE) (40 mM Tris pH 7.6, 20 mM acetic acid, 1 mM EDTA) with ethidium bromide (0.5 µg/ml) to enable separation and detection of DNA bands. Wells were formed by inserting a comb before gel was set. PCR samples were mixed with 6x loading dye (Thermo Fisher Scientific).

Hyperladder I (200- 10,000 bp; Bioline) was loaded into one well to allow identification of DNA sizes. DNA bands were separated at 150 V for approximately 40 min. DNA was visualised in a Gel Doc XR+ Imager and analysed using the Image Lab 2.0 software (both Bio-Rad, Hemel Hempstead, UK).

Extraction and purification of DNA bands

Gel was placed on a blue light transilluminator (Life Technologies) which visualises DNA bands using UV-transmission. Bands were excised using a sterile razor blade, weighed and DNA was purified using the QIAquick Gel-Extraction kit (Qiagen, Venlo, Netherlands) according to the manufacturer's guidelines. Following purification, DNA was eluted in 30 µl of nuclease free water.

Ligation

Amplified DNA fragments (corresponding to the HRG N1/N2-domain coding sequence) were ligated following digestion into similarly digested pETM11 plasmid (in a 3:1 insert:plasmid ratio, 10 µl final volume) using 1 µl of T4 DNA ligase (NEB) in 1 × T4 DNA Ligase Buffer (NEB) for 10 min at room temperature. A control reaction without insert DNA was also set up. The ligation product was chilled on ice prior to bacterial transformation.

Transformation of *E. coli* competent cells

For propagation of ligation product and expression of recombinant protein, three strains of chemically competent *E. coli* were transformed: BL21, Shuffle T7 (NEB) and ArcticExpress (DE3) RP competent cells (Agilent Technologies, Edinburgh, UK). In each case, a 50 µl aliquot of competent cells, was thawed on ice for 10 min and 5 µl of ligation product or 1 µl of purified DNA was added to the cell mixture. The tube was flicked 5 times to facilitate mixing and placed on ice for 30 min. After heat shock at 42^{o}C for 40 s (20 s for ArcticExpress) cells were placed back on ice for 5 min. Next 950 µl of room temperature SOC rich media was pipetted and the mixture was incubated at 37^{o}C (BL21 and ArcticExpress) or 30^{o}C (Shuffle T7) for 60 min, shaken (300 rpm). An aliquot of transformed cells was plated onto a selection plate (LB supplemented with 50 µg/ml of kanamycin) and incubated overnight at 37^{o}C. Shuffle T7 had to be plated on LB agar supplemented with 30 µg/ml of kanamycin and incubated overnight at 30^{o}C. Formed colonies were picked and grown in 10 ml of LB media supplemented with 30 µg/ml kanamycin and grown overnight at 37^{o}C or 30^{o}C (Shuffle T7) in a shaking incubator. Obtained cultures were used either for preparation of glycerol stocks or subsequent protein expression.

Plasmid purification

For diagnostic purposes, five of successfully transformed colonies were grown in 5 ml of LB broth supplemented with 50 µg/ml of kanamycin overnight at 37°C, shaking at 200 rpm. DNA was then purified from 1 ml of culture using a QIAprep Spin Miniprep Kit (Qiagen) according to manufacturer's protocol and eluted from columns with 40 µl of nuclease-free water. DNA concentration and purity were measured using a NanoVue spectrophotometer (GE Healthcare). A ratio of the absorbance at 260 nm and 280 nm of 1.8- 1.9 was regarded as sufficiently pure for downstream applications. Purified DNA was stored at -20°C in water until required.

Generation of glycerol stocks

For long-term storage of bacterial cultures, glycerol stocks were prepared by mixing 0.5 ml of overnight bacterial culture and 0.5 ml of 50% glycerol. Cryogenic vials were stored at -80°C until required.

4.2.5.2. Small scale protein expression

To optimize the production of N1/N2-domain of recombinant protein by competent strains of *E. coli,* the effect of varying two separate growth parameters was investigated: temperature and concentration of inducer, isopropyl β-D-1-thiogalactopyranoside (IPTG; Sigma-Aldrich). Cells were initially grown for 12 h in LB medium supplemented with 30 µg/ml kanamycin. Subsequent cultures were then set up as 1 in 100 dilution of initial culture in 50 ml aliquots of the same medium and grown at optimal temperatures until OD_{600} reached 0.7 AU (mid log growth phase). Protein expression was then induced with 0.01 mM, 0.2 mM or 1 mM of IPTG, respectively and the growth temperature adjusted to either 16°C, 25°C or 30°C. Cultures were incubated for 16 h in a shaking incubator. Aliquots of the bacterial cultures were spun down at 13,000 rpm for 1 min and supernatants transferred to new tubes. Pellets were re-suspended in 50 µl of reducing NuPAGE protein sample buffer and boiled for 15 min. Supernatant was mixed with reducing NuPAGE protein sample buffer and boiled for 5 min. Samples were then spun for 5 min at 14,000 rpm and analysed by SDS-PAGE. Optimal conditions for protein production were determined.

4.2.5.3. Large scale protein expression under non-denaturing conditions

Initial culture of Shuffle T7 *E. coli* strain, expressing N1/N2-domain recombinant protein was set up from glycerol stock in 50 ml LB supplemented with 30 ug/ml of kanamycin. Culture was grown for 12 h at 30°C, with shaking at 200 rpm. The main cultures were set up in 1 L volumes of the same medium at 1:100 dilution of the initial culture and grown at 30°C, with shaking at 200 rpm

until the OD_{600} reached 0.7 AU. Protein expression was induced with 0.02 mM of IPTG and the temperature lowered to 25°C. Cultures were grown for 16 h, shaking at 200 rpm. Bacterial pellet was harvested by centrifugation for 40 min, 6,000 rpm at 4°C, and then frozen until required at -80°C. From each 1 L of bacterial culture around 4.5 g of pellet was harvested. Thawed Shuffle T7 pellet containing the expressed recombinant N1/N2 domain was resuspended in lysis buffer (50 mM Tris, 150 mM NaCl, 20 mM imidazole, pH 8) with the addition of complete EDTA-free protease inhibitor tablets (Roche, Basel, Switzerland) in addition to 1 mg/ml lysozyme and 20 µg/ml DNase (for 1 h at 4°C. Cells were lysed by sonication with Ultrasonic Cell Disruptor (40% amplitude, 10s pulses at 10s intervals for 3 min, on ice). Lysate was cleared by centrifugation at 20,000 rpm at 4°C for 30 min and filtered through a 0.44 µm filter (Millipore). Cleared lysate was applied to a HisTrap column (GE Healthcare), pre-equilibrated with equilibration buffer (50 mM Tris, 150 mM NaCl, 20 mM imidazole, pH 8). Column was washed until the absorbance reached 0 mAU. Protein was eluted with step-wise gradient up to 400 mM imidazole. Fractions were analysed using SDS-PAGE. Chosen fractions were mixed with TEV protease in a 1:10 ratio and dialysed overnight against equilibration buffer. Following dialysis, samples were run through a pre-equilibrated HisTrap column. HRG N1/N2-domain protein fragments with the His-tag cleaved by TEV protease should not bind to the HisTrap column, therefore column flow through was collected. Additionally, the column was washed with buffer containing a high concentration of imidazole (400 mM imidazole, 50 mM Tris, 150 mM NaCl, and pH 8). Eluted fractions were also collected. Column flow through and eluted fractions were analysed using SDS-PAGE. HisTrap flow through was subjected to further purification. Sample was concentrated to 5 ml before final purification, using a Vivaspin 20 column (10 kDa MWCO; GE Healthcare). For the final purification, the size exclusion column HiLoad 16/600 Superdex 75 pg (GE Healthcare) was used with 10 mM Tris, 150 mM NaCl, pH 8 buffer, and with a flow rate of 0.5 ml per minute. The recombinant HRG N1/N2-domain was eluted as a single peak and concentrated to 10 mg/ml. Purified sample was aliquoted and flash frozen in liquid nitrogen before final storage at -80°C until required.

4.2.5.4. Large scale protein expression under denaturing conditions

Bacterial culture of Shuffle T7 *E. coli* strain, expressing the HRG N1/N2-domain recombinant protein was grown as previously described and harvested pellet was frozen for one day. Thawed Shuffle T7 pellet was resuspended in lysis buffer, with the addition of 8 M urea for 1 hour at 4°C with stirring. Cells were then lysed by sonication (40% amplitude, 10s pulses at 10s intervals for

3 min, on ice). Lysate was cleared by centrifugation, filtered and applied onto the HisTrap column, washed with equilibration buffer. Protein was eluted with step gradient of up to 400 mM imidazole (400 mM imidazole, 50 mM Tris, 150 mM NaCl, and pH 8). Eluted fractions were analysed by SDS-PAGE after which selected fractions were pooled together and dialysed twice for 12 h, at 4^{o}C against 5 L of 50 mM Tris, 150 mM NaCl, pH 8 containing 5 mM dithiothreitol (DTT) in order to remove urea and aid refolding of the recombinant protein. Following dialysis, the sample was mixed with TEV protease at a 1:10 ratio to cleave the His-tag. The protein was then dialysed against 50 mM Tris-HCl, 150 mM NaCl, 20 mM imidazole, pH 8.0. Protein digestion and dialysis was carried out for 16 h at 4^{o}C. Digestion was firstly assessed by SDS-PAGE, then fully digested protein was passed again through the HisTrap column and the flow-through (containing His-tag cleaved HRG N1/N2-domain protein) was concentrated using a Vivaspin 20 column (10 kDa MWCO) down to a volume of 5 ml. For further purification, the sample was loaded onto a gel filtration column, HiLoad 16/600 Superdex 75 pg. The running buffer (50 mM Tris, 150 mM NaCl, pH 8) was applied at a flow rate of 1 ml/min. Fractions were concentrated to either 10 mg/ml or 20 mg/ml. Subsequently, another batch of protein was purified using the same method except for the TEV cleavage. All purified samples were aliquoted and flash frozen in liquid nitrogen before final storage at -80^{o}C until required.

4.2.5.5. Purification of recombinant HRG N1/N2-domain-green fluorescent protein (GFP) fusion protein

Molecular cloning

To amplify the cDNA sequence encoding the N1/N2-domains of human HRG for insertion into pEHISGFPTEV *E. coli* expression plasmid (for creation of a HRG N1/N2-GFP fusion protein), 10 ng of template DNA was used (Fig. 4.3; 4.4) As a template, the previously gel purified N1/N2-domain insert (from 5.2.5.1) was used. The PCR amplification reaction contained: 1.5 µl of Velocity DNA polymerase (Bioline, London, UK), 10 µl of 5x Hi-Fi Buffer (contains 10 mM Mg^{2+}), 0.5 µl dNTPs (Sigma Aldrich) and forward (5'-AAAGCGGCCGCGTTAGTCCGACCGATTCGTCTGC-3') and reverse (5'-TTTCTCGAGTCACACCTCGCAATTAATGACAAGGTTCTTC-3') primers (Eurofins Scientific) at a final concentration of 0.6 µM. Additionally, molecular grade water was added to a final volume of 50 µl. PCR cycling was as follows: 1 cycle as initial denaturation at 98^{o}C for 2 min, followed by 40 cycles of denaturation at 98^{o}C for 30 s, annealing at 61^{o}C for 30 s, and extension at 72^{o}C for 45 s. Final extension was in 1 cycle at 72^{o}C for 7 min.

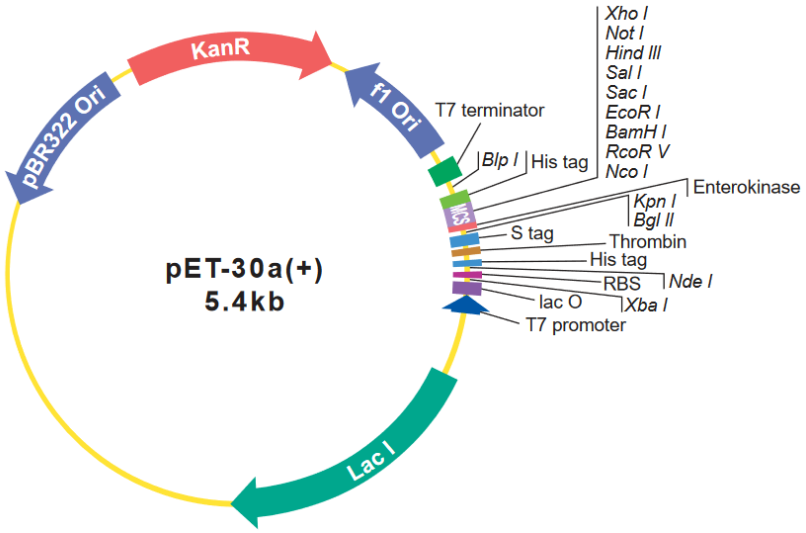

Figure 4.3. pET-30a(+) vector, was used to construct pEHISGFPTEV vector. The GFP encoding sequence was PCR amplified and cloned into pET-30a(+) using NdeI and NcoI restriction sites. pEHISGFPTEV expression vector, used for the N1/N2 – domain expression. The multiple cloning site (MSC) was the location of gene insertion. The expression is driven by the T7-lac promoter. Kanamycin resistance gene allows for the selection of colonies (Novagen, Merck, Darmstadt, Germany).

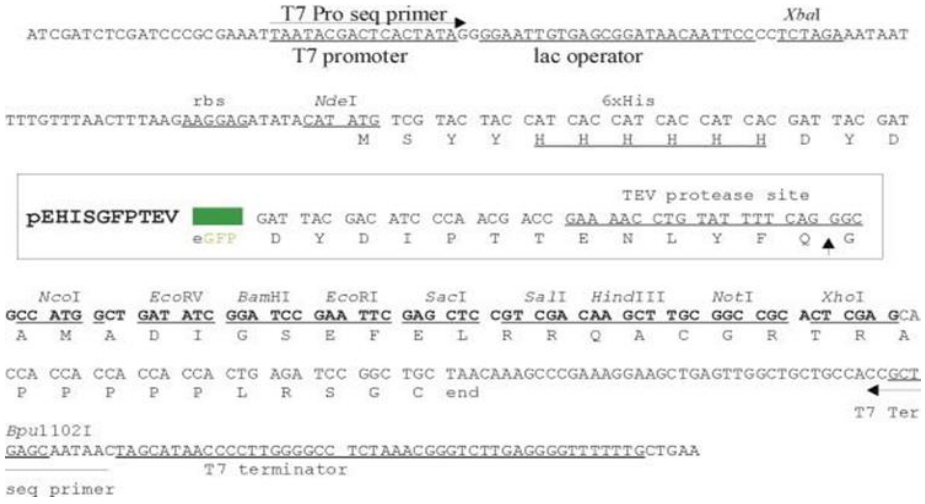

Figure 4.4. Multiple cloning site of pEHISGFPTEV vector. Vector contains the f1 replication origin, kanamycin resistance gene, pB332 DNA replication origin, and lac repressor gene. Moreover, the cloning region shows the T7 promoter, lac operator, hexameric His-tag, TEV protease recognition site, restriction endonuclease sites for cloning, and the T7 terminator regions (Liu and Naismith, 2009).

Product was run on agarose gel, purified and cloned into pEHISGFPTEV vector using NotI and XhoI restriction sites as described above. This vector made by Liu and Naismith (2009) combines the advantages of the GFP-based solubility, His-tag affinity isolation and TEV protease-mediated cleavage of partner proteins. It is based upon the pET30a vector (Novagen, Cambridge, U.S.A.) and therefore has a T7 promoter. A sample of pEHISGFPTEV was kindly given to us by Prof. James H. Naismith (University of St Andrews). Shuffle T7 *E. coli* competent cells were subsequently transformed with the pEHISGFPTEV containing the corresponding HRG N1N2-domain encoding insert. Glycerol stocks were prepared as described above.

Protein purification

An initial culture of Shuffle T7 *E. coli* expressing N1/N2-domain recombinant GFP fusion protein was set up from glycerol stock in 50 ml LB media supplemented with 30 ug/ml of kanamycin. Culture was grown at 30^{o}C for 16 h with shaking (200 rpm). Subsequent 800 ml cultures were set up in the same medium at 1:100 dilution of initial culture and grown at 30^{o}C with shaking (200 rpm) until OD_{600} reached 0.7 AU. Following the addition of 0.7 mM of IPTG, the temperature was lowered to 25^{o}C for an overnight incubation. The next morning, the bacterial pellet was harvested by centrifugation and resuspended in equilibration buffer (50 mM sodium phosphate, 400 mM NaCl, 1 mM β-mercaptoethanol, 10 mM imidazole, pH 7.5) supplemented with 200 µg/ml of lysozyme and EDTA-free protein inhibitor tablet (Roche). Cells were lysed at 4^{o}C for 30 min followed by sonication with Ultrasonic Cell Disruptor, using a large probe, at 50% amplitude in 3 cycles of 30 s with 1 min intervals to prevent sample overheating. The cell lysate was centrifuged at 18,000 rpm for 30 min at 4^{o}C, supernatant filtered through a 0.2 µm filter and loaded onto a pre-equilibrated HisTrap column (GE Healthcare). The column was washed with 10 CV of wash buffer (50 mM sodium phosphate, 400 mM NaCl, 30 mM imidazole, pH 7.5). The target protein was eluted using elution buffer (50 mM sodium phosphate, 400 mM NaCl, 300 mM imidazole, pH 7.5). The eluted fractions were analysed by SDS-PAGE.

4.2.6. Enzyme-linked immunosorbent binding assay (ELISA)

The influence of zinc on binding of full-length human HRG and the HRG N1/N2-domains to complement proteins, C1q, C3 and FH was examined using an ELISA-based method. Also binding between heparin and the HRG N1/N2 domains was examined. For binding studies, native FH and HRG were purified as described previously (Brandstatter et al., 2012; Kassaar et al., 2015) and the N1/N2 domain of HRG expressed and purified as described above. C1q and C3 were

purchased from Fitzgerald Industries International (Acton, MA, U.S.A.). Binding experiments were performed in the absence and presence of zinc (10 µM $ZnCl_2$).

4.2.6.1. Protein biotinylation

Antibodies directed against epitopes within the HRG N1/N2-domain were not commercially available. A strategy was therefore adopted whereby detection of bound protein was carried out using a streptavidin-linked enzyme following biotinylation of the HRG N1/N2 domain protein. For this 4 mg of purified HRG N1/N2-domain protein was biotinylated using the Biotin Protein Labelling Kit (Jena Bioscience, Jena, Germany) in accordance with the manufacturer's instructions. Prior to assay, the biotinylated, protein was dialysed against an "ELISA" working buffer (50 mM HEPES, 150 mM NaCl, 0.2% Tween 20, pH 7.4) for 2 h at room temperature.

4.2.6.2. The effect of zinc on binding of native HRG to complement proteins

To examine the effect of zinc on HRG binding to C1q, C3 and FH, 96-well microtitre plates (Nunc Maxisorp; Sigma-Aldrich) were coated overnight with each protein (50 µl of 10 µg/ml concentration which corresponds to 25 µM C1q, 65 µM FH and 54 µM for C3) diluted in a coating buffer (75 mM sodium carbonate, pH 9.6) at 4^{o}C. Plates were then washed 3 times for 5 min (50 mM HEPES, 150 mM NaCl, 0.05% Tween 20, pH 7.4), as was similarly done after all the incubation steps. Following blocking (100 µl of 0.4% gelatine in wash buffer, supplemented with 0.2% Tween 20 at 25^{o}C for 2 h) plates were incubated for 1 h at 25^{o}C with HRG (purified from human plasma) diluted in binding buffer (50 mM HEPES, pH 7.4, 100 mM NaCl, 2 mM $CaCl_2$). HRG was added at various concentrations ranging from 0-3 µM and was prepared in wash buffer supplemented with 10 µM zinc chloride or without zinc as a control. Plates were then incubated with anti-HRG primary antibody (Abnova, Taipei City, Taiwan), at 1:1000 dilution in blocking solution at 25^{o}C and then with goat-α-rabbit alkaline phosphatase conjugate (Sigma-Aldrich) at 1:10,000 dilution for 1h at 25^{o}C. Bound HRG was detected using *p*-nitrophenylphosphate (Sigma-Aldrich). The reaction was stopped after 1 h using 3 M NaOH. The absorbance at 405 nm was measured using a Dynex MRX microplate reader (Dynex Technologies, Worthing, UK).

4.2.6.3. The effect of zinc on binding of N1/N2 domains of HRG to complement proteins

To examine the effect of zinc on HRG N1/N2-domain binding to C1q, C3 and FH, 96-well microtitre plates were coated with complement proteins and blocked as described above (5.2.6.2). The plates were then incubated with biotinylated HRG N1/N2-domain for 2h at 30^{o}C. Protein was added at various concentrations ranging from 0-10 µM in wash buffer (50 mM

HEPES, 150 mM NaCl, 0.05% Tween 20, pH 7.4) supplemented with 10 µM zinc chloride or without zinc as a control. Plate was then washed 3 times with wash buffer. A streptavidin-alkaline phosphatase conjugate (Thermo Fisher Scientific) was prepared at 1:10,000 dilution in wash buffer (with and without zinc, respectively) and incubated for 1 h at 25°C. Unbound streptavidin was washed away and plate was incubated with *p*-nitrophenylphosphate substrate (dissolved in wash buffer) for 1h at 25°C in the dark. The reaction was stopped with the addition of 3 M NaOH and absorbance at 405 nm was measured as described above.

4.2.6.4. The effect of zinc on binding of heparin to N1/N2-domain of HRG

To examine the effect of zinc on HRG N1/N2-domain binding to heparin, Costar carbohydrate binding plates (Corning, New York, U.S.A.), which have a hydrazide surface that covalently binds to carbohydrate groups, were chemically cross-linked to heparin. Firstly, heparin was activated with periodate to ensure specific orientation of the biomolecule on the surface. For this unfractionated heparin (4 mg) was dissolved in 4 ml of ultrapure water, mixed with 6.4 ml of 15 mM sodium periodate (solution in 0.1 M sodium acetate, pH 5.5) and incubated for 30 min at room temperature. The reaction was stopped by adding 400 µl of 1 % ethylene glycol. The mixture was then dialysed twice against 1 L of 0.1 M sodium acetate, pH 5.5, for 1 h at room temperature. Activated heparin was aliquoted and stored at -20°C for up to 3 weeks. The final concentration of heparin was estimated to be 0.37 mg/ml.

The carbohydrate binding plates were then coated with 20 µg/ml of activated heparin diluted in 0.1 M sodium acetate, pH 5.5, for 1 h at room temperature. Next the plate was washed with ELISA washing buffer (50 mM HEPES, 150 mM NaCl, 0.05% Tween 20, pH 7.4) and plates were blocked with 0.5% fish skin gelatine (Sigma-Aldrich) in wash buffer supplemented with 0.2% Tween 20, pH 8.2 for 2 h at room temperature. Following blocking, biotinylated HRG N1/N2-domain of HRG was applied and incubated at 37°C for 2 h. Protein was added at various concentrations ranging from 0-10 µM in wash buffer with 10 µM zinc chloride or without zinc as a control. Plates were washed 3 times with ELISA wash buffer. The streptavidin-alkaline phosphatase detection method was the same as described above (5.2.6.3). Reaction was stopped with the addition of 3 M NaOH and absorbance at 405 nm was measured.

4.2.6.5. Data presentation

Data obtained from native HRG and N1N2-domanin of HRG binding studies, were fitted in GraphPad Prism v6 software, using a sigmoidal 4-parameter logistic (Sigmoidal 4PL) fit.

4.2.7. Hydroxyapatite-coated magnetic bead binding assay

BcMag hydroxyapatite-modified magnetic beads (supplied by Bioclone, London, UK) are silica-coated superparamagnetic beads around 2 µm in diameter which have hydroxyapatite functional groups added on their surface. These were used to establish a HAP-binding assay to probe the HAP-binding properties of HRG. For this, beads were preconditioned according to manufacturer's instructions. Assays were performed in triplicate using 0.3 mg of beads per sample. Beads were washed twice with 50 mM Tris, 140 mM NaCl, pH 7.4 (or pH 6.5 and pH 8.0, respectively) using a magnetic separator test tube rack and incubated in 400 µl of 0-1 µM human HRG (in the same buffer) for 1 h at room temperature with rotary mixing. The binding buffer was additionally supplemented with 1 mM zinc chloride for some experiments. Protein-bound beads were washed twice with 50 mM Tris, 140 mM NaCl, pH 7.4 (or pH 6.5 and pH 8.0, or the addition of zinc respectively), followed by blocking with 1% BSA dissolved in the same buffer for 1 h at room temperature with rotary mixing. Beads were resuspended in 300 µl of blocking solution with the addition of rabbit anti-human HRG antibody at 1:1000 dilution (Abnova) and incubated for 1 h at room temperature with rotary mixing. This was followed by two washes (with wash buffer as above) and incubation with horseradish peroxidase (HRP)-conjugated anti-rabbit antibody at 1: 10,000 for 1 h at room temperature with rotary mixing. Detection was carried out using o-phenylenediamine dihydrochloride (OPD; Sigma-Aldrich) as a substrate. The absorbance at 492 nm was measured using a Dynex MRX microplate reader (Dynex Technologies).

4.2.8. X-ray crystallography of native HRG and recombinant N1/N2 domains of HRG

In order to gain structural insight into the molecular interaction between HRG and its various binding partners, we aimed to structurally characterise HRG, using X-ray crystallography. N1 and N2 domains were of particular interest as they are thought to participate in complement binding. Previously the group successfully solved the structure of the N2 domain from rabbit HRG (Kassaar, 2014). Nevertheless, the structure of the N1 and N2 domains together (which are thought to fold together to form an interaction site for various molecules including complement proteins and heparins), or indeed the full-length protein remains unknown. Many parameters influence crystals creation therefore only proteins, proven by SDS-PAGE to be of high purity (>95%) and homogeneity, were used for crystallisation trials.

Firstly, crystallisation of the full-length HRG, purified from rabbit plasma was attempted. Protein was concentrated to 18 and 36 mg/ml and used to set up trials with commercially available crystal screens, PEG 4, PEG 2 and WIZARD (Qiagen, Manchester, UK). Secondly, crystal trials with a recombinant fragment of HRG containing the N1 and N2 domains at a concentration of 25 mg/ml were set up using the same commercially available crystal screens, and additionally one custom made screen prepared in the Naismith laboratory (Biomedical Sciences Research Complex, University of St Andrews). The HRG N1/N2-domain crystallisation trials were attempted with and without the addition of a very pure preparation of low molecular weight heparin (200 μM, 1.8 kDa). The principle behind inclusion of heparin was to attempt obtain a heparin-bound structure of the HRG N1/N2 domain fragment. Trials were set up using an Art Robbins Gryphon crystallisation robot by sitting-drop vapour diffusion method. In this method, the protein is in the vapour-liquid equilibrium with precipitant and therefore concentrates over time, it is hoped, to the point when crystals form and grow.

4.3. Results

4.3.1. Protein purification

4.3.1.1. Purification of the native proteins

Purification of human and rabbit HRG

HRG was successfully purified from human/rabbit plasma using a two-step purification method (Fig 4.5, 4.6). Human HRG has a molecular mass of around 70 kDa, rabbit protein is around 58 kDa (Kassaar, 2014). HRG as suggested by its name has an unusually high number of histidine residues, which makes it ideal for purification using a HisTrap column. However, following this procedure, SDS-PAGE analysis revealed that some contaminating proteins remained after this step (Figs. 4.5 A and 4.6 A). Therefore, to ensure maximum sample homogeneity, HRG was further purified by size exclusion chromatography. This final step removed all contaminating proteins, leaving pure HRG (Figs. 4.5 B and 4.6 B). Mass spectrometry studies involving tryptic peptide digestion confirmed the proteins to be human HRG (Fig 4.7 A) with 32% coverage and rabbit HRG (Fig. 4.7 B) with 22% coverage.

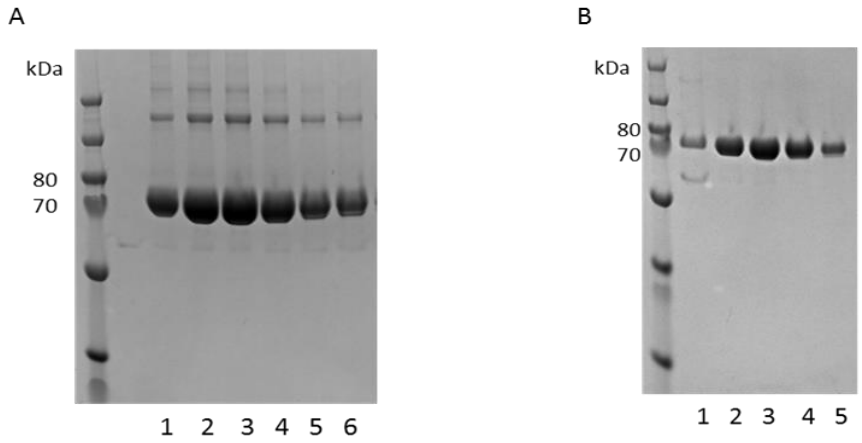

Figure 4.5. SDS-Page images for rabbit HRG purification. On the image, each lane represents samples from 1 ml eluted fractions. (A) After initial purification with HisTrap™ Ni column fractions 1-6 were pooled together. (B) These were then purified further by gel filtration, HiLoad Superdex 200 pg. Here fractions 2-5 were then pooled, freeze-dried and stored at -80°C. LC MS/MS following SDS-PAGE analysis and in-gel tryptic digestion confirmed the purified protein to be rabbit HRG.

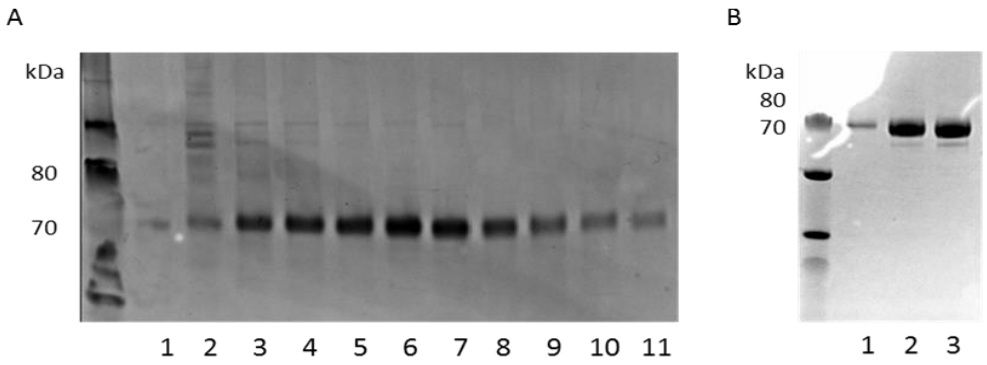

Figure 4.6. SDS-Page images for human HRG purification. On the image, each lane represents samples from 1 ml eluted fractions. After initial purification with HisTrap™ Ni column fractions 3-11 (A) were pooled together. (B) These were then purified further by gel filtration, HiLoad Superdex 200 pg. Here fractions 2-3 were then pooled, freeze-dried and stored at -80°C. LC MS/MS following SDS-PAGE analysis and in-gel tryptic digestion confirmed the purified protein to be human HRG.

A

LIPTDCRTTKPLAEKALDLINKWRRDGYLFQLLRVADAHLDGAESATVYYLVLDVKETDCSVLSRKHWEDCDPDLTKRPSLDVIG
QCRVIATRYSDEYQTLRLNDFNCTTSSVSSALANTKDSPVLFDFIEDTEPFRKSADKALEVYKSESEAYASFRVDRVERVTRVK
GGERTNYYVDFSVRNCSRSHFHRHPNAFGFCRADLSFDVEASNLENPEDVIISCEVFNFEEHGNISGFRPHLGKTPLGTDGS
RDHHHPHKPHKFGCPPPQEGEDFSEGPPSQGGTPPLSPPSGPRCRHRPFGTNETHRFPHHRNFSEHHPHGPPPHGHHPH
GPPPHGHHPHGPPPHGHPPHGPPPHGHPPHGPPPHGHPPHGPPPHGHPPHGPPPHGHPPHGPPPHGHPPHGPPPH
GHPPHGHGFHDHGPCDPPSHKEGPQDLHQHGHGPPPKHPGKRGPGKGHFPFHWRRIGSVYQLPPLQKGEVLPLPEAN
FPSFSLRNHTHPLKPEIQPFPQVASERCPEEFNGEFAQLSKFFPSTFPK

B

ATLQCSWALTPTDCKTTKPLAEKALDLINKWRRDGYLFQLLRVADAHLDGAESATVYYLVLDVKETDCSVLSRKH
WEDCDPDLTKRPSLDVIGQCKVIATRYSDEYQTLRLNDFNCTTSSVSSALANTKDSPVLFDFIEDTEPFRKSADKA
LEVYKSESEAYASFRVDRVERVTRVKGGERTNYYVDFSVRNCSRSHFHRHPAFGFCRADLSFDVEASNLENPEDV
IISCEVFNFEEHGNISGFRPHLGKTPLGTDGSRDHHHPHKPHKFGCPPPQEGEDFSEGPPLQGGTPPLSPPFRPR
CRHRPFGTNETHRFPHHRISVNIIHRPPPHGHHPHGPPPHGHHPHGPPPHGHPPHGPPPRHPPHGPPPHGHP
PHGPPPHGHPPHGPPPHGHPPHGPPPHGHPPHGHGFHDHGPCDPPSHKEGPQDLHQHAMGPPPKHPGKR
GPGKGHFPFHWRRIGSVYQLPPLQKGEVLPLPEANFPQLLLRNHTHPLKPEIQPFPQVASERCPEEFNGEFAQLS
KFFPSTFPK

Figure 4.7. MS/MS sequence analysis for identification of human HRG (A) and rabbit HRG (B). Significant peptide fragments are highlighted in red. 32% of analysed protein shows more than 95% similarities with human HRG and 22% of analysed protein showed more than 95% similarities with rabbit HRG. That allowed as assuming that obtained proteins were human and rabbiting HRG respectively.

Purification of human complement Factor H (FH)

Complement factor H (FH) is the main regulator of alternative complement pathway. FH has a molecular weight of 150 kDa. Prior to binding studies, it was purified from human serum using a three-step chromatography procedure. For initial purification, cation and anion exchange columns were used, however SDS-PAGE revealed that the obtained sample was still a mixture of FH and contaminating proteins (Fig. 4.8 A and B). As a final purification step, size exclusion chromatography was used, which removed most of the contaminating proteins, leaving FH with only a trace of two contaminating proteins of a size similar to FH (Fig. 4.8 C). To reduce the risk of protein degradation all steps were carried either on ice or at 4^{o}C when possible. Mass spectrometry studies involving tryptic peptide digestion confirmed the proteins to be human FH (Fig. 4.9). Fractions 1-7 (Fig. 4.8 C) were pooled and concentrated using Vivaspin protein concentrators. The purified protein was quantified, flash frozen in liquid nitrogen and stored in small aliquots at -80^{o}C to be used for all subsequent studies. Additionally, when stored for longer than 6 months, the sample of protein was analysed by SDS-PAGE gel prior to use. This was necessary to make sure that storing conditions are appropriate and that the protein did not degrade over time.

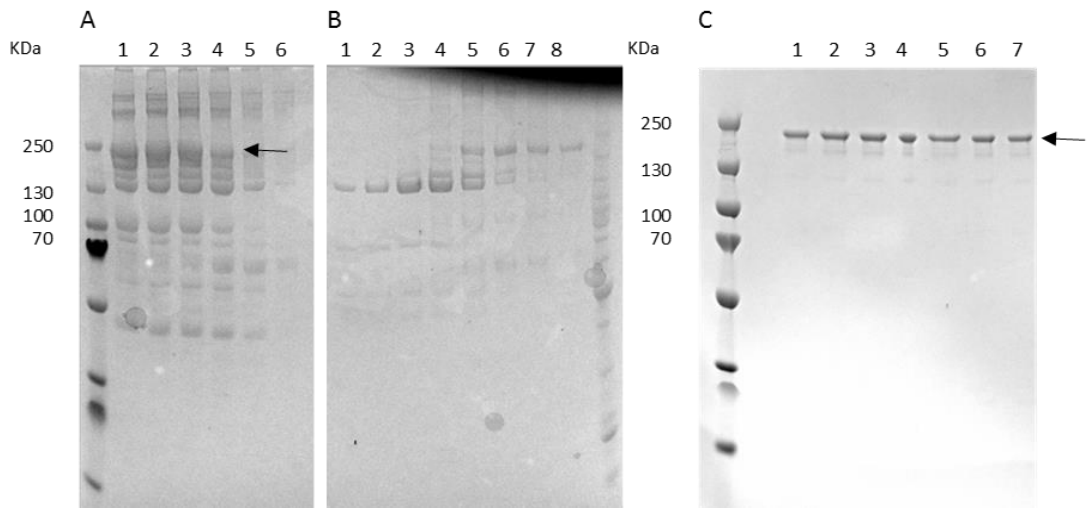

Figure 4.8. SDS-Page images for FH purification after running through 1st (A) (cation exchange column, CEX) and 2nd (B) (anion exchange column, AEX). Each lane represents 5 ml of elutant. After overnight ammonium carbonate dialysis samples were run through the second column. Factor H was identified in fractions 1-5 from CEX column and in fractions 1-6 from AEX. For further purification fractions 1-4 from AEX were pooled and purified using gel filtration column HiLoad Superdex 200 pg (C). Fractions 1-7 were pooled, concentrated and stored at -80^{o}C. FH is marked with an arrow.

MRLLAKIICLMLWAICVAEDCNELPPRRNTEILTGSWSDQTYPEGTQAIYKCRPGYRSLGNIIMVCRKGEWVALNPL
RKCQKRPCGHPGDTPFGTFTLTGGNVFEYGVKAVYTCNEGYQLLGEINYRECDTDGWTNDIPICEVVKCLPVTAPE
NGKIVSSAMEPDREYHFGQAVRFVCNSGYKIEGDEEMHCSDDGFWSKEKPKCVEISCKSPDVINGSPISQKIIYKEN
ERFQYKCNMGYEYSERGDAVCTESGWRPLPSCEEKSCDNPYIPNGDYSPLRIKHRTGDEITYQCRNGFYPATRGNT
AKCTSTGWIPAPRCTLKPCDYPDIKHGGLYHENMRRPYFPVAVGKYYSYYCDEHFETPSGSYWDHIHCTQDGWSP
AVPCLRKCYFPYLENGYNQNYGRKFVQGKSIDVACHPGYALPKAQTTVTCMENGWSPTPRCIRVKTCSKSSIDIEN
GFISESQYTYALKEKAKYQCKLGYVTADGETSGSITCGKDGWSAQPTCIKSCDIPVFMNARTKNDFTWFKLNDTLD
YECHDGYESNTGSTTGSIVCGYNGWSDLPICYERECELPKIDVHLVPDRKKDQYKVGEVLKFSCKPGFTIVGPNSVQ
CYHFGLSPDLPICKEQVQSCGPPPELLNGNVKEKTKEEYGHSEVVEYYCNPRFLMKGPNKIQCVDGEWTTLPVCIVE
ESTCGDIPELEHGWAQLSSPPYYYGDSVEFNCSESFTMIGHRSITCIHGVWTQLPQCVAIDKLKKCKSSNLIILEEHLK
NKKEFDHNSNIRYRCRGKEGWIHTVCINGRWDPEVNCSMAQIQLCPPPPQIPNSHNMTTTLNYRDGEKVSVLCQ
ENYLIQEGEEITCKDGRWQSIPLCVEKIPCSQPPQIEHGTINSSRSSQESYAHGTKLSYTCEGGFRISEENETTCYMGK
WSSPPQCEGLPCKSPPEISHGVVAHMSDSYQYGEEVTYKCFEGFGIDGPAIAKCLGEKWSHPPSCIKTDCLSLPSFE
NAIPMGEKKDVYKAGEQVTYTCATYKMDGASNVTCINSRWTGRPTCRDTSCVNPPTVQNAYIVSRQMSKYPSGE
RVRYQCRSPYEMFGDEEVMCLNGNWTEPPQCKDSTGKCGPPPPIDNGDITSFPLSVYAPASSVEYQCQNLYQLEG
NKRITCRNGQWSEPPKCLHPCVISREIMENYNIALRWTAKQKLYSRTGESVEFVCKRGYRLSSRSHTLRTTCWDGKL
EYPTCAKR

Figure 4.9. LC MS/MS sequence analysis for identification of human FH. Significant peptide fragments are highlighted in red. 13% of analysed protein shows more than 95% similarities with FH, which is sufficient to confirm that the obtained protein is FH.

The method used for FH purification was essentially that carried out previously by Brandstatter et al., (2012) with some minor modifications. Cation and anion exchange columns were substituted with equivalents from other brands. In addition, in the last purification step gel filtration was used rather than hydroxyapatite affinity chromatography.

4.3.1.2. Production and purification of recombinant proteins

HRG is believed to bind most of its ligands via its N-terminus, including heparin (Koide et al., 1989), heparan sulphate, plasminogen and to cell-surface GAG of T-cell lines (Jones, 2004). It is therefore postulated that this region of the protein may interact with complement proteins, heparin and other ligands that modulate the immune system and/or can contribute to the development of some diseases, including AMD. To examine those interactions, the recombinant HRG fragment consisting of the N1/N2 domains was produced using an *E. coli* expression system.

Protein purification under non denaturing conditions

High-level expression of non-native proteins in *E. coli* very often results in the production of misfolded protein, which can generate insoluble protein aggregates. Those aggregates are known as inclusion bodies and are almost exclusively formed by proteins foreign to *E. coli*. It is possible and relatively easy to purify proteins from inclusion bodies, but the refolding is complicated and time consuming. To overcome potential protein insolubility, Shuffle T7 competent cells were chosen for the production of recombinant HRG N1/N2-domain. This strain is engineered to express DsbC isomerase, which facilitates the expression of proteins containing disulfide bonds, in the cytoplasm, and to fix mis-oxidised proteins into their correct form.

After successful cloning of the appropriate coding sequence into the pETM11 vector, a His-tagged HRG N1/N2-domain fragment was expressed in Shuffle T7 cells. Cells were grown on LB agar plates with the addition of kanamycin for selection. After an initial overnight liquid culture, main cultures were set up in 50 ml aliquots to evaluate the conditions that would give highest protein yield. Effect of two parameters was investigated: temperature and concentration of inducer (IPTG). Cultures were grown at optimal temperature until reaching the mid-log growth phase, and then protein production was induced with the addition of 0.01 mM, 0.4 mM or 1 mM of IPTG and the temperature lowered to 16°C, 25°C or 30°C for 16h. The following day a sample of each culture was taken, spun down, lysed and analysed with SDS-PAGE. The culture condition that resulted in the highest protein yield was the one induced with 0.01 mM IPTG and grown at 25°C (Fig. 4.10). This was judged by subjective comparison of the thickness of the bands at 30 KDa at different culture conditions

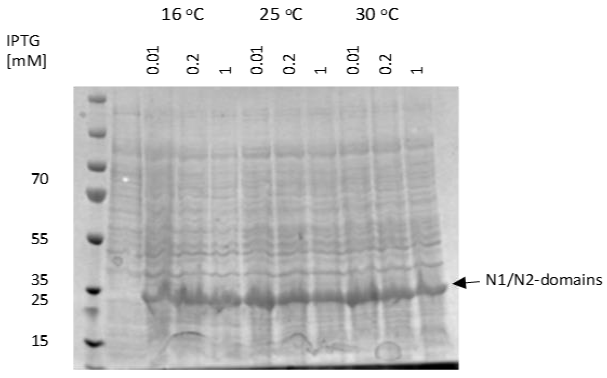

Figure 4.10. Optimizing growth conditions for recombinant HRG N1/N2-domain expression by Shuffle T7 cells. Nine different growth conditions were tested. Each lane represents one of the conditions. Protein production was induced with 0.01, 0.2 and 1 mM of IPTG and then temperature lowered to 16, 25 or 30°C (top row).

Once the growth conditions were optimised, a preparative scale culture for protein expression was set up. Cultures were grown according to the optimal conditions (0.01 mM IPTG and grown at 25°C). Subsequently, the bacterial pellet was lysed in a buffer containing lysozyme, and sonicated. The filtered lysate was loaded onto a HisTrap HP column. The N1/N2-domain was eluted with 30-50% of Elution buffer. Chosen fractions (Fig. 4.11 A, fraction 3-6) were pooled and mixed with TEV protease to cleave the His-tag from the N1/N2-domain. To determine whether the protein bound to the column (and thus whether cleavage was successful), the column flow through was analysed by SDS-PAGE (Fig 4.11 B), which showed no protein of expected size suggesting the His-tag had been successfully removed.

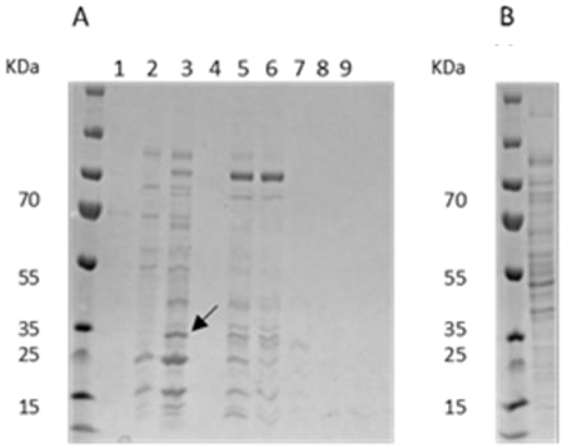

Figure 4.11. SDS-PAGE images for the first step of N1N2-domains purification. On the image, each lane represents samples from 1 ml eluted fractions. Eluted fractions 3, 5 and 6 (A) reveal a band of around 30 kDa (an arrow). Those fractions were then pooled for further purification. The HRG N1/N2-domain fragment is indicated by the arrow. Column flow-through (B) showed no protein of the expected size (30 kDa), therefore all protein present in the sample was bound to the HisTrap™ Ni column.

After dialysis, the cleaved protein was run through a HisTrap HP column. The TEV protease removes the His-tag. Therefore, the cleaved protein should not bind to the column and should be present in the flow through, which was collected. Additionally, fractions bound to the column (and later eluted), were also analysed to check if cleavage was sufficient. SDS-PAGE revealed that only a relatively small amount of protein was present in the flow through (Fig. 4.12 B,

fractions 1-4). SDS-PAGE revealed that TEV cleavage was insufficient, and most of the protein was bound to the column (Fig. 4.12 B, fraction 6).

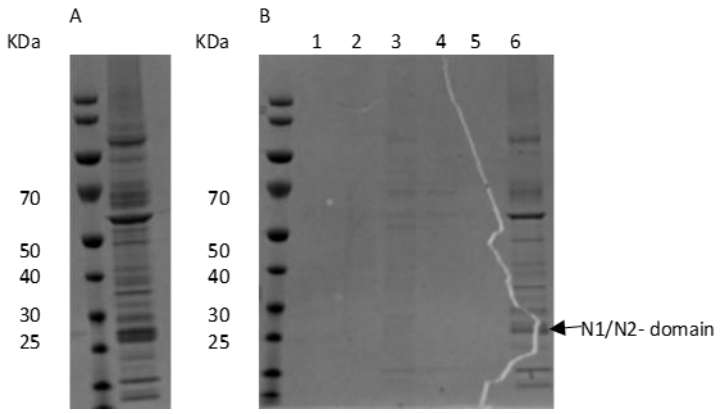

Figure 4.12. SDS-PAGE images for second step of HRG N1/N2-domain purification. On the image, each lane represents samples from 1 ml eluted fractions. After TEV cleavage, prior to the second HisTrap column, the sample was run on the gel, to make sure N1/N2-domain did not degrade during an overnight dialysis (A). Protein without His-tag, should not bind to HisTrap column, yet only trace amount was present in the flow through (B, fractions 1-4). Proteins bound to the column were later eluted with 50 – 100% of elution buffer (B, fraction 6).

Solubility screening

It was suspected that most of the expressed recombinant HRG N1/N2-domain fragment was formed within insoluble inclusion bodies during bacterial growth. To confirm this, a solubility screen was performed. Transformed Shuffle T7 cells were grown, an aliquot of the bacterial culture was lysed, and the supernatant (Fig. 4.13, fraction 2) and pellet (Fig. 4.13, fraction 1) were analysed separately by SDS-PAGE. Additionally, an aliquot of bacterial culture was lysed and sonicated prior to SDS-PAGE analysis, with pellet (Fig. 4.13, fraction 3) and supernatant (Fig. 4.13, fraction 4) run separately. The results strongly suggested that most of the protein was present in insoluble fractions (in pellet, Fig. 4.13, fractions 1 and 3). This soulubility screen provided a proof that solubility was indeed a problem and most of the protein is probably trapped in insoluble inclusion bodies formed during bacterial growth.

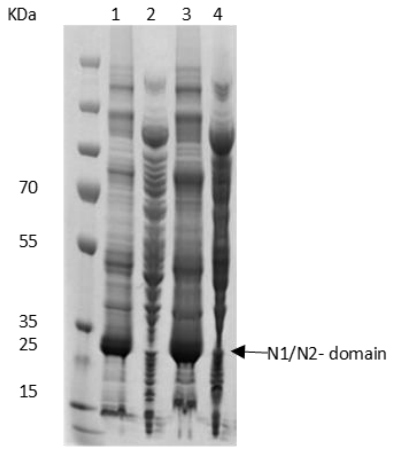

Figure 4.13. SDS-PAGE images of solubility screen for N1/N2-domain in Shuffle T7. On the image each lane represents either the pellet (1 and 3) or the supernatant fraction (2 and 4) of bacterial culture. Samples 1 and 2 were lysed prior to analysis, and samples 3 and 4 lysed and additionally sonicated. All samples were reduced with β-mercaptoethanol prior to analysis.

Culturing *E. coli* at low temperatures to increase protein solubility

It was reported by San-Miguel et al. (2013), that the production of soluble proteins in *E. coli* can be improved when bacteria are cultured at low temperature. To facilitate this they induced protein production at early log phase (OD_{600} = 0.1 AU), then lowered the temperature to 4°C. As a result, they obtained a much higher yield of soluble protein, compared to a standard culture method. A similar method was therefore employed for recombinant HRG N1/N2-domain production. For this, 50 ml cultures of previously transformed Shuffle T7 cells were set up in aliquots and grown until OD_{600}=0.1 AU. IPTG was then added to induce expression and the temperature was lowered to either 4°C (Fig. 4.14 A) or 15°C (Fig. 4.14 B) and cells were incubated for 72 h and 48 h, respectively. Analysis by SDS-PAGE revealed that the HRG N1/N2-domain was still present in the insoluble fractions (Fig. 4.14 A, fractions 1, 3 and 6; Fig. 4.14 B, fractions 1, 3 and 6). Furthermore, more protein was expressed when the culture was grown at 15°C for 48 h, than when grown at 4°C for 72 h.

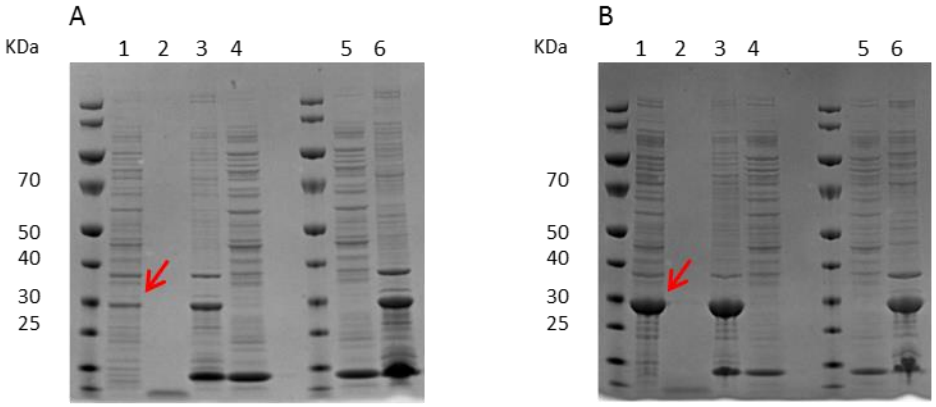

Figure 4.14. SDS-PAGE analysis of solubility screens for expressed HRG N1/N2-domains in Shuffle T7 cells grown at 4°C (A) and 15°C (B). For both each lane represents either pellet (1, 3 and 6) or supernatant fractions (2, 4 and 5) of the bacterial culture. Samples 1 and 2 were not lysed prior to analysis, samples 3 and 4 were lysed, and samples 5 and 6 were lysed and additionally sonicated. All samples were reduced with β-mercaptoethanol prior to analysis. Red arrows show HRG N1/N2-domain at approximately 30 kDa.

This approach may have failed due insufficient *E. coli* chaperonin functioning. Chaperonins are enzymes that assist proper protein folding by stabilising unfolded and partially-folded proteins. *E. coli* chaperonins lose up to 70% (chaperonin complex GroEL/ES) of their activity at low temperatures (Ferrer et al., 2003). However, there are commercially available *E. coli* strains engineered to co-express cold-adapted chaperonins to improve protein processing ability at low temperatures. ArcticExpress competent cells express chaperonins Cpn10 and Cpn60 from the psychrophilic bacterium, *Oleispira antarctica*, which exhibit very high activity at low temperatures (4-12°C). For HRG N1/N2-domain expression, the DE3 lysogen strain was chosen, as it is designed for T7 promoter-driven expression (as per PETM11 expression plasmid). An aliquot of ArcticExpress cells was transformed with pETM11 containing the HRG N1/N2-domain insert. Cultures were set up and grown at 37°C until OD_{600} = 0.6 AU, then protein production was induced by the addition of IPTG and temperature lowered to 4°C and 10°C for up to 72 h. The resultant bacteria were collected, lysed and sonicated. Pellets (Fig. 4.15 A) and supernatants (Fig. 4.15 B) were reduced with β-mercaptoethanol and analysed separately by SDS-PAGE. A band corresponding to protein of expected size was present in pellet fractions only (Fig. 4.15 A, black arrow). No protein of 30 kDa was seen in supernatant fractions (Fig. 4.15 B). That led to

the conclusion that the recombinant N1/N2-domain was still insoluble when expressed in these cells.

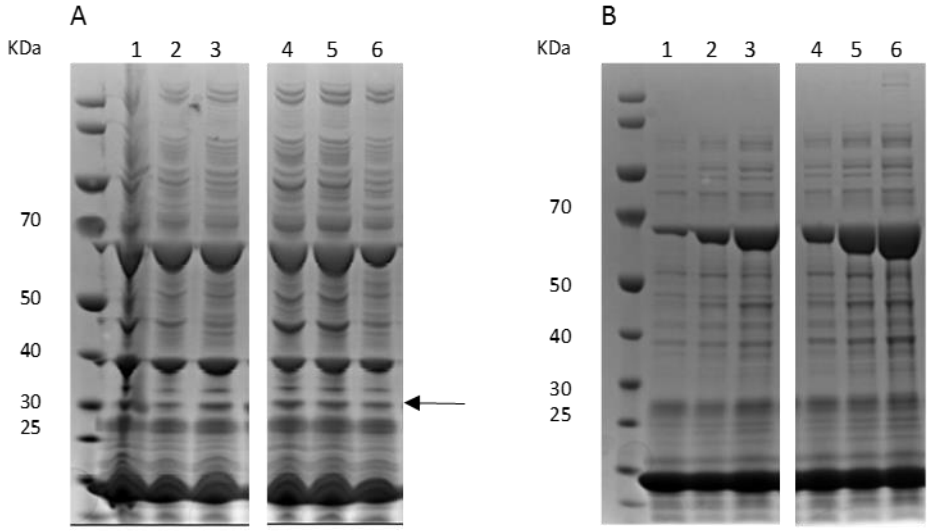

Figure 4.15. SDS-PAGE analysis of solubility screens for expressed HRG N1/N2-domains in ArcticExpress cells grown at low temperatures. The images represent either pellet (A) or supernatant fractions (B) of the bacterial culture. Samples 1-3 represent the culture grown at 4^{o}C, samples 4-6 at 10^{o}C. Samples 1-3 and 4-6 were taken at 24 h intervals.

GFP fusion protein

Green fluorescent protein (GFP) from the jellyfish, *Aequorea victoria* is widely used in biological assays. It is non-toxic for *E. coli* cells and highly soluble, which makes it a perfect fusion partner to increase solubility of recombinant proteins. To this end, expression of a HRG N1/N2 domain-GFP fusion was attempted to determine whether this might aid in the production of a soluble fragment for further study. In order to achieve this the coding sequence of the HRG N1/N2 domain was cloned into the pEHISGFPTEV expression vector. This plasmid allows production of an N-terminal, TEV protease cleavable His-tagged GFP fusion protein. It uses a T7 promoter and a T7 terminator and therefore is suitable for expressing a target protein in *E. coli* strains expressing T7 RNA polymerase such as Shuffle T7.

The coding sequence for the HRG N1/N2-domain was cloned into pEHISGFPTEV using NotI and XhoI restriction sites. Shuffle T7 competent cells were transformed, colonies were picked and grown for DNA isolation. Plasmid minipreps were performed and the resulting DNA was

quantified and subjected to further analysis (commercial sequencing and diagnostic restriction digest) to confirm that cloning was successful. For protein purification, a transformed culture was grown in LB until the mid-log growth phase, then protein production was induced with IPTG and grown overnight at 25°C. Following centrifugation and lysis, the filtered bacterial lysate was then applied to a pre-equilibrated HisTrap HP column. Eluted fractions were analysed by SDS-PAGE revealing a protein of expected size (Fig. 4.16 A, red arrow). The desired protein should be around 61.7 kDa as it is a fusion of HRG N1/N2-domain, which has a calculated mass of 30 KDa plus 31.7 kDa corresponding to HisGFP. Fractions 3-8 were pooled and dialysed overnight with TEV protease to cleave GFP fusion protein. SDS-PAGE of a digested sample showed a band of around 30 kDa, thought to be the HRG N1/N2-domain. However mass spectrometry analysis identified this protein to be TEV protease (Fig. 4.16 B), suggesting that both proteolytic cleavage did not work and proteins remained fused or, perhaps more likely, that the expressed fusion protein was not soluble.

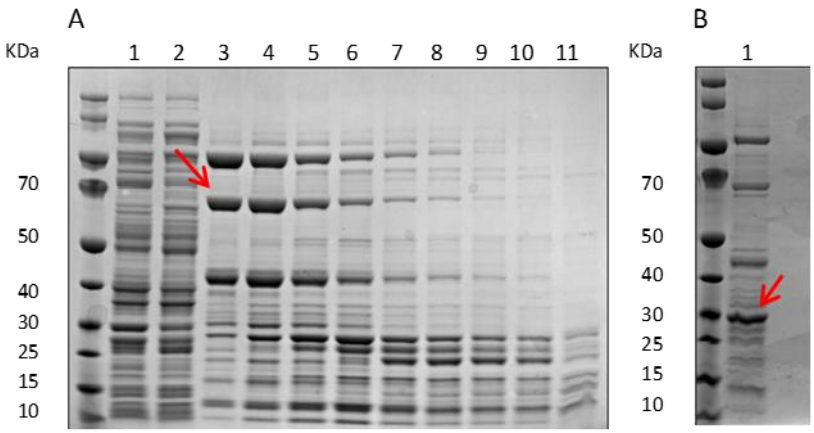

Figure 4.16. SDS-PAGE analysis of HRG N1/N2-GFP fusion protein purification after preliminary purification with HisTrap (A) column and after TEV cleavage (B). Each line represents 1 ml of elutant. The HRG N1/N2-GFP fusion protein had a calculated molecular weight of 61.7 kDa (red arrow), therefore after initial purification (A) fractions 3-8 were pooled and dialysed over-night with TEV protease. The next day, the sample was run on SDS-PAGE which revealed a protein of appropriate size to be present (B, red arrow). However, LC MS/MS analysis identified the protein as TEV protease rather than HRG N1/N2.

Denaturing conditions

Two strains of competent *E. coli* cells, Shuffle T7 and ArcticExpress, were used with various culture conditions, but neither resulted in the expression of soluble, recombinant HRG N1/N2. Formation of inclusion bodies prevented the production of soluble protein. Therefore, to recover protein from those aggregates, purification of the protein over denaturing conditions, followed by refolding to its native state was attempted.

An initial culture of transformed Shuffle T7 competent cells was grown from glycerol stock. The following day, two 1 L cultures were set up. When OD_{600}=0.7 AU, protein production was induced with IPTG and temperature was lowered to 25°C for an overnight culture. The bacterial pellet was lysed with addition of 8 M urea to denature proteins. The lysate was loaded onto a HisTrap HP column. Eluted fractions 4-16 (Fig. 4.17 A) were pooled together and dialysed twice against a buffer containing DTT, which reduces unwanted disulphide bond formation to help the protein refold into its native structure. The protein sample was mixed with TEV protease in order to cleave the His tag, and was then dialysed overnight. The following day, the sample was run through a HisTrap HP column. After TEV cleavage, the protein should not bind to the HisTrap HP column and therefore be present only in the column flow through. SDS-PAGE analysis revealed a protein of the expected size in both the column flow through (Fig. 4.17 A, fractions 1-7) and fractions eluted from the HisTrap column (Fig. 4.18 A, fractions 8-15). That would suggest that except His tags, the protein has some other histidine residues in its structure.

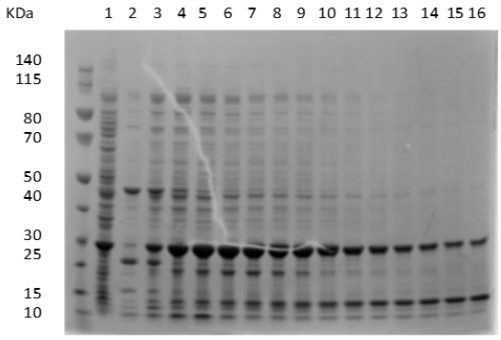

Figure 4.17. SDS-PAGE analysis of expressed HRG N1/N2-domains following first HisTrap purification, purified under denaturing conditions. Each lane represents samples from 1 ml eluted fractions, except lane number 1, which shows the lysed and filtered sample prior to loading. Protein was eluted using an imidazole gradient. Fractions 4-16 revealed a band of approximately 30 kDa, which corresponds to HRG N1/N2-domains. Those fractions were then pooled for further purification.

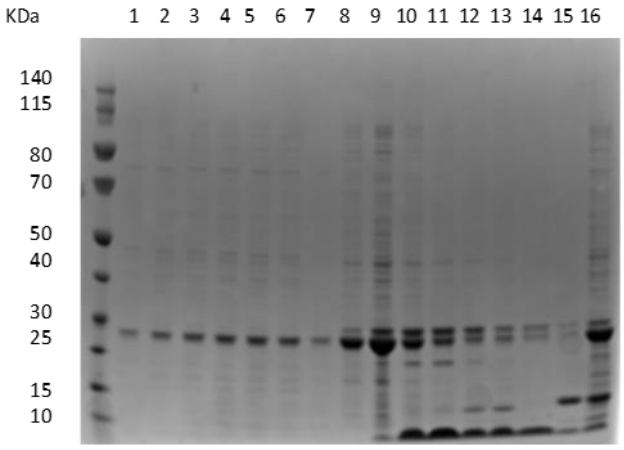

Figure 4.18. SDS-PAGE analysis of expressed HRG N1/N2-domain following second HisTrap step, purified under denaturing conditions. After an overnight proteolytic cleavage, sample was loaded onto HisTrap column. Each lane represents samples from 1 ml fractions. Both, column flow through (fractions 1-7) and eluted fractions (8-15), revealed the band of around 30 kDa, which corresponds to the HRG N1/N2-domain.

The column flow through and fractions eluted from the column were treated separately. Firstly, column flow through was run through a size exclusion column (Fig. 4.19) and concentrated to 10 mg/ml. Mass spec analysis proved the protein to be the N1/N2 domain of HRG with 54 % coverage (Fig. 4.20). Unfortunately, the protein was still not completely pure as there was a trace of an additional contaminant, identified by mass spectrometry as the *E. coli* molecular chaperone, Dnak. However, the obtained protein (estimated to be around 90% pure) was deemed of sufficient purity to set up crystallisation trials and to be used in subsequent binding studies. Next, the fractions eluted from a HisTrap HP column were purified by size exclusion chromatography. It was not possible to separate two proteins, whose molecular weights were very similar using this method (Fig. 4.21). The higher band is most likely the HRG N1/N2-domain (30 kDa) and the lower band is TEV protease (28 kDa) (Fig. 4.20). The purity of this sample was not satisfactory and therefore was not used for further experiments.

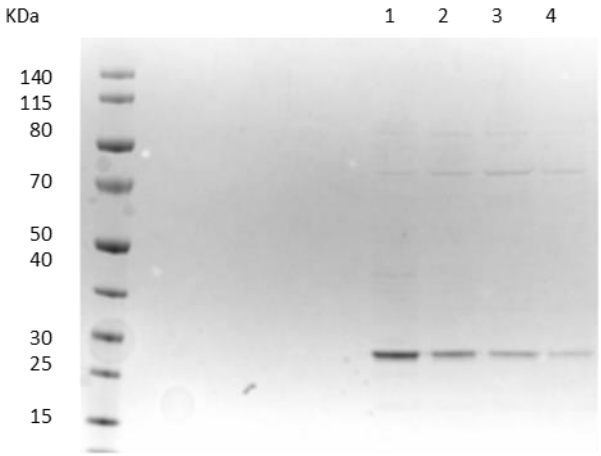

Figure 4.19. SDS-PAGE analysis of expressed HRG N1/N2-domain from column flow through purified by size exclusion chromatography. Each lane represents samples from 1 ml fractions (1-4), which revealed the band of around 30 kDa corresponding to the HRG N1/N2-domain. A trace amount of the 75 kDa *E. coli* protein, Dnak was also present in these fractions.

MKHHHHHHPMSDYDIPTTENLYFQGAMAVSPTDSSAVEPEAEKALDLINKRRRDGYLFQLLRIADAHL
DRVEATTVYYLVLDVQESDCSVLSRKYWADCEPPDSRRPSEIVIGQCKVIATRHSHESQDLRVIDFAC
TTSSVSSALANTKDSPVLIDFFEDTERYRKQANKAPEKYKEENDDFASFRVDRIERVARVRGGEGTGY
FVDFSVRASPRHHFPRHPNVFGFCRADLFYDVEALDLESPKNLVINCEV

Figure 4.20. LC MS/MS sequence analysis for identification of recombinant N1/N2-domain purified over denaturing conditions revealed 54% coverage. Identified peptide fragments are highlighted in red.

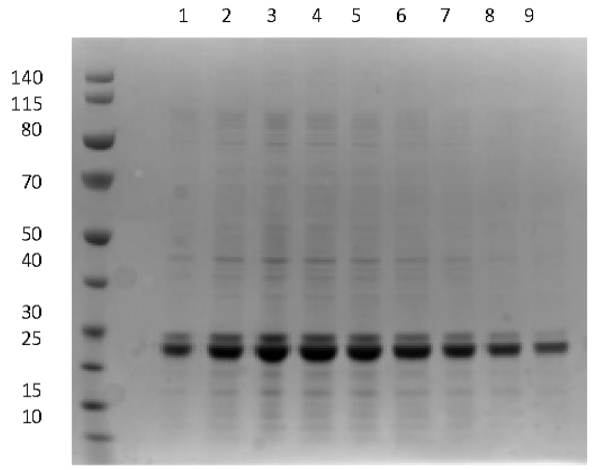

Figure 4.21. SDS-PAGE analysis of expressed HRG N1/N2-domain from the second HisTrap column purified by size exclusion chromatography. Each lane represents samples from 1 ml fractions (1-9), which each revealed the band of around 30 kDa corresponding to the HRG N1/N2-domain (larger of the bands is HRG N1/N2-domain and the smaller one TEV protease, 28 kDa). It was not possible to separate two proteins using size exclusion due to the similarity in their molecular weights.

Many approaches were attempted to express the recombinant HRG N1/N2-domain. Besides many parameters being assessed, including temperature, IPTG concentrations and length of culture, expression and purification under native conditions failed. Overexpressed non-native proteins in *E. coli* system are sometimes insoluble and form protein aggregates. To enhance protein solubility the protein was purified with the addition of denaturant, 8 M Urea. This approach helped, and finally, soluble HRG N1/N2-domain protein fragment was produced. This was extremely important as it is thought that most of the interactions between HRG and immune system molecules, including complement proteins, occur via N-terminus. Synthesis of this protein allowed to subsequent binding studies and crystal trials to be performed.

4.3.2. The role of zinc in the regulation of HRG–complement protein interactions

Complement proteins constitute a major part of innate immunity. They make up approximately 5% of the total protein content of human blood plasma (Nayak et al., 2010). C1q is the first component of the classical pathway. C3 is a central complement protein and supports the

activation of all three pathways of complement activation. It is probably the most versatile and multifunctional complement protein, possessing structural features that allow it to interact with at least 25 different proteins (Sahu and Lambris, 2001). Factor H is not a complement protein in the strictest sense, but through its interactions with the variety of proteins, acts as a main regulator of the alternative complement pathway.

As zinc is known to affect both complement protein and HRG functioning and that it has been demonstrated that HRG can interact with a number of complement proteins, we explored whether those interactions are influenced by zinc. Binding studies with purified HRG and complement proteins FH, C1q and C3, were performed using an ELISA based method. The binding studies were conducted in the absence/presence of 10 μM zinc, which is within the physiological range for plasma (10-20 μM; Sarkar, 1989). However, it is important to point out that under normal conditions most of the total zinc is bound to albumin and other plasma proteins including HRG. Despite this, it appears that there are circumstances where levels of "labile" zinc in plasma can achieve such concentrations in vivo. These include local sites at the surface of platelets and immune cells following zinc release (Leung et al., 1983) or under pathological conditions where zinc binding to serum albumin is disrupted (Kassaar et al., 2015).

To examine HRG complement protein binding, microtiter plates were coated overnight with 10 μg/ml of complement proteins C1q, C3 and FH. The following day plates were blocked with 0.4% gelatine, to avoid non-specific binding. Various concentrations of HRG were added to the plate and levels of bound protein were detected using an HRG-specific primary antibody and an alkaline phosphatase-linked secondary antibody. For each binding study, control and experimental groups were run on the same plate in parallel to make the results fully comparable.

The results revealed that native HRG has very high affinities for the three examined complement proteins as indicated by Kd values which are all in nanomolar range. Moreover, zinc has inhibitory effect on those interactions, with the affinity of HRG towards FH decreasing more than twice, from Kd of 0.66 nM to Kd of 1.46 nM after the addition of zinc (Fig. 4.22 A). The inhibitory effect of zinc was also observed on the affinity of HRG towards C3, with Kd increased from 0.44 nM to 1 nM when 10 μM zinc was added during the binding (Fig. 4.22 C). The affinity of HRG towards C1q also decreased after the addition of zinc, however the effect was less pronounced than that observed for C3 and FH, Kd increased from 0.64 nM to 0.97 nM (Fig. 4.22 B).

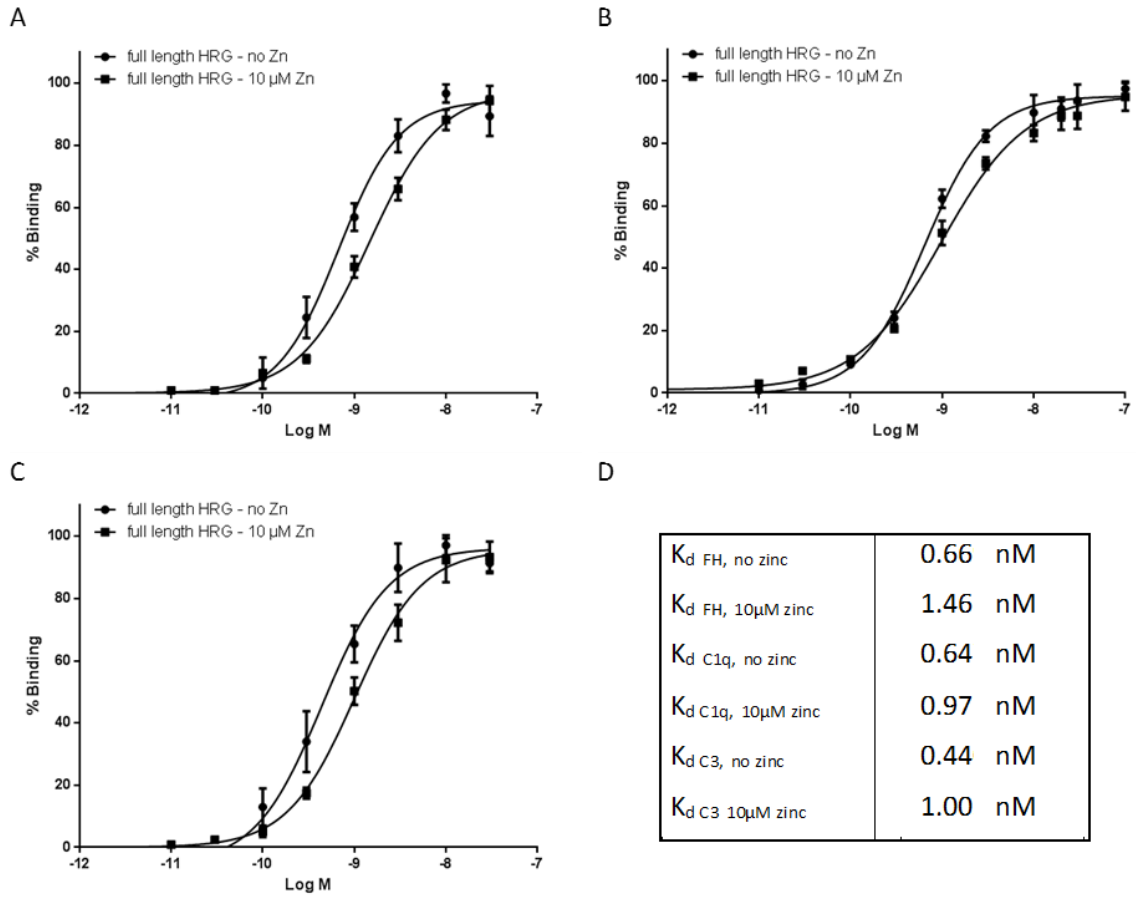

Figure 4.22. Binding of full-length human histidine rich glycoprotein to complement proteins: FH (A), C1q (B) and C3 (C). Dissociation constant (K_d) values were calculated using Graphpad Prism v6 (software) with Sigmoidal 4PL fit. The experiment was performed in the presence and absence of 10 µM zinc. Assays were performed in triplicate. Error bars represent calculated S.D.

It has been postulated that HRG interacts with many of its ligands through its N-terminus; therefore, the next step was to examine the interaction of a recombinant HRG N1/N2-domain fragment with C1q, C3 and FH. Due to the unavailability of an N-terminally directed anti-HRG antibody, the recombinant fragment was biotinylated to allow detection using alkaline phosphatase-linked streptavidin. Covalent cross-linking of biotin to the protein is rapid and specific, and does not interfere with the proteins function. The results revealed that zinc has no effect on the binding affinity of biotinylated N1/N2-domain towards FH with the K_d values *ca.* 0.23 µM (Fig 4.23 A), and toward C1q with the K_d values 0.22 µM (Fig. 4.23 B). In the contrary, zinc had a strong stimulatory effect on the binding affinity of N1/N2-domain towards C3, and the K_d decreased from 2.798 µM to 0.406 µM (Fig. 4.23 C).

Moreover, the results may suggest that the HRG N1/N2-domain fragment (Fig. 4.23) has much lower affinity for the three examined complement proteins compared to full-length protein as the K_d values are all in micro molar range (Fig. 4.22). However, due to differences in the experimental procedures, the results from the two experiments cannot be directly compared. For full-length protein, a two-step, antibody detection method was used, whereas for the HRG N1/N2 domain the protein was biotinylated, which in itself may have influenced complement protein binding.

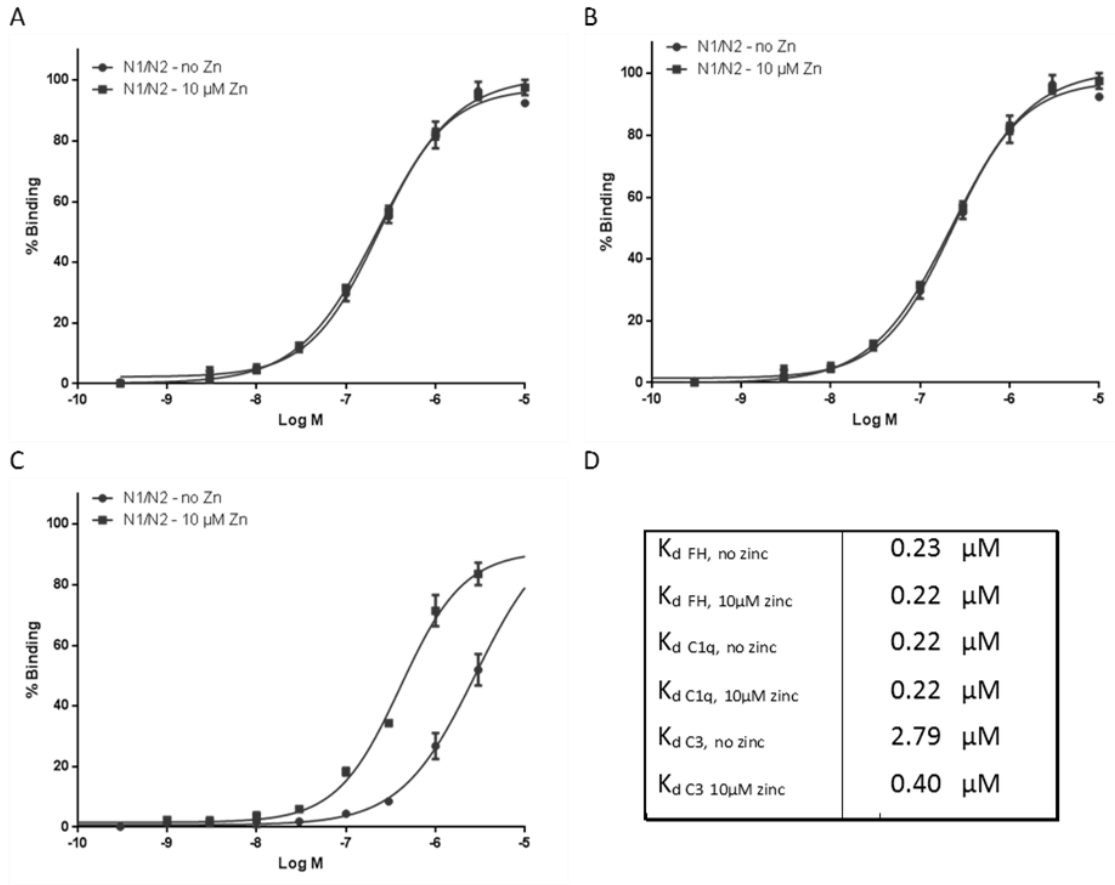

Figure 4.23. Binding of the N1N2-domain of HRG to complement proteins: FH (A), C1q (B) and C3 (C). K_d values were calculated using Graphpad Prism v6 (software) with Sigmoidal 4PL fit. The experiment was performed in the presence and absence of 10 µM zinc. Assays were performed in triplicate. Error bars represent calculated S.D.

Heparin is a known ligand for HRG (Koide et al., 1989) and is thought that this may occur, at least in part, via the proteins N-domain (Kassaar et al., 2015). It has been speculated that HRG can

bind heparins through both zinc-dependent and zinc-independent mechanisms, with the zinc-dependent mechanism being of higher affinity and involving the HRR region of the protein (Kassaar et al., 2015). The interaction of HRG with heparins is important for binding of the protein to the surface of cells (via heparan sulfate) including immune cells (Jones, 2004) and also plays a significant role in the neutralisation of heparins to promote coagulation (Borza and Morgan, 1998). To aid determination of whether the N1/N2 domain of HRG participates in heparin binding and whether zinc may influence this process, the binding of biotinylated recombinant HRG N1/N2-domain fragment to heparin-coated plates was performed in the presence of different concentrations of the fragment with and without 10 µM zinc. The results show that the addition of zinc did not affect the binding affinity of N1/N2-domain toward heparin, with K_d values remaining approximately the same (from 0.17 nM to 0.13 nM after the addition of zinc; Fig. 4.24). Additionally the affinity of binding is very strong as K_d values are in the nanomolar range. This interaction is therefore ~1000 times stronger than the binding observed between the HRG N1/N2-domain and complement proteins (Fig. 4.23).

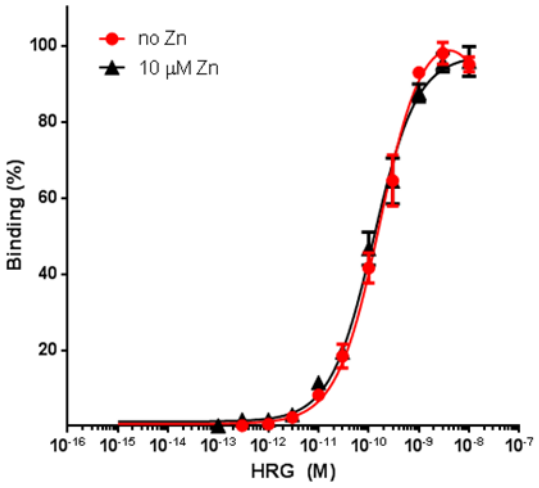

$K_{d\ no\ zinc}$ =0.17 nM

$K_{d\ 10\ \mu M\ zinc}$ = 0.13 nM

Figure 4.24. Binding of N1N2-domain of HRG to unfractionated heparin. K_d values were calculated using Graphpad Prism v6 (software). The experiment was performed in triplicate in the presence and absence of 10 µM zinc. Error bars represent calculated S.D.

4.3.3. The role of zinc and pH in the regulation of HAP-protein interactions

4.3.3.1. The influence of zinc on HAP-protein interactions using an ELISA based method

Numerous insoluble HAP spherules are present within sub-retinal pigment epithelial (RPE) deposits. These deposits are associated with cell death in age-related macular degeneration (AMD). Metals, such as zinc, iron and copper are also present in sub-RPE deposits and may alter the binding characteristics of HAP. The influence of zinc on HAP binding by human HRG and FH was examined.

BcMag^{TM} Hydroxyapatite-Modified Magnetic Beads are silica-coated superparamagnetic, 2 µm diameter beads with HAP functional groups added on the surface. A series of experiments were performed using these beads in an ELISA-based method. Each condition was prepared and run in triplicate. The first step was to establish whether elevated zinc has an influence on human HRG-HAP interactions. Two supraphysiological zinc concentrations were picked in relevance to AMD; 100 µM and 1 mM. Although the experiment was performed in 1.5 ml tubes, after the enzymatic reaction was stopped, samples were transferred onto 96-well microtitre plates and the absorbance was measured using a plate reader.

Results were plotted using GraphPad Prism v6 and dissociation constant values (K_d) calculated automatically using a "one site binding" model. No difference in the affinity of binding was observed between HAP beads pre-conditioned with 1 mM zinc and a non-zinc treated control, with the K_d = 4.17 nM ± 0.98 nM and K_d= 4.72 nM ± 0.95 nM respectively (Fig. 4.25). However, when HAP beads were pre-conditioned with 1 mM zinc and additionally the same concentration of zinc was present during HRG binding, the affinity of human HRG towards HAP increased almost 2-fold (K_d= 1.92 nM ± 0.43 nM; Fig. 4.25). Therefore, it suggested that pre-incubation of the beads with 1 mM zinc does not permanently change the surface of beads in the way that would influence the binding. Nevertheless, zinc at this concentration enhances the interaction between hydroxyapatite and human HRG.

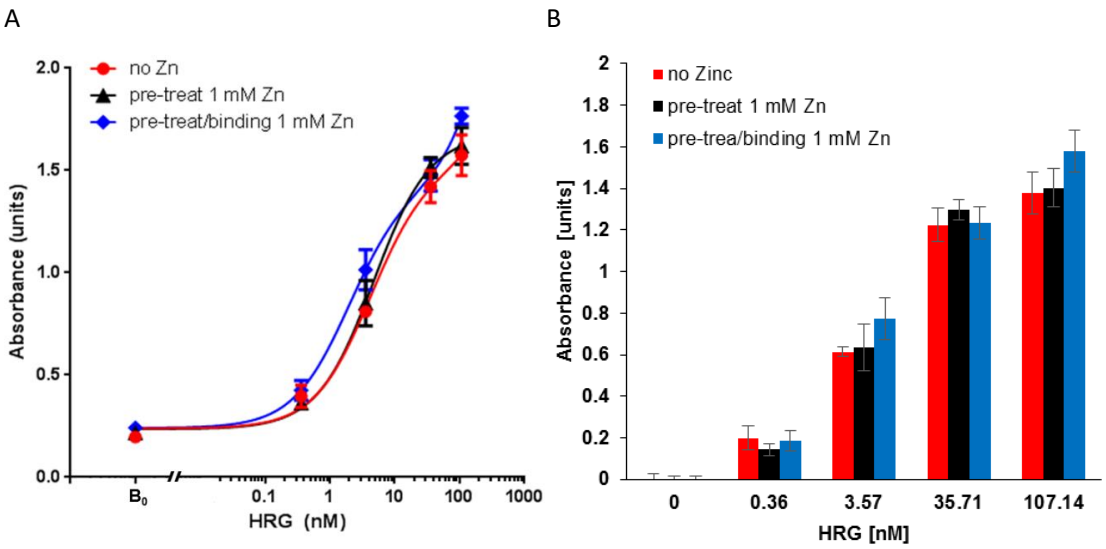

Figure 4.25. The influence of zinc on HRG-hydroxyapatite binding. Results are presented as binding curve (A) and bar chart (B) representing the same set of data. When HAP beads were pre-treated with zinc, no influence on binding was seen. However, when zinc was additionally present during HRG binding, the binding affinity increased significantly. K_d values were calculated using Graphpad Prism v6. Error bars on both graphs represent ± S.D.

4.3.3.2. Binding of HRG and FH to pre-coated HAP magnetic beads

It has been shown recently that protein aggregates on HAP spherules within drusen include FH (Thompson et al., 2015) as well as HRG (Fig. 4.1). The mechanism of formation of these aggregates is still unknown. To explore this, a HAP binding assay incorporating a pre-incubation of HAP beads with either HRG or FH was established. The aim being to examine if either of these two proteins has the potential to initiate deposit formation by binding directly to HAP spherules and facilitate further protein binding. Firstly, FH binding to HAP spherules with and without pre-coating with HRG was assessed and corresponding data was fitted using a sigmoidal fit (Fig. 4.26). When HAP beads were pre-coated with HRG prior to FH, no significant difference in the binding affinity of FH toward HAP was observed, K_d value being 17.86±23.51 nM, and 54.53±66.50 nM respectively. That shows that the FH was still able to bind to HAP beads, even pre-coated with HRG. To test the second model, where FH binds to the HAP spherules firstly and then HRG binds to FH, beads were pre-coated with FH and HRG was bound on top to form binding curve (Fig. 4.27). The data was again fitted using a sigmoidal fit. When beads were pre-coated with FH, HRG was still able to bind to HAP, however decrease in binding affinity of HRG toward HAP was observed, with 2-fold increase in K_d values, from 0.67 ±0.13 nM, to 1.53 ±0.3 nM, compared to HRG binding to bare beads.

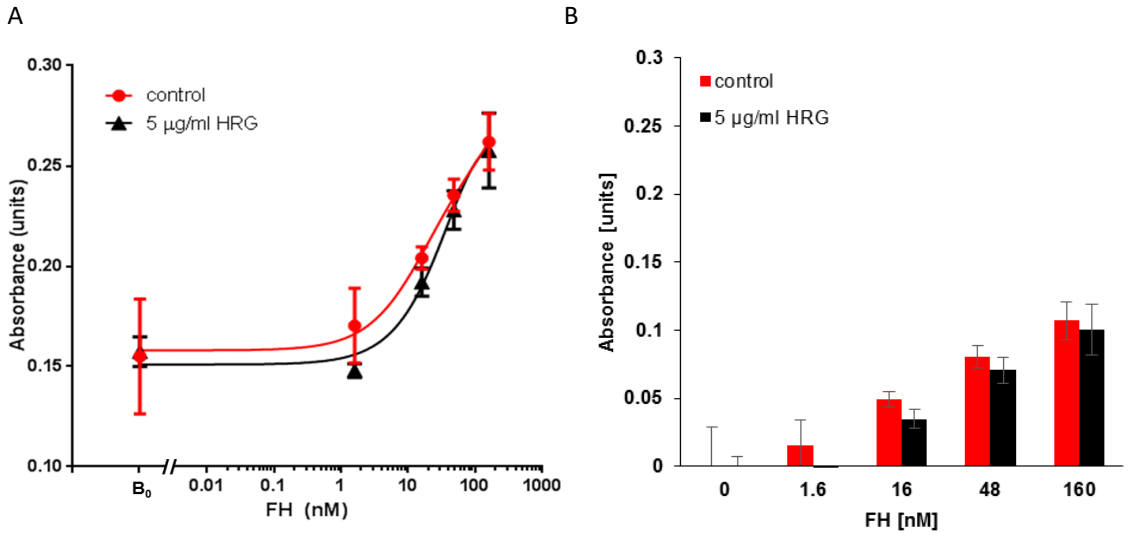

Figure 4.26. Binding of FH to hydroxyapatite pre-coated with HRG. HAP beads were either precoated with human HRG prior to FH binding, or left without HRG as a control. Results are presented as binding curve (A) and bar chart (B) representing the same data set. No difference in affinity of binding was observed. K_d values were calculated using Graphpad Prism v6. Error bars on both graphs represent ± S.D.

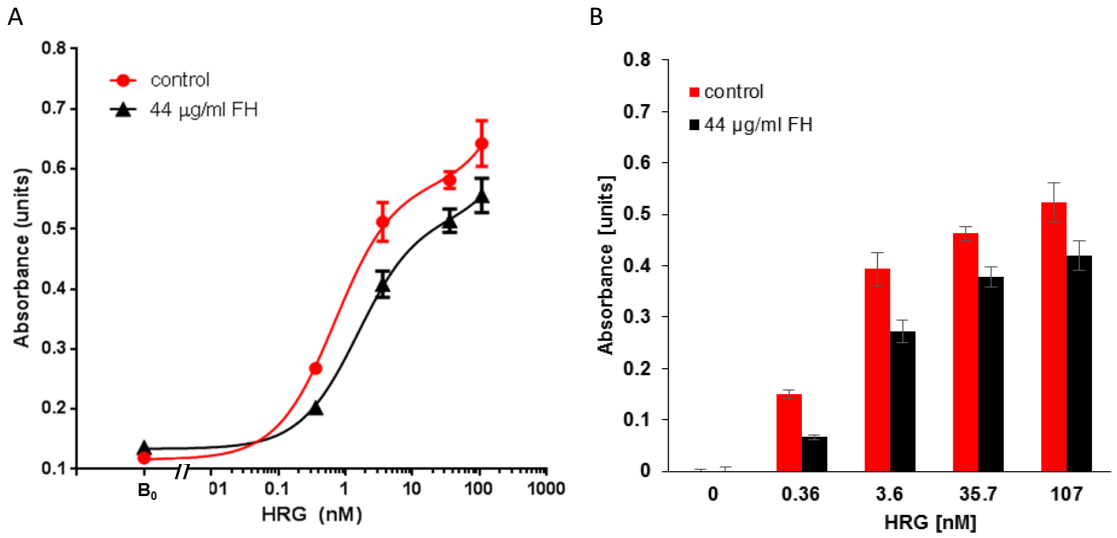

Figure 4.27. Binding of HRG to hydroxyapatite pre-coated with FH. Hydroxyapatite beads were either precoated with FH prior to HRG binding, or left without HRG as a control. Results are presented as binding curve (A) and bar chart (B) representing the same data set. Increased affinity of binding was observed when beads were pre-coated with HRG. K_d values were calculated using Graphpad Prism v6. Error bars on both graphs represent ± S.D.

4.3.3.3. The influence of pH on HAP-HRG interaction

The natural pH of the eye is 7.11±1.5 (Thai-Lim et al., 2014) but can become more alkaline during aging (Coles and Jaros, 1984). Potential small changes in pH that could happen at the Bruch's membrane in the eye could be a factor in drusen formation. Therefore, the next step was to examine the influence of pH on HRG-HAP as a factor in drusen formation. Three experimental groups were prepared in buffers of equal composition (140 mM NaCl, 50 mM Tris) but of varying pH of 6.5, 7.5 and 8.0. Values picked are close to physiological pH of human blood and are likely to represent that of the mammalian retina, which is 7.1-7.8 (Dmitriev and Mangel, 2001). Slightly elevated or acidic pH may occur during aging or in some pathological conditions, including inflammation. After the enzymatic reaction was stopped, samples were transferred onto 96-well plates and the absorbance was measured using a plate reader. The data was fitted using sigmoidal fit and K_d values were calculated.

No changes in binding affinities of human HRG towards HAP were observed upon pH alterations, with K_d value calculated to be 2.36 ±0.92 nM, for the binding at pH 6.5 and 2.49 0.61 nM at pH 8.0, compared to the control, where Kd value was 2.51 ±1.05 nM (Fig. 4.28). As elevated zinc (Fig. 4.25) and pH (Fig. 4.28) separately showed no influence on examined interaction, it was interesting to see whether those two parameters combined will show any impact.

Firstly, pH 6.5 combined with 1 mM zinc was examined (Fig. 4.29 A). Secondly, pH 8.0 together with zinc (Fig. 4.29 B). For both experiments, control was prepared at pH 7.5 and without the addition of zinc. Unfortunately, the data obtained could not be fitted to a simple "one site binding" model, therefore K_d values could not be calculated. Nonetheless, based on the absorbance, the data suggest that low pH in combination with addition of 1 mM zinc had no effect on the binding of HRG to the HAP beads. Alkaline pH together with 1 mM zinc potentiates the binding, which is represented as an increase in absorbance (Fig. 4.29 B).

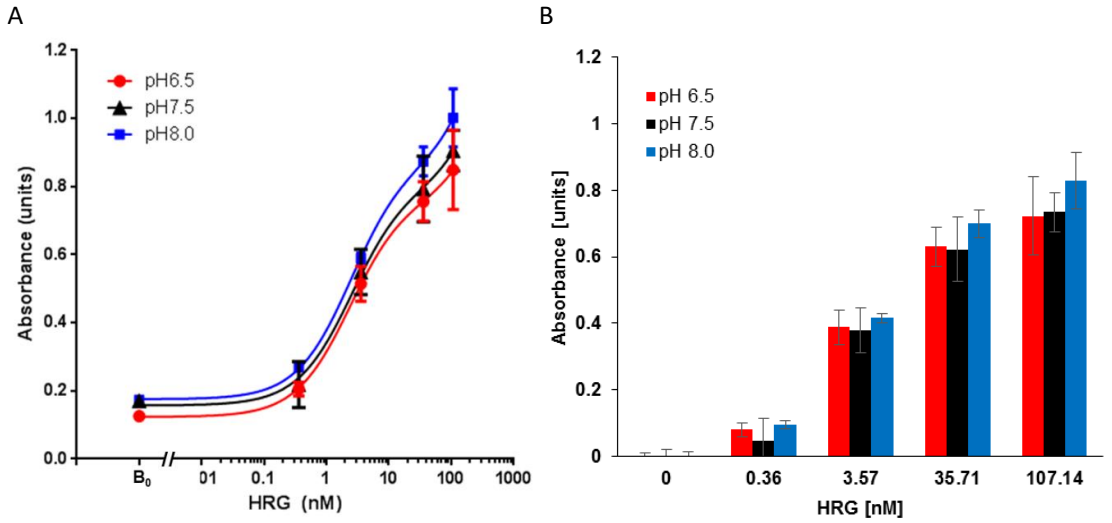

Figure 4.28. The influence of pH on HRG-hydroxyapatite binding. Results are presented as binding curve (A) and bar chart (B) representing the same data set. Neither low, nor elevated pH had an influence on the interaction between HAP and HRG as compared to the control (pH 7.5). K_d values were calculated using Graphpad Prism v6. Error bars on both graphs represent ± S.D.

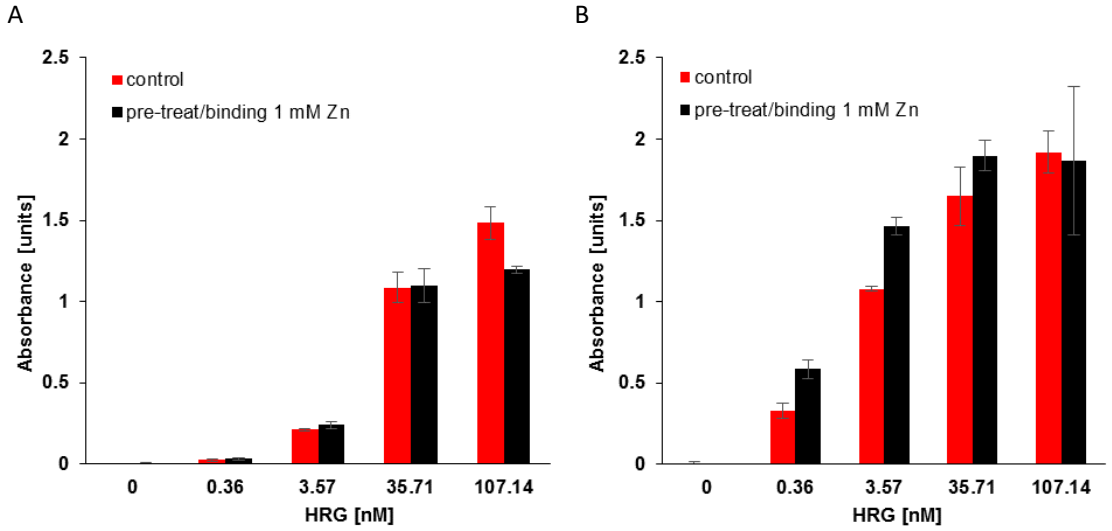

Figure 4.29. The combined influence of altered pH and zinc on HRG-HAP binding. Results are presented as bar charts. (A) Low pH (pH 6.5) together with 1 mM zinc does not influence the interaction between HRG and HAP magnetic beads. (B) High pH (pH 8.0) combined with 1 mM zinc, increase the binding of HRG to HAP magnetic beads. Control represents the binding of HRG to HAP magnetic beads at pH 7.5 and without the addition of zinc. Error bars on both graphs represent ± S.D.

4.3.4. Crystallography

In order to gain structural information relating to HRG-complement interactions we aimed to structurally characterise HRG using X-ray crystallography. Of particular interest was the N1 and N2 domains, which together are thought to participate in complement protein and heparin binding. Previously, our research group successfully solved the structure of the N2 domain of rabbit HRG (Kassaar, 2014). However, the structure of the N1 and N2 domains together, or indeed the whole protein, remains unknown. Crystallisation was attempted using two approaches. Firstly, we attempted to crystallise the whole protein purified from plasma. Secondly, we aim to crystallise the recombinant HRG N1/N2 fragment.

Many parameters influence crystal creation, including protein purity, homogeneity and concentration. For the crystallisation trials, a vapour diffusion method was used in which protein is put in the vapour-liquid equilibrium with precipitant and therefore concentrated over time to the point when crystals are being formed.

Crystallisation was attempted with rabbit HRG (18 and 36 mg/ml) purified from plasma. Trials were set up using an Art Robbins Gryphon crystallisation robot. The first crystals appeared after 3 months. In house analysis of these crystals revealed that they were unable to diffract X-ray effectively. Later crystals were re-analysed at the synchrotron at DIAMOND, but were also unable to diffract sufficiently to allow structural characterisation.

Recombinant N1/N2 domain, purified under denaturing conditions was used to set up crystallisation trials. Obtained protein was of satisfactory purity (approx. 95%) as revealed by SDS-PAGE (Fig. 4.30) and then concentrated to 25 mg/ml. Crystal trials were set using three commercially available crystal trials (PEG 4, PEG 2 and WIZARD) and one of the in house trials, with the addition of 200 µM, low molecular weight heparin (1.8 kDa) and also without heparin. Crystallography plates were checked in weekly intervals over 3 months; however, no crystals were observed.

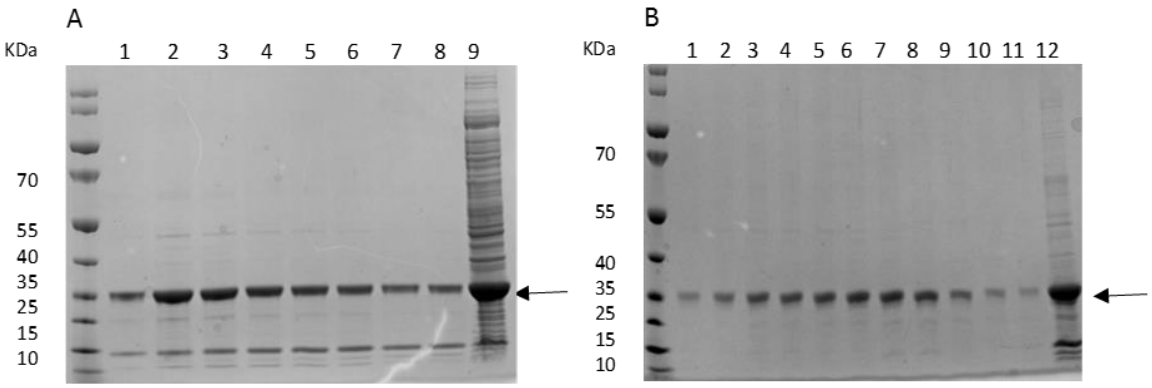

Figure 4.30. SDS-Page images for N1/N2-domain purification after running through HisTrap (A) and size exclusion column (HiLoad Superdex 75 pg) (B). Each line represents 1 ml of elutant. Last line on each gel shows the purity of the sample before loading onto column. Fractions 1-11 (B) were pooled, concentrated and crystal trials were set up. The presence of the N1/N2-domain is indicated by an arrow (A and B).

4.4. Discussion

4.4.1. The role of zinc in the regulation of HRG–complement protein interactions

HRG is known to modulate the activity of several complement proteins: C8, C9, D and S-protein. These interactions occur in a time- and concentration-dependent manner (Chang et al., 1992). HRG has also been shown to bind to C1q, FH, C4b-binding protein, C4 and C3 (Manderson et al., 2009). The results presented here, confirm that HRG binds strongly to several complement proteins, C1q, C3 and Factor H. Furthermore, it is shown for the first time that these interactions are zinc-dependent.

To examine whether the interaction between HRG and complement proteins occurs via HRG N-terminus, and if zinc plays any role in this interaction, a series of binding experiments were performed utilising a recombinant fragment of HRG constituting the N1/N2 domains. The results showed that zinc decreases the affinity of full length HRG for complement proteins C1q, FH and C3. The greatest effect was observed for FH and C3 where the Kd was increased 2-fold. When the same study was repeated with N1/N2-domain of HRG, zinc showed no effect on binding between N1/N2-domain and FH, and between N1/N2-domain and C1q. However, the affinity of HRG N1/N2-domain towards C3 was increased almost 7-fold by the presence of zinc. The results suggest for the first time, that binding of complement proteins to HRG is not solely dependent on the N-terminus, as it was previously thought. Other protein domains are likely contribute to the binding.

The idea that zinc can influence HRG activity came after finding that activated platelets can release zinc in localised areas and simultaneously HRG (Leung et al., 1983). HRG activation by zinc is possible when plasma fatty acid levels are elevated. In those conditions albumin binds fatty acids and does not bind zinc, which in fact leaves more zinc available to bind HRG (Stewart et al., 2003; Stewart et al., 2009; Lu et al., 2012). Zinc is crucial for proper innate and adaptive immune response (Maares and Haase, 2016). It is known that zinc modulates HRG immune complex clearance activity. In the presence of physiological zinc concentrations, HRG potentiates the binding of IgG containing immune complexes to FcγRI receptor on THP1 cells (Gorgani et al., 1999a). Insufficient clearance of immune complexes and apoptotic cells is dangerous and can lead to systemic lupus erythematosus-like symptoms (Skattum et al., 2011). HRG has also a big role in apoptotic and necrotic cells clearance. By binding to human monocyte-

derived macrophages and apoptotic Jurkat T-cells via FcγRI receptor, HRG accelerates apoptosis (Gorgani et al., 2002). Interestingly, C1q also takes part in apoptotic and necrotic cell clearance (Elward et al., 2005).

It was suggested that the binding affinities of HRG to IgG and C1q are affected by physiological concentrations of zinc, such that HRG's interaction with C1q is weakened (Gorgani et al., 1997a). Those results correspond to current findings as it was also observed that the affinity of HRG for C1q is lower, after addition of 10 µM zinc. It was also shown that micromolar zinc concentrations potentiate FH functioning through its ability to bind cofactor C3b resulting in strong inhibition of complement functions and causing protein precipitation (Blom et al., 2003). Additionally, FH forms oligomers consisting of 4-10 molecules in the presence of zinc, which could form aggregates and therefore block binding sites and decrease the affinity between FH and HRG (Perkins et al., 1991). The results presented here show decreased binding between FH and HRG, and between C3 and HRG in the presence of micromolar zinc.

Previous evidence together with current results and in vitro experiments showed that the formation of potentially harmful insoluble immune complexes (IICs) is partially inhibited at physiological HRG concentrations (~ 2 µM) (Gorgani et al., 1997a). This leads us to propose a new model of interaction between HRG and complement proteins. At physiological zinc concentrations, C3 binds HRG with high affinity. Moreover, zinc inhibits binding between HRG and FH. That may allow FH to bind with its ligand, C3b, which is crucial to control complement function through its inhibition. When the level of zinc is low, HRG binds FH. The complement pathway is not inhibited when it lacks the main regulatory protein (FH), and can result in the eventual destruction of "self" tissue.

It appears zinc can influence immune responses by affecting both alternative and classical complement pathways. However, the current investigation was limited to only three complement proteins (C1q, C3 and FH). Considerably more work should be done to determine the influence of zinc on the complement system as a whole in vivo.

Heparin and its derivative heparan sulfate, are other known ligands for HRG (Jones et al., 2004, Vanwildemeersch et al., 2006). The polysaccharide heparan sulphate is ubiquitously expressed on cell surfaces. It has multiple roles in inflammatory responses including initial adhesion of leukocytes to the inflamed endothelium, the subsequent chemokine-mediated transmigration through the vessel wall and the establishment of both acute and chronic inflammatory reactions (Parish, 2006).

It was shown previously that, two regions of HRG interact with heparin, N1/N2 region and the HRRs. Additionally it was shown that binding to the HRR is Zn^{2+}-dependent (Jones et al., 2004, Vanwildemeersch et al., 2006). Later Kassaar et al. (2015) demonstrated that the binding of heparin occurs in a Zn^{2+}-independent manner, for small heparin chains. However, when larger heparin chains are used, binding affinity of HRG towards heparin is enhanced by Zn^{2+}. It was suggested by Kassaar et al (2015) that heparin binding via the N1/N2 domain is Zn^{2+}-independent and that binding via the HRR is Zn^{2+}-dependent. The results presented in this chapter revealed no difference in the binding affinity of the N1/N2 domain towards unfractionated heparin in the presence of 10 μM Zn^{2+}, which is in agreement with this theory.

4.4.2. The role of zinc and pH in the regulation of HAP-protein interactions

AMD is the leading cause of irreversible vision loss in the elderly population of developed countries. Late, advanced stage of AMD is diagnosed as either “wet” neovascular AMD, "dry" atrophic AMD or as both forms (Khan et al., 2016). In this disease, maculopathy is caused by the formation of sub-RPE deposits on Bruch’s membrane called drusen. Small numbers of hard drusen is normal for the ageing eye, however the soft drusen indicate AMD-related changes (Ardeljan and Chan, 2013). They are composed of proteins from both degraded retinal cells and plasma, including vitronectin, clusterin (ApoJ), apolipoprotein E (ApoE), (serum), amyloid P (SAP) and amyloid-b (Thompson et al., 2015), and complement proteins (C2, C3, C9) (Johnson et al., 2001; Johnson et al., 2002). They are also recently linked to blood circulation specific proteins like albumin, haptoglobin (Anderson et al., 2002) and histidine-rich glycoprotein (HRG; Dr Imre Lengyel, UCL Institute of Ophthalmology, unpublished data). It has been recently discovered that soft sub-RPE deposits include cholesterol containing lipid droplets coated by insoluble hydroxyapatite (HAP) (Thompson et al., 2015). It has been also shown that proteins can form aggregates on drusen’s surfaces (Kobayashi et al., 2014) and those aggregates include FH (Thompson et al., 2015) and HRG (Dr Imre Lengyel, UCL Institute of Ophthalmology, unpublished data).

HAP is a calcium-containing mineral usually found in bones. Nonetheless, it can be found in other tissues as calcification is a normal process during ageing, or as a response to inflammation or injury (Anderson et al., 2002). The mechanism by which it occurs is different for different tissues. Most of those calcified deposits are just results of other primary age-related changes. These can cause age-related, irreversible tissue damage including calcification of the pineal gland during Alzheimer’s disease, calcified atherosclerosis lesions and HAP spherules in AMD.

It is known that some proteins including HRG can bind to HAP. This led to the idea of using HAP-coated beads as a model of HAP spherules in the AMD affected eye. This allowed characterisation of the HAP-associated binding properties of HRG and give clues as to how this protein contribute to deposit formation.

It has been suggested that one of the factors that increases sub-RPE deposits formation is a local increase in zinc levels. In AMD, the Bruch's membrane contains almost three times more zinc than in a healthy eye. There is even higher zinc content in the deposits (Lengyel et al., 2007) and therefore it is feasible that interaction between HRG, complement proteins and HAP are essential for drusen formation and it occurs when zinc levels are elevated (Perkins et al. 2010). Naturally, zinc should then increase the binding of HRG to HAP spherules. To test this hypothesis, HAP-coated magnetic beads were pre-conditioned with high concentration of zinc prior to HRG binding. No difference in binding was observed compared to the control (not preconditioned with zinc). However, when beads were pre-conditioned with zinc and additionally zinc was present during HRG binding, the affinity of HRG towards HAP increased almost twice. That suggests, that zinc does not bind strongly to the surface of the beads and can be washed away. The increased affinity of binding in the presence of zinc is likely a result of zinc interacting with HRG to alter its ability to interact with HAP.

The inflammation process also promotes drusen formation (Anderson et al., 2002). Complement activation as part of the inflammatory response, should normally result in phagocytosis and removal of degraded plasma proteins and organelles from RPE. Polymorphisms in a number of complement proteins including FH, C2, C3 and C9, result in not fully functional complement pathways (Perkins et al., 2010; Yates et al., 2007; Khan et al., 2016). This may cause inadequate removal of cellular and non-cellular debris. One of the factors known to regulate the response from alternative complement pathway is pH (Fishelson et al., 1987), and since it is feasible that drusens are formed in the place of local inflammation (Anderson et al., 2002), the influence of pH on HAP-HRG interaction was examined as a possible factor contributing to AMD development. Neither slightly alkaline (pH 8.0) nor acidic (pH 6.5) environment had any influence on the interaction when compared to binding at a physiological pH 7.5. The obtained results did not prove whether HRG is initiating deposit formation by accumulating on HAP spherules. It seemed that next, it should be examined whether combined elevated zinc levels and pH changes would alter the binding between HRG and HAP. Those conditions would be a more representative model for AMD onset. At pH 6.0, high zinc levels had no influence on

binding, however at alkaline pH 8.0, zinc increased the binding affinity of HRG to HAP. The natural pH of the eye is 7.11±1.5 (Thai-Lim et al., 2014), however, it becomes more alkaline during aging, especially in females (Coles and Jaros, 1984). It is then possible, that in the aging eye, where pH is increased and in the presence of zinc, the formation of HAP coated deposits is favoured.

As mentioned before, polymorphisms in the gene coding for FH are risk factors for AMD development. Additionally, FH has been identified in sub-retinal deposits as one of the proteins coating HAP spherules (Fig. 5.1). Already knowing that HRG binds to HAP, it is very likely that HAP spherules would bind plasma proteins, including HRG, then FH and other proteins can bind on top, building up deposits. Alternatively HAP spherules could be initially coated with FH, with HRG binding on to. This is of course a very simplified picture, compared to many proteins present in the eye in vivo. It is however possible that protein locally produced, and therefore abundant in the eye can initiate deposit formation (Mandal and Ayyagari, 2006). The results showed that FH can bind to HAP even when beads were pre-coated with HRG. In contrast, when beads were pre-coated with FH, the binding of HRG to HAP was restricted, meaning there was less space for HRG binding.

Current results, together with previous research, supports the idea that together, FH-HRG binding, the interaction between HRG, complement proteins, and HAP are essential for drusen formation, which occurs when zinc levels and pH are elevated. Additionally, results presented in this chapter show for the first time that interaction between HAP and proteins present in the eye during AMD, is zinc and pH dependent.

It is possible that not only HRG and FH, but also other proteins involved in inflammatory reaction can bind to the surface of drusen and contribute to sub-RPE deposit formation. Those would include amyloid beta and vitronectin (Thompson et al., 2015). This study investigated only the influence of Zn^{2+} and pH on HAP binding properties of HRG and FH. To get more detailed insight into factors controlling the formation of sub-RPE deposits prior to the development of AMD and possibly other diseases with significant tissue calcification, HAP binding properties of other complement factors, including C3 and C1q should be investigated. It is also known that zinc is not the only metal present in sub-RPE. Iron accumulation has been demonstrated in the eyes affected with AMD and therefore its influence on HAP binding should also be examined (Hahn, 2013).

4.4.3. Attempts to structurally characterise HRG

HRG can interact with numerous ligands, including: haem, plasminogen (Lijnen et al., 1980), heparanases (Poon et al., 2010b), fibrinogen (Leung et al., 1983), heparin (Kassaar et al, 2015) and also components of the immune system including the complement proteins within both the classical and alternative pathways, antibodies, Fc receptors on immunoglobulins and membrane attack complex components. HRG also modulates formation and function of immune complexes. The interactions of HRG with its ligands occur mainly through the N- and C-terminal domains. Of particular interest was the N1 and N2 domains, which together are thought to participate in complement protein and heparin binding.

Previously, our research group successfully solved the structure of the N2 domain of rabbit HRG (Kassaar, 2014). However, the structure of the N1 and N2 domains together, or indeed the whole protein, remains unknown. Crystallisation was attempted using two approaches. Firstly, we attempted to crystallise the whole protein purified from plasma. Secondly, we aimed to crystallise the recombinant HRG N1/N2 fragment; and also N1/N2 fragment with the addition of 200 μM, low molecular weight heparin (1.8 kDa).

Despite trying variety of concentrations of protein in combination with commercial and in-house crystallisation screens, only two sets of crystals were formed, both from rabbit HRG protein. Unfortunately they were unable to diffract effectively. Many parameters influence crystal creation, including protein purity, homogeneity and concentration. To maximise the chances of gaining crystals, only the protein of the highest obtained purity was used to set up the trials. For the crystallisation trials, a vapour diffusion method was used in which protein is put in the vapour-liquid equilibrium with precipitant and therefore concentrated over time to the point when crystals are being formed The use of Art Robbins Gryphon crystallisation robot, allows high throughput crystallization screening. For each crystal screen used, 96-different conditions were set up.

Chapter 5. Conclusion

Collectively, the aim of this thesis was to examine the complex roles of zinc in many aspects of immune response. The role of zinc in adaptive immunity was shown by the influence of zinc on DC function as antigen presenting cells, and by observed changes in zinc homeostasis during DCs maturation. In innate immunity zinc influences both alternative and classical complement pathways and can contribute to the formation and clearance of immune complexes. Also characterisation of the HAP-associated binding properties of HRG give clues as to how this protein contribute to calcified deposit formation in the inflammatory diseases associated with tissue calcification.

The importance of zinc for cellular immunity is well described; however, the exact mechanisms by which zinc acts are still not clear. Here we show that LPS-mediated stimulation of TLR4 influences zinc homeostasis in DCs, the key antigen presenting cells (Fig. 5.1).

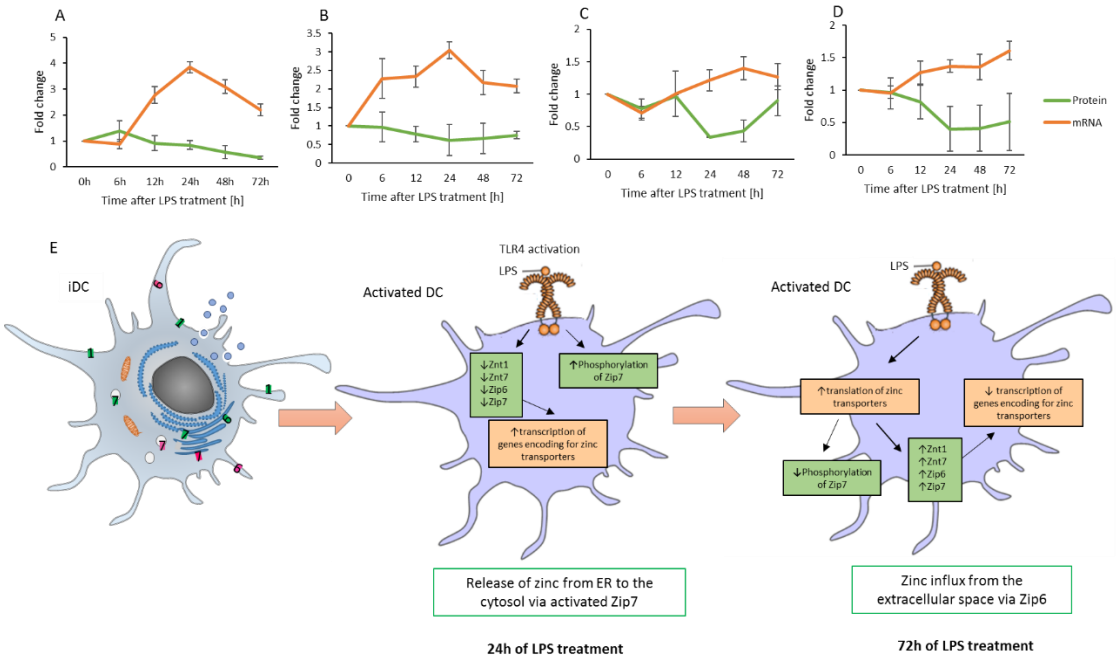

Figure 5.1. Zinc homeostasis in moDC upon LPS stimulation. NIR Western blot analysis of zinc transporters ZnT1 (A), ZnT7 (B), Zip6 (C) and Zip7 (D) and real-time PCR of the relative amounts of mRNA transcripts encoding for those transporters. DCs were treated with LPS for up to 72h. NIR WB results were normalised to the amount of β-actin and qPCR results were normalised to the amount of two housekeeping genes, β-actin and RPLP0. Results (A-D) are presented as a fold

change of the untreated control (0h). Results are the mean ± S.D. based upon three (NIR WB) or six (qPCR) independent experiments. Upon 24h of LPS treatment the expression of all examined zinc transporters (ZnT1, ZnT7, Zip6 and Zip7) decreased, followed by the increase in relative amounts of mRNA transcripts encoding for those transporters (E). After 72h of LPS treatment the relative amounts of zinc transporters increased, followed by the decrease in the relative amounts of mRNA transcripts.

The results presented here have firstly confirmed that our monocyte-derived DCs exhibit a characteristic morphological appearance, which helps to validate our cell model. Microscopy imaging in both bright field and using fluorescence antibodies revealed an abundance of cytoplasmic projections upon LPS-induced maturation, which are characteristic for DCs. Furthermore, the presented results demonstrated the importance of zinc transporters in maintaining intracellular zinc level during DC maturation. It was shown by qPCR that the levels of mRNA transcript encoding for ZnT1, ZnT7, Zip6 and Zip7 were altered upon LPS-induced maturation of DCs. These alterations were also reflected in the expression of zinc transporter proteins, by western blotting (WB) and immunofluorescence (IF) which revealed a decrease in the expression of all examined zinc transporters after 24 h of LPS-induced maturation. It was also shown that the Zip7 transporter, which is located on ER, was gradually activated during DCs maturation. The phosphorylation of this transporter was measured using flow cytometry, WB and visualised with IF. The microscopy results have also revealed that only minor fluctuations in intracellular zinc levels occur during DCs maturation. The zinc levels were assessed using flow cytometry with zinc-specific membrane permeable fluorophore, ZnAF-2F DA.

The data have therefore demonstrated that TLR4 signalling upon LPS binding, alters the expression of zinc transporters, most likely to maintain a stable concentration of intracellular free zinc. This indicates the importance of zinc at every level of DCs maturation, beginning with antigen recognition, through antigen processing and cell migration to the lymphatic organs to finally, antigen presentation to T-cells. This helps build a fuller picture of zinc homeostasis and its importance for the initiation of immune response.

Here we also presented a global picture of proteomic changes that occur in maturing DCs. Due to the novel method used (SWATH proteomics), changes are described for the first time in a fully quantitative manner. The results showed 3-7 fold increases in the expression of histocompatibility complex proteins (MHC I), involved in the antigen presentation, along with

other upregulated proteins involved in either response to cytokines or cell remodelling. Most of the identified proteins however, were downregulated upon LPS induced maturation. Those were mostly proteins involved in carbon metabolism, but also ribosomal and ER proteins responsible for protein translation and post-translational modifications. Among the downregulated proteins were also members of antigen presentation pathways, including MHC II.

The presented proteomic data suggest that during the maturation process, DCs likely respond to self-secreted interferon, which is shown by the 30 to 40-fold increase in the IFN induced proteins upon maturation. It is therefore possible that DCs generate a self-enhancement (or positive-feedback) loop, which mostly results in the expression of MHC I. Secondly, the results suggest that many cellular processes are slowed during cell maturation. It is however also possible that the global decrease in protein expression observed is simply a consequence of the downregulation of translational machinery. Finally, the results presented reveal that MHC I plays a key role in LPS-mediated antigen presentation. This is a little surprising as it is widely acknowledged to be a role for MHC II. It should be highlighted that further study including further time points is required to be sure that other important changes are overlooked. Therefore LPS may indeed be presented via MHC II in the early stage of maturation and later (around 24 h), MHC I takes over the antigen presenting role and presents proteins that were stored for several hours in cytoplasmic aggregates. This potential insight into antigen presentation alters the current understanding of the mechanisms mediating this immune response.

In addition, presented study for the first time uses HAP to induce DC maturation and provides quantitative analysis of subsequent proteomic changes. In a similar manner to LPS-induced maturation, most of the identified proteins were downregulated upon HAP-induced maturation. The majority of these are key metabolic enzymes and proteins forming part of the translation machinery. This observation brings important insight into the pathology of inflammatory diseases associated with tissue calcification, such as age-related macular degeneration, atherosclerosis and Alzheimer's disease and into the mechanisms of bone graft rejection. To further understand the proteomic changes that occur during DCs maturation, future work should examine the changes in early stages of maturation. In addition, it would be beneficial to identify proteome profiles related to the functionally different dendritic cell phenotypes, which could then serve as diagnostic tool in interpretation of clinical proteomic data.

The importance of zinc was also shown in innate immunity through its role in regulating the interaction of complement proteins with HRG. The results revealed that in the presence of physiological concentrations of zinc the affinity of full length HRG to complement proteins C1q, FH and C3 is decreased, with the greatest effect observed for FH and C3 where the binding affinity decreased 2-fold. When a similar study was carried out using a recombinant protein constituting only the N1/N2-domain of HRG, the presence of zinc had no effect on binding between N1/N2-domain and FH or C1q. However, the affinity of HRG N1/N2-domain towards C3 was increased almost 7-fold by the presence of zinc. These results suggest for the first time that binding of complement proteins to HRG is not solely dependent on the N-terminus, as it was previously thought. Other protein domains are likely contribute to the binding. It appears zinc can influence immune responses by affecting both alternative and classical complement pathways. However, the current investigation was limited to only three complement proteins (C1q, C3 and FH). Considerably more work should be done to determine the influence of zinc on the complement system as a whole in vivo.

The effect of zinc in modulating interactions between the N1/N2 domain and heparin was also assessed. However, no difference in the binding affinity of the HRG N1/N2 domain towards unfractionated heparin was identified in the presence and absence of physiological zinc concentrations. It had been previously suggested that the heparin binding via the N1/N2 domain is Zn^{2+}-independent and that binding via the HRR region of HRG is Zn^{2+}-dependent, which is in agreement with presented results. This interaction between HRG and different heparins is believed to be important in innate immunity. For example, it is known that the heparin derivative, heparan sulfate plays a multiple roles regulating inflammatory responses.

Following establishment of a novel magnetic bead assay, it was revealed that zinc together with pH can influence HRG-hydroxyapatite interactions. Such interactions may be involved in the onset of the eye disease, AMD. Protein binding to HAP-coated spherules (that form in an age-dependent manner) have recently been implicated as playing a crucial role in the development of AMD. Here we demonstrated that HRG and the complement protein, FH (which is associated with familial forms of the disease) can bind to HAP beads. The binding of FH to HAP was still possible even when beads were pre-coated with HRG. In contrast, when beads were pre-coated with FH, the binding of HRG to HAP was restricted. The results also demonstrated that the binding of HRG to HAP beads was enhanced when the high, supraphysiological zinc concentration was present, but not influenced by the alteration of pH. Nonetheless, alkaline pH together with 1

mM zinc potentiated the binding of HRG to the HAP beads, but low pH in combination with addition of 1 mM zinc had no effect. The study was limited only to FH and HRG interaction with HAP beads and the role of zinc in this interaction. However it is known that other plasma proteins and proteins involved in inflammatory reaction as well as HRG and FH can bind to HAP spherules in vivo. To get more detailed insight into factors controlling the formation of sub-RPE deposits prior to the development of AMD and possibly other diseases with significant tissue calcification, the HAP binding properties of other complement factors including C3 and C1q should be investigated. It is also known that zinc is not the only metal present in human retina. Therefore other divalent cations previously detected in retina, such as iron and copper should be also investigated in relation to drusen formation.

The last very ambitious aim of this study was to structurally characterise HRG. Current structural information relating this protein had mostly come from sequence analysis and spectroscopic studies. The only published X-ray crystal structure is available for the N2 domain of rabbit HRG, which shares great homology with human N2 domain. Crystallisation was attempted using two approaches. Firstly, we attempted to crystallise the whole protein purified from rabbit and human plasma. Unfortunately, despite multiple crystal growth conditions being tested, including attempts with a variety of concentrations of protein in combination with commercial and in-house crystallisation screens, only two sets of crystals were formed, both with plasma-purified rabbit HRG protein. Unfortunately however, these crystals were unable to diffract effectively to yield a 3-D structure.

One of the many parameters influencing crystal formation is protein purity and homogeneity. Our group have previously crystallised native N2 domain, therefore it was suspected that the problem laid within PRR and HRR domains, which have a high probability of being disordered and thus not amenable for production of crystals that would diffract to high resolution. The second approach was to crystallise a recombinant form of HRG constituting on the N1/N2 domains and thus omitting PRR and HRR domains. Crystals were set up with and without the addition of low molecular weight heparin (1.8 kDa). This would bring an answer on how exactly HRG and heparins interact. So far it is only known that HRG can bind heparins via N-terminus and HRR domains. These attempts unfortunately failed to yield any crystals. The recombinant protein used for crystallisation trials was purified using denaturing and subsequent refolding method following expression in *E. coli*. This might have led to heterogeneity of the resultant protein and therefore hindered crystal formation. Future attempts should focus on establishing

a better recombinant system for the expression of soluble recombinant full length and truncated HRG. There are also other alternative strategies for structural characterisation of the molecules. One of them, cryo-electron microscopy (cryo-EM), is a form of transmission electron microscopy where the sample is studied at cryogenic temperatures. This method in contrast to crystallography, allows the observation of protein structure without forced crystal formation and therefore in its native state. Another method that could be used is a multi-dimensional nuclear magnetic resonance spectroscopy (3D-NMR). This method is used to assign specific resonance signals to specific atoms in an isotopically enriched protein. Nevertheless, structural characterisation of HRG using 3D-NMR may be difficult as there are many histidine residues present and these would be very difficult to individually assign to signals in the resultant spectra hindering solution of the structure.

References

AL-ALWAN M.M., ROWDEN G., LEE T.D., WEST K.A. (2001) Fascin is involved in the antigen presentation activity of mature dendritic cells. *J Immunol*, 166:338–345.

ALCHI B., JAYNE D. (2010) Membranoproliferative glomerulonephritis. *Pediatr Nephrol,* 25:1409.

ALGVERE P.V., KVANTA A., SEREGARD S. (2016) Drusen maculopathy: a risk factor for visual deterioration. *Acta Ophthalmol*, 94: 427–433.

ALLEN J.I., PERRI R.T., MCCLAIN C.J., KAY N.E. (1983) Alterations in human natural killer cell activity and monocyte cytotoxicity induced by zinc deficiency. *J Lab Clin Med,* 102**:**577-89.

ALLOATTI A., KOTSIAS F., GAMELAS MAGALHAES J., AMIGORENA S. (2016) Dendritic cell maturation and cross-presentation: timing matters! *Immunol Rev*, 272:97-108.

AMULIC B., CAZALET C., HAYES G.L., METZLER K.D., ZYCHLINSKY A. (2012) Neutrophil function: from mechanisms to disease. *Annu Rev Immunol*, 30:459-489.

ANDERSON D.H., MULLINS R.F., HAGEMAN G.S. JOHNSON L.V. (2002) A role for local inflammation in the formation of drusen in the aging eye. *Am J Ophthalmol,* 134:411–431.

ANDONOVA, M., BORISSOV, I. & SOTIROV, L. (2001) Changes in some factors of the innate immunity and serum zinc and iron concentrations in pigs following intravenous administration of Escherichia coli lipopolysaccharide. *Onderstepoort J Vet Res,* 68**:**91-9.

ANDRE F., CHAPUT N., SCHARTZ N.E., FLAMENT C., et al. (2004) Exosomes as potent cell-free peptide-based vaccine. Dendritic cell-derived exosomes transfer functional MHC class I/peptide complexes to dendritic cells. *J Immunol*, 172:2126–2136.

ARDELJAN D., CHAN C.C. (2013) Aging is not a disease: distinguishing age-related macular degeneration from aging. *Prog Retin Eye Res,* 37:68-89.

ANDERSON D.H., RADEKE M.J., GALLO N.B., CHAPIN E.A., JOHNSON P.T., et al. (2010) The pivotal role of the complement system in aging and age-related macular degeneration: hypothesis re-visited*. Prog Retin Eye Res*, 29:95–112.

ANGENIEUX C., FRICKER D., STRUB J.M., LUCHE S., et al. (2001) Gene induction during differentiation of human monocytes into dendritic cells: an integrated study at the RNA and protein levels. *Funct Integr Genomics*, 1:323–329.

ANTONIOU A.N., POWIS S.J., ELLIOTT T. (2003) Assembly and export of MHC class I peptide ligands. *Curr Opin Immunol*, 15:75–81.

APCHER S., MANOURY B., FAHRAEUS R. (2012) The role of mRNA translation in direct MHC class I antigen presentation. *Curr Opin Immunol*, 24:71–76.

APCHER S., MILLOT G., DASKALOGIANNI C., SCHERL A., MANOURY B., FAHRAEUS R. (2013) Translation of pre-spliced RNAs in the nuclear compartment generates peptides for the MHC class I pathway. *Proc Natl Acad Sci USA*, 110:17951–17956.

ASGARI, E., ZHOU, W. & SACKS, S. (2010) Complement in organ transplantation. *Curr Opin Organ Transplant,* 15**:**486-91.

AYDEMIR T.B., LIUZZI J.P., MCCLELLAN S., ROBERT J. COUSINS R.J. (2009) Zinc transporter ZIP8 (SLC39A8) and zinc influence IFN-γ expression in activated human T cells. *J Leukoc Biol,* 86:337–348.

BACH J.F., DARDENNE M. (1989) Thymulin, a zinc dependent hormone. *Med Oncol Tumor Pharmacother*, 6(1):25-9.

BANCHEREAU J., BRIERE F., CAUX C., DAVOUST J., et al. (2000) Immunobiology of dendritic cells. *Annu Rev Immunol*, 18:767–811.

BAO B., PRASAD A.S., BECK F.W., BAO G.W., SINGH T., ALI S., SARKAR F.H. (2011) Intracellular free zinc up-regulates IFN-gamma and T-beta essential for Th1 differentiation in Con-A stimulated HUT-78 cells. *Biochem Biophys Res Commun*, 407:703-707.

BELL S.G., VALLEE B.L. (2009) The metallothionein/thionein system: an oxidoreductive metabolic zinc link. *Chembiochem*, 10:55–62.

BERG J.M, TYMOCZKO J.L., STRYER L. (2012) *Biochemistry.* 7th ed. Basingstoke : W.H. Freeman.

BLEWETT H.J., TAYLOR C.G. (2012) Dietary zinc deficiency in rodents: effects on T-cell development, maturation and phenotypes. *Nutrients*, 4:449–466.

BLOM A.M., KASK L., RAMESH B., HILLARP A. (2003) Effects of zinc on factor I cofactor activity of C4b-binding protein and factor H. *Arch Biochem Biophys,* 418**:**108-18.

BLUM J.S., WEARSCH P.A., CRESSWELL P. (2013) Pathways of antigen processing. *Annu Rev Immunol*, 31:443–473.

BOGUNOVIC D., BYUN M., DURFEE L.A., ABHYANKAR A., SANAL O. ET AL. (2012) Mycobacterial disease and impaired IFN-gamma immunity in humans with inherited ISG15 deficiency. *Science,* 337:1684-1688.

BONAVENTURA P., BENEDETTI G., ALBARÈDE B., MIOSSEC P. (2015) Zinc and its role in immunity and inflammation. *Autoimmun Rev*, 14:277–285.

BANGE F.-C., FLOHR T., BUWITT U., BOETTGER E.C. (1992) An interferon-induced protein with release factor activity is a tryptophanyl-tRNA synthetase. *FEBS Lett*, 300:162-166.

BORZA D.B., TATUM F.M., MORGAN W.T. (1996) Domain structure and conformation of histidine-proline-rich glycoprotein. *Biochemistry*, 35:1925-1934.

BORZA D.B., MORGAN W.T. (1998) Histidine-proline-rich glycoprotein as a plasma pH sensor. Modulation of its interaction with glycosaminoglycans by pH and metals. *J Biol Chem,* 273:5493-9.

BOURGUIGNON L.Y., XIA W., WONG G. (2009) Hyaluronan-mediated CD44 interaction with p300 and SIRT1 regulates beta-catenin signaling and NFkappaB-specific transcription activity leading to MDR1 and Bcl-xL gene expression and chemoresistance in breast tumor cells. *J Biol Chem*, 284:2657-2671.

BRANDSTATTER H., SCHULZ P., POLUNIC I., KANNICHT C., KOHLA G., ROMISCH J. (2012) Purification and biochemical characterization of functional complement factor H from human plasma fractions. *Vox Sang,* 103**:**201-12.

BRIEGER A., RINK L., HAASE H. (2013) Differential Regulation of TLR-Dependent MyD88 and TRIF Signaling Pathways by Free Zinc Ions. *J Immunol,* 191:1808-1817.

BUBECK D. (2014) The making of a macromolecular machine: assembly of the membrane attack complex. *Biochemistry,* 53:1908–15.

BUSCHE M.N., STAHL G.L. (2010) Role of the complement components C5 and C3a in a mouse model of myocardial ischemia and reperfusion injury. *Ger Med Sci,* 8.

CAI L., HOLOWECKYJ N., SCHALLER M.D., BEAR J.E. (2005) Phosphorylation of coronin 1B by protein kinase C regulates interaction with Arp2/3 and cell motility. *J Biol Chem,* 280:31913–23.

CAI L., MAKHOV A.M., SCHAFER D.A., BEAR J.E. (2008) Coronin 1B antagonizes cortactin and remodels Arp2/3-containing actin branches in lamellipodia. *Cell,* 134:828-842.

CARON E., ESPONA L., KOWALEWSKI D.J., et al. (2015) An open-source computational and data resource to analyze digital maps of immunopeptidomes. *Elife*, 8;4.

CARPENE E., ANDREANI G., ISANI G. (2007) Metallothionein functions and structural characteristics. *J Trace Elem Med Biol*, 21: 35–39.

CEPPI M., CLAVARINO G., GATTI E., SCHMIDT E.K., DE GASSART A., et al. (2009) Ribosomal protein mRNAs are translationally-regulated during human dendritic cells activation by LPS. *Immunome Res*, 27:5-5.

CHANG N.S., LEU R.W., RUMMAGE J.A., ANDERSON J.K., MOLE J.E. (1992) Regulation of Complement Functional Efficiency by Histidine-Rich Glycoprotein. *Blood,* 79**:**2973-2980.

CHANG R.Y., ETHERIDGE N., NOUWENS A.S., DODD P.R. (2015) SWATH analysis of the synaptic proteome in Alzheimer's disease. *Neurochem Int*, 87:1-12.

CHATURVEDI A., PIERCE S.K. (2009) How location governs Toll like receptor signalling. *Traffic*, 10(6): 621–628.

CHAVAKIS T., MAY A.E., PREISSNER K.T., KANSE S.M. (1999) Molecular mechanisms of zincdependent leukocyte adhesion involving the urokinase receptor and beta2-integrins. *Blood*, 93:2976–83.

CHEN M., FORRESTER J.V., XU H. (2007) Synthesis of complement factor H by retinal pigment epithelial cells is down-regulated by oxidized photoreceptor outer segments. *Exp Eye Res*, 84:635–645.

CHEN M., MUCKERSIE E., ROBERTSON M., FORRESTER J.V., XU H. (2008) Up-regulation of complement factor B in retinal pigment epithelial cells is accompanied by complement activation in the aged retina. *Exp Eye Res*, 87:543–550.

CHEN P., ABACHERLI L.E., NADLER S.T. (2009) MMP7 shedding of syndecan-1 facilitates re-epithelialization by affecting α2β1 integrin activation. *PLoS One*, 4: 6565.

CHEN M., MUCKERSIE E., FORRESTER J.V., XU H. (2010) Immune activation in retinal aging: a gene expression study*. Invest Ophthalmol Vis Sci*, 51:5888–5896.

CHEN L., YANG S., JAKONCIC J., ZHANG J.J., HUANG X.Y. (2010b) Migrastatin analogues target fascin to block tumour metastasis. *Nature,* 464:1062-1066.

CIPRIANI V., LEUNG H.T, PLAGNOL V., BUNCE C., KHAN J.C., et al. (2012) Genome-wide association study of age-related macular degeneration identifies associated variants in the TNXB-FKBPL–NOTCH4 region of chromosome 6p21.3. *Hum Mol Genet*, 21:4138–4150.

CLARK A., WEYMANN A., HARTMAN E., TURMELLE Y., CARROLL M., THURMAN J.M. (2008) Evidence for non-traditional activation of complement factor C3 during murine liver regeneration. *Mol Immunol,* 45:3125–32.

COLES W.H., JAROS P.A. (1984) Dynamics of ocular surface pH. *Brit J Ophthalmol*, 68:549-552.

COLLARD C.D., MONTALTO M.C., REENSTRA W.R., BURAS J.A., STAHL G.L. (2001) Endothelial oxidative stress activates the lectin complement pathway: role of cytokeratin 1. *Am J Pathol,* 159**:**1045-1054.

COUSINS, R. J., LIUZZI, J. P. & LICHTEN, L. A. (2006) Mammalian zinc transport, trafficking, and signals. *J Biol Chem,* 281**:**24085-9.

COUSINS R.J. (2010) Gastrointestinal factors influencing zinc absorption and homeostasis. *Int J Vitam Nutr Res*, 80:243–248.

CRAMPTON S.P., VOYNOVA E., BOLLAND S. (2010) Innate pathways to B-cell activation and tolerance. *Ann N Y Acad Sci*, 1183:58–68.

CURCIO C.A., OWSLEY C., JACKSON G.R. (2000) Spare the rods, save the cones in aging and age-related maculopathy. *Invest Ophthalmol Vis Sci*, 41:2015–8.

DARDENNE, M., PLEAU, J. M., NABARRA, B., LEFRANCIER, P., DERRIEN, M., et al. (1982) Contribution of zinc and other metals to the biological activity of the serum thymic factor. *Proc Natl Acad Sci U.S.A.,* 79**:**5370-3.

DARINGER N.M., SCHWARZ K.A., LEONARD J.N. (2015) Contributions of Unique Intracellular Domains to Switchlike Biosensing by Toll-like Receptor 4. *J Biol Chem*, 290(14): 8764–8777.

DAVIES M.D., GANGON R.E., LEE L.Y. (2005) The Age-Related Eye Disease Study severity scale for age-related macular degener-Dry AMD Mechanisms, Targets, and Imaging. *Arch Ophthalmol,* 54:1484–1498.

DELAMARRE L., HOLCOMBE H., MELLMAN I. (2003) Presentation of exogenous antigens on major histocompatibility complex (MHC) class I and MHC class II molecules is differentially regulated during dendritic cell maturation. *J Exp Med.,* 198(1):111-22.

DEVINE L., SUN J., BARR M., KAVATHAS P. (1999) Orientation of the Ig domains of CD8 alpha beta relative to MHC class I. *J Immunol*, 162: 846–51.

DIXELIUS J., OLSSON A.K., THULIN A., LEE C., JOHANSSON I., CLAESSON-WELSH L. (2006) Minimal active domain and mechanism of action of the angiogenesis inhibitor histidine-rich glycoprotein. *Cancer Res,* 66**:**2089-97.

DMITRIEV A.V., MANGEL S.C. (2001) Circadian clock regulation of pH in the rabbit retina. *J Neurosci*, 21:2897-902.

DORE-DUFFY P, PETERSON M, CATALANOTTO F, MARLOW S, HO SY, OSTROM M, et al. (1990) Zinc profiles in rheumatoid arthritis. *Clin Exp Rheumatol*, 8:541–546.

DOWLING J.K., MANSELL A. (2016) Toll-like receptors: the swiss army knife of immunity and vaccine development. *Clin Transl Immunol*, 5:85.

DOWLING J.K., DELLACASAGRANDE J. (2016) Toll-like receptors: ligands, cell-based models and readouts for receptor action. *Methods Mol Biol,* 1390:3–27.

DOWNING P.R., KELLER J.C., BOACKLE R.J. (1989) Interaction of dental cements with the complement system. *Dent Mater,* 5**:**83-9.

DRASIN, T. & SAHUD, M. (1996) Blood-type and age affect human plasma levels of histidine-rich glycoprotein in a large population. *Thromb Res,* 84**:**179-88.

DUBBEN S., HÖNSCHEID A., WINKLER K., RINK L., HAASE H. (2010) Cellular zinc homeostasis is a regulator in monocyte differentiation of HL-60 cells by 1 alpha,25-dihydroxyvitamin D3. *J Leuko Biol,* 87:833-844.

DUTHIE M.S., WINDISH H.P., FOX C.B., REED S.G. (2011) Use of defined TLR ligands as adjuvants within human vaccines. *Immunol Rev*, 239:178–196

EASTERBROOKSMITH, S. B., VANDENBERG, R. J. & ALDEN, J. R. (1988) The Role of Fc-Fc Interactions in Insoluble Immune-Complex Formation and Complement Activation. *Mol Immunol,* 25**:**1331-1337.

EDWARDS A.O. (2008) Genetics of age-related macular degeneration. *Adv Exp Med Biol*, 613:211–219.

EIDE D.J. (2004) The SLC39 family of metal ion transporters. *Pflugers Arch,* 447**:**796-800.

ELWARD K., GRIFFITHS M., MIZUNO M., HARRIS C.L., NEAL J.W., MORGAN B.P., GASQUE P.(2005) CD46 plays a key role in tailoring innate immune recognition of apoptotic and necrotic cells. *J Biol Chem*, 280:36342-54.

ENG B.H., GUERINOT M.L., EIDE D., SAIER M.H. (1998) Sequence analyses and phylogenetic characterization of the ZIP family of metal ion transport proteins. *J Membr Biol*, 166:1–7.

FAKHOURI F., DE JORGE E.G., BRUNE F., AZAM P., COOK H.T., PICKERING M.C. (2010) Treatment with human complement factor H rapidly reverses renal complement deposition in factor H-deficient mice. *Kidney Int,* 78**:**279-86.

FEENEY-BURNS L., ELLERSIECK M.R. (1985) Age-related changes in the ultrastructure of Bruch's membrane. *Am J Ophthalmol*, 100:686–97.

FERREIRA G.B., OVERBERGH L., VAN ETTEN E., LAGE K., et al. (2008) Protein-induced changes during the maturation process of human dendritic cells: 2-D DIGE approach. *Proteomics Clin Appl*, 2:1349–1360.

FERREIRA V.P., HERBERT A.P., CORTÉS C., MCKEE K.A., BLAUM B.S., et al. (2009) The binding of factor H to a complex of physiological polyanions and C3b on cells is impaired in atypical hemolytic uremic syndrome. *J Immunol,* 1950:7009–7018.

FERREIRA G.B., MATHIEU C., OVERBERGH L. (2010) Understanding dendritic cell biology and its role in immunological disorders through proteomic profiling. *Proteomics Clin Appl*, 4:190-203.

FERRER M., CHERNIKOVA T.N., YAKIMOV M.M., GOLYSHIN P.N., TIMMIS K.N. (2003) Chaperonins govern growth of Escherichia coli at low temperatures. *Nat Biotechnol,* 21:1266-7.

FETT A.L., HERMANN M.M., MUETHER P.S., KIRCHHOF B., FAUSER S. (2012) Immunohistochemical localization of complement regulatory proteins in the human retina. *Histol Histopathol,* 27:357–364.

FINNEY L.A., O'HALLORAN T.V. (2003) Transition metal speciation in the cell: insights from the chemistry of metal ion receptors. *Science,* 300:931–936.

FISHELSON Z., HORSTMANN R.D., MÜLLER-EBERHARD H.J. (1987) Regulation of the alternative pathway of complement by pH. *J Immunol,* 138:3392-3395.

FITZGERALD K.A., ROWE D.C., BARNES B.J., CAFFREY D.R., VISINTIN A., et al. (2003) LPS-TLR4 signaling to IRF-3/7 and NF-kappaB involves the toll adapters TRAM and TRIF. *J Exp Med*, 198:1043–1055.

FORRESTER J.V., XU H., LAMBE T., CORNALL R. (2008) Immune privilege or privileged immunity? *Mucosal Immunol*, 1:372–381.

FORRESTER J.V., XU H., KUFFOVA L., DICK A.D., MCMENAMIN P.G. (2010) Dendritic cell physiology and function in the eye. *Immunol Rev*, 234:282–304.

FORRESTER J.V., XU H. (2012) Good news-bad news: the yin and yang of immune privilege in the eye. *Front Immunol,* 3:338.

FOSTER M., SAMMAN S. (2012) Zinc and Regulation of Inflammatory Cytokines: Implications for Cardiometabolic Disease. *Nutrients*, 4:676–694.

FU C.L., HORN M.K. (2002) Histidine-rich glycoprotein plus zinc to neutralize heparin. *J Lab Clin Med*, 139:211-217.

GABORIAUD C., THIELENS N.M., GREGORY L.A., ROSSI V., FONTECILLA-CAMPS J.C., ARLAUD G.J. (2004) Structure and activation of the C1 complex of complement: unraveling the puzzle. *Trends Immunol,* 25:368–73.

GABORIAUD C., LING W.L., THIELENS N.M., BALLY I., ROSSI V. (2014) Deciphering the fine details of c1 assembly and activation mechanisms: "mission impossible"? *Front Immunol*, 5:565.

GAITHER L.A., EIDE D.J. (2000) Functional expression of the human hZIP2 zinc transporter. *Journal of Biological Chemistry*, 275:5560–5564.

GAY N.J., GANGLOFF M. (2007) Structure and function of Toll receptors and their ligands. *Annu Rev Biochem,* 76:141–165.

GEISSE S., GRAM H., KLEUSER B., KOCHER H.P. (1996) Eukaryotic expression systems: A comparison. *Protein Expr Purif,* 8:271–82.

GHAI R., WATERS P., ROUMENINA L.T., GADJEVA M., KOJOUHAROVA M.S., et al. (2007) C1q and its growing family. *Immunobiology,* 212:253–66.

GILLET L.C., NAVARRO P., TATE S., RÖST H., SELEVSEK N., et al. (2012) Targeted data extraction of the MS/MS spectra generated by data-independent acquisition: a new concept for consistent and accurate proteome analysis. *Mol Cell Proteomics*, 11:O111-016717.

GORGANI N.N., PARISH C.R., EASTERBROOK SMITH S.B., ALTIN J.G. (1997a) Histidine-rich glycoprotein binds to human IgG and C1q and inhibits the formation of insoluble immune complexes. *Biochemistry,* 36**:**6653-62.

GORGANI N.N., PARISH C.R., SMITH S.B.E., ALTIN J.G. (1997b) Histidine-rich glycoprotein binds to human IgG and C1q and inhibits the formation of insoluble immune complexes. *Biochemistry,* 36**:**6653-6662.

GORGANI N.N., ALTIN J.G., PARISH C.R. (1999a) Histidine-rich glycoprotein regulates the binding of monomeric IgG and immune complexes to monocytes. *Int Immunol*, 11:1275-1282.

GORGANI N.N., PARISH C.R., ALTIN J.G. (1999b) Differential binding of histidine-rich glycoprotein (HRG) to human IgG subclasses and IgG molecules containing kappa and lambda light chains. *J Biol Chem,* 274**:**29633-40.

GORGANI N.N., SMITH B.A., KONO D.H., THEOFILOPOULOS A.N. (2002) Histidine-rich glycoprotein binds to DNA and Fc gamma RI and potentiates the ingestion of apoptotic cells by macrophages. *J Immunol,* 169**:**4745-51.

GORODETSKY R., MOU X., BLANKENFELD A., MARX G. (1993) Platelet multielemental composition, lability, and subcellular localization. *Am J Hematol,* 42**:**278-83.

GRANDJEAN-LAQUERRIÈRE A., et al. (2007) Involvement of toll-like receptor 4 in the inflammatory reaction induced by hydroxyapatite particles. *Biomaterials,* 28:400–4.

GRANUCCI F., FERRERO E., FOTI M., AGGUJARO D., VETTORETTO K., RICCIARDI-CASTAGNOLI P. (1999) Early events in dendritic cell maturation induced by LPS. *Microbes Infect*, 1:1079–1084.

GREEN N.M., MARSHAK-ROTHSTEIN A. (2011) Toll-like receptor driven B cell activation in the induction of systemic autoimmunity. *Semin Immunol* 23:106–112.

GREEN N.M., MOODY K.S., DEBATIS M., MARSHAK-ROTHSTEIN A. (2012) Activation of autoreactive B cells by endogenous TLR7 and TLR3 RNA ligands. J Biol Chem, 287:39789-99.

GREGERSON D.S., YANG J. (2003) CD45-positive cells of the retina and their responsiveness to in Vivo and in Vitro treatment with IFN-gamma or anti–CD40. *Invest Ophthalmol Vis Sci,* 44:3083–3093.

GRIFFIN J.P., CHU R., HARDING C.V. (1997) Early endosomes and a late endocytic compartment generate different peptide-class II MHC complexes via distinct processing mechanisms. *J Immunol,* 158**:**1523-1532.

GRUBER K., MAYWALD M., ROSENKRANZ E., HAASE H., PLUMAKERS B., RINK L. (2013) Zinc deficiency adversely influences interleukin-4 and interleukin-6 signaling. *J Biol Regul Homeost Agents*, 27:661–71.

GUERRIER T., POCHARD P., LAHIRI A., YOUINOU P., PERS J.O., et al. (2014) TLR9 expressed on plasma membrane acts as a negative regulator of human B cell response. *J Autoimmun*, 51:23–29

GUNDACKER N.C., HAUDEK V.J., WIMMER H., SLANY A., GRISS J., et al. (2009) Cytoplasmic proteome and secretome profiles of differently stimulated human dendritic cells. *J Proteome Res*, 8:2799-811.

GUNZEL D., ZIMMERMANN F., DURRY S., SCHLUE W.R. (2001) Apparent intracellular Mg2 + buffering in neurons of the leech Hirudo medicinalis. *Biophys J*, 80:1298–1310.

HAASE H., MARET W. (2005) Protein tyrosine phosphatases as targets of the combined insulinomimetic effects of zinc and oxidants. *Biometals*, 18:333–338.

HAASE H., OBER-BLOBAUM J.L., ENGELHARDT G., HEBEL S., HEIT A., et al. (2008) Zinc signals are essential for lipopolysaccharide-induced signal transduction in monocytes. *J Immunol*, 181:6491–6502.

HAASE H., RINK L. (2009) The immune system and the impact of zinc during aging. *Immun Ageing,* 6:9.

HAHN P., ACQUAH K., COUSINS S.W., LEE P.P., SLOAN F.A. (2013) Ten-year incidence of age-related macular degeneration according to diabetic retinopathy classification among medicare beneficiaries. *Retina.* 33:911-9.

HAINE J.L., HAUSER M.A., SCHMIDT S., SCOTT W.K., OLSON L.M., et al. (2005) Complement factor H variant increases the risk of age-related macular degeneration. *Science,* 308:416-421.

HAINES J.L., HAUSER M.A., SCHMIDT S. ET AL. (2005) Complement factor H variant increases the risk of age-related macular degeneration. *Science* 308:419–421.

HAMBIDGE K.M., KREBS N.F. (2007) Zinc deficiency: a special challenge. *J Nutr*, 137:1101–5.

HAMMER G.C, MA A. (2013) Molecular Control of Steady-State Dendritic Cell Maturation and Immune Homeostasis. *Annu Rev Immunol,* 31:743–91

HARBOE M., MOLLNES T.E. (2008) The alternative complement pathway revisited. *J Cell Mol Med,* 12**:**1074-1084.

HASAN R., RINK L., HAASE H. (2012) Zinc signals in neutrophil granulocytes are required for the formation of neutrophil extracellular traps. *Innate Immun*, 19:253-264.

HASAN R., RINK L., HAASE H. (2016) Chelation of free Zn Impairs chemotaxis, phagocytosis, oxidative burst, degranulation, and cytokine production by neutrophil granulocytes. *Biol Trace Elem Res*, 171:79-88.

HASEGAWA H., SUZUKI K., SUZUKI K., NAKAJI S., SUGAWARA K. (2000) Effects of zinc on the reactive oxygen species generating capacity of human neutrophils and on the serum opsonic activity in vitro. *Luminescence*, 15:321–327.

HAVERLAND N.A., FOX H., CIBOROWSKI P. (2014) Quantitative proteomics by SWATH-MS reveals altered expression of nucleic acid binding and regulatory proteins in HIV-1-infected macrophages. *J Proteome Res*, 13:2109–2119.

HAVERLAND N.A., VILLENEUVE L.M., CIBOROWSKI P., FOX H.S. (2016) The Proteomic Characterization of Plasma or Serum from HIV-Infected Patients. *Methods Mol Biol*, 1354:293-310.

HEINEN S., HARTMANN A., LAUER N., WIEHL U., DAHSE H-M., SCHIRMER S., et al. (2009) Factor H-related protein 1 (CFHR-1) inhibits complement C5 convertase activity and terminal complex formation. *Blood,* 114:2439–47.

HEYNEMAN C.A. (1996) Zinc deficiency and taste disorders. *Ann Pharmacother*, 30 :186–7.

HIRANO T., KIKUCHI K., URANO Y., NAGANO T. (2002) Improvement and Biological Applications of Fluorescent Probes for Zinc, ZnAFs. *JACS*, 124:6555.

HOEBE K., JANSSEN E. M., KIM S. O., ALEXOPOULOU L., FLAVELL R. A., HAN J., BEUTLER B. (2003) Upregulation of costimulatory molecules induced by lipopolysaccharide and double-stranded RNA occurs by Trif-dependent and Trif independent pathways. *Nat. Immunol*. 4:1223–1229.

HOFER, J., JANECKE, A. R., ZIMMERHACKL, L. B., RIEDL, M., ROSALES, A., et al. (2013) Complement factor H-related protein 1 deficiency and factor H antibodies in pediatric patients with atypical hemolytic uremic syndrome. *Clin J Am Soc Nephrol,* 8**:**407-15.

HOGSTRAND C., KILLE P., NICHOLSON R.I., TAYLOR K.M. (2009) Zinc transporters and cancer: a potential role for ZIP7 as a hub for tyrosine kinase activation. *Trends Mol Med*, 15:101–111.

HOJYO S., FUKADA T. (2016) Zinc transporters and signaling in physiology and pathogenesis. *Arch Biochem Biophys*, 1-8.

HSIANG T.Y., ZHAO C., KRUG R.M. (2009) Interferon-induced ISG15 conjugation inhibits influenza A virus gene expression and replication in human cells. *J Virol,* 83:5971-5977.

HUANG L., KIRSCHKE C.P., ZHANG Y., YAN Y.Y. (2005) The ZIP7 gene (Slc39a7) encodes a Zinc transporter involved in Zinc homeostasis of the Golgi apparatus. *J Biol Chem*, 280:15456–15463.

HUANG Y. H., SNUDERL M., JAIN R.K. (2011) Polarization of Tumor-Associated Macrophages: A Novel Strategy for Vascular Normalization and Antitumor Immunity. *Cancer Cell,* 19**:**1-2.

HUANG L., TEPAAMORNDECH S. (2013) The SLC30 family of zinc transporters - a review of current understanding of their biological and pathophysiological roles. *Mol Aspects Med* 34: 548–60.

HUGHES E.A., HAMMOND C., CRESSWELL P. (1997) Misfolded major histocompatibility complex class I heavy chains are translocated into the cytoplasm and degraded by the proteasome. *Proc. Natl Acad. Sci. USA*, 94:1896–1901.

HUGHES A.E., ORR N., ESFANDIARY H., DIAZ-TORRES M., GOODSHIP T., CHAKRAVARTHY U. (2006) A common CFH haplotype, with deletion of CFHR1 and CFHR3, is associated with lower risk of age-related macular degeneration. *Nat Genet*, 38:1173–1177.

HUJANEN E.S., SEPPA S.T., VIRTANEN K. (1995) Polymorphonuclear leukocyte chemotaxis induced by zinc, copper and nickel in vitro. *Biochim Biophys Acta*, 1245:145–52.

HULETT M.D., PARISH C.R. (2000) Murine histidine-rich glycoprotein: cloning, characterization and cellular origin. *Immunol Cell Biol,* 78**:**280-7.

IBS K.H., RINK L. (2003) Zinc-altered immune function. *J Nutr,* 133**:**1452S-6S.

IRMLER M., STEINER V., RUEGG C., WAJANT H., TSCHOPP J. (2000) Caspase-induced inactivation of the anti-apoptotic TRAF1 during Fas ligand-mediated apoptosis. *FEBS Lett*, 468:129-133.

JAGER R.D., MIELER W.F., MILLER J.W. (2008) Age-related macular degeneration. *N Engl J Med*, 358:2606–2617.

JACK D.L., KLEIN N.J., TURNER M.W. (2001) Mannose-binding lectin: targeting the microbial world for complement attack and opsonophagocytosis. *Immunol Rev,* 180**:**86-99.

JEONG J., EIDE D.J. (2013) The SLC39 family of zinc transporters. *Mol Aspects Med*, 34:612–619.

JIANG X., CHEN Z.J. (2011) The role of ubiquitylation in immune defence and pathogen evasion. *Nat Rev Immunol*, 12:35-48.

JOFFRE O.P., SEGURA E., SAVINA A., AMIGORENA S. (2012) Cross-presentation by dendritic cells. *Nature Reviews Immunology* 12:557-569.

JOHNSON L.V., LEITNER W.P., STAPLES M.K., ANDERSON D.H. (2001) Complement activation and inflammatory processes in drusen formation and age-related macular degeneration. *Exp Eye Res,* 73:887–8.

JOHNSON L.V., LEITNER W.P., RIVEST A.J., STAPLES M.K., RADEKE M.J., ANDERSON D.H. (2002) The Alzheimer's A beta-peptide is deposited at sites of complement activation in pathologic deposits associated with aging and age-related macular degeneration. *Proc Natl Acad Sci U.S.A.*, 99:11830–11835.

JONES T., KAZAMA Y., ODANI S., HINO H., KATO I. (1989) Analyses of heparin-binding domain by limited proteolysis and by monoclonal antibodies. *Thromb Haemost*, 62:473.

JONES A.L., HULETT M.D., PARISH C.R. (2004) Histidine-rich glycoprotein binds to cell-surface heparan sulfate via its N-terminal domain following $Zn2^{+}$ chelation. *J Biol Chem*, 279:30114–30122.

JONES A.L., HULETT M.D., PARISH C.R. (2005a) Histidine-rich glycoprotein: A novel adaptor protein in plasma that modulates the immune, vascular and coagu-lation systems*. Immunol Cell Biol,* 83:106-118.

JONES A.L., POON I.K., HULETT M.D., PARISH C.R. (2005c) Histidine-rich glycoprotein specifically binds to necrotic cells via its amino-terminal domain and facilitates necrotic cell phagocytosis. *J Biol Chem,* 280**:**35733-41.

KABU K., YAMASAKI S., KAMIMURA D., ITO Y., HASEGAWA A., et al. (2006) Zinc is required for Fc epsilon RI-mediated mast cell activation. *J Immunol*, 177:1296-305.

KACPRZYK, L., RYDENGARD, V., MORGELIN, M., DAVOUDI, M., PASUPULETI, M., et al. (2007) Antimicrobial activity of histidine-rich peptides is dependent on acidic conditions. *Biochim Biophys Acta,* 1768**:**2667-2680.

KAGAN J.C., SU T., HORNG T., CHOW A., AKIRA S., MEDZHITOV R. (2008) TRAM couples endocytosis of Toll-like receptor 4 to the induction of interferonbeta. *Nat Immunol* 9:361–368.

KAMATH A.T., POOLEY J., O'KEEFFE M.A., VREMEC D., ZHAN Y., et al. (2000) The development, maturation, and turnover rate of mouse spleen dendritic cell populations. *J Immunol,* 165:6762–70.

KAMBE T. (2011) An overview of a wide range of functions of ZnT and Zip Zinc transporters in the secretory pathway. *Biosci Biotechnol Biochem*, 75:1036–1043.

KAMBE T. (2013) Overview of and update on the physiological functions of Mammalian zinc transporters. *Nihon Eiseigaku Zasshi,* 68**:**92-102.

KARLSTETTER M., SCHOLZ R., RUTAR M., WONG W.T., PROVIS J.M., LANGMANN T. (2015) Retinal microglia: just bystander or target for therapy? *Prog Retin Eye Res*, 45:30–57.

KASSAAR O., MCMAHON S.A., THOMPSON R., BOTTING C.H., NAISMITH J.H., STEWART A.J. (2014) Crystal structure of histidine-rich glycoprotein N2 domain reveals redox activity at an interdomain disulfide bridge: implications for angiogenic regulation. *Blood,* 123:1948-55.

KASSAAR O., SCHWARZ-LINEK U., BLINDAUER C.A., STEWART A.J. (2015) Plasma free fatty acid levels influence Zn(2+) -dependent histidine-rich glycoprotein-heparin interactions via an allosteric switch on serum albumin. *J Thromb Haemost,* 13:101-10.

KAWAI T., AKIRA S. (2010) The role of pattern-recognition receptors in innate immunity: update on toll-like receptors. *Nat Immunol*, 11:373–384.

KAYAGAKI N., et al. (2007) DUBA: a deubiquitinase that regulates type I interferon production. *Science*, 318:1628–1632.

KEGG database: Kyoto Encyclopedia of Genes and Genomes – GenomeNet. Available at: www.genome.jp/kegg *(Accessed: August 2016).*

KHAN K.N., MAHROO O.A., KHAN R.S., MOHAMED M.D., MCKIBBIN M., et al. (2016) Differentiating drusen: Drusen and drusen-like appearances associated with ageing, age-related macular degeneration, inherited eye disease and other pathological processes. *Prog Retin Eye Res,* 53:70-106.

KING L.E., FRENTZEL J.W., MANN J.J., FRAKER P.J. (2005) Chronic zinc deficiency in mice disrupted T cell lymphopoiesis and erythropoiesis while B cell lymphopoiesis and myelopoiesis were maintained. *J Am Coll Nutr,* 24:494–502.

KITABAYASHI C., FUKADA T., KANAMOTO M., OHASHI W., HOJYO S., ATSUMI T. (2010) Zinc suppresses Th17 development via inhibition of STAT3 activation. *Int Immunol*, 22: 375–86.

KITAMURA, H., MORIKAWA, H., KAMON, H., IGUCHI, M., HOJYO, S., et al. (2006) Toll-like receptor-mediated regulation of zinc homeostasis influences dendritic cell function. *Nat Immunol,* 7**:**971-977.

KISHORE U., GHAI R., GREENHOUGH T.J., SHRIVE A.K., BONIFATI D.M., et al. (2004) Structural and functional anatomy of the globular domain of complement protein C1q. *Immunol Lett,* 95:113–28.

KLEIN R., PETO T., BIRD A., VANNEWKIRK M.R. (2004) The epidemiology of age related macular degeneration. *Am J Ophthalmol*, 137:486–95.

KLENOTIC P.A., HUANG P., PALOMO J., KAUR B., VAN MEIR E.G., et al. (2010) Histidine-rich glycoprotein modulates the anti-angiogenic effects of vasculostatin. *Am J Pathol,* 176**:**2039-2050.

KLUSZYNSKI B.A., KIM C., FAULK W.P. (1997) Zinc as a cofactor for heparin neutralization by histidine-rich glycoprotein. *J Biol Chem,* 272**:**13541-7.

KOBAYASHI S., TANAKA T., MATSUYOSHI N., IMAMURA S. (1996) Keratin 9 point mutation in the pedigree of epidermolytic hereditary palmoplantar keratoderma perturbs keratin intermediate filament network formation. *FEBS Lett,* 386:149-155.

KOBAYASHI S., KORE-EDA S., TANAKA T. (1999) Demonstration of the pathogenic effect of point mutated keratin 9 in vivo. *FEBS Lett*, 447:39-43.

KOBAYASHI H., OKAMOTO H., MURAKAMI A., IWATA T. (2014) Plasma proteome analysis on cynomolgus monkey *(Macaca fascicularis)* pedigrees with early onset drusen formation. *Exp Anim,* 63:305-310.

KOIDE T., FOSTER D., YOSHITAKE S., DAVIE E.W. (1986) Amino acid sequence of human histidine-rich glycoprotein derived from the nucleotide sequence of its cDNA. *Biochemistry,* 25**:** 2220-5.

KOLANOWSKI S.T., VAN SCHIJNDEL G.M., VAN HAM S.M., TEN BRINKE A. (2016) Adaptation to replating of dendritic cells synergizes with Toll-like receptor stimuli and enhances the pro-inflammatory cytokine profile. *Cytotherapy*, 18:902-10.

KOLB H., KOLB-BACHOFEN V. (1998) Nitric oxide in autoimmune disease: cytotoxic or regulatory mediator? *Immunology Today,* 19**:**556-561.

KOLEV M., LE FRIEC G., KEMPER C. (2014) Complement – tapping into new sites and effector systems. *Nat Rev Immunol,* 14:811–20.

KREZEL A., MARET W. (2007) Dual nanomolar and picomolar Zn(II) binding properties of metallothionein. *J Am Chem Soc,* 129:10911–10921.

LE NAOUR F., HOHENKIRK L., GROLLEAU A., MISEK D.E. et al. (2001) Profiling changes in gene expression during differentiation and maturation of monocyte-derived dendritic cells using both oligonucleotide microarrays and proteomics. *J Biol Chem,* 276:17920–17931.

LANG S.M., BYNOE M.O., KARKI R., TARTELL M.A., MEANS R.E. (2013) Kaposi's sarcoma-associated herpesvirus K3 and K5 proteins down regulate both DC-SIGN and DC-SIGNR. *PLoS One*, 8:e58056.

LANGE T. (2009) Proinflammatory and osteoclastogenic effects of beta-tri-calciumphosphate and hydroxyapatite particles on human mononuclear cells in vitro. *Biomaterials*, 30:5312–8.

LANGE T., SCHILLING A.F., PETERS F., MUJAS J., WICKLEIN D., AMLING M. (2011) Size dependent induction of proinflammatory cytokines and cytotoxicity of particulate beta-tric-alciumphosphatein vitro. *Biomaterials*, 32:4067–75.

LAU L.I.,CHIOU S.H.,LIU C.J.,YEN M.Y.,WEI Y.H. (2011) Theeffectofphoto-oxidative stress and inflammatory cytokine on complement factor H expression in retinal pigment epithelial cells. *Invest Ophthalmol Vis Sci*. 52:6832–6841.

LAW S.K.A., REID K.B.M. (1995) *Complement*, second ed. IRL Press, Oxford.

LECHNER J., CHEN M., HOGG R.E., TOTH L., SILVESTRI G., et al. (2016) Higher plasma levels of complement C3a, C4a and C5a increase the risk of subretinal fibrosis in neovascular age-related macular degeneration. *Immun Ageing*, 13:4.

LEE H.D., KOO B.H., KIM Y.H., JEON O.H., KIM D.S. (2012) Exosome release of ADAM15 and the functional implications of human macrophage-derived ADAM15 exosomes. *FASEB J,* 26:3084-3095.

LEHMANN HEUSS N.D., MCPHERSON S.W., ROEHRICH H., GREGERSON D.S. (2010) Dendritic cells are early responders to retinal injury. *Neurobiol Dis*, 40:177–184.

LELOUARD H., GATTI E., CAPPELLO F., GRESSER O., CAMOSSETO V., PIERRE P. (2002) Transient aggregation of ubiquitinated proteins during dendritic cell maturation. *Nature,* 417:177–182.

LELOUARD H., ET AL. (2004) Dendritic cell aggresome-like induced structures are dedicated areas for ubiquitination and storage of newly synthesized defective proteins. *J Cell Biol*, 164:667–675.

LELOUARD H., et al. (2007) Regulation of translation is required for dendritic cell function and survival during activation. *J Cell Biol*, 179:1427–1439.

LENGYEL I., FLINN J.M., PETO T., LINKOUS D.H., CANO K., et al. (2007) High concentration of zinc in sub-retinal pigment epithelial deposits. *Exp Eye Res,* 84:772-780.

LEUNG L.L., HARPEL P.C., NACHMAN R.L., RABELLINO E.M. (1983) Histidine-rich glycoprotein is present in human platelets and is released following thrombin stimulation. *Blood,* 62**:**1016-21.

LI Y., YOUSSOUFIAN H. (1997) MxA overexpression reveals a common genetic link in four Fanconi anemia complementation groups. *J Clin Invest,* 100:2873-2880.
LIJNEN H.R., HOYLAERTS M., COLLEN D. (1980) Isolation and characterization of a human plasma protein with affinity for the lysine binding sites in plasminogen. Role in the regulation of fibrinolysis and identification as histidine-rich glycoprotein. *J Biol Chem,* 255**:**10214-22.
LIU H., SADYGOV R.G., AND YATES J.R. (2004) A model for random sampling and estimation of relative protein abundance in shotgun proteomics. *Anal Chem*, 76:4193–4201.
LIU Y.J. (2005). IPC: professional type 1 interferon-producing cells and plasmacytoid dendritic cell precursors. *Annu Rev Immunol*, 23:275–306.
LIU H., NAISMITH J.H. (2009) A simple and efficient expression and purification system using two newly constructed vectors. *Protein Expr Purif,* 63:102-11.
LIU M.M., CHAN C.C., TUO J. (2012) Genetic mechanisms and age-related macular degeneration: common variants, rare variants, copy number variations, epigenetics, and mitochondrial genetics. *Hum Genomics,* 6:13.
LIU M.J., BAO S., GALVEZ-PERALTA M., PYLE C.J., RUDAWSKY A.C. (2013) ZIP8 regulates host defense through zinc-mediated inhibition of NF-κB. *Cell Rep*, 3:386–400.
LIUZZI J.P., LICHTEN L.A., RIVERA S., BLANCHARD R.K., AYDEMIR T.B., et al. (2005) Interleukin-6 regulates the zinc transporter Zip14 in liver and contributes to the hypozincemia of the acute-phase response. *Proc Natl Acad Sci U S A,* 102**:**6843-8.
LONGHURST C.M., WHITE M.M., WILKINSON D.A., JENNINGS L.K. (1999) A CD9, alphaIIbbeta3, integrin-associated protein, and GPIb/V/IX complex on the surface of human platelets is influenced by alphaIIbbeta3 conformational states. *Eur J Biochem,* 263:104-111.
LÖFFEK S., SCHILLING O., FRANZKE C.W. (2011) Biological role of matrix metalloproteinases: a critical balance. *Eur Respir J*, 38: 191-208.
LU J.H., TEH B.K., WANG L., WANG Y.N., TAN Y.S., et al. 2008. The classical and regulatory functions of C1q in immunity and autoimmunity. *Cell Mol Immunol,* 5**:**9-21.
LU J., STEWART A.J., SLEEP D., SADLER P.J., PINHEIRO T.J., BLINDAUER C.A. (2012) A molecular mechanism for modulating plasma Zn speciation by fatty acids. *J Am Chem Soc,* 134**:** 1454-7.
LUO C., CHEN M., XU H. (2011) Complement gene expression and regulation in mouse retina and retinal pigment epithelium/choroid. *Mol Vis*, 17:1588–1597.
LUTTY G.A., HASEGAWA T., BABA T., GREBE R., BHUTTO I., MCLEOD D.S. (2010) Development of the human choriocapillaris. *Eye (Lond),* 24:408–415.
MAARES M., HAASE H. (2016) Zinc and immunity: An essential interrelation. *Arch Biochem Biophys*, 16:30074-1.
MANDAL M.N., AYYAGARI R. (2006) Complement factor H: spatial and temporal expression and localization in the eye. *Invest Ophthalmol Vis Sci,* 47:4091-7.
MANDERSON G.A., MARTIN M., ONNERFJORD P., SAXNE T., SCHMIDTCHEN A., et al. (2009) Interactions of histidine-rich glycoprotein with immunoglobulins and proteins of the complement system. *Mol Immunol,* 46:3388-3398.
MANGANI S., MEYER-KLAUCKE W., MOIR A.J.G., RANIERI-RAGGI M., MARTINI D., RAGGI A. (2003) Characterization of the Zn binding site of the HPRG protein associated with rabbit skeletal muscle AMP deaminase. *J Biol Chem,* 278:3176-3184.
MANN M., HENDRICKSON R.C., PANDEY A. (2001) Analysis of proteins and proteomes by mass spectrometry. *Annu Rev Biochem,* 70:437–73.
MANTEGAZZA A.R., MAGALHAES J.G., AMIGORENA S., MARKS M.S. (2013) Presentation of phagocytosed antigens by MHC class I and II. *Traffic*, 14(2): 135–152.
MARET W., SANDSTEAD H.H. (2006) Zinc requirements and the risks and benefits of zinc supplementation. *J Trace Elem Med Biol*, 20: 3–18.

MARET W. (2006) Zinc coordination environments in proteins as redox sensors and signal transducers. *Antioxid Redox Signal,* 8:1419–1441.

Maret W. (2008) Metallothionein redox biology in the cytoprotective and cytotoxic functions of zinc. *Experimental gerontology*, 43:363–369.

MARET W., LI Y. (2009) Coordination dynamics of zinc in proteins. *Chem Rev*, 109:4682–707.

MARET W. (2015) Analyzing free zinc(II) ion concentrations in cell biology with fluorescent chelating molecules. *Metallomics*, 7:202-11.

MARIANI E., CATTINI L., NERI S., MALAVOLTA M., MOCCHEGIANI E., et al. (2006) Simultaneous evaluation of circulating chemokine and cytokine profiles in elderly subjects by multiplex technology: relationship with zinc status. *Biogerontology*, 7:449–59.

MARIANI E., NERI S., CATTINI L., MOCCHEGIANI E., MALAVOLTA M., et al. (2008) Effect of zinc supplementation on plasma IL-6 and MCP-1 production and NK cell function in healthy elderly: interactive influence of þ647 MT1a and -174 IL-6 polymorphic alleles. *Exp Gerontol,* 43:462-471.

MARTINEZ-BARRICARTE R., RECALDE S., FERNANDEZ-ROBREDO P., MILLAN I., OLAVARRIETA L., VINUELA A., PEREZ-PEREZ J., GARCIA-LAYANA A., RODRIGUEZ DE CORDOBA S. (2012) Relevance of complement factor H-related 1 (CFHR1) genotypes in age-related macular degeneration. *Invest Ophthalmol Vis Sci*, 53:1087–1094.

MARX G., KORNER G., MOU X.O., GORODETSKY R. (1993) Packaging Zinc, Fibrinogen, and Factor-Xiii in Platelet Alpha-Granules. *J Cell Physiol,* 156**:**437-442.

MATSUSHITA M., FUJITA T. (2001) Ficolins and the lectin complement pathway. *Immunol Rev,* 180**:**78-85.

MAYER L.S., UCIECHOWSKI P., MEYER S., SCHWERDTLE T., RINK L., HAASE H. (2014) Differential impact of zinc deficiency on phagocytosis, oxidative burst, and production of pro-inflammatory cytokines by human monocytes. *Metallomics*, 6:1288-1295.

MERLE N.S., CHURCH S.E., FREMEAUX-BACCHI V., ROUMENINA L.T. (2015) Complement system part I - molecular mechanisms of activation and regulation. *Front Immunol*. 6:262.

MERAD M., MANZ M.G. (2009) Dendritic cell homeostasis. *Blood*, 113:3418–3427.

METZ C.H., SCHRÖDER A.K., OVERBECK S., KAHMANN L., PLÜMÄKERS B., RINK L. (2006) T-helper type 1 cytokine release is enhanced by in vitro zinc supplementation due to increased natural killer cells. *Nutrition,* 23:157-163.

MILLER L.A., USACHENKO J., MCDONALD R.J., HYDE D.M. (2000) Trafficking of neutrophils across airway epithelium is dependent upon both thioredoxin- and pertussis toxin-sensitive signaling mechanisms. *J Leukoc Biol,* 68:201-208.

MILON B., DHERMY D., POUNTNEY D., BOURGEOIS M., BEAUMONT C. (2001) Differential subcellular localization of hZip1 in adherent and non-adherent cells. *FEBS Lett*, 507:241–246.

MITCHELL W.A., MENG I., NICHOLSON S.A., ASPINALL R. (2006) Thymic output, ageing and zinc. *Biogerontology,* 7**:**461-70.

MONROE K.M., MCWHIRTER S.M., VANCE R.E. (2010) Induction of type I interferons by bacteria. *Cell Microbiol*, 12:881–890.

MONTGOMERY D.W., CHVAPIL M., ZUKOSKI C.F. (1979) Effects of zinc chloride on guinea pig complement component activity in vitro: concentration-dependent inhibition and enhancement. *Infect Immun,* 23**:**424-31.

MORELLI A.E., LARREGINA A.T., SHUFESKY W.J., SULLIVAN M.L.G., STOLZ D.B., et al. (2004) Endocytosis, intracellular sorting, and processing of exosomes by dendritic cells. *Blood,* 104**:**3257-3266.

MORGAN W.T. (1978) Human serum histidine-rich glycoprotein. Interactions with heme, metal ions and organic ligands. *Biochim Biophys Acta*, 535:319-333.

MORGAN W.T. (1981) Interactions of the histidine-rich glycoprotein of serum with metals. *Biochemistry,* 20**:**1054-61.

MUNICH S., SOBO-VUJANOVIC A., BUCHSER W.J., BEER-STOLZ D., VUJANOVIC N.L. (2012) Dendritic cell exosomes directly kill tumor cells and activate natural killer cells via TNF superfamily ligands. *Oncoimmunology,* 1**:**1074-1083.

MUZZIOLI M., STECCONI R., DONNINI A., RE F., PROVINCIALI M. (2007) Zinc improves the development of human CD34þ cell progenitors towards Natural Killer cells and induces the expression of GATA- 3 transcription factor. *Int J Biochem Cell Biol*, 39:955-965.

NADRA I., MASON J.C., PHILIPPIDIS P., FLOREY O., SMYTHE C.D., et al. (2005) Proinflammatory activation of macrophages by basic calcium phosphate crystals via protein kinase C and MAP kinase pathways: a vicious cycle of inflammation and arterial calcification? *Circ Res*, 96:1248–56.

NAKADA S., TAI I., PANIER S., AL-HAKIM A., IEMURA S., et al. (2010) Non-canonical inhibition of DNA damage-dependent ubiquitination by OTUB1. *Nature*, 466:941-946.

NAN R., TETCHNER S., RODRIGUEZ E., PAO P.J., GOR J., et al. (2013) Zinc-induced Self-association of Complement C3b and Factor H: implications for inflammation and age-related macular degeneration. *J Biol Chem,* 288**:**19197-210.

NAYAK A., FERLUGA J., TSOLAKI A.G., KISHORE U. (2010) The non-classical functions of the classical complement pathway recognition subcomponent C1q. *Immunol Lett,* 131**:**139-150.

NEEFJES J., JONGSMA M.L.M., PAUL P., BAKKE O. (2011) Towards a systems understanding of MHC class I and MHC class II antigen presentation. *Nature Reviews Immunology*, 11:823-836.

NICE T.J., DENG W., COSCOY L., RAULET D.H. (2010) Stress-regulated targeting of the NKG2D ligand Mult1 by a membrane-associated RING-CH family E3 ligase. *J Immunol*, 185:5369–5376.

NILSEN N.J., VLADIMER G.I., STENVIK J., ORNING M.P., ZEID-KILANI M.V. et al. (2015) A role for the adaptor proteins TRAM and TRIF in toll-like receptor 2 signaling. *J Biol Chem*, 290:3209–3222.

NILSSON B., EKDAHL K.N. (1998) Components of the alternative pathway. *The Complement System*, 23–49. Springer. Berlin.

NILSSON B., NILSSON EKDAHL K. (2012) The tick-over theory revisited: is C3 a con-tact-activated protein? *Immunobiology,* 217:1106–10.

NISHIDA K., HASEGAWA A., NAKAE S., OBOKI K., SAITO H., et al. (2009) Zinc transporter Znt5/Slc30a5 is required for the mast cell-mediated delayed-type allergic reaction but not the immediate-type reaction. *J Exp Med*, 206:1351-64.

OHANA E., HOCH E., KEASAR C., KAMBE T., YIFRACH O., HERSHFINKEL M. (2009) Identification of the Zn2þ binding site and mode of operation of a mammalian Zn2þ transporter. *J Biol Chem*, 284:17677–17686.

OH J., SHIN J.S. (2015) Molecular mechanism and cellular function of MHCII ubiquitination. *Immunol Rev*, 266:134–144.

OKUMURA A., PITHA P.M., HARTY R.N. (2008) ISG15 inhibits Ebola VP40 VLP budding in an L-domain-dependent manner by blocking Nedd4 ligase activity. *Proc Natl Acad Sci U.S.A.,* 105:3974-3979.

ONG S.E., MANN M. (2005) Mass spectrometry-based proteomics turns quantitative. *Nat Chem Biol*, 1:252–62.

OVERBECK S., UCIECHOWSKI P., ACKLAND M.L., FORD D., RINK L. (2008) Intracellular zinc homeostasis in leukocyte subsets is regulated by different expression of zinc exporters ZnT-1 to ZnT-9. *J Leukoc Biol*, 83:368–80.

PALM N.W., ROSENSTEIN R.K., MEDZHITOV R. (2012) Allergic host defences. *Nature,* 484 (7395): 465–472.

PALMITER R.D., HUANG L. (2004) Efflux and compartmentalization of zinc by members of the SLC30 family of solute carriers. *Pflugers Arch,* 447**:**744-51.

PATEL V.I., METCALF J.P. (2016) Identification and characterization of human dendritic cell subsets in the steady state: a review of our current knowledge. *J Investig Med.* 64:833-847.

PARISH C.R. (2006) The role of heparan sulphate in inflammation. *Nat Rev Immunol,* 6:633-643.

PASSERINI A., ANDREINI C., MENCHETTI S., ROSATO A., FRASCONI P. (2007) Predicting zinc binding at the proteome level. *BMC Bioinformatics*, 8:39.

PEREIRA S.R., FACA V.M., GOMES G.G., CHAMMAS R., et al. (2005) Changes in the proteomic profile during differentiation and maturation of human monocyte-derived dendritic cells stimulated with granulocyte macrophage colony stimulating factor/interleukin-4 and lipopolysaccharide. *Proteomics*, 5:1186–1198.

PERKINS S.J., NEALIS A.S., SIM R.B. (1991) Oligomeric domain structure of human complement factor H by x-ray and neutron solution scattering. *Biochemistry,* 30**:**2847-2857.

PERKINS S.J., NAN R., OKEMEFUNA A.I., LI K., KHAN S., MILLER A. (2010) Multiple interactions of complement Factor H with its ligands in solution: a progress report. *Adv Exp Med Biol,* 703**:**25-47.

PERKINS S.J., NAN R., LI K., KHAN S., MILLER A. (2012) Complement Factor H–ligand interactions: Self-association, multivalency and dissociation constants. *Immunobiology*, 217:281–297.

PERKINS D.J. VOGEL S.N. (2015) Space and time: new considerations about the relationship between toll-like receptors (TLRs) and type I interferons (IFNs). *Cytokine*, 74:171–174.

PICKERING M.C., WALPORT M.J. (2000) Links between complement abnormalities and systemic lupus erythematosus. *Rheumatology (Oxford),* 39:133–41.

PICOTTI P., BODENMILLER B., MUELLER L.N., DOMON B., AEBERSOLD R. (2009) Full dynamic range proteome analysis of S. cerevisiae by targeted proteomics. *Cell*, 138:795–806.

PICHLMAIR A., LASSNIG C., EBERLE C.A., GORNA M.W., BAUMANN C.L., et al. (2011) IFIT1 is an antiviral protein that recognizes 5'-triphosphate RNA. *Nat Immunol*, 12:624-630.

PINET V.M., LONG E.O. (1998) Peptide loading onto recycling HLA-DR molecules occurs in early endosomes. *Eur JImmunol,* 28**:**799-804.

PLÒCIENNIKOWSKA A., HROMADA-JUDYCKA A., BORZECKA K., KWIATKOWSKA K. (2014) Co-operation of TLR4 and raft proteins in LPS-induced pro-inflammatory signalling. *Cell Mol Life Sci*, 72: 557–581.

POON I.K., YEE D.Y., JONES A.L., WOOD R.J., DAVIS D.S., et al. (2010a). Histidine-rich glycoprotein binds heparanase and regulates its enzymatic activity and cell surface interactions. *Int J Biochem Cell Biol,* 42**:**1507-16.

POON I.K.H., PARISH C.R., HULETT M.D. (2010b) Histidine-rich glycoprotein functions cooperatively with cell surface heparan sulfate on phagocytes to promote necrotic cell uptake. *J Leukoc Biol,* 88**:**559-569.

PORCELLI S., BRENNER M.B., GREENSTEIN J.L., BALK S.P., TERHORST C., BLEICHER P.A. (1989) Recognition of cluster of differentiation 1 antigens by human CD4-CD8-cytolytic T lymphocytes. *Nature,* 341 (6241):447–50.

POWIS S.J., SOO C.Y., ZHENG Y., CAMPBELL E.C., RICHES A. (2011) Nanoparticle Tracking Analysis of Cell Exosome and Nanovesicle Secretion. *Microscopy and Analysis*, 25:7-9.

PRASAD A.S. (2009) Zinc: role in immunity, oxidative stress and chronic inflammation. *Curr Opin Clin Nutr Metab Care*, 12:646-652.

PRASAD A.S. (2000) Effects of zinc deficiency on Th1 and Th2 cytokine shifts. *J Infect Dis*, 182:62–8.

PRASAD A.S. (2012) Discovery of human zinc deficiency: 50 years later. *J Trace Elem Med Biol,* 26**:**66-9.

REIS E SOUSA C. (2006) Dendritic cells in a mature age. *Nat Rev Immunol,* 6:476–483.

RICHARDS J., LE NAOUR F., HANASH S., BERETTA L. (2002) Integrated genomic and proteomic analysis of signalling pathways in dendritic cell differentiation and maturation. *Ann NY Acad Sci*, 975:91–100.

RICHES K., FRANKLIN L., MAQBOOL A., PECKHAM M., ADAMS M., et al. (2013) Apolipoprotein(a) acts as a chemorepellent to human vascular smooth muscle cells via integrin alphaVbeta3 and RhoA/ROCK-mediated mechanisms. *Int J Biochem Cell Biol*, 45:1776-1783.

RICKLIN D., HAJISHENGALLIS G., YANG K., LAMBRIS J.D. (2010) Complement: a key system for immune surveillance and homeostasis. *Nat Immunol,* 11**:**785-97.

RINK L., GABRIEL P. (2000) Zinc and the immune system. *Proc Nutr Soc,* 59**:**541-52.

ROCK K.L., FARFAN-ARRIBAS D.J., COLBERT J.D., GOLDBERG A.L. (2014) Re-examining class-I presentation and the DRiP hypothesis. *Trends Immunol*, 35:144–152.

ROBINET M., MAILLARD S., CRON M.A., BERRIH-AKNIN S., LE PANSE R. (2016) Review on Toll-Like Receptor Activation in Myasthenia Gravis: Application to the Development of New Experimental Models. *Clin Rev Allerg Immu*, 1–15.

ROCHE P.A., MARKS M.S., CRESSWELL P. (1991) Formation of a Nine-Subunit Complex by Hla Class-Ii Glycoproteins and the Invariant Chain. *Nature,* 354**:**392-394.

ROMANI L. (2004) Immunity to fungal infections. *Nature Rev. Immunol.* 4:11-24.

RONCA F., RAGGI A. (2015) Structure-function relationships in mammalian histidine-proline-rich glycoprotein. *Biochimie.* 118:207-220.

ROUMENINA L.T., KANTARDJIEV A.A., ATANASOV B.P., WATERS P., GADJEVA M., et al. (2005) Role of $Ca2^{+}$ in the electrostatic stability and the functional activity of the globular domain of human C1q. *Biochemistry,* 44:14097–109.

ROUMENINA L.T., POPOV K.T., BUREEVA S.V., KOJOUHAROVA M., GADJEVA M., et al. (2008) Interaction of the globular domain of human C1q with *Salmonella typhimurium* lipopolysaccharide. *Biochim Biophys Acta,* 1784:1271–6.

RUGJEE K.N., ROY CHAUDHURY S., AL-JUBRAN K., RAMANATHAN P., MATINA T., (2013) Fluorescent protein tagging confirms the presence of ribosomal proteins at Drosophila polytene chromosomes. *Peer J*, 1:e15.

RYDENGARD V., NORDAHL E.A., SCHMIDTCHEN A. (2006) Zinc potentiates the antibacterial effects of histidine-rich peptides against Enterococcus faecalis. *FEBS J,* 273**:**2399-2406.

RYDENGÅRD V., OLSSON A.K., MÖRGELIN M., SCHMIDTCHEN A. (2007) Histidine-rich glycoprotein exerts antibacterial activity. *FEBS J*, 274:377-89.

RYDENGÅRD V., SHANNON O., LUNDQVIST K., KACPRZYK L., CHALUPKA A., et al. (2008) Histidine-Rich Glycoprotein Protects from Systemic Candida Infection. *PLoS Pathog*, 4: e1000116.

SAHU A., LAMBRIS J.D. (2001) Structure and biology of complement protein C3, a connecting link between innate and acquired immunity. *Immunol Rev,* 180**,** 35-48.

SAN-MIGUEL T., PÉREZ-BERMÚDEZ P., GAVIDIA I. (2013) Production of soluble eukaryotic recombinant proteins in E. coli is favoured in early log-phase cultures induced at low temperature. *Springerplus*, 2:89.

SARKAR B. (1989) Metal–protein interactions in transport, accumulation, and excretion of metals. *Biol Trace Elem Res*, 21:137–44.

SAUNDERS R.E., GOODSHIP T.H.J., ZIPFEL P.F., PERKINS S.J. (2006) Factor H-associated haemolytic uraemic syndrome: a web database of the structural consequences of disease-associated mutations. *Hum Mutat*, 27:21–30.

SAYADI A., NGUYEN A.T., BARD F.A., BARD-CHAPEAU E.A. (2013) Zip14 expression induced by lipopolysaccharides in macrophages attenuates inflammatory response. *Inflamm Res,* 62:133–43.

SCHWEIGEL-RÖNTGEN M. (2014) The Families of Zinc (SLC30 and SLC39) and Copper (SLC31) Transporters. *Curr Top Membr*, 73:321-55.

SCOTT B.J., BRADWELL A.R. (1983) Identification of the serum binding proteins for iron, zinc, cadmium, nickel, and calcium. *Clin Chem,* 29**:**629-33.

SEDDON J.M., COTE J., PAGE W.F., AGGEN S.H., NEALE M.C. (2005) The US twin study of age-related macular degeneration: relative roles of genetic and environmental influences. *Arch Ophthal*, 123:321–7.

SELBI W., DE LA MOTTE C., HASCALL V., PHILLIPS A. (2004) MP-7 modulates hyaluronan-mediated proximal tubular cell-monocyte interaction. *J Am Soc Nephrol*, 15:1199-1211.

SENSI S.L., PAOLETTI P., BUSH A.I., SEKLER I. (2009) Zinc in the physiology and pathology of the CNS. *Nat rev Neurosci*, 10:780–791.

SHI X., LENG L., WANG T., WANG W., DU X., LI J., MCDONALD C., CHEN Z., MURPHY J.W., LOLIS E., NOBLE P., KNUDSON W., BUCALA R. (2006) CD44 is the signaling component of the macrophage migration inhibitory factor-CD74 receptor complex. *Immunity*, 25:595-606.

SHIN .JS., EBERSOLD M., PYPAERT M., DELAMARRE L., HARTLEY A., MELLMAN I. (2006) Surface expression of MHC class II in dendritic cells is controlled by regulated ubiquitination. *Nature*, 444:115–118.

SIMANTOV R., FEBBRAIO M., CROMBIE R., ASCH A.S., NACHMAN R. L., SILVERSTEIN R.L. (2001) Histidine-rich glycoprotein inhibits the antiangiogenic effect of thrombospondin-1. *J Clin Invest,* 107**:**45-52.

SKATTUM L., VAN DEUREN M., VAN DER POLL T., TRUEDSSON L. (2011) Complement deficiency states and associated infections. *Mol Immunol,* 48**:**1643-55.

SKERKA C., CHEN Q., FREMEAUX-BACCHI V., ROUMENINA L.T. (2013) Complement factor H related proteins (CFHRs). *Mol Immunol,* 56:170–80.

SMITH P.K., KROHN R.I., HERMANSON G.T., MALLIA A.K., GARTNER F.H., et al. (1985) Measurement of protein using bicinchoninic acid. *Anal Biochem*, 150:76-85.

SOO C.Y., SONG Y., ZHENG Y., CAMPBELL E.C., RICHES A.C., GUNN-MOORE F., POWIS S.J. (2012) Nanoparticle tracking analysis monitors microvesicle and exosome secretion from immune cells. *Immunology*, 136:192-7.

SORENSEN C.B., KROGH-PEDERSEN H., PETERSEN T.E. (1993) Determination of the disulphide bridge arrangement of bovine histidine-rich glycoprotein. *FEBS Lett,* 328**:**285-90.

SPITS H., ARTIS D., COLONNA M., DIEFENBACH A., DI SANTO J.P., EBERL G., KOYASU S., LOCKSLEY R.M., MCKENZIE A.N., MEBIUS R.E., POWRIE F., VIVIER E. (2013) Innate lymphoid cells — a proposal for uniform nomenclature. Nature Rev Immunol, 13, 145–149.

STAWOWCZYK M., VAN SCOY S., KUMAR K.P., REICH N.C. (2011) The interferon stimulated gene 54 promotes apoptosis. *J Biol Chem*, 286:7257-7266.

STEFANIDOU M., MARAVELIAS C., DONA A., SPILIOPOULOU C. (2006) Zinc: a multipurpose trace element. *Arch Toxicol,* 80:1–9.

STEWART A.J., BLINDAUER C.A., BEREZENKO S., SLEEP D., SADLER P.J. (2003) Interdomain zinc site on human albumin. *Proc Nat Acad Sci USA,* 100**:**3701-3706.

STEWART A.J., BLINDAUER C.A., SADLER P.J. (2009) Plasma fatty acid levels may regulate the Zn(2+)-dependent activities of histidine-rich glycoprotein. *Biochimie,* 91**:**1518-22.

STATHAKIS D.G., BURTON D.Y., MCIVOR W.E., KRISHNAKUMAR S., WRIGHT T.R., O'DONNELL J.M. (1999) The catecholamines up (Catsup) protein of Drosophila melanogaster functions as a negative regulator of tyrosine hydroxylase activity. *Genetics*,153:361–382.

STRAUSS O. (2005) The retinal pigment epithelium in visual function. *Physiol Rev*, 85:845–81.

STREILEIN J.W. (1999) Immunoregulatory mechanisms of the eye. *Prog Retin Eye Res*, 18:357–370.

STURFELT G., TRUEDSSON L. (2005) Complement and its breakdown products in SLE. *Rheumatology (Oxford),* 44**:**1227-32.

SUMMERSGILL H., ENGLAND H., LOPEZ-CASTEJON G., LAWRENCE C.B., LUHESHI N.M., PAHLE J. (2014) Zinc depletion regulates the processing and secretion of IL-1beta. *Cell Death Dis,* 5:1040.

SUZUKI T., ISHIHARA K., MIGAKI H., NAGAO M., YAMAGUCHI-IWAI Y., KAMBE T. (2005) Two different zinc transport complexes of cation diffusion facilitator proteins localized in the secretory pathway operate to activate alkaline phosphatases in vertebrate cells*. J Biol Chem*, 280:30956–30962.

SWEIGARD J.H., YANAI R., GAISSERT P., SAINT-GENIEZ M., KATAOKA K., THANOS A. (2014) The alternative complement pathway regulates pathological angiogenesis in the retina. *FASEB J,* 28:3171-82.

TAKAHASHI M., MORI S., SHIGETA S., FUJITA T. (2007) Role of MBL-associated serine protease (MASP) on activation of the lectin complement pathway. *Adv Exp Med Biol,* 598**:**93-104.

TAN Y.F., LEONG C.F., CHEONG S.K. 2010. Observation of dendritic cell morphology under light, phase-contrast or confocal laser scanning microscopy. *Malaysian J Pathol,* 32:97 – 102.

TAN P.L., BOWES RICKMAN C., KATSANIS N. (2016) AMD and the alternative complement pathway: genetics and functional implications. *Hum Genomics*, 10:23.

TAYLOR K.M., NICHOLSON R.I. (2003) The LZT proteins; the LIV-1 subfamily of zinc transporters. *Biochim Biophys Acta,* 1611:16–30.

TAYLOR K.M., HISCOX S.E., NICHOLSON R. (2004) Zinc transporter LIV-1: a link between cellular development and cancer progression. *Trends Endocrinol Metab*, 15:461-463.

TAYLOR K.M., MORGAN H.E., JOHNSON A., NICHOLSON R.I. (2004b) Structure-function analysis of HKE4, a member of the new LIV-1 subfamily of zinc transporters. *Biochem J*, 377:131–139.

TAYLOR M.W., GROSSE W.M., SCHALEY J.E., SANDA C., WU X. (2004c) Global effect of PEG-IFN-alpha and ribavirin on gene expression in PBMC in vitro. *J Interferon Cytokine Res*, 24:107–118.

TAYLOR K.M., MORGAN H.E., JOHNSON A., NICHOLSON R.I. (2005) Structure-function analysis of a novel member of the LIV-1 subfamily of zinc transporters, ZIP14. *FEBS Lett*, 579: 427–432.

TAYLOR M.W., TSUKAHARA T., BRODSKY L., SCHALEY J., SANDA C. (2007) Changes in gene expression during pegylated interferon and ribavirin therapy of chronic hepatitis C virus distinguish responders from nonresponders to antiviral therapy. *J Virol,* 81:3391–3401.

TAYLOR K.M., VICHOVA P., JORDAN N., HISCOX S., HENDLEY R., NICHOLSON R.I. (2008) ZIP7-mediated intracellular zinc transport contributes to aberrant growth factor signaling in antihormone-resistant breast cancer Cells. *Endocrinology*, 149:4912–4920.

TAYLOR K.M. (2008b). A distinct role in breast cancer for two LIV-1 family zinc transporters. *Biochem Soc Trans*, 36:1247–1251.

TAYLOR K.M., HISCOX S., NICHOLSON R.I., HOGSTRAND C., KILLE P. (2012) Protein kinase CK2 triggers cytosolic Zinc signalling pathways by phosphorylation of Zinc channel ZIP7. *Sci Signaling* 5:11.

TEILLET F., DUBLET B., ANDRIEU J-P., GABORIAUD C., ARLAUD G.J., THIELENS N.M. (2005) The two major oligomeric forms of human mannan-binding lectin: chemical characterization, carbohydrate-binding properties, and interaction with MBL-associated serine proteases. *J Immunol,* 1950:2870–7.

THAI LIM L., AH-KEE E.Y, COLLINS C.E. (2014) Common eye drops and their implications for pH measurements in the management of chemical eye injuries. *Int J Ophthalmol*, 7:1067–1068.

THERY C., DUBAN L., SEGURA E., VERON P., et al. (2002) Indirect activation of naive CD41 T cells by dendritic cell-derived exosomes. *Nat Immunol*, 3:1156–1162.

THOMPSON R.B., REFFATTO V., BUNDY J.G., KORTVELY E., FLINN J.M. et al.(2015) Identification of hydroxyapatite spherules provides new insight into subretinal pigment epithelial deposit formation in the aging eye. *Proc Natl Acad Sci U.S.A.,* 112:1565-1570.

THORNTON J., EDWARDS R., MITCHELL P., HARRISON R.A., BUCHAN I., KELLY S.P. (2005) Smoking and age-related macular degeneration: a review of association. *Eye (Lond),* 19:935–44.

TILL G.O., HANSCH G.M. (1998) *The Complement System*. Springer-Verlag, Berlin, 23–49.

TODD D.J., LEE A.H., GLIMCHER L.H. (2008) The endoplasmic reticulum stress response in immunity and autoimmunity. *Nat Rev Immunol,* 8:663-674.

TRIANTAFYLLOPOULOU A., FRANZKE C.W., SESHAN S.V. (2010) Proliferative lesions and metalloproteinase activity in murine lupus nephritis mediated by type I interferons and macrophages. *Proc Natl Acad Sci USA*, 107: 3012–3017.

TROMBETTA E.S., EBERSOLD M., GARRETT W., PYPAERT M., MELLMAN I. (2003) Activation of lysosomal function during dendritic cell maturation. *Science,* 299:1400–3.

TSUCHIDA-STRAETEN N., ENSSLEN S., SCHAFER C., WOLTJE M., DENECKE B., et al. (2005) Enhanced blood coagulation and fibrinolysis in mice lacking histidine-rich glycoprotein (HRG). *J Thromb Haemost,* 3**:**865-72.

TUBEK S., GRZANKA P., TUBEK I. (2008) Role of zinc in hemostasis: A review. *Biol Trace Elem Res,* 121**:**1-8.

TURLEY S.J., INABA K., GARRETT W.S., EBERSOLD M., UNTERNAEHRER J. (2000) Transport of peptide-MHC class II complexes in developing dendritic cells. *Science,* 288:522–27.

TURNER M.W. (1996) Mannose-binding lectin: the pluripotent molecule of the innate immune system. *Immunol Today,* 17**:**532-40.

TYERS M., MANN M. (2003) From genomics to proteomics. *Nature,* 422:193–7.

TZIMA E., READER J.S., IRANI-TEHRANI M., EWALT K.L., SCHWARTZ M.A., SCHIMMEL P. (2003) Biologically active fragment of a human tRNA synthetase inhibits fluid shear stress-activated responses of endothelial cells. *Proc Natl Acad Sci U.S.A.,* 100:14903-14907.

USUKI K., SARAS J., WALTENBERGER J., MIYAZONO K., PIERCE G., et al. (1992) Platelet-derived endothelial cell growth factor has thymidine phosphorylase activity. *Biochem Biophys Res Commun*, 184:1311-1316.

VALÉS-GÓMEZ M., ERSKINE R.A., DEACON M.P., STROMINGER J.L., REYBURN H.T. (2000) The role of zinc in the binding of killer cell Ig-like receptors to class I MHC proteins. *Proc Natl Acad Sci U S A*, 98:1734-9.

VALLEE B.L., FALCHUK K.H. (1993) The Biochemical Basis of Zinc Physiology. *Physiol Rev,* 73**:**79-118.

VAN NIEL G., WUBBOLTS R., STOORVOGEL W. (2008) Endosomal sorting of MHC class II determines antigen presentation by dendritic cells. *Curr Opin Cell Biol,* 20**:**437-44.

VANWILDEMEERSCH M., OLSSON A.K., GOTTFRIDSSON E., CLAESSON-WELSH L., LINDAHL U., SPILLMANN D. (2006) The anti-angiogenic His/Pro-rich fragment of histidine-rich glycoprotein binds to endothelial cell heparan sulfate in a Zn^{2+}-dependent manner. *J Biol Chem,* 281:10298–304.

VAUTIER S., DA GLÓRIA SOUSA M., BROWN G.D. (2010) C-type lectins, fungi and Th17 responses. *Cytokine Growth Factor Rev*. 21(6): 405–412.

VELARD F., BRAUX J., AMEDEE J., LAQUERRIERE P. (2013) Inflammatory cell response to calcium phosphate biomaterial particles: An overview. *Acta Biomaterialia*, 9:4956–4963.

VERBOVETSKI I., BYCHKOV H., TRAHTEMBERG U., SHAPIRA I., HAREUVENI M., et al. (2002) Opsonization of apoptotic cells by autologous iC3b facilitates clearance by immature dendritic cells, down-regulates DR and CD86, and up-regulates CC chemokine receptor 7. *J Exp Med,* 196:1553–61.

VERDIJK P., VAN VEELEN P.A., DE RU A.H., HENSBERGEN P.J., MIZUNO K., et al. (2004) Morphological changes during dendritic cell maturation correlate with cofilin activation and translocation to the cell membrane. *Eur J Immunol*, 34:156–164.

VILLADANGOS J.A., SCHNORRER P., WILSON N.S. (2005) Control of MHC class II antigen presentation in dendritic cells: a balance between creative and destructive forces. *Immunol Rev,* 207**:**191-205.

VILLADANGOS J.A., SCHNORRER P. (2007) Intrinsic and cooperative antigen-presenting functions of dendritic-cell subsets in vivo. *Nat Rev Immunol,* 7**:**543-55.

VUJANOVIC N.L. (2011) Role of TNF superfamily ligands in innate immunity. *Immunol Res,* 50**:**159-174.

VYAS J.M., VAN DER VEEN A.G., PLOEGH H.L. (2008) The known unknowns of antigen processing and presentation. Nature Rev. Immunol. 8:607–618.

WALKER J.A., JILLIAN L.B., ANDREW N.J.M. (2013) Innate lymphoid cells—how did we miss them?". Nature Rev Immunol*,* 13 (2): 75–87.

WALLIS R., MITCHELL D.A., SCHMID R., SCHWAEBLE W.J., KEEBLE A.H. (2010) Paths reunited: Initiation of the classical and lectin pathways of complement activation. *Immunobiology,* 215**:**1-11.

WALSH H.A., BOTTING N.P. (2002) Purification and biochemical characterization of some of the properties of recombinant human kynureninase. *Eur J Biochem*, 269:2069-2074.

WAN Y., PETRIS M.J., PECK S.C. (2014) Separation of zinc-dependent and zinc-independent events during early LPS-stimulated TLR4 signaling in macrophage cells. *FEBS Lett*, 588:2928-35.

WANG F., KIM B.E., DUFNER-BEATTIE J., PETRIS M.J., ANDREWS G., EIDE D.J. (2004) Acrodermatitis enteropathica mutations affect transport activity, localization and zinc responsive trafficking of the mouse ZIP4 zinc transporter. *Hum Mol Genet*, 13: 563–571.

WARNER J.R., MCINTOSH K.B. (2009) How common are extraribosomal functions of ribosomal proteins? *Mol Cell*, 34:3-11.

WELLENREUTHER G., CIANCI M., TUCOULOU R., MEYER-KLAUCKE W., HAASE H. (2009) The ligand environment of zinc stored in vesicles. *Biochem Biophys Res Commun,* 380**:**198-203.

WELLINGHAUSEN N., DRIESSEN C., RINK L. (1996) Stimulation of human peripheral blood mononuclear cells by zinc and related cations. *Cytokine*, 8:767-771.

WELLINGHAUSEN N., MARTIN M., RINK L. (1997) Zinc inhibits interleukin-1-dependent T cell stimulation. *Eur J Immunol,* 27:2529-2535.

WENKEL H., STREILEIN J.W. (2000) Evidence that retinal pigment epithelium functions as an immune-privileged tissue. *Invest Ophthalmol Vis Sci*, 41:3467–3473.

WEST M.A., WALLIN R.P., MATTHEWS S.P., SVENSSON H.G. ET AL. (2004) Enhanced dendritic cell antigen capture via tolllike receptor-induced actin remodeling. *Science,* 305:1153–1157.

WEST A.P., KOBLANSKY A.A., GHOSH S. (2006) Recognition and signaling by toll-like receptors. *Annu Rev Cell Dev Biol,* 22:409–437.

WHITEHOUSE R.C., PRASAD A.S., RABBANI P.I., COSSACK Z.T. (1982) Zinc in Plasma, Neutrophils, Lymphocytes, and Erythrocytes as Determined by Flameless Atomic-Absorption Spectrophotometry. *Clinical Chemistry,* 28**:**475-480.

WICOVSKY A., HENKLER F., SALZMANN S., SCHEURICH P., KNEITZ C., WAJANT H. (2009) Tumor necrosis factor receptor-associated factor-1 enhances proinflammatory TNF receptor-2 signaling and modifies TNFR1-TNFR2 cooperation. *Oncogene* 28:1769-1781.

WONG W.L., SU X., LI X., CHEUNG C.M., KLEIN R., et al. (2014) Global prevalence of age-related macular degeneration and disease burden projection for 2020 and 2040: a systematic review and meta-analysis. *Lancet Glob Health*, 2:106–116.

XU H., DAWSON R., FORRESTER J.V, LIVERSIDGE J. (2007) Identification of novel dendritic cell populations in normal mouse retina. *Invest Ophthalmol Vis Sci*, 48:1701–1710.

XU H., CHEN M., FORRESTER J.V. (2009) Para-inflammation in the aging retina. *Prog Retin Eye Res*, 28:348–368.

XU H., CHEN M. (2016) Targeting the complement system for the management of retinal inflammatory and degenerative disease. *Eur J Pharmacol,* 787:94-104.

YAMAMOTO K., TAKAHASHI M. (1975) Inhibition of the terminal stage of complement-mediated lysis (reactive lysis) by zinc and copper ions. *Int Arch Allergy Appl Immunol,* 48**:**653-63.

YAMASAKI S., SAKATA-SOGAWA K., HASEGAWA A., SUZUKI T., KABU K., et al. (2007) Zinc is a novel intracellular second messenger. *J Cell Biol,* 177:637–645.

YAMASHIRO S., YAMAKITA Y., ONO S., MATSUMURA F. (1998) Fascin, an actin-bundling protein, induces membrane protrusions and increases cell motility of epithelial cells. *Mol Biol Cell*, 9:993-1006.

YANAGIHARA S., KOMURA E., NAGAFUNE J., WATARAI H. ET AL. (1998) EBI1/CCR7 is a new member of dendritic cell chemokine receptor that is up-regulated upon maturation. *J Immunol,* 161:3096–3102.

YATES J.R., SEPP T., MATHARU B.K. (2007) Complement C3 variant and the risk of age-related macular degeneration. *New Engl J Med,* 357:553–561.

YU L., WANG L., CHEN S. (2010) Endogenous toll-like receptor ligands and their biological significance. *J Cell Mol Med,* 14(11): 2592–2603.

ZHANG M., CHEN L., WANG S., WANG T. (2009) Rab7: roles in membrane trafficking and disease. *Biosci Rep*, 29:193-209.

ZHU H., BILGIN M., SNYDER M. (2003). Proteomics. *Annu Rev Biochem,* 72:783–812.

ZHOU L.J., TEDDER T.F. (1996) CD14+ blood monocytes can differentiate into functionally mature CD83+ dendritic cells. *Proc Natl Acad Sci U S A*, 93:2588–2592.

ZIPFEL P.F., SKERKA C. (1999) FHL-1/reconectin: a human complement and immune regulator with cell-adhesive function. *Immunol Today*, 20:135-40.

.

Appendices

Appendix 1

B-actin

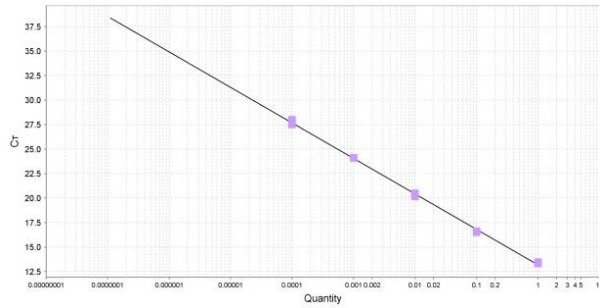

RPLP0

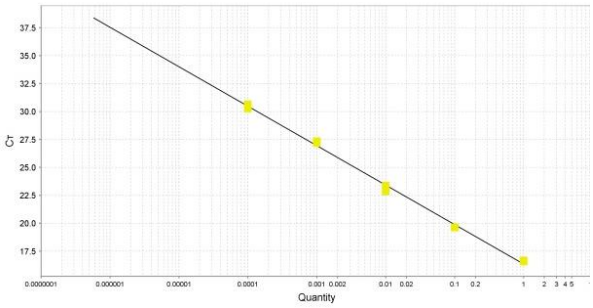

SLC30A1

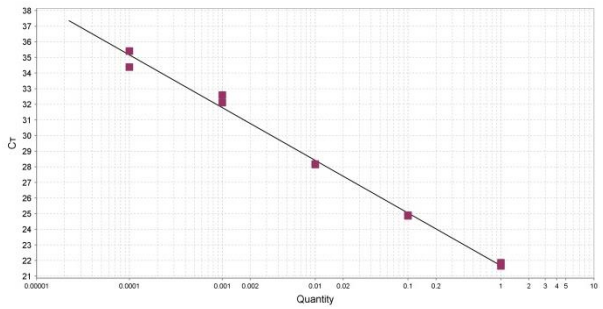

SLC30A7

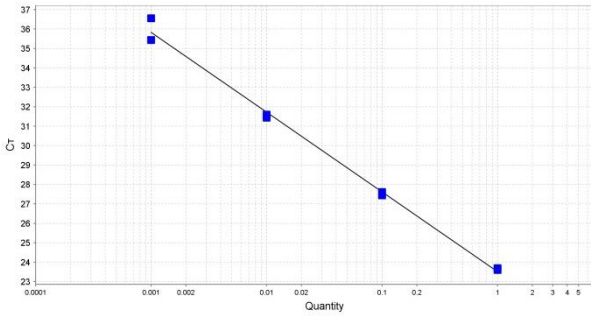

SLC39A6

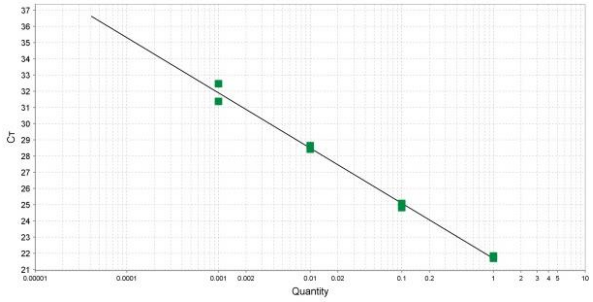

SLC39A7

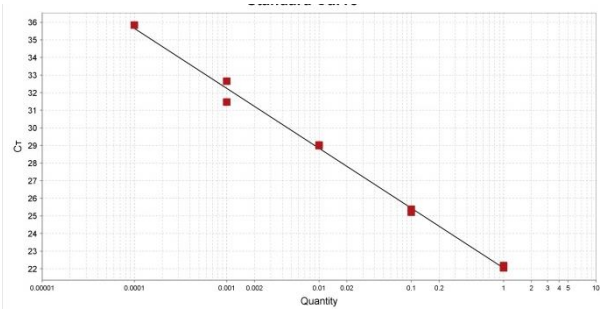

B

Target	R2	Primer efficiency	Error
ZnT1	0.993	97.91	0.101
ZnT7	0.995	75.3	0.119
Zip6	0.994	96.65	0.109
Zip7	0.995	96.77	0.092
B-actin	0.998	88.9	0.051
RPLP0	0.996	91.96	0.075

Figure 1. Standard amplification curves were plotted for each primer pair using serial dilution of DNA (A). Reaction efficiencies and correlation coefficient (R2) (B) were calculated automatically by ViiA™ 7 Real-Time PCR System Software based on standard curves plotted.

University of St Andrews
from first to foremost

600 YEARS
1413 – 2013

Project Title	**Investigation of immune cell behaviour**
Researchers Name(s)	**Dr Simon Powis, Miss Fiona Cooke, Professor Malte Gather, Dr Marcel Schubert, Dr Andrew Morton, Giorgio Bartalucci, Mohammad Hassan, Dagmara Wiatrek, Alisdair Pollock**
Supervisor(s)	**Dr Simon Powis**
Department/Unit	**School of Medicine**
Ethical Approval Code (Approval allocated to Original Application)	**MD10814**
Original Application Approval Date	**14th February 2014**
Amendment Application Approval	**6th March 2015**

Ethical Amendment 2 Approval

Thank you for submitting your amendment application which was considered by the School of Medicine Ethics Convener on the 6th March 2015. The following documents were reviewed:

1. Ethical Amendment Application Form YES

The University Teaching and Research Ethics Committee (UTREC) approves this study from an ethical point of view. Please note that where approval is given by a School Ethics Committee that committee is part of UTREC and is delegated to act for UTREC.

Approval is given for ten years from the original application only. Ethical Amendments do not extend this period but give permission to an amendment to the original approval research proposal only. If you are unable to complete your research within the original 10 year validation period, you will be required to write to your School Ethics Committee and to UTREC (where approval was given by UTREC) to request an extension or you will need to re-apply. You must inform your School Ethics Committee when the research has been completed.

Any serious adverse events or significant change which occurs in connection with this study and/or which may alter its ethical consideration, must be reported immediately to the School Ethics Committee, and an Ethical Amendment Form submitted where appropriate.

Approval is given on the understanding that the 'Guidelines for Ethical Research Practice' (http://www.st-andrews.ac.uk/media/UTRECguidelines%20Feb%2008.pdf) are adhered to.

Yours sincerely

Dr Gordon Cramb
Convenor of the School Ethics Committee